HOLTEC
INTERNATIONAL

LICENSING REPORT

for

CAPACITY EXPANSION

of

THE LA SALLE COUNTY STATION UNIT 1

COMMONWEALTH EDISON COMPANY

CHICAGO, ILLINOIS

by

HOLTEC INTERNATIONAL
CHERRY HILL, NJ

HOLTEC REPORT HI-92765

This report, with certain added appendices, also serves as the Design Report for this project.

HOLTEC INTERNATIONAL

REVIEW AND CERTIFICATION LOG

DOCUMENT NAME: LICENSING REPORT FOR CAPACITY EXPANSION OF THE LA SALLE COUNTY STATION UNIT 1

HOLTEC DOCUMENT I.D. # HI-92765

HOLTEC PROJECT NUMBER 1174J

CUSTOMER/CLIENT UST&D/CECo

REVISION BLOCK				
ISSUE NO.	AUTHOR & DATE	REVIEWER & DATE	QUALITY ASSURANCE & DATE	PROJECT MANAGER & DATE
ORIGINAL	YW 4/20/92	A.S. 4/20/92	4/20/92	YW 4/20/92
REV. 1	5/22/92	5/21/92	5/21/92	5/21/92
REV. 2				
REV. 3				
REV. 4				
REV. 5				
REV. 6				

* Must be Project Manager or his Designee.

NOTE: Signatures and printed names are required in the review block.

This document conforms to the requirements of the design specification and the applicable sections of the governing codes.

SUMMARY OF REVISIONS LOG

Report HI-92765

Preliminary Issue: February 14, 1992
Contains sections 1, 2, 3, 4, 5, 6, 7, and 10 of report.

Revision 0: April 15, 1992
Contains all sections of the report.

Revision 1: May 20, 1992
Contains all sections of the report.

TABLE OF CONTENTS

TABLE OF CONTENTS

TABLE OF CONTENTS

TABLE OF CONTENTS

1.0- INTRODUCTION

The La Salle County Station (LSCS) installation consists of two Boiling Water Reactors (3323 MWt thermal output, 1130 MWe) supplied by the General Electric Company of San Jose, California. This licensing application deals with the proposed capacity expansion in the Unit 1 spent fuel pool at La Salle County Station site. The LSCS Unit 1 reactor features a core consisting of 764 fuel assemblies. The plant is located at a distance of approximately 15 miles southwest of the town of Morris, Illinois. The site is owned and operated by the Commonwealth Edison Company, henceforth also referred to as the Owner or Licensee.

LSCS Unit 1 began commercial operation in 1983. Its spent fuel pool is of 408" x 480" (nominal) planform section with the spheroidal drywell wall constituting the southend wall. The pool is presently equipped with 1080 storage cells in a low density layout.

This licensing application is for reracking the LSCS Unit 1 pool with new maximum density racks. As described in Section 2 of this report, the reracking is proposed to be carried out in 1993 in one campaign.

The new spent fuel storage racks are free-standing and self supporting. The principal construction materials for the new racks are ASME 240-Type 304 stainless steel sheet and plate stock, and SA564 (precipitation hardened stainless steel) for the adjustable support spindles. The only non-stainless material utilized in the rack is the neutron absorber material which is a boron carbide aluminum cermet manufactured under a U.S. patent and sold under the brand name Boral™ by AAR Brooks and Perkins, Livonia, Michigan.

The new racks are designed and analyzed in accordance with Section III, Division 1, Subsection NF of the ASME Boiler and Pressure Vessel Code. The material procurement and fabrication of the rack modules conforms to 10CFR 50 Appendix B requirements.

The present and anticipated refueling schedule for the LSCS Unit 1 pool contemplates a normal batch size of 256 assemblies discharged at 18 month cycles.

The proposed reracking campaign (ca. 1993) will increase the number of storage locations to 4029 (including control rod storage locations), which will provide over 18 years of refueling discharges while maintaining the full core discharge capability.

This Licensing Report documents the design and analyses performed by the Contractors, Holtec International of Cherry Hill, New Jersey, and Sargent & Lundy Engineers of Chicago, Illinois, to demonstrate that the new spent fuel racks satisfy all governing requirements of the applicable codes and standards, in particular, "OT Position for Review and Acceptance of Spent Fuel Storage and Handling Applications", USNRC (1978) and 1979 Addendum thereto.

The safety assessment of the proposed rack modules involved demonstration of its hydrothermal, criticality and structural adequacy. Hydrothermal adequacy requires that fuel cladding will not fail due to excessive thermal stress, and that the steady state pool bulk temperature will remain within the limits prescribed for the spent fuel pool. Demonstration of structural adequacy primarily involves analyses showing that, under the postulated seismic events, the primary stresses in the module structure will remain below the ASME Code allowables. The structural qualification also includes analytical demonstration that the subcriticality of the

stored fuel will be maintained under accident scenarios such as fuel assembly drop, accidental misplacement of fuel outside a rack, etc.

The criticality safety analysis presented in Section 4 of this report shows that the neutron multiplication factor for the stored fuel array is bounded by the USNRC limit of 0.95 under assumptions of 95% probability and 95% confidence. Consequences of the inadvertent placement of a fuel assembly are also evaluated as part of the criticality analysis. The criticality analysis also sets the requirements on the length of the B-10 screen and the areal B-10 density.

The thermal-hydraulic, criticality, seismic and mechanical accident analyses were performed by Holtec International using its computer codes which have been used in numerous rerackin. applications. Likewise, radiological and pool structural evaluations were performed by Sargent & Lundy Engineers using methods and procedures which have been applied in several dockets.

This Licensing Report contains documentation of the analyses performed to demonstrate the large margins of safety with respect to all USNRC specified criteria.

The analyses presented herein clearly demonstrate that the rack module arrays possess wide margins of safety from all three - thermal-hydraulic, criticality, and structural - vantage points. The No Significant Hazard Consideration evaluation presented along with this licensing report is based on the descriptions and analyses synopsized in the subsequent sections of this report.

This document has been prepared for submission to the U.S. Nuclear Regulatory Commission for securing regulatory approval for the modification of the LSCS-1 pool as proposed herein.

2.0 MODULE LAYOUT AND RERACKING OPERATION

2.1 Module Layout

This section provides general information on the new storage modules for the La Salle County Station Unit 1 spent fuel pool. The information presented in this and the next section provide the basis for the detailed criticality, thermal-hydraulic and seismic analyses presented in the subsequent sections of this report.

The La Salle County Station Unit 1 high density spent fuel storage racks consist of individual cells with 6.05" (nom.) inside square dimension, each of which accommodates a single Boiling Water Reactor (BWR) fuel assembly. The fuel assembly can be stored in the storage locations in channelled or unchannelled configuration. Table 2.1.1 gives the essential storage cell design data.

As mentioned in the preceding section, the reracking of the La Salle County Station Unit 1 pool is expected to begin in March, 1993 for scheduled completion in late 1993.

The rack modules proposed to be emplaced in the pool are in twenty-one discrete modules, denoted as Modules A, B, C, D, F, K, L, M, N, P, Q, R, S and T, respectively. Table 2.1.2 gives the rack module data.

As indicated in Table 2.1.2, the proposed rerack will provide 4029 storage locations in the spent fuel pool, including 4 for storing control rod guide tubes/defective fuel containers, and 43 cells for control rods and other miscellaneous items. Figure 2.1.1 shows the module layout for the enhanced storage. The module prismatic nominal dimensions and weights are presented in Table 2.1.3.

The new modules for the La Salle County Station Unit 1 fuel pool are qualified as quasi-impacting freestanding racks, i.e., each module is freestanding and is shown to undergo minimal kinematic displacements during the postulated seismic events. Thus, rack-to-rack impacts are limited to the baseplate region or to the top of the racks. Impact between the racks in the cellular region containing active fuel is not permissible.

The rack module support legs are of remotely adjustable type. Figure 2.1.2 shows a typical new rack module for the La Salle County Station Unit 1 fuel pool.

2.2 Heavy Load Consideration for the Proposed Reracking Operation

The existing LSCS-1 racks are of the low density unpoisoned type which are anchored to the pool floor and laterally supported from the walls. At the start of the reracking operation, all nuclear fuel stored in the Unit 1 pool will be transferred over to the Unit 2 pool (which communicates with the Unit 1 pool through a transfer canal). Thus, there will be no active fission products source in the Unit 1 spent fuel pool during the rack change-out operation.

CECo has developed a "defense-in-depth" approach to execute the LSCS-1 reracking which places a strong emphasis on equipment redundancy, personnel training and proceduralized execution.

A remotely engagable lift rig, meeting NUREG-0612 stress criteria, will be used to lift the empty modules. The rig designed for handling the La Salle racks is identical in its physical attributes to the rigs utilized to rerack Millstone Point Unit One (1988), Vogtle Unit Two (1989), Indian Point Unit Two (1990), Ulchin Unit Two (1990), Hope Creek (1990), Laguna Verde Unit One (1990), and Kuosheng (1991). The rig consists of independently loaded lift rods with a "cam type" lift configuration which ensures that failure of one traction rod will not result in uncontrolled

lowering of the load being carried by the rig (which complies with the duality feature called for in Section 5.1.6(1) of NUREG 0612). The rig has the following additional attributes:

a. The stresses in the lift rods are self limiting inasmuch as an increase in the magnitude of the load reduces the eccentricity between the upward force and downward reaction (moment arm).

b. It is impossible for a traction rod to lose its engagement with the rig in locked position. Moreover, the locked configuration can be directly verified from above the pool water without the aid of an underwater camera.

c. The stress analysis of the rig is carried out using a finite element code, and the primary stress limits postulated in ANSI 14.6 (1978) are shown to be met.

d. The rig is load tested with 150% of the maximum weight to be lifted. The test weight is maintained in the air for one hour. All critical weld joints are liquid penetrant examined, after the load test, to establish the soundness of all critical joints.

The La Salle Reactor Building crane will be used for the reracking operation. The installation procedures call for all modules to be empty while being handled.

The Reactor Building crane is a single-trolley top-running electric overhead travelling bridge crane with a 125-ton capacity main hoist, a 10-ton capacity auxiliary hoist and a span of 124 feet 8 inches. The crane was tested to 125% of rated capacity (156.25 tons for the main hoist and 12.5 tons for the auxiliary hoist). A single failure proof 15 ton auxiliary hoist will be used to avoid immersion of the main crane hook in the pool water.

Pursuant to the defense-in-depth approach of NUREG-0612, the following additional measures of safety will be undertaken for the reracking operation.

(i) The crane and hoist will be given a preventive maintenance checkup and inspection prior to reracking and in accordance with station procedures.

(ii) Safe load paths have been developed for moving the old and new racks in the Reactor Building. The "old" or "new" racks will not be carried over any region of the pool containing fuel.

(iii) The rack upending or laying down will be carried out in an area which is not overlapping to any safety related component.

(iv) Crew members involved in the rigging of all heavy loads associated with the La Salle rerack project shall be trained in proper rigging techniques as well as safe travel path requirements for the loads. Lifting and upending of the new racks will be done in accordance with the manufacturer's design requirements to prevent potential damage during handling. All training of personnel shall be documented.

(v) All heavy loads will be lifted in such a manner that the center of the lift points is aligned with the center of the load being lifted.

(vi) Turnbuckles are utilized to "fine tune" the verticality of the rack being lifted.

In addition to the above design, testing and operation measures, CECo has also considered the consequences of a postulated rack drop on the integrity of the pool structure. The following analyses were performed:

a. The heaviest rack module (out of all existing and new racks) was postulated to free fall from the top of the water surface level to the pool floor.

b. The fall of a rack is assumed to occur in its normal vertical configuration which minimizes the retarding effect of water drag.

c. The falling rack is assumed to impact the pool slab undergoing an elastic/plastic impact.

d. The maximum impact load is compared with the gross seismic slab impact load during the SSE event (presented in Section 6 of this report).

Analyses show that the maximum load due to the rack drop event is well below the cumulative impact load produced during the seismic event. Thus, the pool structure integrity analyses performed in support of this submittal and documented in Section 8 of this report bound the rack drop scenario.

The "old" racks will be "hydrolased" while underwater in the pool, and approved for shipping per the requirements of 10 CFR71 and 49 CFR 171-178 before being brought to the Reactor Building Trackway. They will be housed in special shipping containers, and transported to a processing facility for volume reduction. Non-decontaminatable portions of the racks will be handled in accordance with 10CFR61.

All phases of the reracking activity will be conducted in accordance with written procedures which will be reviewed and approved by the Commonwealth Edison Company.

Our proposed compliance with the objectives of NUREG-0612 follows the guidelines contained in section 5 of that document. The guidelines of NUREG-0612 call for measures to "provide an adequate defense-in-depth for handling of heavy loads near spent fuel...". The NUREG-0612 guidelines cite four major causes of load handling accidents, namely,

i. operator errors
ii. rigging failure
iii. lack of adequate inspection
iv. inadequate procedures

The La Salle rerack program ensures maximum emphasis to mitigate the potential load drop accidents by implementing measures to eliminate shortcomings in all aspects of the operation including the four aforementioned areas. A summary of the measures specifically planned to deal with the major causes is provided below.

Operator errors: As mentioned above, CECo plans to provide comprehensive training to the installation crew for the rerack project.

Rigging failure: The lifting device designed for handling and installation of the racks in the La Salle fuel pool has redundancies in the lift legs, and lift eyes such that there are four independent load paths. Failure of any one load bearing member would not lead to uncontrolled lowering of the load. The rig complies with all provisions of ANSI 14.6 - 1978, including compliance with the primary stress criteria, load testing at 150% of maximum lift load, and dye examination of critical welds.

The La Salle rig design is similar to the rigs used in the rerack of numerous other plants, such as Hope Creek, Millstone Unit 1, Indian Point Unit Two, Ulchin II, and Laguna Verde.

Lack of adequate inspection: The designer of the racks will develop a set of inspection points which have proven to have eliminated any incidence of rack or erroneous installation in numerous prior rerack projects.

Inadequate procedures: CECo plans procedures to cover the entire gamut of operations pertaining to the rerack effort, such as mobilization, rack handling, upending, lifting, installation, verticality, alignment, dummy gage testing, site safety, and ALARA compliance.

The series of procedures planned for the La Salle rerack are the successor of the procedures implemented successfully in other projects in the past.

In addition to the above, a complete inspection of the fuel handling crane and relubrication of its moving parts in accordance with station procedures before the start of reracking is planned. Safe load paths have been developed as required by NUREG-0612.

Table 2.2.1 provides a synopsis of the requirements delineated in NUREG-0612, and our intended compliance.

In summary, the measures implemented in La Salle reracking are similar to those utilized in the most recent successful rerack projects (such as Indian Point Unit 2, concluded in October, 1990 and Hope Creek concluded in March, 1992).

Table 2.1.1

DESIGN DATA FOR NEW RACKS

I.D. (inside dimension)	6.05 inch (nom.)
Cell Nominal Pitch	6.264 inch
Boral Loading (min.)	0.022 gm per sq.cm. (B-10)
Boral plate (nom.) width:	5 inch
Boral picture frame (bounding) size	5.125" x 150-1/2"
Boral length:	150 inches
Cell height:	167.75 inch
Baseplate thickness:	3/4 inch
Bottom plenum height:	6-3/4" (nominal)
Number of supports per module:	Four (minimum)
Support Type:	Remotely adjustable
Control rod cell I.D.:	9.82 inch (square)
Control rod guide tube or failed fuel container cell I.D.:	11.5 inch (square)

Table 2.1.2

MODULE DATA FOR RERACKING

MODULE		NUMBER OF CELLS			
I.D.	Qty.	N-S Direction	E-W Direction	Total Cells Per Rack	Total No. of Cells for This Rack Type
A	1	17	15	255	255
B	4	14	15	210	840
C	1	17	13	221	221
D	4	14	13	182	728
F	2	14	18	252	504
K	1	9	18	162	162
L	1	17	18	242	242 (17x18-4x16)
M	1	17	15	231	231 (17x15-4x6)
N	1	12	15	201	201 (12x15+21)
P	1	12	15	192	192 (12x15+12)
Q	1	12	13	138	138 (9x13+21)
R	1	12	13	138	138 (9x13+21)
S	1	13	13	169	169
T	1	2	4	8	8
TOTAL:	21	———	———	———	4029*

* Including 47 cells for failed fuel containers, control rods and control rod guide tubes.

Table 2.1.3

MODULE DIMENSIONS AND WEIGHT FOR NEW RACKS

Module I.D.	DIMENSION (inches)* North-South	East-West	Shipping Weight in Pounds
A	106.76	94.2	26800
B	87.92	94.2	22500
C	106.76	81.64	23200
D	87.92	81.64	20000
F	87.92	113.04	26500
W	56.52	113.04	17800
L	106.76	113.04	25400
M	106.76	94.2	24300
N	105.6	94.2	24200
P	105.6	94.2	23000
Q	75.36	81.64	15000
R	75.36	81.64	15000
S	81.64	81.64	17800
T	23.25	43.15	2400

* Nominal rectangular planform dimensions.

Table 2.2.1

HEAVY LOAD HANDLING COMPLIANCE MATRIX (NUREG-0612)

Criterion		Compliance
1.	Are safe load paths defined for the movement of heavy loads to minimize the potential of impact, if dropped on irradiated fuel?	Yes
2.	Will procedures be developed to cover: identification of required equipment, inspection and acceptance criteria required before movement of load, steps and proper sequence for handling the load, defining the safe load paths, and special precautions?	Yes
3.	Will crane operators be trained and qualified?	Yes
4.	Will special lifting devices meet the guidelines of ANSI 14.6-1978?	Yes
5.	Will non-custom lifting devices be installed and used in accordance with ANSI B30.9-1971?	Yes
6.	Will the cranes be inspected and tested prior to use in rerack?	Yes
7.	Does the crane meet the intent of ANSI B30.2-1976 and CMMA-70?	Yes

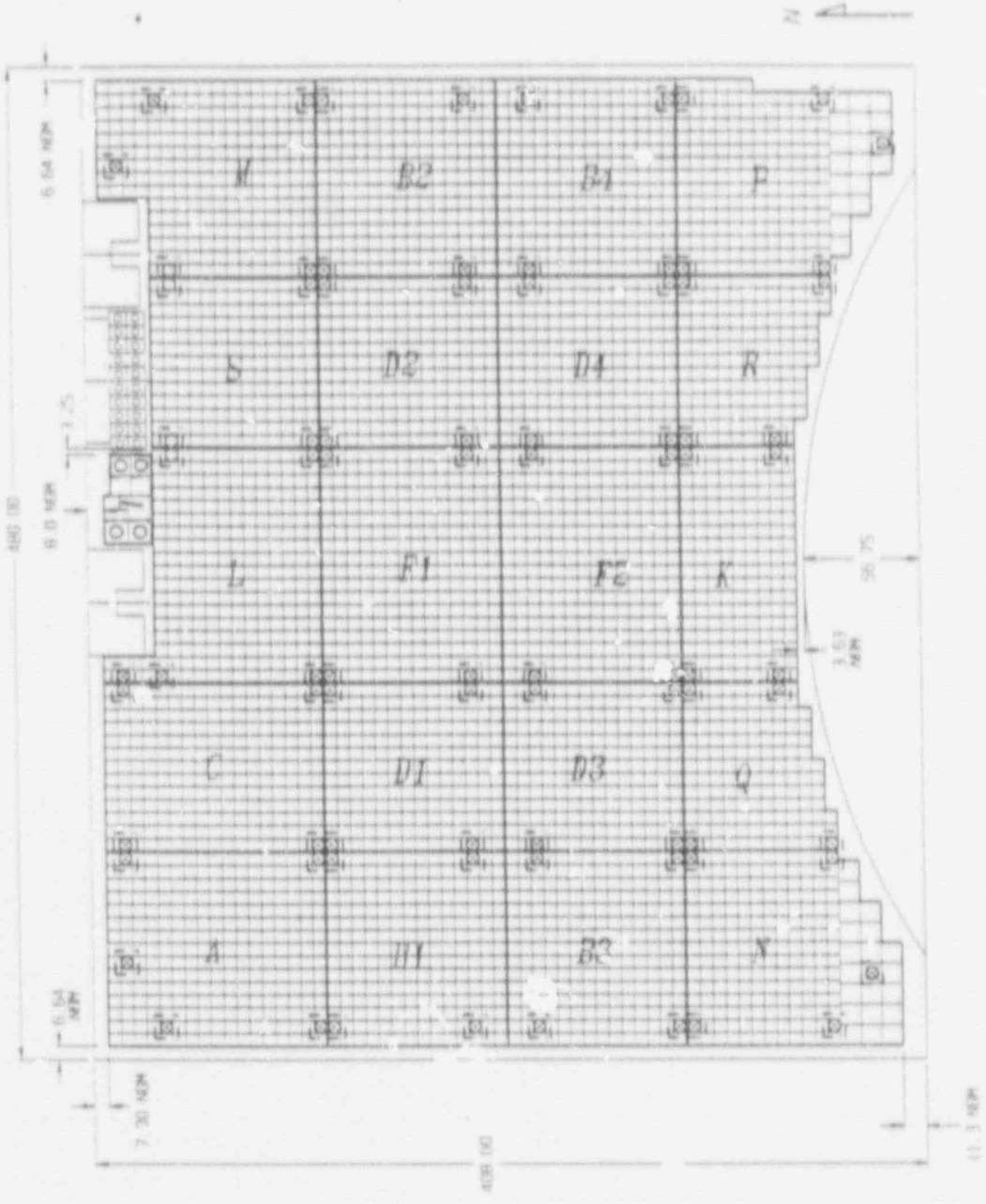

LAYOUT FOR LA SALLE UNIT 1 FUEL POOL

FIG 2.1.1

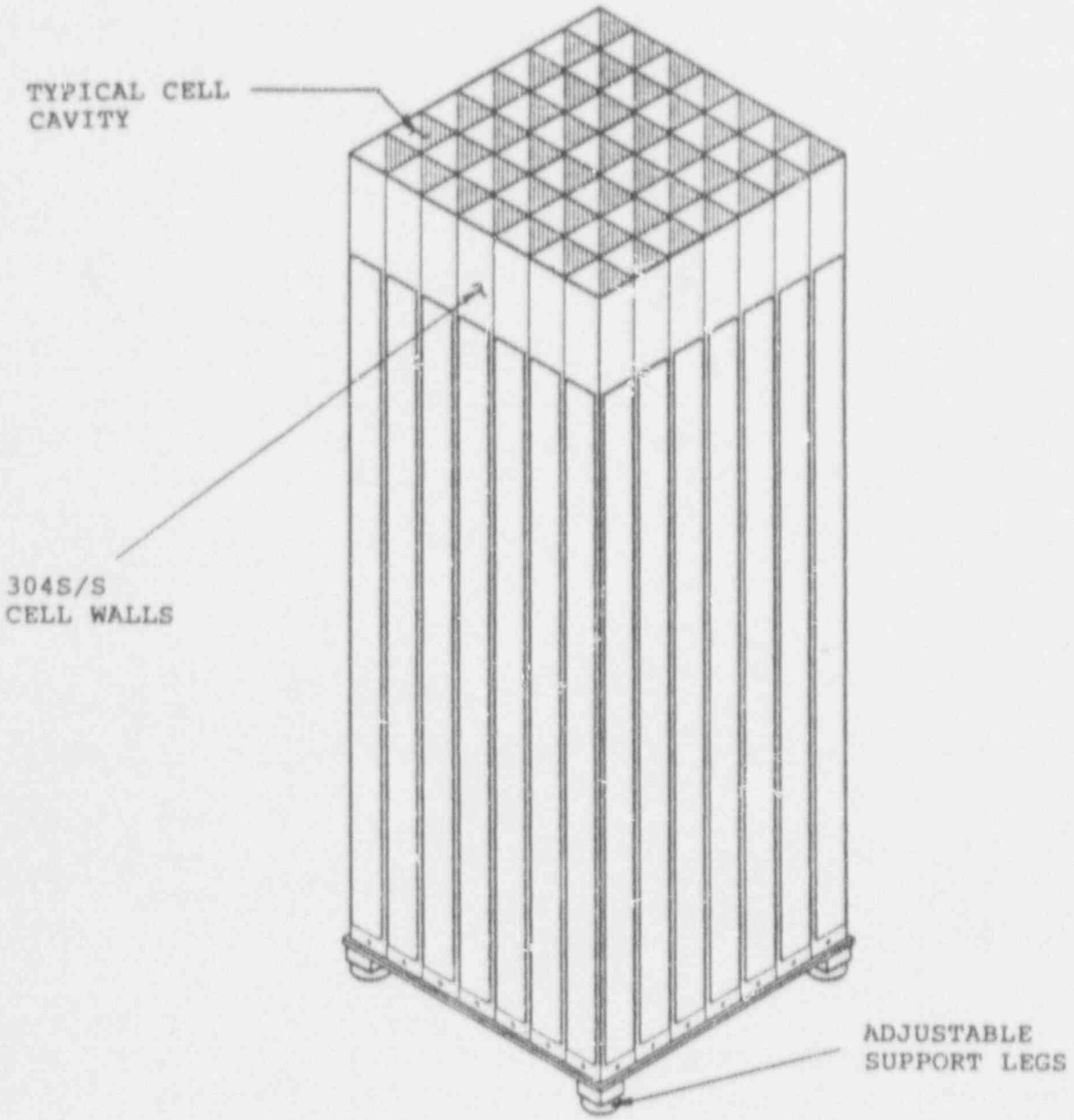

PICTORIAL VIEW OF FUEL RACK MODULE

FIGURE 2.1.2

3.0 RACK FABRICATION AND APPLICABLE CODES

The purpose of this section is to provide a comprehensive resume of the concepts and features underlying the design of the racks for the La Salle County Station Unit 1.

3.1 Design Objective

The central objective governing the design of the new high density storage racks for the La Salle County Station Unit 1 fuel pool is defined in the following six criteria:

(i) The rack module is fabricated in such a manner that there is no weld splatter on the storage cell surfaces which would come in contact with the fuel assembly. Weld splatter on the lateral surface of the storage cell, which can come in contact with fuel assemblies, can be detrimental to its structural integrity.

(ii) The storage locations are designed and constructed in such a way that redundant flow paths for the coolant are available in case the main designated flow path is blocked.

(iii) The fabrication process based on the rack design involves operational sequences which permit immediate and convenient verification by the inspection staff to ensure that the "poison" panels are correctly installed.

(iv) The storage cells are connected to each other by autogenously produced corner welds which leads to a honeycomb lattice construction. The extent of welding is selected to "detune" the racks from the ground motion such that the rack displacements are minimized.

(v) The baseplate provides a conformal contact surface for the "nose" of the fuel assembly.

(vi) The module design affords built-in flexibility in the fabrication process so as to maintain the desired cell pitch even if certain "boxes" are slightly oversize.

The foregoing objective is fully realized in the module design for the La Salle County Station Unit 1 racks as described in the following.

3.2 Anatomy of the Rack Module

The new high density rack module design employs storage cell locations with a single poison panel sandwiched between adjacent austenitic steel surfaces.

A complete description of the rack geometry is best presented by first introducing its constituent parts. The principal parts are denoted as: (1) the storage box subassembly (2) the baseplate (3) the neutron absorber material, (4) picture frame sheathing, and (5) support legs.

Each part is briefly described below with the aid of sketches.

(1) Storage cell box subassembly: The so-called "boxes" are fabricated from two precision formed channels by seam welding them together in a seam welding machine equipped with copper chill bars, and pneumatic clamps to minimize distortion due to welding heat input. Figure 3.2.1 shows the "box".

The minimum weld penetration is 80% of the box metal gage which is 13 gage (0.09" thick). The boxes are manufactured to 6.05" nominal I.D. (inside dimension).

As shown in Figure 3.2.1, each box has a minimum of two lateral holes punched near its bottom edge to provide auxiliary flow holes. In the next step, a picture frame sheathing is press formed in a precision die. The sheathing is shown attached to the box in Figure 3.2.2. The sheathing is made to an offset of 0.089" to ensure an unconstrained installation of Boral™ plates. The "picture frame sheathing" is attached to each side of the box with the poison material (Boral™) installed in the sheathing cavity. The top of the sheathing is connected using a smooth continuous fillet weld near the top of the box. The edges of the sheathing and the box are welded together to form a smooth lead-in edge. The box with integrally connected sheathing is referred to as the "composite box".

The "composite boxes" are arranged in a checkerboard array to form an assemblage of storage cell locations (Figure 3.2.3). The inter-box welding and pitch adjustment is accomplished by small longitudinal austenitic stainless connectors shown as small circles in Figure 3.2.3.

An assemblage of box assemblies thus prepared is welded edge to edge as shown in Figure 3.2.3 resulting in a honeycomb structure with axial, flexural and torsional rigidity depending on the extent of intercell welding provided. Figure 3.2.3 shows that two edges of each interior box are connected to the contiguous boxes resulting in a well defined path for "shear flow".

(2) Baseplate: The baseplate, 3/4 inch thick, provides a continuous horizontal surface for supporting the fuel assemblies. The baseplate has a concentric hole with a 45^0, 1/4" deep chamfer in each cell location to provide a conformal contact seating surface for the nose of the fuel assembly.

The baseplate is attached to the cell assemblage by fillet welds.

The baseplate projects beyond the cellular region of the rack modules by 3/16" (nominal). These baseplate projections serve as the designated impact locations for the racks in the event that the modules undergo kinematic movements during a seismic event.

(3) The neutron absorber material: Boral™ is used as the neutron absorber material. Boral™ is manufactured by AAR Brooks and Perkins of Livonia, Michigan. More on this material follows in the next section.

(4) Picture Frame Sheathing: The sheathing is a part of the "composite box assembly" described earlier. The sheathing serves as the locater and retainer of the poison material. As such, it is made in repeatable precise dimensions. This is accomplished by press-forming stainless sheet stock in a specially high tolerance die.

Figure 3.2.4 shows three storage cells in elevation with the fuel assembly shown in phantom in one cell. The poison screen extends over 150" vertical distance, straddling the active fuel length of all fuel assemblies to be used in the La Salle County Station Unit 1 reactors.

Support Legs: As stated earlier, all support legs are the adjustable type (Figure 3.2.5). The top (female) position is made of austenitic steel material. The bottom part is made of 17:4 Ph series stainless steel to avoid galling.

The support leg is equipped with a socket to enable remote leveling of the rack after its placement in the pool.

The fabrication details for the La Salle rack modules are similar to those of other recently reracked BWR pools such as J.A. FitzPatrick and Kuosheng Units 1 and 2.

3.3 Materials of Construction

The principal material of construction utilized in the fabrication of the La Salle County Station Unit 1 high density racks is austenitic stainless steel (ASME 240 and 479-304). One notable exception is the support spindle material which is made out of a special high strength (precipitation hardened) stainless steel (A564-630).

In addition to the structural and non-structural stainless material, the racks employ Boral™, a patented product of AAR Brooks and Perkins, as the neutron absorber material. A brief description of Boral™ and a list of fuel pools in which it is used follows.

Boral™ is a thermal neutron poison material composed of boron carbide and 1100 alloy aluminum. Boron carbide is a compound having a high boron content in a physically stable and chemically inert form. The 1100 alloy aluminum is a light-weight metal with high tensile strength which is protected from corrosion by a highly resistant oxide film. The two materials, boron carbide and aluminum, are chemically compatible and ideally suited for long-term use in the radiation, thermal and chemical environment of the spent fuel pool.

Boral's use in the spent fuel pools as a preferred neutron absorbing material can be attributed to the following reasons:

(i) The content and placement of boron carbide provides a very high removal cross section for thermal neutrons.

(ii) Boron carbide, in the form of fine particles, is homogenously dispersed throughout the central layer of the Boral™ panels.

(iii) The boron carbide and aluminum materials in Boral™ are not detrimentally affected by long-term exposure to gamma radiation.

(iv) The neutron absorbing central layer of Boral™ is clad with permanently bonded surfaces of aluminum.

(v) Boral™ is stable, strong, durable, and corrosion resistant.

Boral™ is manufactured under the control and surveillance of a Quality Assurance/Quality Control Program that conforms to the requirements of 10 CFR 50 Appendix B, "Quality Assurance Criteria for Nuclear Power Plants".

As indicated in Table 3.3.1, Boral™ has been licensed by the USNRC for use in numerous BWR and PWR spent fuel storage racks.

Boral™ Material Characteristics

Aluminum: 1100 alloy aluminum is the metallic ingredient of Boral™. The excellent corrosion resistance of the 1100 alloy aluminum is provided by the protective oxide film that develops on its surface from exposure to the atmosphere or water. This film prevents the loss of metal from general corrosion or pitting corrosion and the film remains stable between a pH range of 4.5 to 8.5.

Boron Carbide: The boron carbide contained in Boral™ is a fine granulated powder that conforms to ASTM C-750-80 nuclear grade Type III. The particles range in size between 60 and 200 mesh and the material conforms to the chemical composition and properties listed in Table 3.3.2.

A large body of test data and plant operating experience data is available in the publications in the public domain by Boral's manufacturer.

3.4 Codes, Standards, and Practices for the Spent Fuel Pool Modification

The fabrication of the rack modules is performed under a strict quality assurance program which meets 10 CFR 50 Appendix B requirements.

The following codes, standards and practices were used for all applicable aspects of the design, construction, and assembly of the spent fuel storage racks. Additional specific references related to detailed analyses are given in each section.

a. Design Codes

(1) AISC Manual of Steel Construction, 8th Edition, 1980 (provides detailed structural criteria for linear type supports).

(2) ANSI N210-1976, "Design Objectives for Light Water Reactor Spent Fuel Storage Facilities at Nuclear Power Stations" (contains guidelines for fuel rack design).

(3) American Society of Mechanical Engineers (ASME), Boiler and Pressure Vessel Code, Section III, 1986 Edition.

(4) ANSI/AISC-N690-1984 - Nuclear Facilities - Steel Safety Related Structure for Design, Fabrication and Erection

(5) ASNT-TC-1A - June, 1980 American Society for Nondestructive Testing (Recommended Practice for Personnel Qualifications).

b. Material Codes - Standards of ASME or ASTM, AS NOTED:

(1) E165 - Standard Methods for Liquid Penetrant Inspection

(2) SA240 - Standard Specification for Heat-Resisting Chromium and Chromium-Nickel Stainless Steel Plate, Sheet and Strip for Fusion-Welded Unfired Pressure Vessels

(3) A262 - Detecting Susceptibility to Intergranular Attack in Austenitic Stainless Steel

(4) SA276 - Standard Specification for Stainless and Heat-Resisting Steel Bars and Shapes

(5) SA479 - Steel Bars for Boilers & Pressure Vessels

(6) C750 - Standard Specification for Nuclear-Grade Boron Carbide Powder

(7) C992 - Standard Specification for Boron-Based Neutron Absorbing Material Systems for Use in Nuclear Spent Fuel Storage Racks

(8) SA312 - Specification for Seamless and Welded Austenitic Stainless Steel Pipe

(9) SA564 - Specification for Hot Rolled and Cold-Finished Age-Hardening Stainless and Heat Resisting Steel Bars and Shapes

(10) American Society of Mechanical Engineers (ASME), Boiler and Pressure Vessel Code, Section II-Parts A and C, 1986 Edition.

(11) ASTM A262 Practices A and E - Standard Recommended Practices for Detecting Susceptibility to Intergrannular Attack in Stainless Steels

(12) ASTM A380 - Recommended Practice for Descaling, Cleaning and Marking Stainless Steel Parts and Equipment

c. Welding Codes

(1) ASME Boiler and Pressure Vessel Code, Section IX - Welding and Brazing Qualifications, 1986 Edition.

(2) AWS D1.1 - Welding Standards

d. Quality Assurance, Cleanliness, Packaging, Shipping, Receiving, Storage, and Handling Requirements

(1) NQA-2-Part 2.2 1983 - Packaging, Shipping, Receiving, Storage, and Handling of Items for Nuclear Power Plants (During Construction Phase)

(2) NQA-1-1983 - Basic Requirements and Supplements

(3) ASME Boiler and Pressure Vessel, Section V, Nondestructive Examination, 1986 Edition.

(4) ANSI - N45.2.11, 1974 Quality Assurance Requirements for the Design of Nuclear Power Plants.

(5) ANSI - N45.2.6 - Qualifications of Inspection, Examination, and Testing Personnel for Nuclear Power Plants (Regulatory Guide 1.58).

(6) ANSI N45.2.13 - Quality Assurance Requirements for Control of Procurement of Equipment Materials and Services for Nuclear Power Plants (Regulatory Guide 1.123).

(7) ANSI N45.2.23 - Qualification of Quality Assurance Program Audit Personnel for Nuclear Power Plants (Regulatory Guide 1.146).

(8) N45.2.9 - Requirements for Collection, Storage and Maintenance of Quality Assurance Records for Nuclear Power Plants - 1974

(9) N45.2.10 - Quality Assurance Terms and Definitions - 1973

e. Governing NRC Design Documents

(1) "OT Position for Review and Acceptance of Spent Fuel Storage and Handling Applications," dated April 14, 1978, and the modifications to this document of January 18, 1979.

(2) NRC Standard Review Plan Rev. 3, 1981, NUREG 0800 - 9.1.2, Spent Fuel Storage

(3) NRC Standard Review Plan, Rev. 2, July 1981 NUREG 0800 - 9.1.1, New Fuel Storage

(4) NRC Standard Review Plan, Rev. 1, July 1981, NUREG 0800 - 3.8.4, Other Seismic Category I Structures

(5) NRC Standard Review Plan, Rev. 1, July 1981, NUREG 0800 - 3.8.5, Foundations

f. Other ANSI Standards (not listed in the preceding)

(1) N210 - Design Objective for Light Water Reactor Spent Fuel Storage Facilities at Nuclear Power Plants

(2) ANSI/ASN 8.1 - 1983, Nuclear Criticality Safety in Operations with Fissionable Materials Outside Reactors

(3) ANSI/ASN 8.7 - 1974, Guide for Nuclear Criticality Safety in the Storage of Fissile Materials

(4) ANSI/ANS 8.11 - 1975, Validation of Calculation Methods for Nuclear Criticality Safety

g. Code-of-Federal Regulations

(1) 10 CFR 21 - Reporting of Defects and Non-compliance

(2) 10 CFR 50 - Appendix A - General Design Criteria for Nuclear Power Plants

(3) 10 CFR 50 - Appendix B - Quality Assurance Criteria for Nuclear Power Plants and Fuel Reprocessing Plants

(4) 10CFR Part 20 - Radiation Protection Standards

(5) 29CFR Section 1910.401 - OSHA Standards for Commercial Diving Operations

h. Regulatory Guides

(1) RG 1.13 - Spent Fuel Storage Facility Design Basis

(2) RG 1.25 - Assumptions Used for Evaluating the Potential Radiological Consequences of a Fuel Handling Accident in the Fuel Handling and Storage Facility of Boiling and Pressurized Water Reactors.

(3) RG 1.28 - (endorses ANSI N45.2) - Quality Assurance Program Requirements, June, 1972.

(4) RG 1.29 - Seismic Design Classification

(5) RG 1.38 - (endorses ANSI N45.2.2) Quality Assurance Requirements for Packaging, Shipping, Receiving, Storage and Handling of Items for Water-Cooled Nuclear Power Plants, March, 1973.

(6) RG 1.44 - Control of the Use of Sensitized Stainless Steel

(7) RG 1.58 - (endorses ANSI N45.2.6) Qualification of Nuclear Power Plant Inspection, Examination, and Testing Personnel. Rev. 1, September, 1980

(8) RG 1.64 - (endorses ANSI N45.2.11) Quality Assurance Requirements for the Design of Nuclear Power Plants, October, 1973.

(9) RG 1.74 - (endorses ANSI N45.2.10) Quality Assurance Terms and Definitions, February, 1974.

(10) RG 1.88 - (endorses ANSI N45.2.9) Collection, Storage and Maintenance of Nuclear Power Plant Quality Assurance Records. Rev. 2, October, 1976.

(11) RG 1.92 - Combining Modal Responses and Spatial Components in Seismic Response Analysis

(12) RG 1.123 - (endorses ANSI N45.2.13) Quality Assurance Requirements for Control of Procurement of Items and Services for Nuclear Power Plants.

(13) NRC Regulatory Guide 3.41 Rev., May 1977 - Validation of Calculation Methods for Nuclear Criticality Safety

(14) NRC Regulatory Guide 1.26 Rev. 3, Feb. 1976, Quality Group Classifications and Standards for Water, Steam and Radioactive Containing Components of Nuclear Power Plants

i. Branch Technical Position

(1) CPB 9.1-1 - Criticality in Fuel Storage Facilities

(2) ASB 9-2 - Residual Decay Energy for Light-Water Reactors for Long-Term Cooling

j. Standard Review Plan

(1) SRP 3.7.1 - Seismic Design Parameters

(2) SRP 3.7.2 - Seismic System Analysis

(3) SRP 3.7.2 - Seismic Subsystem Analysis

(4) SRP 3.8.4 - Other Seismic Category I Structures (including Appendix D)

(5) SRP 9.1.2 - Spent Fuel Storage

(6) SRP 9.1.3 - Spent Fuel Pool Cooling and Cleanup System

k. Other

La Salle County Station updated Final Safety Analysis Report (UFSAR)

Table 3.3.1

BORAL™ EXPERIENCE LIST (DOMESTIC AND FOREIGN)

Pressurized Water Applications

Plant	Utility	Vented Construction	Mfg. Year
Bellefonte 1, 2	Tennessee Valley Authority	No	1981
D.C. Cook 1,2	Indiana & Michigan Electric	No	1979
Indian Point 3	NY Power Authority	Yes	1987
Maine Yankee	Maine Yankee Atomic Power	Yes	1977
Salem 1, 2	Public Service Elec & Gas	No	1980
Seabrook	New Hampshire Yankee	No	---
Sequoyah 1,2	Tennessee Valley Authority	No	1979
Yankee Rowe 1964/1983	Yankee Atomic Power	Yes	
Zion 1,2	Commonwealth Edison Co.	Yes	1980
Byron 1,2	Commonwealth Edison Co.	Yes	1988
Braidwood 1,2	Commonwealth Edison Co.	Yes	1988
Yankee Rowe	Yankee Atomic Electric	Yes	1988
Three Mile Island Unit One	GPU Nuclear	Yes	1991
Zion	Commonwealth Edison Co.	Yes	1991

Boiling Water Applications

Browns Ferry 1,2,3	Tennessee Valley Authority	Yes	1980
Brunswick 1,2	Carolina Power & Light	Yes	1981
Clinton	Illinois Power	Yes	1981
Cooper	Nebraska Public Power	Yes	1979
Dresden 2,3	Commonwealth Edison Co.	Yes	1981
Duane Arnold	Iowa Elec. Light & Power	No	1979
J.A. FitzPatrick	NY Power Authority	No	1979
E.I. Hatch 1,2	Georgia Power	Yes	1981
Hope Creek	Public Service Elec & Gas	Yes	1985
Humboldt Bay	Pacific Gas & Electric	Yes	1986
LaCrosse	Dairyland Power	Yes	1976
Limerick 1,2	Philadelphia Electric	No	1980
Monticello	Northern States Power	Yes	1978
Peachbottom 2,3	Philadelphia Electric	No	1980
Perry, 1,2	Cleveland Elec. Illuminating	No	1979
Pilgrim	Boston Edison	No	1978
Shoreham	Long Island Lighting	Yes	---
Susquehanna 1,2	Pennsylvania Power & Light	No	1979
Vermont Yankee 1978/1986	Vermont Yankee Atomic Power	Yes	
Hope Creek	Public Service Elec & Gas	Yes	1989
Shearon Harris	Carolina Power & Light Co.	Yes	1991

Table 3.3.1 (continued)

Foreign Installations Using Boral™

France	
12 PWR Plants	Electricite de France
South Africa	
Koeberg 1,2	ESCOM
Switzerland	
Beznau 1,2	Nordostschweizerische Kraftwerke AG
Gosgen	Kernkraftwerk Gosgen-Daniken AG
Taiwan	
Chin-Shan 1,2	Taiwan Power Company
Kuosheng 1,2	Taiwan Power Company
Mexico	
Laguna Verde 1 & 2	Comision Federal de Electricidad

Table 3.3.2

BORON CARBIDE CHEMICAL COMPOSITION, WEIGHT %*

Total boron	70.0 min.
B^{10} isotopic content in natural boron	18.0
Boric oxide	3.0 max.
Iron	2.0 max.
Total boron plus total carbon	94.0 min.

BORON CARBIDE PHYSICAL PROPERTIES

Chemical formula	B_4C
Boron content (weight)	78.28%
Carbon content (weight)	21.72%
Crystal Structure	rombohedral
Density	2.51 gm./cc-0.0907 lb/cu. in.
Melting Point	2450^0C - 4442^0F
Boiling Point	3500^0C-6332^0F

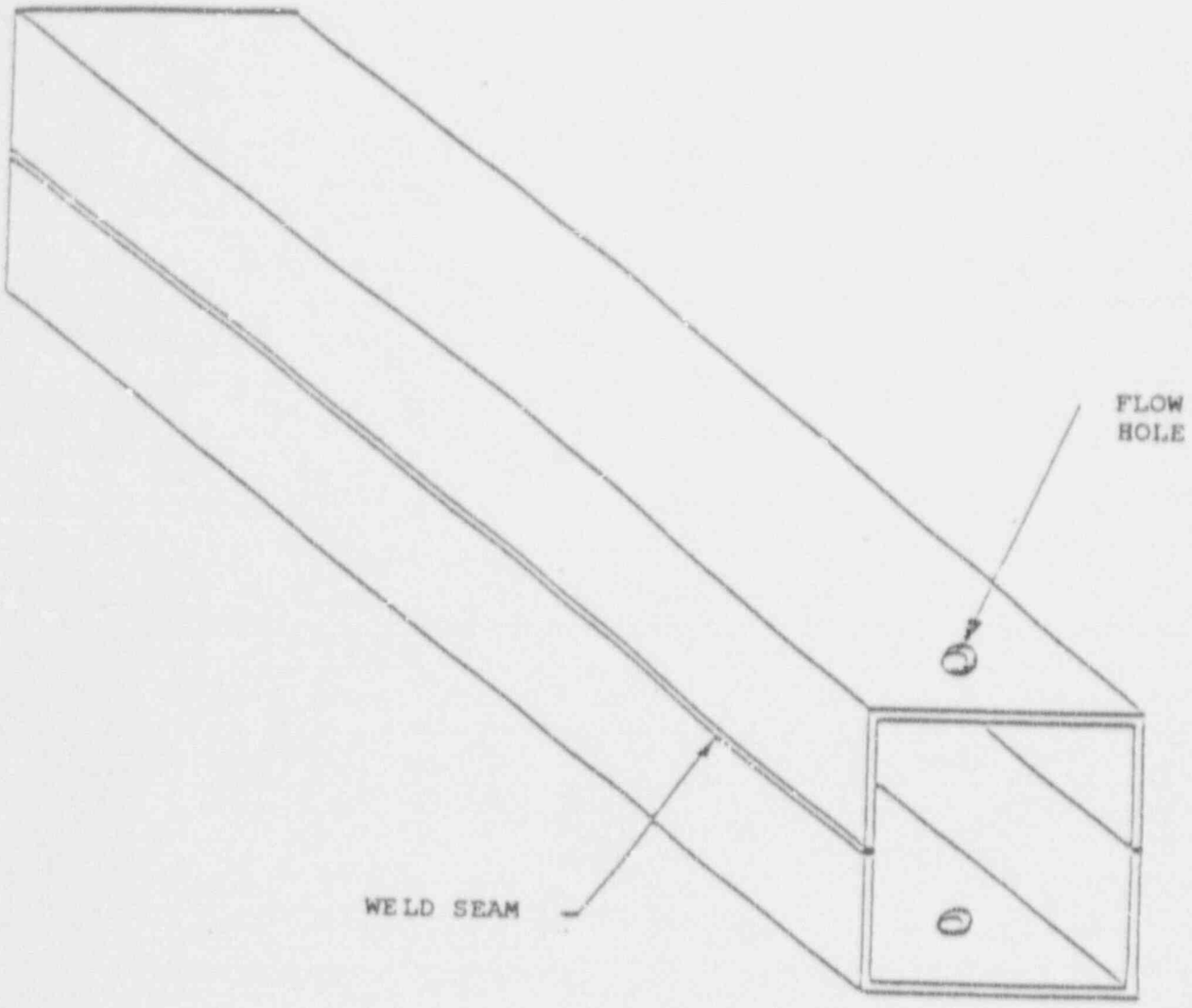

FIGURE 3.2.1 SEAM WELDING PRECISION FORMED CHANNELS

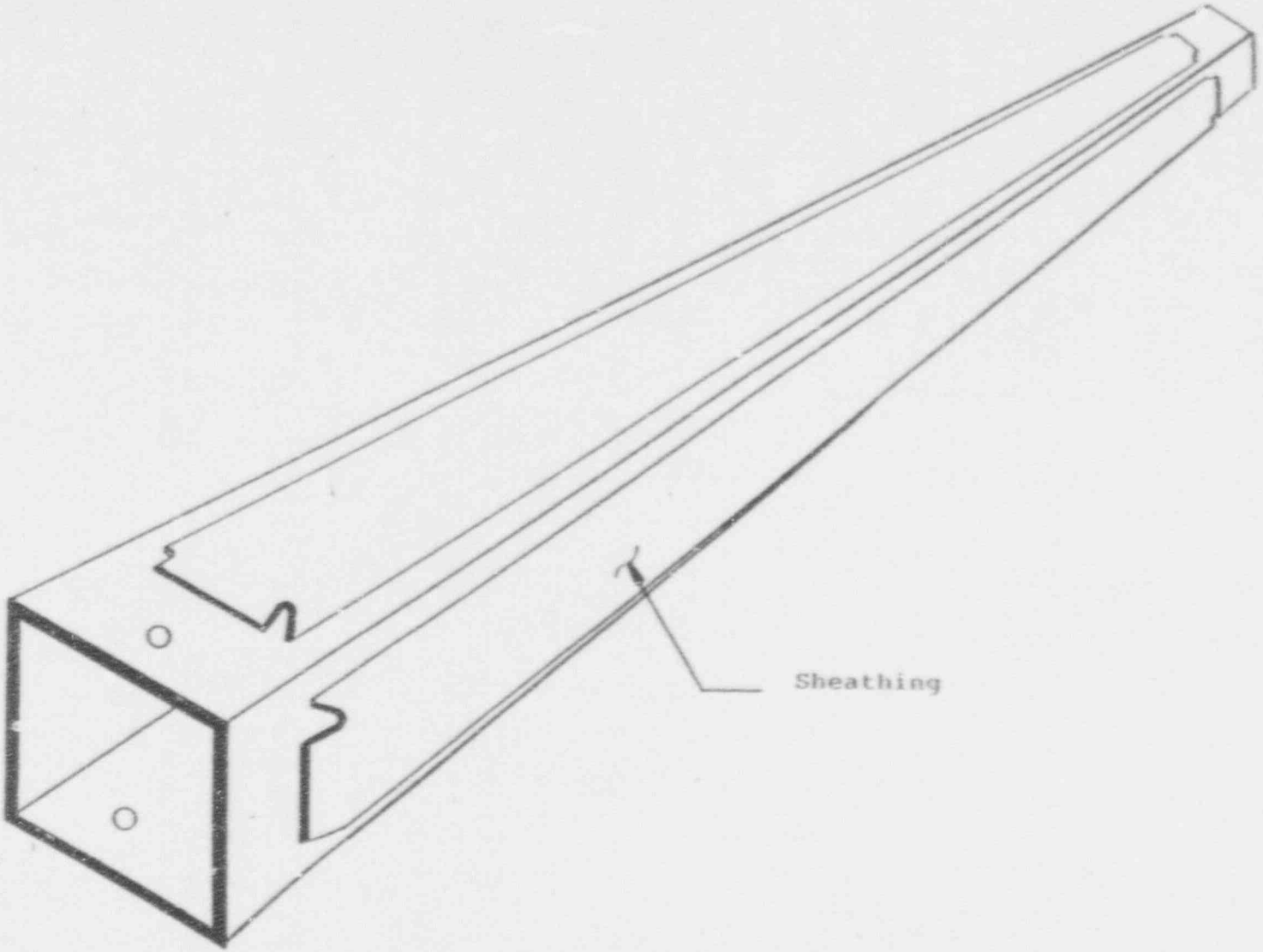

FIGURE 3.2.2 SHEATHING SHOWN INSTALLED ON THE BOX

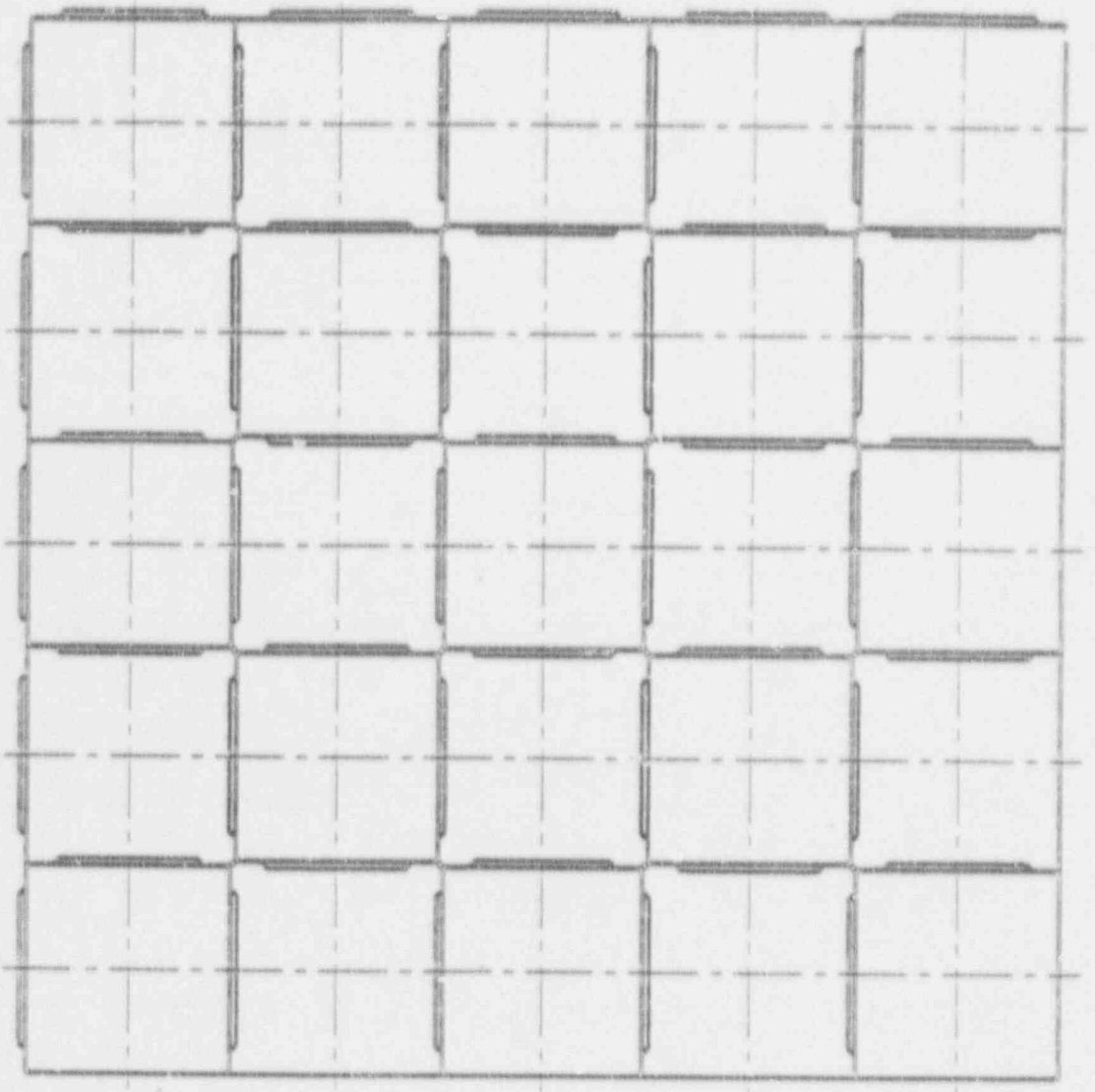

FIGURE 3.2.3 A CROSS SECTIONAL VIEW OF AN ARRAY OF STORAGE BOXES

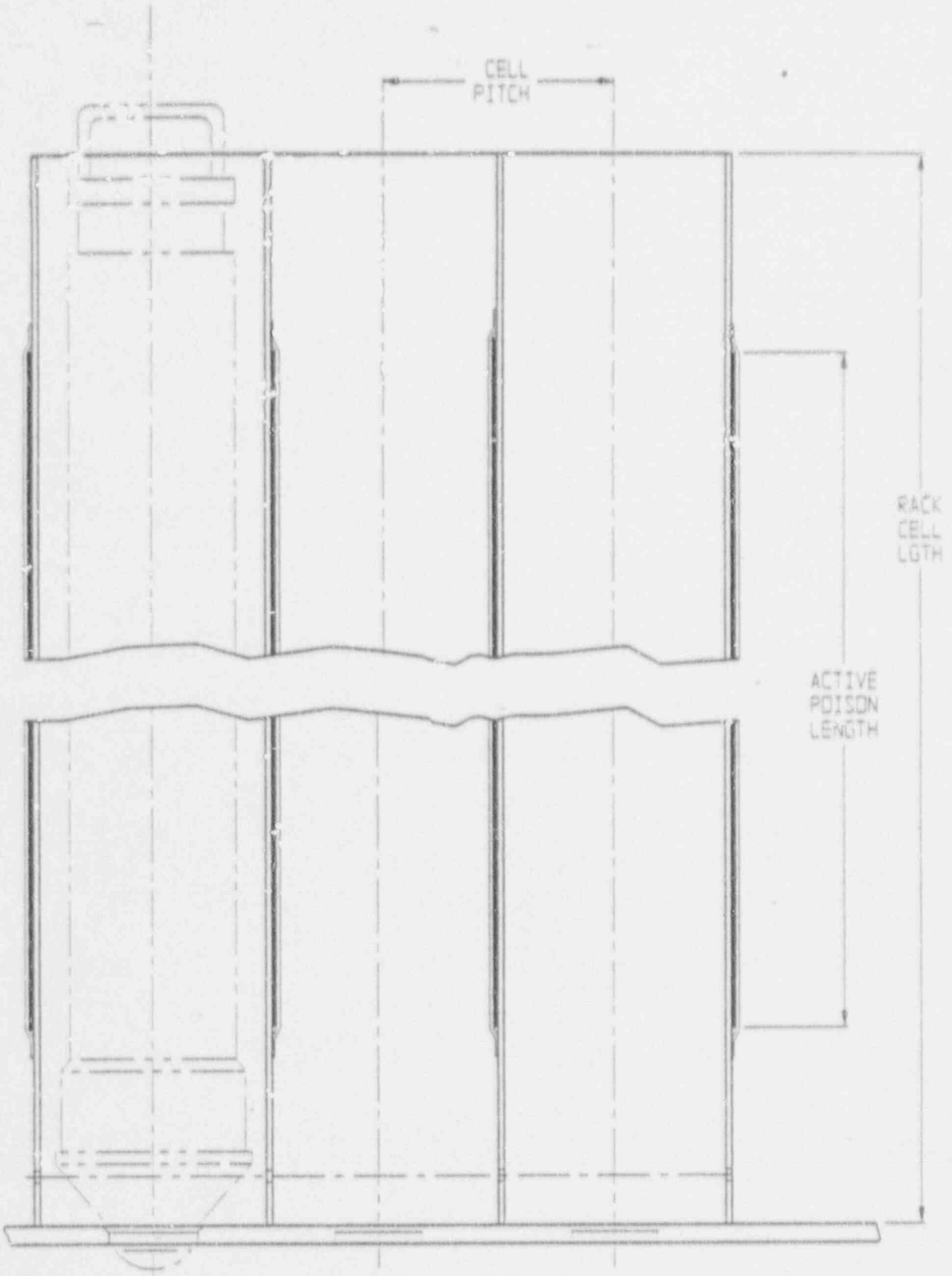

FIG. 3.4 THREE CELLS
IN ELEVATION VIEW

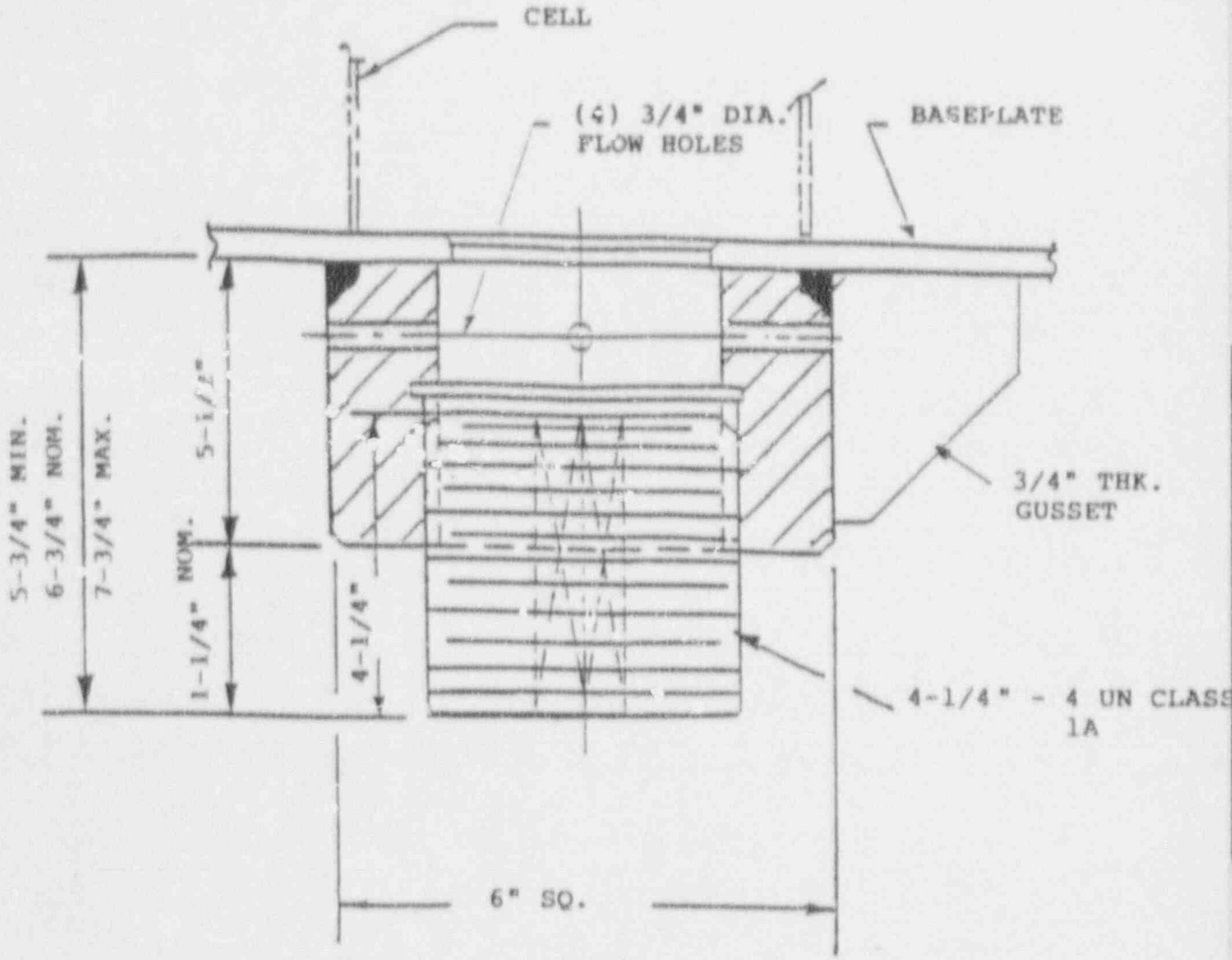

FIGURE 3.2.5 ADJUSTABLE SUPPORT

4.0 CRITICALITY SAFETY ANALYSES

4.1 DESIGN BASES

The high density spent fuel storage racks for the La Salle County Station are designed to assure that the neutron multipli-cation factor (k_{eff}) is less than 0.95 with the racks fully loaded with fuel of the highest anticipated reactivity and the pool flooded with pure water at a temperature corresponding to the highest reactivity. The design basis fuel for the storage rack is an 8x8 BWR fuel rod assembly with a uniform enrichment of 3.75 wt% U-235 in the enriched zone. The maximum calculated reactivity of the storage rack includes a margin for uncertainty in reactivity calculations and in mechanical tolerances, statistically combined, such that the true k_{eff} will be less than 0.95 with a 95% probability at a 95% confidence level. Reactivity effects of abnormal and accident conditions have also been evaluated to assure that under credible abnormal conditions, the reactivity will be less than the limiting design basis value.

Applicable codes, standards, and regulations, or pertinent sections thereof, include the following:

- General Design Criterion 62, Prevention of Criticality in Fuel Storage and Handling.
- USNRC Standard Review Plan, NUREG-0800, Section 9.1.2, Spent Fuel Storage, Rev. 3, July 1981
- USNRC letter of April 14, 1978, to all Power Reactor Licensees - OT Position for Review and Acceptance of Spent Fuel Storage and Handling Applications, including the modification letter dated January 18, 1979.
- USNRC Regulatory Guide 1.13, Spent Fuel Storage Facility Design Basis, Rev. 2 (proposed), December, 1981.

- USNRC Regulatory Guide 3.41, Validation of Calculational Methods for Nuclear Criticality Safety (and related ANSI N16.9-1975).

- ANS-8.17-1984, Criticality Safety Criteria for the Handling, Storage and Transportation of LWR Fuel Outside Reactors.

To assure the true reactivity will always be less than the calculated reactivity, the following conservative assumptions were made:

- The racks are assumed to contain the most reactive fuel authorized to be stored in the Unit 1 pool.

- Moderator is pure, unborated water at a temperature corresponding to the highest reactivity (4°C).

- Criticality safety analyses are based upon the k_{eff} of an infinite radial array of storage cells, ie, no credit is taken for radial neutron leakage (except as necessary in the assessment of abnormal/accident conditions).

- Neutron absorption in minor structural members is neglected, i.e., spacer grids are replaced by water.

4.2 SUMMARY OF CRITICALITY SAFETY ANALYSES

4.2.1 Normal Operating Conditions

The storage racks are designed to accommodate an 8 x 8 GE type fuel assembly of 3.5% average enrichment, including the two 6-inch natural UO_2 blankets, without gadolinium burnable poison. In the 138 inch enriched zone, the uniform average enrichment is 3.743% U-235, conservatively taken as 3.75 % U-235 for design purposes. The basic calculations supporting the criticality safety of the La Salle fuel storage racks are summarized in Table 4.2.1, indicating a maximum k_∞ in the storage rack of 0.943* (95% probability at the 95% confidence level) including all known uncertainties. Thus, the fuel storage rack satisfies the design basis requirement of a maximum k_{eff} less than or equal to 0.95 without credit for the gadolinium burnable poison normally in the fuel.

The design basis criterion of a uniform enrichment of 3.75% without gadolinium burnable poison is very conservative. With the gadolinium burnable poison loading usually contained in BWR fuel, the actual reactivity will be considerably lower, even at the peak in reactivity over burnup, where the gadolinium is essentially consumed. For this reason, the racks could safely accommodate fuel of higher enrichments, with credit for the gadolinium burnable poison that is normally contained in BWR fuel.

Calculations were made for fuel of 4.25% average enrichment (4.6% enrichment in the 138-inch enriched fuel zone) with rods containing 2% gadolinium (as Gd_2O_3), although normally fuel assemblies of this enrichment would contain substantially more gadolinium. To illustrate trends, the calculations included fuel of 4.4% enrichment, with both 6 and 8 gadolinium-containing rods in each

---

* k_∞ is calculated for an infinite array, neglecting radial neutron leakage.

assembly. The maximum k_∞ for the uniform 4.6% enriched case with 2% Gd_2O_3 was 0.9241, including uncertainties, corresponding to a k_∞ of 1.355 in the standard* core geometry. It is evident that a considerable margin exists below the USNRC guideline on k_{eff} (0.95) and that the racks could safely accommodate fuel of appreciably higher enrichments. The maximum k_∞ of 0.9241 includes a conservative allowance of 0.0100 δk for possible differences in calculational results between a fuel vendor and those reported here. Furthermore, the use of a uniform enrichment is conservative with respect to the distributed enrichments conventionally used in BWR fuel.

4.2.2 Abnormal and Accident Conditions

None of the credible abnormal or accident conditions that have been identified will result in exceeding the limiting reactivity (k_{eff} of 0.95). The effects on reactivity of credible abnormal and accident conditions are summarized in Table 4.2.2. No other credible accident events or abnormal configurations have been identified that might have any adverse effect on the storage rack criticality safety. The double contingency principle specifically invoked in the definitive USNRC letter of April 14, 1978 precludes the necessity of considering the occurrence of more than a single unlikely and independent accident condition concurrently.

---

* The standard core geometry is defined as an infinite array of fuel assemblies on a 6-inch lattice spacing at 20°C, without any control absorber or voids.

4.3 REFERENCE FUEL STORAGE CELL

4.3.1 Fuel Assembly Design Specification

The design basis fuel assembly is a standard 8x8 array of BWR fuel rods containing UO_2 clad in Zircaloy (62 fuel rods with 2 water rods). For the nominal design case, fuel of uniform 3.75 wt% U-235 enrichment was assumed, which, at 95% theoretical UO_2 density, corresponds to 18.18 grams U-235 per axial centimeter of fuel assembly. Design parameters are summarized in Table 4.3.1.

4.3.2 Storage Rack Cell Specifications

The design basis storage rack cell consists of an egg-crate structure, illustrated in Figure 4.3.1, with fixed neutron absorber material (Boral) of 0.0238 g/cm^2 boron-10 areal density (0.022 g B-10/cm^2 minimum) positioned between the fuel assembly storage cells. The storage cell design for analysis is conservatively based upon a nominal center-to-center lattice spacing of 6.264 inches and a larger spacing would result in a lower reactivity. Manufacturing tolerances, used in evaluating uncertainties in reactivity, are indicated in Figure 4.3.1. The 0.090-in. stainless-steel box which defines the fuel assembly storage cell has a nominal inside dimension of 6.05 in. This allows adequate clearance for inserting or removing the fuel assemblies, with or without the Zircaloy flow liner. Boral panels are not needed or used on the exterior walls of modules facing non-fueled regions, i.e., the pool walls.

4.4 ANALYTICAL METHODOLOGY

Criticality analyses of the high density spent fuel storage racks were performed using both the CASMO-3 code[1] (a two-dimensional multi-group transport theory code) and the KENO-5a code[2] (a Monte Carlo code), using the 27-group SCALE* cross-section library[3] with the NITAWL subroutine for U-238 resonance shielding effects (Nordheim integral treatment). CASMO-3 was also used as a means of evaluating small reactivity increments associated with manufacturing tolerances.

Benchmark calculations are presented in Appendix A and indicate a bias of 0.0000 ± 0.0024 for CASMO-3 and 0.0101 ± 0.0018 (95%/95%) for NITAWL-KENO-5a. These methods of analysis and the benchmarking calculations have previously been used in the evaluation of spent fuel storage racks that have been reviewed and accepted by the USNRC.

In the geometric model used in the calculations, each fuel rod and its cladding was described explicitly and reflecting boundary conditions (zero neutron current) were used in the axial direction and at the centerline of the Boral and steel plates between storage cells. These boundary conditions have the effect of creating an infinite array of storage cells in the X and Y directions. In KENO-5a, the axial height of 150 inches (Z direction) was used with the top and bottom 6 inch natural UO_2 blankets included.

---

* SCALE is an acronym for Standardized Computer Analysis for Licensing Evaluation, a standard cross-section set developed by ORNL for the USNRC.

4.5 CRITICALITY ANALYSES AND TOLERANCE VARIATIONS

4.5.1 Nominal Design Case

For the design basis reactivity calculations with a uniform enrichment of 3.75%, the nominal storage cell infinite multiplication factor, k_∞, is 0.9348 (CASMO-3). With a δk of 0.0070 for all known uncertainties statistically combined, the maximum k_∞ in the fuel rack is 0.943 which is substantially less than the design basis limit of 0.95 for k_{eff}. Independent calculations with NITAWL-KENO-5a (500,000 histories in 1000 generations) gave a k_∞ (including all uncertainties) of 0.9346 ± 0.0070 (95%/95%, maximum k_∞ of 0.942) which is in good agreement with the CASMO calculation (see Table 4.2.1). The K-factor for 95% probability at a 95% confidence level was determined from NBS Handbook 91[4].

4.5.2 Uncertainties Due to Rack Manufacturing Tolerances

The reactivity effects due to manufacturing tolerances are summarized in Table 4.5.1 and discussed in the following sections:

4.5.2.1 Boron Loading Variation

The Boral absorber panels used in the storage cells are nominally 0.082-inch thick, with a B-10 areal density of 0.0238 g/cm^2. The manufacturing tolerance limit is ±0.0018 g/cm^2 in B-10 loading, which assures that the minimum boron-10 areal density will not be less than 0.022 $gram/cm^2$. Differential CASMO-3 calculations indicate that this tolerance limit results in an incremental reactivity uncertainty of ±0.0051 δk.

4.5.2.2 Boral Width Tolerance Variation

The reference storage cell design uses a Boral panel width of 5.00 ± 1/16 inches. For a reduction in width of the maximum tolerance, the calculated positive reactivity increment is +0.0019 δk.

4.5.2 3 Storage C .l Lattice Pitch Variation

The design storage cell lattice spacing between fuel assemblies is 6.264 inch. For the manufacturing tolerance of ±0.04 inch, the corresponding maximum uncertainty in reactivity is ± 0.0022 δk as determined by differential CASMO-3 calculations. Increasing the lattice pitch reduces reactivity, e.g., at a lattice spacing of 6.304 inches, the reactivity would be 0.0022 δk lower.

4.5.2.4 Stainless Steel Thickness Tolerances

The nominal thicknesses of the stainless steel box and the steel backing plate are 0.090 inch and 0.035 inches respectively. The maximum positive reactivity effect for a mean stainless steel thickness tolerance (± 0.005 inches) was calculated (by CASMO-3) to be ± 0.0010 δk.

4.5.2.5 Fuel Enrichment and Density Variation

The nominal design enrichment is 3.75 wt% U-235. CASMO-3 calculations of the sensitivity to small enrichment variations yielded an uncertainty of 0.0029 δk for the estimated ±0.05 tolerance on percent U-235 enrichment.

The design basis calculation assumed a UO_2 stack density of 95% theoretical density, corresponding to a density of 10.412 g/cm^3. Calculations were also made to determine the sensitivity to a conservative tolerance in UO_2 fuel density of ± 0.20 in density

or a maximum density of 10.612 g/cm^3. These calculations indicate that the storage rack k_∞ is increased by 0.0024 δk. A lower fuel density would result in a correspondingly lower value of reactivity. Thus, the uncertainty associated with the tolerance on fuel density is ±0.0024 δk.

4.5.3 Zirconium Flow Channel

The design basis calculations assumed the presence of a flow channel. Elimination of the zirconium flow channel results in a small (~ 0.0065 δk) decrease in reactivity.

4.5.4 Water Gap Spacing between Modules

For normal storage conditions with a water gap between modules, the array k_{eff} of a module would be less than the reference design k_∞ and Boral panels along the walls of the modules facing the water gap would not be necessary. However, as an additional and precautionary measure, the rack design provides for Boral panels on storage cells on one of the two module walls along the water gap. With this conservative configuration, the design assures that, even under abnormal or accident conditions, the storage rack reactivity will remain less than the 0.95 k_{eff} regulatory limit.

4.6 HIGHER ENRICHMENT FUEL

Higher enrichments were also considered, including fuel of 4.4% enrichment with both 6 and 8 fuel rods containing 2 wt% gadolinium oxide (Gd_2O_3) and fuel of 4.6% enrichment with 8 2% Gd_2O_3 containing rods in the assemblies. Burnup calculations were performed with CASMO-3 which accounts for the highly self-shielded gadolinium cross-sections. The restart option in CASMO-3 was then used to analytically place the spent fuel assemblies into the storage rack or into the standard core geometry.

Figure 4.6.1 shows the reactivity variation with burnup for both the 4.4% and 4.6% enriched fuel. In both cases, the peak reactivity over burnup is substantially less than the rack design basis enrichment without gadolinium. The peak reactivity of 0.8973 k_∞ occurs at a burnup of 9 MWD/KgU. Adding the calculational and manufacturing uncertainties, a correction for bulging of the zirconium flow channel, an estimate of the potential uncertainty in depletion calculations and including a conservative allowance for the possible difference between the calculations reported here and the fuel vendor calculations, the results are listed below:

	4.4% E	4.6% E
Calculated Reactivity at the peak over burnup	0.8893	0.8973
δk for Uncertainties (95%/95%)	0.0073	0.0073
δk for bulging of the Zr channel	0 0050	0.0050
δk for depletion uncertainty	0.0045	0.0045
Allowance for difference with vendor calculations	0.0100	0.0100
Maximum k_∞	0.9161	0.9241

Whether the assemblies contain 6 or 8 Gd-rods is of little significance since the evaluation is performed at the peak reactivity over burnup where the gadolinium is almost completely consumed.

From the data presented above, it is evident that there is a considerable margin below the USNRC limiting criterion on k_{eff}. The racks are therefore capable of accepting fuel with enrichments greater than 4.6%, particularly since fuel of the higher enrichments will normally contain appreciable more gadolinium burnable poison than the modest assumption used for the present analyses.

Figure 4.6.2 illustrates the correlation between the reactivities in the rack and those in the standard core geometry. For the 4.6% enriched case, the maximum in reactivity in Figure 4.6.1 at 9 MWD/KgU corresponds to a k_∞ in the standard core geometry (20°C) of 1.332 with residual gadolinium included or 1.355 with residual gadolinium set to zero. Thus, any fuel which has a k_∞ of 1.332 (or 1.355 with residual gadolinium excluded) or less at 20°C in the standard core geometry and an average enrichment of 4.6% or less in the enriched zone* will be acceptable for storage in the Lasalle Unit 1 spent fuel racks. There is also a reserve margin in reactivity available which could be used in the future should the need arise to qualify the racks for even higher enrichment.

---

* Individual rod enrichments may exceed 4.6%E as long as the average enriched-zone enrichment is 4.6% or less.

4.7 ABNORMAL AND ACCIDENT CONDITIONS

4.7.1 Temperature and Water Density Effects

The moderator temperature coefficient of reactivity is negative and a conservative moderator temperature corresponding to the maximum water density (4°C) was assumed for the reference design. This assures that the true reactivity will always be lower than the calculated value regardless of temperature or water density.

Temperature effects on reactivity have been calculated and the results are shown in Table 4.7.1. Introducing voids in the water in the storage cells (to simulate boiling) decreased reactivity, as shown in the table. Boiling at the submerged depth of the racks would occur at approximately 252°F.

4.7.2 Abnormal Location of a Fuel Assembly

It is theoretically possible to suspend a fuel assembly of the highest allowable reactivity outside and adjacent to the fuel rack, although such a condition is highly unlikely. Neutron leakage, inherent along the module edge, significantly reduces the reactivity consequences of an extraneous fuel assembly. Three dimensional KENO-5a calculations show that the k_{eff}, with an assembly outside and adjacent to a rack module, is less than the design basis k_∞ of an infinite radial array. Thus, the abnormal location of a fuel assembly will have a negligible reactivity effect.

4.7.3 Eccentric Fuel Assembly Positioning

The fuel assembly is normally located in the center of the storage rack cell with bottom fittings and spacers that

mechanically restrict lateral movement of the fuel assemblies. Nevertheless, calculations with the fuel assembly moved into the corner of the storage rack cell (four-assembly cluster at closest approach), resulted in a substantial negative reactivity effect. Thus, the nominal case, with the fuel assembly positioned in the center of the storage cell, yields the maximum reactivity.

4.7.4 Dropped Fuel Assembly

For a drop on top of the rack, the fuel assembly will come to rest horizontally on top of the rack with a minimum separation distance from the fuel of more than 12 inches which is sufficient to preclude neutron coupling (i.e., an effectively infinite separation). Maximum expected deformation under seismic or accident conditions will not reduce the minimum spacing between

fuel assemblies to less than 12 inches. Consequently, fuel assembly drop accidents will not result in a significant increase in reactivity (<0.0001 δk) due to the separation distance.

4.7.5 Fuel Rack Lateral Movement

Normally, the individual rack modules in the spent fuel pool are separated by a water gap. Lateral motion of a fuel rack, postulated as a consequence of the design basis earthquake, could reduce or eliminate this water gap spacing. Since the exterior walls of one of the modules along the gap contains Boral, closing the gap would not result in any increase above the design basis reactivity. Consequently, rack module movement would have negligible reactivity consequences, and the reactivity would remain below the design basis k_{∞}.

4.8 COMPARISON WITH RECENT BWR STORAGE RACK DESIGNS

The specification of 3.75% enrichment as a design basis, without consideration of the gadolinium burnable poison present, is very conservative. The La Salle storage rack design may be compared with other recent BWR rack designs as shown in the following tabulation:

Plant	Design Basis Enrichment	B-10 g/cm^2 Loading
Lasalle County Station	3.75%	0.0238
Hope Creek	3.4%	0.0170
Fitzpatrick	3.3%	0.0137
Laguna Verde (Mexico)	3.15	0.012
Kuosheng (Taiwan)	3.15	0.012

4.9 LARGE STORAGE CELLS FOR SPECIAL RERACKED STORAGE NEEDS

The reracked La Salle fuel pool will contain four large square cells of 11.5" inside dimension which are sized to store the control rod drive tube or the defective fuel container. Calculations confirm that these cells are suitable for storing defective fuel containers loaded with a fuel assembly, yielding a k_∞ of - 0.74 with fresh unburned fuel.

4.10 REFERENCES FOR SECTION 4

1. A. Ahlin, M. Edenius, H. Haggblom, "CASMO - A Fuel Assembly Burnup Program," AE-RF-76-4158, Studsvik report (proprietary).

   A. Ahlin and M. Edenius, "CASMO - A Fast Transport Theory Depletion Code for LWR Analysis," ANS Transactions, Vol. 26, p. 604, 1977.

   "CASMO-3, A Fuel Assembly Burnup Program, Users Manual", Studsvik/NFA-87/7, Studsvik Energitechnik AB, November 1986

   M. Edenius et al., "CASMO Benchmark Report," Studsvik/RF-78-6293, Aktiebolaget Atomenergi, March 1978.

2. L.M. Petrie and N.F. Landers, "KENO-Va, An Improved Monte Carlo Criticality Program,", Oak Ridge National Laboratory, NUREG/CR-0200, Volume 2, Section F11. December 1984.

3. R.M. Westfall et al., "SCALE: A Modular Code System for Performing Standardized Computer Analyses for Licensing Evaluation," NUREG/CR-0200, 1979.

   Green, Lucious, Petrie, Ford, White, Wright, "PSR-63/AMPX-1 (code package), AMPX Modular Code System for Generating Coupled Multigroup Neutron-Gamma Libraries from ENDF/B," ORNL-TM-3706, Oak Ridge National Laboratory, March 1976.

4. M.G. Natrella, Experimental Statistics National Bureau of Standards, Handbook 91, August 1963.

Table 4.2.1

SUMMARY OF CRITICALITY SAFETY ANALYSES

	CASMO		KENO
Temperature for analysis	4°C	4°C	4°C
Gadolinia Content	None	2%	None
Fuel Burnup @ Max k_{eff}	0	9	0
Fuel Enrichment, wt% U-235	3.75	4.6	3.75
Reference k_∞	0.9350	0.8973	0.9245
Calculational Bias	0.0000	0.0000	0.0101
Uncertainties			
Calculational	±0.0024	±0.0024	±0.0018
KENO statistics	NA	NA	±0.0010
Tolerances[1]	±0.0071	±0.0071	±0.0071
Removal of flow channel	negative	-	negative
Eccentric position	negative	-	negative
Statistical combination[2] of uncertainties	±0.0075	±0.0075	±0.0074
Effect of Channel Bulge	NA	0.0050	NA
Allowance for Vendor Calcs	NA	0.0100	NA
Uncertainty in Depletion Calcs.	NA	0.0045	NA
Total	0.9350 ± 0.0075	0.9168 ± 0.0075	0.9346 ± 0.0074
Maximum reactivity	0.943	0.924	0.942

(1) See Table 4.5.1

(2) Square root of sum of squares of all independent uncertainties.

Table 4.2.2

REACTIVITY EFFECTS OF ABNORMAL AND ACCIDENT CONDITIONS

Accident/Abnormal Condition	Reactivity Effect
Temperature increase	Negative (Table 4.7.1)
Void (boiling)	Negative (Table 4.7.1)
Assembly dropped on top of rack	Negligible
Movement of rack modules	Negligible
Misplacement of a fuel assembly	Negligible

Table 4.3.1

FUEL ASSEMBLY DESIGN SPECIFICATIONS

FUEL ROD DATA	
Cladding outside diameter, in.	0.483
Cladding inside diameter, in.	0.419
Cladding material	Zr-2
UO_2 density (stack), g/cc UO_2 Tolerance	10.412 ± 0.200
Pellet diameter, inch	0.411
Enrichment (Rack design basis, uniform % U-235)	3.75
WATER ROD DATA	
Number of Water Rods	2
Inside diameter, inch	0.531
Outside diameter	0.591
Material	Zr-2
FUEL ASSEMBLY DATA	
Fuel rod array	8 x 8
Number of fuel rods	62
Fuel rod pitch, inch	0.640
Fuel channel, material	Zr-2
Inside dimension, inch	5.258
Outside dimension, inch	5.476

Table 4.5.1

Reactivity Uncertainties[1] due to Manufacturing Tolerances

Quantity	Nominal Value	Tolerance	δk_∞
Boron Loading	0.0238 g/cm^2	±0.0018 g/cm^2	±0.0051
Boral width	5.00 inches	±1/16 inches	±0.0019
Lattice spacing	6.264 inches	±0.040 inches	±0.0017
SS thickness	0.09 and 0.035 inches	±0.005 inches mean	±0.0010
Fuel enrichment	3.75% U-235	±0.05% U-235	±0.0029
Fuel density	10.412 g/cm^3	±0.20 g/cm^3	±0.0024
Statistical combination of uncertainties [1]			±0.0069

[1] Square root of sum of squares of all independent tolerance effects.

Table 4.7.1

EFFECT OF TEMPERATURE AND VOID ON CALCULATED REACTIVITY OF STORAGE RACK

Case	Incremental Reactivity Change, δk
4°C (39°F)	Reference
20°C (68°F)	-0.003
80°C (176°F)	-0.016
122°C (252°F)	-0.028
122°C, 20% void	-0.039

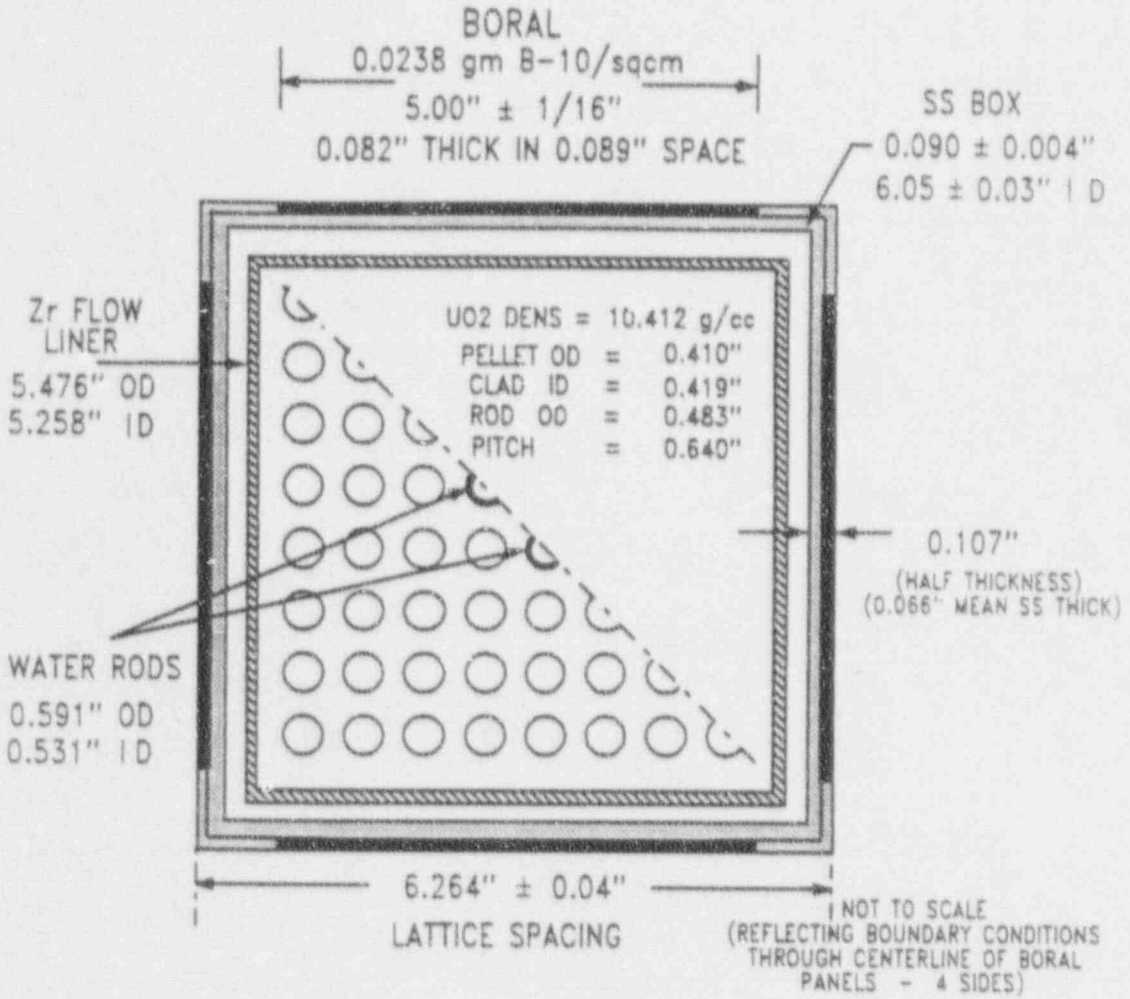

FIG. 4.3.1 STORAGE CELL CROSS SECTION FOR CALCULATIONAL MODEL

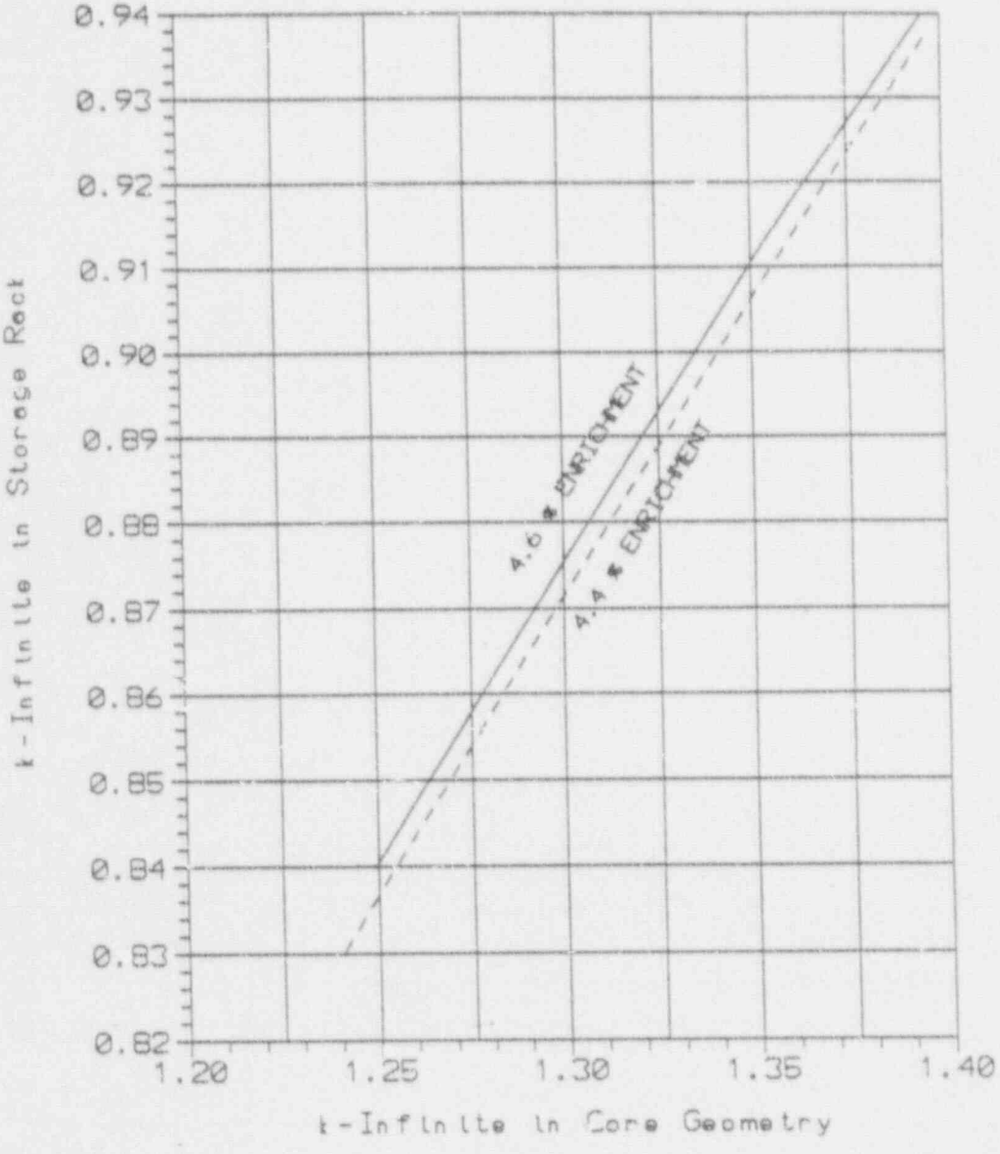

Figure 4.6.2 Correlation Between Reactivity in the Core and in the Rack for 4.4% AND 4.6% Enriched Fuel

APPENDIX A

BENCHMARK CALCULATIONS

by

Stanley E. Turner, PhD, PE

HOLTEC INTERNATIONAL

March, 1992

1.0 — INTRODUCTION AND SUMMARY

The objective of this benchmarking study is to verify both the NITAWL-KENO-5a[1,2] methodology with the 27-group SCALE cross-section library and the CASMO-3 code[3] for use in criticality safety calculations of high density spent fuel storage racks. Both calculational methods are based upon transport theory and have been benchmarked against critical experiments that simulate typical spent fuel storage rack designs as realistically as possible. Results of these benchmark calculations with both methodologies are consistent with corresponding calculations reported in the literature.

Results of the benchmark calculations show that the 27-group (SCALE) NITAWL-KENO-5a calculations consistently underpredict the critical eigenvalue by 0.0101 ± 0.0018 δk (with a 95% probability at a 95% confidence level) for critical experiments[4] that are as representative as possible of realistic spent fuel storage rack configurations and poison worths.

Extensive benchmarking calculations of critical experiments with CASMO-3 have also been reported[5], giving a mean k_{eff} of 1.0004 ± 0.0011 for 37 cases. With a K-factor of 2.14[6] for 95% probability at a 95% confidence level, and conservatively neglecting the small overprediction, the CASMO-3 bias then becomes 0.0000 ± 0.0024. CASMO-3 and NITAWL-KENO-5a intercomparison calculations of infinite arrays of poisoned cell configurations (representative of typical spent fuel storage rack designs) show very good agreement, confirming that 0.0000 ± 0.0024 is a reasonable bias and uncertainty for CASMO-3 calculations. Reference 5 also documents good agreement of heavy nuclide concentrations for the Yankee core isotopics, agreeing with the measured values within experimental error.

The benchmark calculations reported here confirm that either the 27-group (SCALE) NITAWL-KENO or CASMO-3 calculations are acceptable for criticality analysis of high-density spent fuel storage racks. Where possible, reference calculations for storage rack designs should be performed with both code packages to provide independent verification.

2.0 NITAWL-KENO 5a BENCHMARK CALCULATIONS

Analysis of a series of Babcock & Wilcox critical experiments[4], including some with absorber panels typical of a poisoned spent fuel rack, is summarized in Table 1, as calculated with NITAWL-KENO-5a using the 27-group SCALE cross-section library and the Nordheim resonance integral treatment in NITAWL. Dancoff factors for input to NITAWL were calculated with the Oak Ridge SUPERDAN routine (from the SCALE[2] system of codes). The mean for these calculations is 0.9899 ± 0.0028 (1 σ standard deviation of the population). With a one-sided tolerance factor corresponding to 95% probability at a 95% confidence level[6], the calculational bias is + 0.0101 with an uncertainty of the mean of of ± 0.0018 for the sixteen critical experiments analyzed.

Similar calculational deviations have been reported by ORNL[7] for some 54 critical experiments (mostly clean critical without strong absorbers), obtaining a mean bias of 0.0100 ± 0.0013 (95%/95%). These published results are in good agreement with the results obtained in the present analysis and lend further credence to the validity of the 27-group NITAWL-KENO-5a calculational model for use in criticality analysis of high density spent fuel storage racks. No trends in k_{eff} with intra-assembly water gap, with absorber panel reactivity worth, with enrichment or with poison concentration were identified.

Additional benchmarking calculations were also made for a series of French critical experiments[9] at 4.75% enrichment and for several of the BNWL criticals with 4.26% enriched fuel. Analysis of the French criticals (Table 2) showed a tendency to overpredict the reactivity, a result also obtained by ORNL[10]. The calculated k_{eff} values showed a trend toward higher values with decreasing core size. In the absence of a significant enrichment effect (see Section 3 below), this trend and the overprediction is attributed to a small inadequacy in NITAWL-KENO-5a in calculating neutron leakage from very small assemblies.

Similar overprediction was also observed for the BNWL series of critical experiments[11], which also are small assemblies (although significantly larger than the French criticals). In this case (Table 2), the overprediction appears to be small, giving a mean k_{eff} of 0.9990 ± 0.0037 (1 σ population standard deviation). Because of the small size of the BNWL critical experiments and the absence of any significant enrichment effect, the overprediction is also attributed to the failure of NITAWL-KENO-5a to adequately treat neutron leakage in very small assemblies.

Since the analysis of high-density spent fuel storage racks generally does not entail neutron leakage, the observed inadequacy of NITAWL-KENO-5a is not significant. Furthermore, omitting results of the French and BNWL critical experiment analyses from the determination of bias is conservative since any leakage that might enter into the analysis would tend to result in overprediction of the reactivity.

3. CASMO-3 BENCHMARK CALCULATIONS

The CASMO-3 code is a multigroup transport theory code utilizing transmission probabilities to accomplish two-dimensional calculations of reactivity and depletion for BWR and PWR fuel assemblies. As such, CASMO-3 is well-suited to the criticality analysis of spent fuel storage racks, since general practice is to treat the racks as an infinite medium of storage cells, neglecting leakage effects.

CASMO-3 is a modification of the CASMO-2E code and has been extensively benchmarked against both mixed oxide and hot and cold critical experiments by Studsvik Energiteknik[5]. Reported analyses[5] of 37 critical experiments indicate a mean k_{eff} of 1.0004 ± 0.0011 (1σ). To independently confirm the validity of CASMO-3 (and to investigate any effect of enrichment), a series of calculations were made with CASMO-3 and with NITAWL-KENO-5a on identical poisoned storage cells representative of high-density spent fuel storage racks. Results of these intercomparison calculations* (shown in Table 3) are within the normal statistical variation of KENO calculations and confirm the bias of 0.0000 ± 0.0024 (95%/95%) for CASMO-3.

Since two independent methods of analysis would not be expected to have the same error function with enrichment, results of the intercomparison analyses (Table 3) indicate that there is no significant effect of fuel enrichment over the range of enrichments involved in power reactor fuel. Furthermore, neglecting the French and BNWL critical benchmarking in the determination of bias is a conservative approach.

---

*Intercomparison between analytical methods is a technique endorsed by Reg. Guide 5.14, "Validation of Calculational Methods for Nuclear Criticality Safety".

REFERENCES TO APPENDIX A

1. Green, Lucious, Petrie, Ford, White, and Wright, "PSR-63-/NITAWL-1 (code package) NITAWL Modular Code System for Generating Coupled Multigroup Neutron-GAmma Libraries from ENDF/B", ORNL-TM-3706, Oak Ridge National Laboratory, November 1975.

2. R.M. Westfall et. al., "SCALE: A Modular System for Performing Standardized Computer Analysis for Licensing Evaluation", NUREG/CR-0200, 1979.

3. A. Ahlin, M. Edenius, and H. Haggblom, "CASMO - A Fuel Assembly Burnup Program", AE-RF-76-4158, Studsvik report.

   A. Ahlin and M. Edenius, "CASMO - A Fast Transport Theory Depletion Code for LWR Analysis", ANS Transactions, Vol. 26, p. 604, 1977.

   "CASMO-3 A Fuel Assembly Burnup Program, Users Manual", Studsvik/NFA-87/7, Studsvik Energitechnik AB, November 1986

4. M.N. Baldwin et al., "Critical Experiments Supporting Close Proximity Water Storage of Power Reactor Fuel", BAW-1484-7, The Babcock & Wilcox Co., July 1979.

5. M. Edenius and A. Ahlin, "CASMO-3: New Features, Benchmarking, and Advanced Applications", Nuclear Science and Engineering, 100, 342-351, (1988)

6. M.G. Natrella, Experimental Statistics, National Bureau of Standards, Handbook 91, August 1963.

7. R.W. Westfall and J. H. Knight, "SCALE System Cross-section Validation with Shipping-cask Critical Experiments", ANS Transactions, Vol. 33, p. 368, November 1979

8. S.E. Turner and M.K. Gurley, "Evaluation of NITAWL-KENO Benchmark Calculations for High Density Spent Fuel Storage Racks", Nuclear Science and Engineering, 80(2):230-237, February 1982.

9. J.C. Manaranche, et. al., "Dissolution and Storage Experiment with 4.75% U-235 Enriched UO_2 Rods", Nuclear Technology, Vol. 50, pp 148, September 1980

10. A.M. Hathout, et. al., "Validation of Three Cross-section Libraries Used with the SCALE System for Criticality Analysis", Oak Ridge National Laboratory, NUREG/CR-1917, 1981.

11. S.R. Bierman, et. al., "Critical Separation between Subcritical Clusters of 4.29 Wt. % ^{235}U Enriched UO_2 Rods in Water with Fixed Neutron Poisons", Batelle Pacific Northwest Laboratories, NUREG/CR/0073, May 1978 (with August 1979 errata).

Table 1

RESULTS OF 27-GROUP (SCALE) NITAWL-KENO-5a CALCULATIONS OF B&W CRITICAL EXPERIMENTS

Experiment Number	Calculated k_{eff}	σ
I	0.9922	± 0.0006
II	0.9917	± 0.0005
III	0.9931	± 0.0005
IX	0.9915	± 0.0006
X	0.9903	± 0.0006
XI	0.9919	± 0.0005
XII	0.9915	± 0.0006
XIII	0.9945	± 0.0006
XIV	0.9902	± 0.0006
XV	0.9836	± 0.0006
XVI	0.9863	± 0.0006
XVII	0.9875	± 0.0006
XVIII	0.9880	± 0.0006
XIX	0.9882	± 0.0005
XX	0.9885	± 0.0006
XXI	0.9890	± 0.0006
Mean	0.9899	± 0.0007[1]
Bias (95%/95%)	0.0101	± 0.0018

[1] Standard Deviation of the Mean, calculated from the k_{eff} values.

Table 2

RESULTS OF 27-GROUP (SCALE) NITAWL-KENO-5a CALCULATIONS OF FRENCH and BNWL CRITICAL EXPERIMENTS

French Experiments		
Separation Distance, cm	Critical Height, cm	Calculated k_{eff}
0	23.8	1.0231 ± 0.0036
2.5	24.48	1.0252 ± 0.0043
5.0	31.47	1.0073 ± 0.0013
10.0	64.34	0.9944 ± 0.0014

BNWL Experiments		
Case	Expt. No.	Calculated k_{eff}
No Absorber	004/032	0.9964 ± 0.0034
SS Plates (1.05 B)	009	0.9988 ± 0.0038
SS Plates (1.62 B)	011	1.0032 ± 0.0033
SS Plates (1.62 B)	012	0.9986 ± 0.0036
SS Plates	013	0.9980 ± 0.0038
SS Plates	014	0.9936 ± 0.0036
Zr Plates	030	1.0044 ± 0.0035
Mean		0.9990 ± 0.0037

Table 3

RESULTS OF CASMO-3 AND NITAWL-KENO-5a
BENCHMARK (INTERCOMPARISON) CALCULATIONS

Enrichment[1] Wt. % U-235	k_∞ NITAWL-KENO-5a[2]	k_∞ CASMO-3	$\lvert\delta k\rvert$
2.5	0.8408 ± 0.0016	0.8379	0.0029
3.0	0.8831 ± 0.0016	0.8776	0.0055
3.5	0.9097 ± 0.0016	0.9090	0.0007
4.0	0.9334 ± 0.0016	0.9346	0.0012
4.5	0.9569 ± 0.0018	0.9559	0.0010
5.0	0.9766 ± 0.0018	0.9741	0.0025
		Mean	0.0023

(1) Infinite array of assemblies typical of high-density spent fuel storage racks.

(2) k_∞ from NITAWL-KENO-5a corrected for bias.

5.0 THERMAL-HYDRAULIC CONSIDERATIONS

5.1 Introduction

This section provides a summary of the methods, models, analyses and numerical results to demonstrate the compliance of the reracked La Salle County Station (LSCS) Unit 1 spent fuel pool with the provisions of Section III of the USNRC "OT Position Paper for Review and Acceptance of Spent Fuel Storage and Handling Applications", (April 14, 1978).

Similar methods of thermal-hydraulic analysis have been used in previous licensing efforts on high density spent fuel racks for Fermi 2 (Docket 50-341), Quad Cities 1 and 2 (Dockets 50-254 and 50-265), Rancho Seco (Docket 50-312), Grand Gulf Unit 1 (Docket 50-416), Oyster Creek (Docket 50-219), Virgil C. Summer (Docket 50-395), Diablo Canyon 1 and 2 (Docket Nos. 50-275 and 50-323), Byron Units 1 and 2 (Docket 50-454, 455), St. Lucie Unit One (Docket 50-335), Millstone Point I (50-245), Vogtle Unit 2 (50-425), Kuosheng Units 1 & 2 (Taiwan Power Company), Ulchin Unit 2 (Korea Electric Power Company), and J.A. FitzPatrick (New York Power Authority), Zion (Commonwealth Edison Company), Sequoyah (TVA), and Three Mile Island Unit One (GPU Nuclear), among others.

The analyses to be carried out for the thermal-hydraulic qualification of the rack array may be broken down into the following categories:

(i) Pool decay heat evaluation and pool bulk temperature variation with time.

(ii) Determination of the maximum pool local temperature at the instant when the bulk temperature reaches its maximum value.

(iii) Evaluation of the maximum fuel cladding temperature to establish that bulk nucleate boiling at any location resulting in two phase conditions environment around the fuel is not possib

(iv) Evaluation of the time-to-boil if all heat rejection paths from the cooler are lost.

(v) Compute the effect of a blocked fuel cell opening on the local water and maximum cladding temperature.

The following sections present a synopsis of the methods employed to perform such analyses and final results.

5.2 Spent Fuel Pool Cooling System and Cleanup System Description

The La Salle County Station Unit 1 Spent Fuel Pool Cooling System (SFPCS) consists of two identical cooling trains. Each cooling train consists of one 3000 gpm centrifugal pump and one 14.6×10^6 Btu/hr tube-and-shell heat exchanger. The system takes suction from the fuel pool and subsequently pumps water through the filter-demineralizer (cleanup) system and then to the heat exchangers. Heat from the fuel pool water is rejected by the heat exchangers to the Service Water System (SWS). The fuel pool water is cooled and purified through the circulation. Neither the SFPCS nor the cleanup system are Seismic Category I.

In the event of excessive heat load, the pool can be cooled by means of spooling in suction and return lines to the Residual Heat Removal (RHR) "B" loop pump and heat exchanger (41.6×10^6 Btu/hr) of the unit for supplementary cooling of the pool. The flow rate is approximately 7500 gpm through the RHR heat exchanger and back to the RHR return in the fuel pool. All pipes and valves to and from the "B" loop of the RHR System are designed as Seismic Category I and can be isolated from the fuel pool cooling system, thus providing a completely independent seismic designed system for cooling the pool.

The level of the fuel pool is maintained through the use of makeup to the pool. Normal makeup is received from the cycled condensate storage system of the unit. However, a Seismic Category I fuel pool emergency makeup system, which is capable of a makeup of 300 gpm to the pool, is present should it be necessary to provide

emergency makeup. The emergency fuel pool makeup system is part of the core standby cooling system equipment cooling water system (CSCS-ECWS) which is also Seismic Category I, thus ensuring a reliable source of water. Redundant pumps are provided. Makeup to the fuel pool during normal and abnormal conditions is provided by redundant pumps, thus ensuring an adequate means of maintaining the fuel pool level.

5.3 Decay Heat Load Calculations

The decay heat load calculation is performed in accordance with the provisions of "USNRC Branch Technical Position ASB9-2, "Residual Decay Energy for Light Water Reactors for Long Term Cooling", Rev. 2, July, 1981.

5.4 Discharge Scenarios

The LSCS Unit 1 fuel pool cooling system is sized to comply with the cooling capacity requirements implicit in the USNRC SRP 9.1.3. Therefore, calculations validating the SRP compliance of the cooling system are not presented. Instead, we present the discharge scenarios which correspond to the actual La Salle refueling practices.

Accordingly, two discharge scenarios are considered assuming the pool is already filled with 12 refueling batches (256 fuel bundles per batch) at 18 month cycles. Each discharge scenario consists of one refueling batch of 256 assemblies and one full core offload of 764 assemblies to simulate the emergency full core offload condition. The spent fuel pool is assumed to have a total of 4026 storage locations. The assumed final discharges will result in a total of 4092 fuel assemblies in the pool which bounds the actual pool capacity. More fuel assemblies implies higher decay heat load. Therefore, the bounding heat load in the pool will be calculated in the analyses. The two discharge scenarios are intended to

demonstrate that the Spent Fuel Pool Cooling System alone can handle the emergency full core offload in spite of the increased fuel inventory in the fuel pool.

For the two dishcarge scenarios, it is assumed that the normally scheduled outage (Batch #13) occurs 18 months after the previous outage and fuel discharge to the pool begins at the rate of 10 assemblies per hour, 100 hours after reactor shutdown. The reactor is restarted after 45 days of outage. Two spent fuel pool cooling trains are assumed in operation during the discharges. No credit is taken for the additional cooling provided by the RHR heat exchanger.

Case (I): Thirty days after restart of the reactor, the unit experiences an unshceduled shutdown, and the core is offloaded to the pool after 100 hours of decay in the reactor.

Case (II): Reanalysis of the above case with 30 days replaced with 60 days.

Figure 5.4.1 illustrates the above two scenarios. Table 5.4.1 provides the major input for the scenarios.

5.5 Bulk Pool Temperatures

The bulk temperature calculations are performed using a highly conservative mathematical model. As shown in Figure 5.5.1, only the cooling contribution of the spent fuel cooler is considered. The Residual Heat Removal heat exchanger, which is concurrently cooling the water mass in the reactor cavity and the spent fuel pool, is not considered in this analysis in the interest of conservatism.

Similarly, in order to perform the analysis conservatively, the heat exchangers are assumed to be fouled to their design maximum. Thus, the temperature effectiveness, p, for the heat exchanger utilized in the analysis is the lowest postulated value calculated

from heat exchanger thermal hydraulic codes. p is assumed to remain constant in the calculation.

The mathematical formulation can be explained with reference to the simplified heat exchanger alignment of Figure 5.5.1.

Referring to the Spent Fuel Pool Cooling System, the governing differential equation can be written by utilizing conservation of energy:

$$C \frac{dT}{d\tau} = Q_L - Q_{HX} \qquad (5\text{-}1)$$

$$Q_L = P_{com} + Q(\tau) - Q_{EV}(T, t_a)$$

where:

C: Thermal capacitance of the pool (net water volume times water density and times heat capacity), Btu/°F.

Q_L: Heat load to the heat exchanger, Btu/hr.

$Q(\tau)$: Heat generation rate from recently discharged fuel, which is a specified function of time, τ, Btu/hr.

$P_{com} = \beta P_o$: Heat generation rate from "old" fuel, Btu/hr. (P_o = average assembly operating power, Btu/hr)

Q_{HX}: Heat removal rate by the heat exchanger, Btu/hr.

$Q_{EV}(T, t_a)$: Heat loss to the surroundings, which is a function of pool temperature T and ambient temperature t_a, Btu/hr.

Q_{HX} is a non-linear function of time if we assume the temperature effectiveness p is constant during the calculation. Q_{HX} can, however, be written in terms of effectiveness p as follows:

$$Q_{HX} = W_t C_t p (T - t_i) \qquad (5\text{-}2)$$

$$p = \frac{t_o - t_i}{T - t_i}$$

where:

W_t: Coolant flow rate, lb./hr.

C_t: Coolant specific heat, Btu/lb.°F.

p: Temperature effectiveness of heat exchanger.

T: Pool water temperature, °F

t_i: Coolant inlet temperature, °F

t_o: Coolant outlet temperature, °F

p is determined by the heat exchanger design basis performance. Q(τ) is specified according to the provisions of "USNRC Branch Technical Position ASB9-2, "Residual Decay Energy for Light Water Reactors for Long Term Cooling", Rev. 2, July, 1981. Q(τ) is a function of decay time, number of assemblies, and in-core exposure time. During the fuel transfer, the heat load in the pool will increase with respect to the rate of fuel transfer and equals Q(τ) after the fuel transfer.

Q_{EV} is a non-linear function of pool temperature and ambient temperature. Q_{EV} contains the heat evaporation loss through the pool surface, natural convection from the pool surface and heat conduction through the pool walls and slab. Experiments show that the heat conduction takes only about 4% of the total heat loss [5.5.1], therefore, it can be neglected. The evaporation heat and natural convection heat loss can be expressed as:

$$Q_{EV} = m \Gamma A_s + h_C A_s \Theta \qquad (5\text{-}3)$$

where:

m: Mass evaporation rate, lb./hr. $ft.^2$

Γ: Latent heat of pool water, Btu/lb.

A_s: Pool surface area, $ft.^2$

h_c: Convection heat transfer coefficient at pool surface, $Btu/ft.^2$ hr. °F

$\theta = T - t_a$: The temperature difference between pool water and ambient air, °F

The mass evaporation rate m can be obtained as a non-linear function of θ. We, therefore, have

$$m = h_D(\theta)\ (W_{ps} - W_{as}) \qquad (5\text{-}4)$$

where:

W_{ps}: Humidity ratio of saturated moist air at pool water surface temperature T.

W_{as}: Humidity ratio of saturated moist air at ambient temperature t_a

$h_D(\theta)$: Diffusion coefficient at pool water surface. h_D is a non-linear function of θ, lb./hr. $ft.^2$ °F

The non-linear single order differential equation (5-1) is solved using Holtec's Q.A. validated numerical integration code "ONEPOOL".

The next step in the analysis is to determine the temperature rise profile of the pool water if all forced indirect cooling modes are suddenly lost.

If the cooling makeup water is added at the rate of G lb/hr and the cooling water is at temperature, t_{cool}, the governing enthalpy balance equation for this condition can be written as

$$[C + G(C_t)(\tau - \tau_o)]\ \frac{dT}{d\tau} = P_{core} + Q(\tau + \tau_{ins}) + G\ (C_t)\ (t_{cool} - T)$$

where water is assumed to have specific heat of unity (C_t = 1.0 Btu/lb.°F), and the time coordinate τ is measured from the instant of loss-of-cooling. τ_o is the time coordinate when the direct addition (fire hose) cooling water application is begun. τ_{ins} is the time coordinate measured from the instant of reactor shutdown

to the instant of loss-of-cooling. T is the dependent variable (pool water temperature). For conservatism, Q_{EV} is conservatively assumed to remain constant after pool water temperature reaches and rises above 170°F.

A Q.A. validated numerical quadrature code is used to integrate the foregoing equation. The pool water heat up rate, time-to-boil, and subsequent water evaporation-time profile are generated and compiled for safety evaluation.

5.6 Local Pool Water Temperature

In this section, a summary of the methodology, calculations and results for local pool water temperature is presented.

5.6.1 Basis

In order to determine an upper bound on the maximum fuel cladding temperature, a series of conservative assumptions are made. The most important assumptions are listed below:

- The fuel pool will contain spent fuel with varying time-after-shutdown (τ_s). Since the heat emission falls off rapidly with increasing τ_s, it is conservative to assume that all fuel assemblies are from the latest batch discharged simultaneously in the shortest possible time and they all have had the maximum postulated years of operating time in the reactor. The heat emission rate of each fuel assembly is assumed to be equal and maximum.

- As shown in the pool layout drawings, the modules occupy an irregular floor space in the pool. For the hydrothermal analysis, a circle circumscribing the actual rack floor space is drawn (Fig. 5.6.1). It is further assumed that the cylinder with this circle as its base is packed with fuel assemblies at the nominal layout pitch.

- The actual downcomer space around the rack module group varies. The nominal downcomer gap available in the pool is assumed to be the total gap available around the

idealized cylindrical rack; thus, the maximum resistance to downward flow is incorporated into the analysis (Figs. 5.6.2 and 5.6.3) (i.e. minimum gap between the pool wall and rack module, including seismic kinematic effect).

- No downcomer flow is assumed to exist between the rack modules.

- No heat transfer is assumed to occur between pool water and the surroundings (wall, etc.)

- The effect of the truncation of the sparger line in the fuel pool is appropriately accounted for by setting the bottom plenum temperature equal to the spatial average temperature of the pool.

5.6.2 Model Description

In this manner, a conservative idealized model for the rack assemblage is obtained. The water flow is axisymmetric about the vertical axis of the circular rack assemblage, and thus, the flow is two-dimensional (axisymmetric three-dimensional). Fig. 5.6.2 shows a typical "flow chimney" rendering of the thermal hydraulics model. The governing equation to characterize the flow field in the pool can now be written. The resulting integral equation can be solved for the lower plenum velocity field (in the radial direction) and axial velocity (in-cell velocity field), by using the method of collocation. The hydrodynamic loss coefficients which enter into the formulation of the integral equation are also taken from well-recognized sources (Ref. 5.6.1) and wherever discrepancies in reported values exist, the conservative values are consistently used. Reference 5.6.2 gives the details of mathematical analysis used in this solution process.

After the axial velocity field is evaluated, it is a straightforward matter to compute the fuel assembly cladding temperature. The knowledge of the overall flow field enables pinpointing of the storage location with the minimum axial flow (i.e, maximum water outlet temperatures). This is called the most "choked" location. In order to find an upper bound on the temperature in a typical cell, it is assumed that it is located at the most choked location. Knowing the global plenum velocity field, the revised axial flow

through this choked cell can be calculated by solving the Bernoulli's equation for the flow circuit through this cell. Thus, an absolute upper bound on the water exit temperature and maximum fuel cladding temperature is obtained. In view of these aforementioned assumptions, the temperatures calculated in this manner overestimate the temperature rise that will actually occur in the pool. Holtec's earlier computer code THERPOOL* based on the theory of Ref. 5.6.2, automates this calculation. The analysis procedure embodied in THERPOOL has been accepted by the Nuclear Regulatory Commission on several dockets. The Code THERPOOL for local temperature analyses includes the calculation of void generations. The effect of void on the conservation equation, crud layer in the clad, and the clad stress calculation when a void exists, are all incorporated in THERPOOL. The major inputs for the local temperature analysis are given in Table 5.6.1.

5.7 Cladding Temperature

The maximum specific power of a fuel array q_A can be given by:

$$q_A = q\ F_{xy} \qquad (1)$$

where:

F_{xy} = radial peaking factor
q = average fuel assembly specific power

The maximum temperature rise of pool water in the most disadvantageously placed fuel assembly is computed for all loading cases. Having determined the maximum local water temperature in the pool, it is now possible to determine the maximum fuel cladding temperature. A fuel rod can produce F_z times the average heat emission rate over a small length, where F_z is the axial rod peaking

---

* THERPOOL has been used in qualifying the spent fuel pool reracking of over 20 projects, including Enrico Fermi Unit 2 (1980, Quad Cities I and II (1981), Oyster Creek (1984), V.C. Summer (1984), Rancho Seco (1983), Grand Gulf I (1985), Diablo Canyon I and II (1986), St. Lucie Unit One (1987), Millstone Point Unit One (1989), Hope Creek (1990), TMI Unit One (1991), and others.

factor. The axial heat distribution in a rod is generally a maximum in the central region, and tapers off at its two extremities. The peaking factors used for the La Salle County Unit 1 spent fuel pool are shown in Table 5.7.1.

It can be shown that the power distribution corresponding to the chopped cosine power emission rate is given by

$$q(x) = q_A \sin \frac{\pi (a + x)}{1 + 2a}$$

where:

l: active fuel length

a: chopped length at both extremities in the power curve

x: axial coordinate with origin at the bottom of the active fuel region

The value of a is given by

$$a = \frac{l\, z}{1 - 2z}$$

where:

$$z = \frac{1}{\pi\, F_z} - \left[\frac{1}{\pi^2\, F_z^2} - \frac{1}{\pi\, F_z} + \frac{2}{\pi^2} \right]^{1/2}$$

where F_z is the axial peaking factor.

The cladding temperature T_c is governed by a third order differential equation which has the form of

$$\frac{d^3 T}{d x^3} + \alpha_1 \frac{d^2 T}{d x^2} - \alpha_2 \frac{dT}{dx} = f(x)$$

where α_1, α_2 and f(x) are functions of x, and fuel assembly geometric properties. The solution of this differential equation with appropriate boundary conditions provides the fuel cladding temperature and local water temperature profile.

In order to introduce some additional conservatism in the analysis, we assume that the fuel cladding has a crud deposit of .005 ^{0}F-sq.ft.-hr/Btu crud resistance, which covers the entire surface.

5.8 Results

It is shown in the calculations that the decay heat load of the "old" fuel assemblies in the pool (12 refueling batches of 256 assemblies per batch at 18 month cycles) is 4.8[illegible] x 10^{6} Btu/hr during the final discharges specified in Section [illegible] Table 5.8.1 gives the general input for the bulk pool temperature analyses. The maximum bulk pool temperature results are presented in Table 5.8.2. The time varying bulk pool temperatures and heat load in the pool are plotted vs. time-after-shutdown in Figure 5.8.1 to 5.8.4. It is shown from the analyses that the maximum bulk pool temperature resulted from an emergency full core offload is 127.2°F at 180 hours after-reactor-shutdown. The maximum heat load to the cooling system is 37.83 x 10^{6} Btu/hr. The maximum calculated temperature is well below the temperature guidelines for both normal and abnormal conditions specified in the Standard Review Plan, Section 9.1.3.

The foregoing results for the bulk pool temperature were obtained assuming that the total flow rate of the spent fuel pool water through the two coolers is 6000 gpm. System flow calculations indicate, however, that the total flow rate is expected to be limited to 5050 gpm. This decrease from the design basis flow rate is estimated to cause less than 12°F elevation of the maximum bulk pool temperature. Thus, referring to Table 5.8.2, the maximum pool water temperature will remain bounded by 140°F.

The loss-of-cooling events have been considered for the specified discharge scenarios. The loss of all forced cooling is assumed to occur at both instants of peak heat load and peak pool temperature, respectively. Table 5.8.3 summarizes the results of the time-to-

boil and maximum evaporation rate. The calculated minimum time from the loss of pool cooling until the pool boils is 5.91 hours and the maximum boil-off rate is 80.65 gpm, which is well below the capacity of the Seismic Category I makeup water system for the spent fuel pool. It is estimated that the boiling interval period will be reduced by less than 10% due to the aforementioned reduction in the system flow rate.

Table 5.8.4 gives the results of the maximum local water temperature and maximum local fuel cladding temperature for the limiting discharge scenario (Case II). Calculations are performed assuming non-blockage and 50% blockage, respectively. The blockage is assumed to occur in the thermally limiting storage cell by a horizontally placed (misplaced) fuel assembly. It is shown that the calculated maximum local temperatures will not cause local nucleate boiling at any location in the racks. This conclusion remains valid even under the scenario of reduction in the system flow rate, which is estimated to elevate the local temperature in Table 5.8.4 by less than 15°F.

5.9 References for Section 5

5.5.1 Wang, Yu, "Heat Loss to the Ambient From Spent Fuel Pools: Correlation of Theory with Experiment", Holtec Report HI-90477, Rev. 0, April 3, 1990.

5.6.1 General Electric Corporation, R&D Data Books, "Heat Transfer and Fluid Flow", 1974 and updates.

5.6.2 Singh, K.P. et al., "Method for Computing the Maximum Water Temperature in a Fuel Pool Containing Spent Nuclear Fuel", Heat Transfer Engineering, Vol. 7, No. 1-2, pp. 72-82 (1986).

Table 5.4.1

DATA FOR DISCHARGE SCENARIOS

Number of assemblies in refueling batch:	256
Number of assemblies in full core:	764
Number of fuel pool coolers in parallel:	2
Fuel normal exposure time, hrs.:	39420
Fuel transfer rate, assemblies/hr.:	10

Table 5.6.1

DATA FOR LOCAL TEMPERATURE

Type of fuel assembly	GE 8x8
Fuel cladding outer diameter, inches	0.483
Fuel cladding inside diameter, inches	0.419
Storage cell inside dimension, inches	6.05
Active fuel length, inches	150
Number of fuel rods/assembly	62
Operating power per fuel assembly $P_o \times 10^{-6}$, Btu/hr	14.864
Cell pitch, inches	6.264
Cell height, inches	167.75
Bottom height, inches	6.75
Plenum radius, feet	26

Table 5.7.1

Factor	Value
Radial	1.60
Total	2.50

Table 5.8.1

FUEL SPECIFIC POWER AND POOL CAPACITY DATA

Net water volume of pool, $ft.^3$	41780
Fuel pool thermal capacity, 10^6 Btu/°F	2.5
Average operating power of a fuel assembly, 10^6 Btu/hr	14.864
Decay heat load of "old" discharges, 10^6 Btu/hr	4.81
Coolant (WS) inlet temperature, °F	95
Coolant (WS) flow rate, 10^6 lb/hr	2.0

Table 5.8.2

SFP BULK POOL TEMPERATURE

	Maximum Pool Temp., °F	Coincident Time After Reactor Shut-down, hrs.	Coincident Heat Load to SFP Hxs 10^6 Btu/hr	Coincident Evaporation Heat Losses 10^6 Btu/hr
Discharge in Case 1	126.5	180	36.80	0.150
Discharge in Case 2	127.2	180	37.60	0.162

Table 5.8.3

Case Number	Remarks	Time-to-Boil (Hours) (Without Make-up Water)	Maximum Evaporation Rate (GPM)
1A	Loss-of-Cooling at Max. Heat Load	6.10	78.88
1B	Loss-of-Cooling at Max. Pool Temperature	6.12	78.43
2A	Loss-of-Cooling at Max. Heat Load	5.91	80.65
2B	Loss-of-Cooling at Max. Pool Temperature	5.93	80.19

Table 5.8.4

MAXIMUM LOCAL POOL WATER AND FUEL CLADDING TEMPERATURE FOR THE LIMITING CASE (Case II)

	Maximum Local Pool Water Temp., °F	Maximum Local Fuel Cladding Temp., °F
No Blockage	163.2	210.7
50% Blockage	169.0	215.1

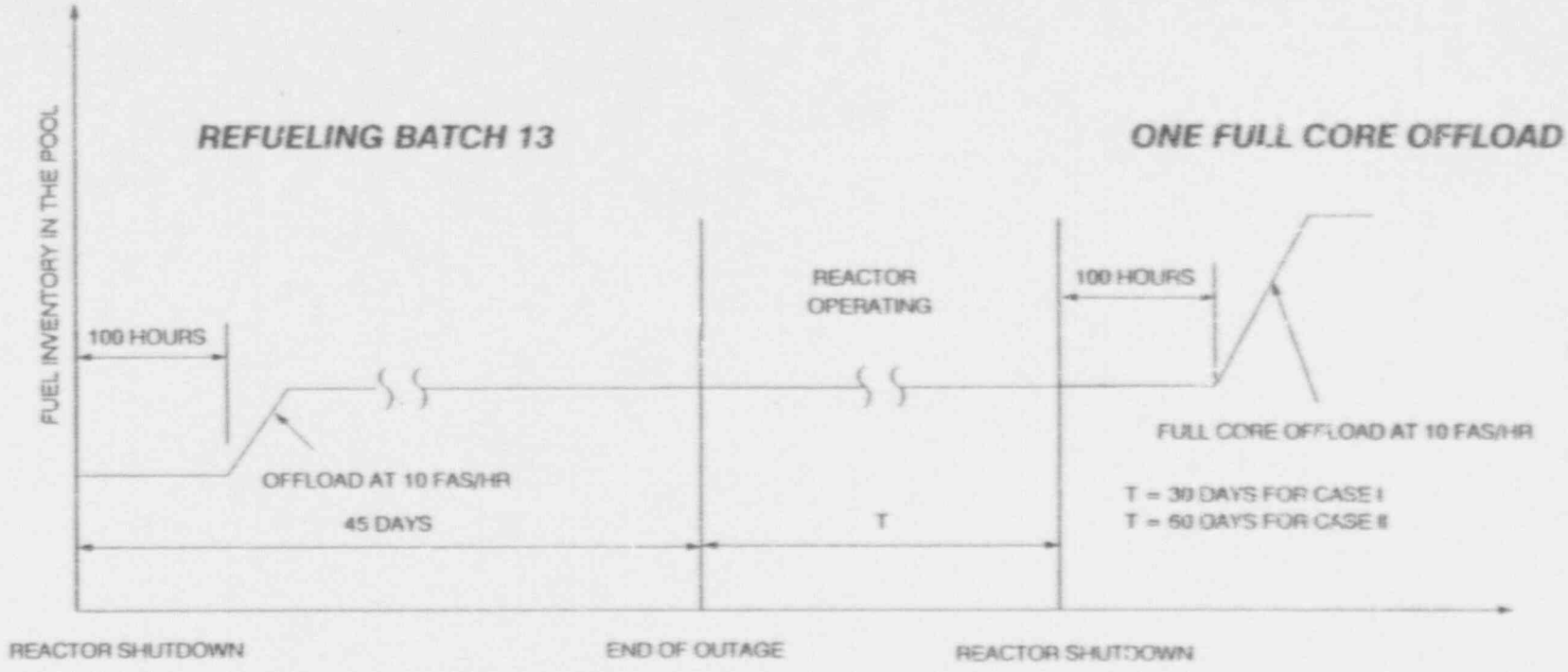

FIGURE 5.4.1 DISCHARGE SCENARIO CASE I & II

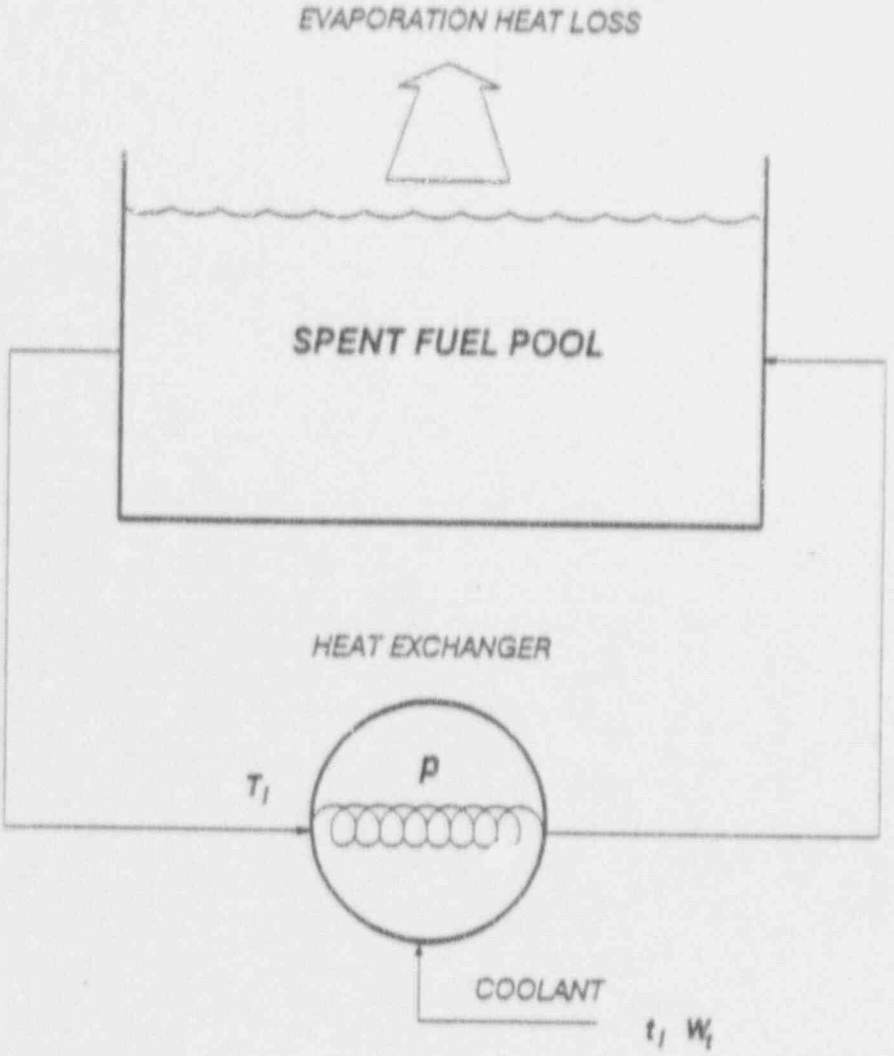

FIGURE 5.5.1 BULK POOL TEMPERATURE ANALYSIS MODEL

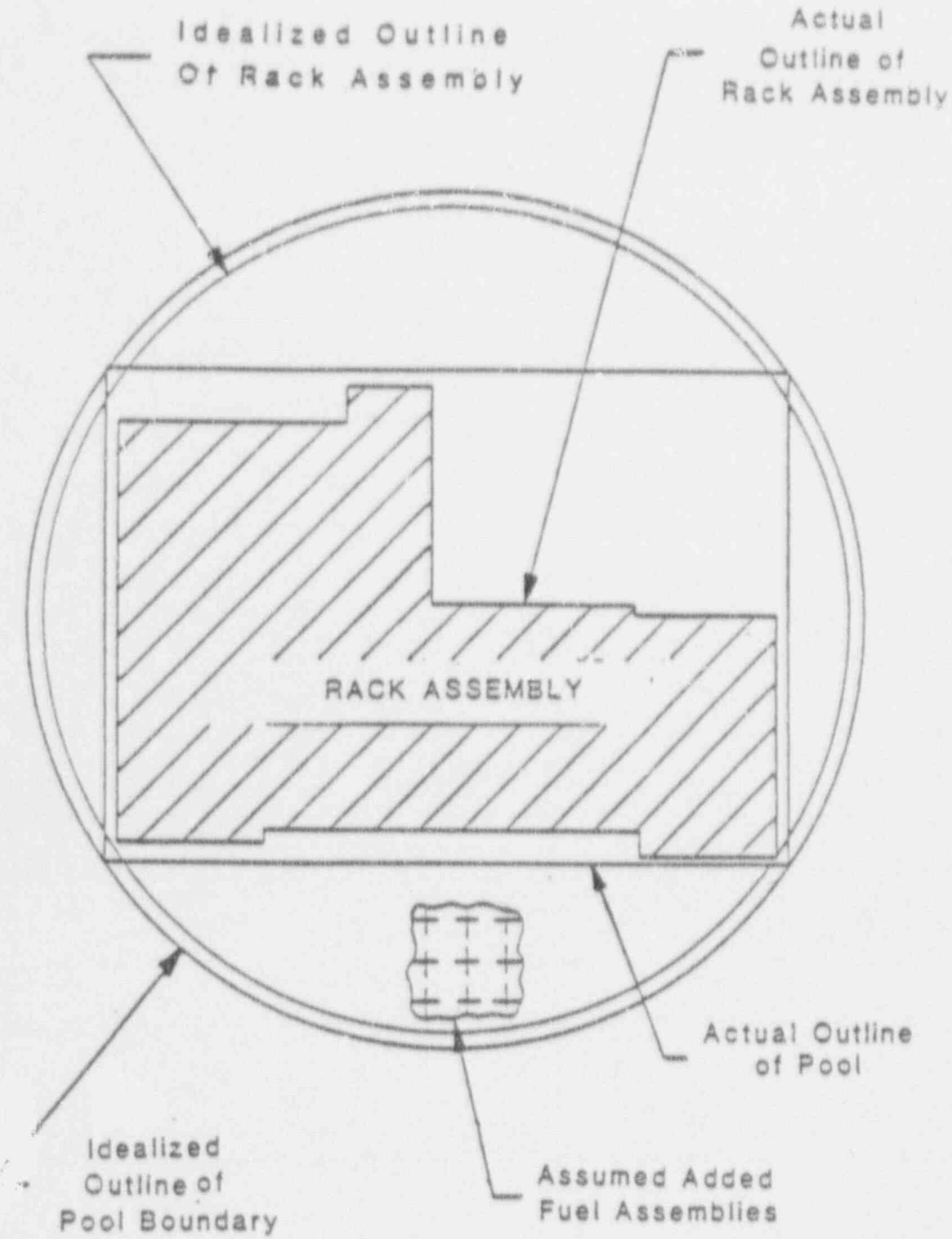

FIGURE 5.6.1 IDEALIZATION OF RACK ASSEMBLY

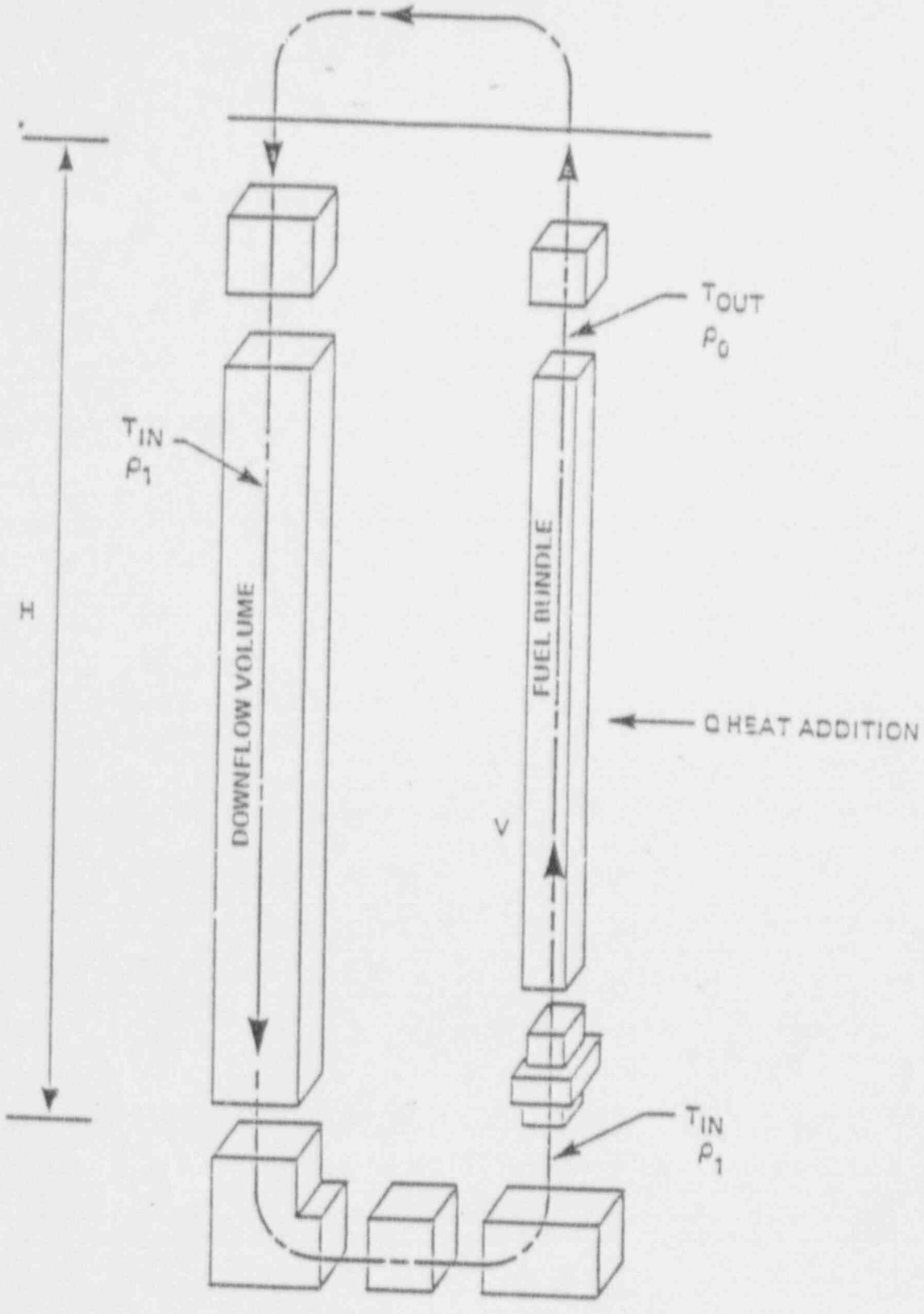

FIGURE 5.6.2 THERMAL CHIMNEY FLOW MODEL

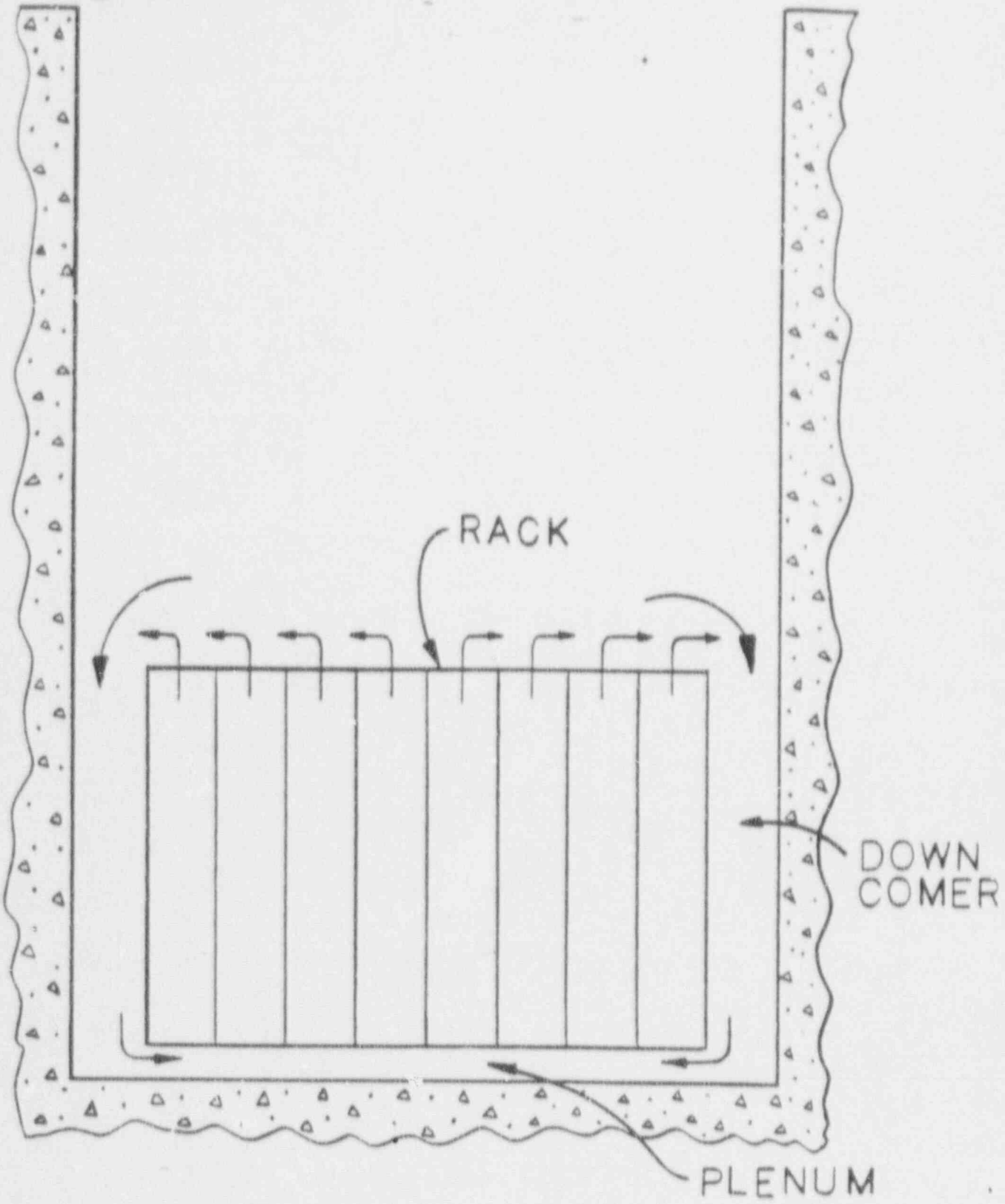

FIGURE 5.6.3 CONVECTION CURRENTS IN THE POOL

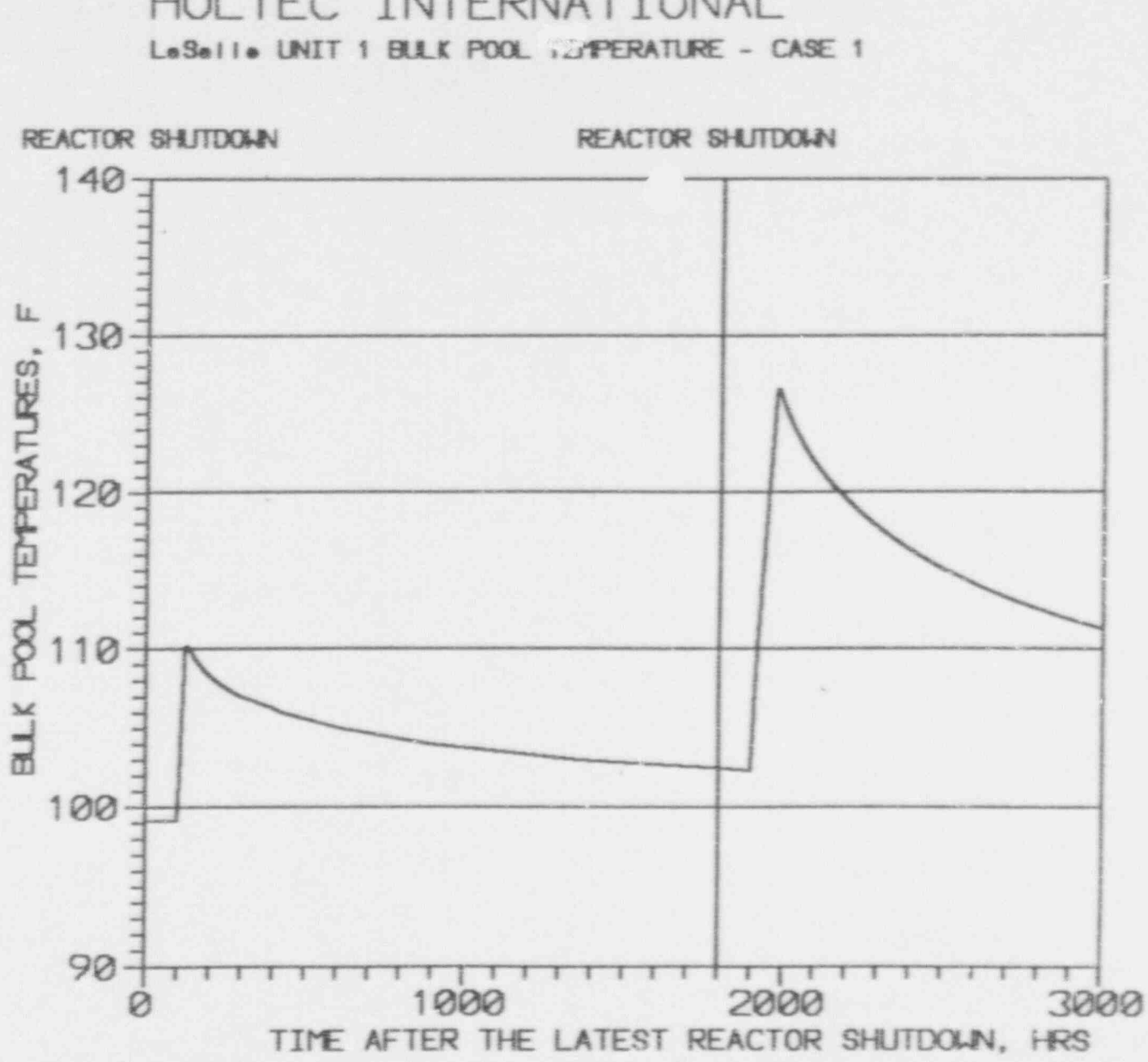
HOLTEC INTERNATIONAL
LaSalle UNIT 1 BULK POOL TEMPERATURE - CASE 1
REACTOR SHUTDOWN
REACTOR SHUTDOWN
140
130
120
110
100
90
BULK POOL TEMPERATURES, F
0
1000
2000
3000
TIME AFTER THE LATEST REACTOR SHUTDOWN, HRS

FIGURE 5.8.1

HOLTEC INTERNATIONAL

LaSalle UNIT 1 BULK POOL TEMPERATURE - CASE II

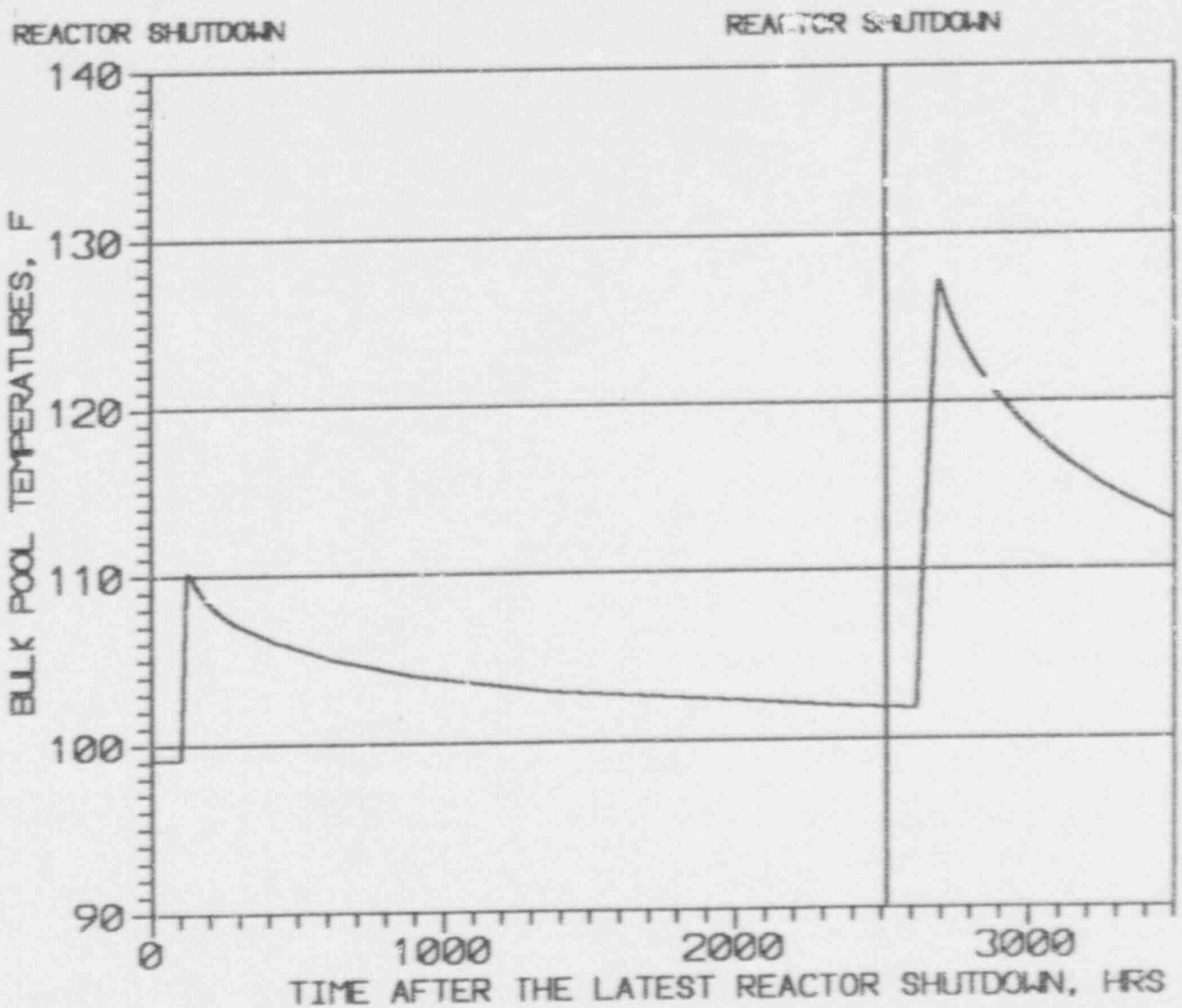

FIGURE 5.8.2

HOLTEC INTERNATIONAL

LaSalle UNIT 1 - CASE 1

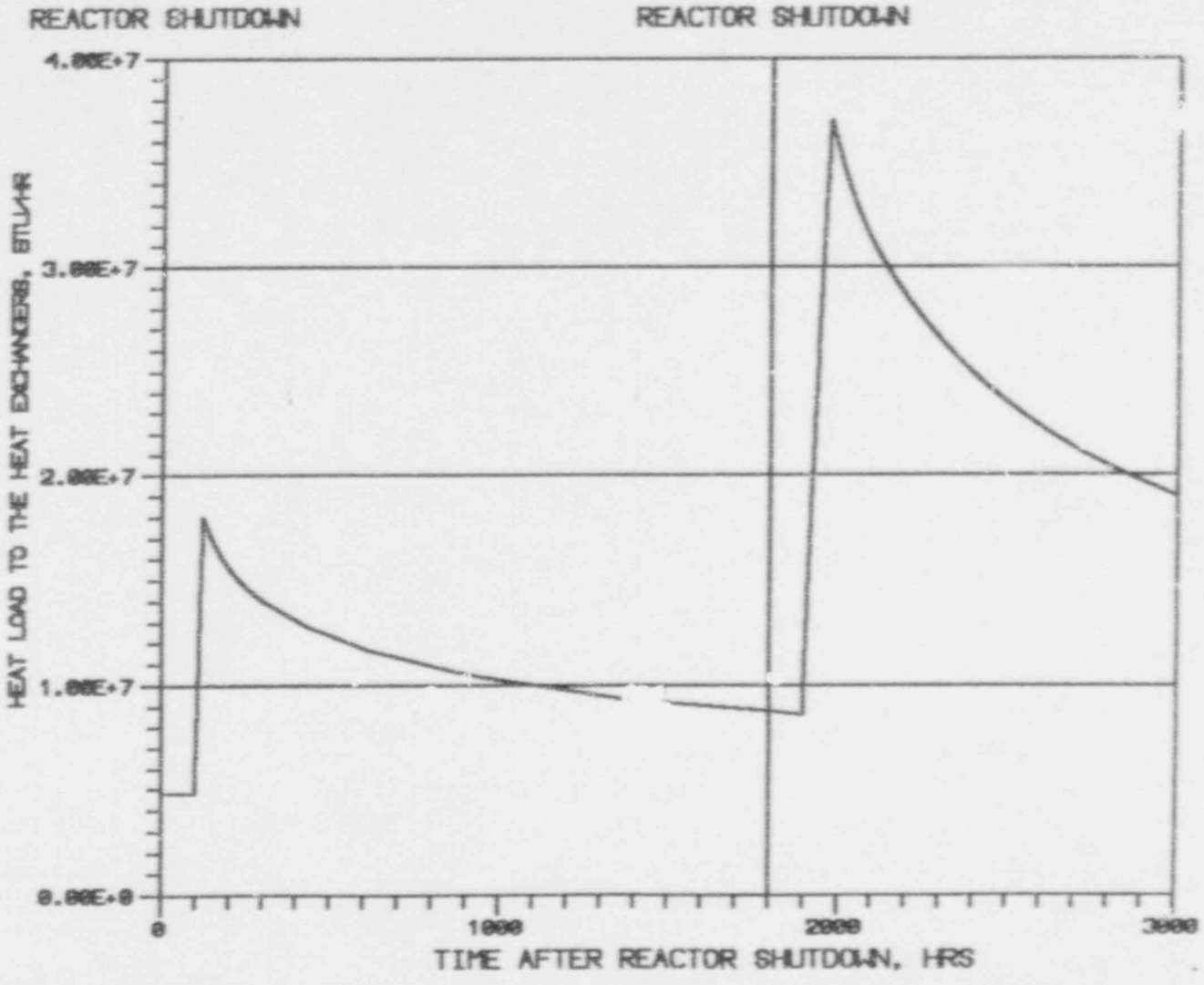

FIGURE 5.8.3

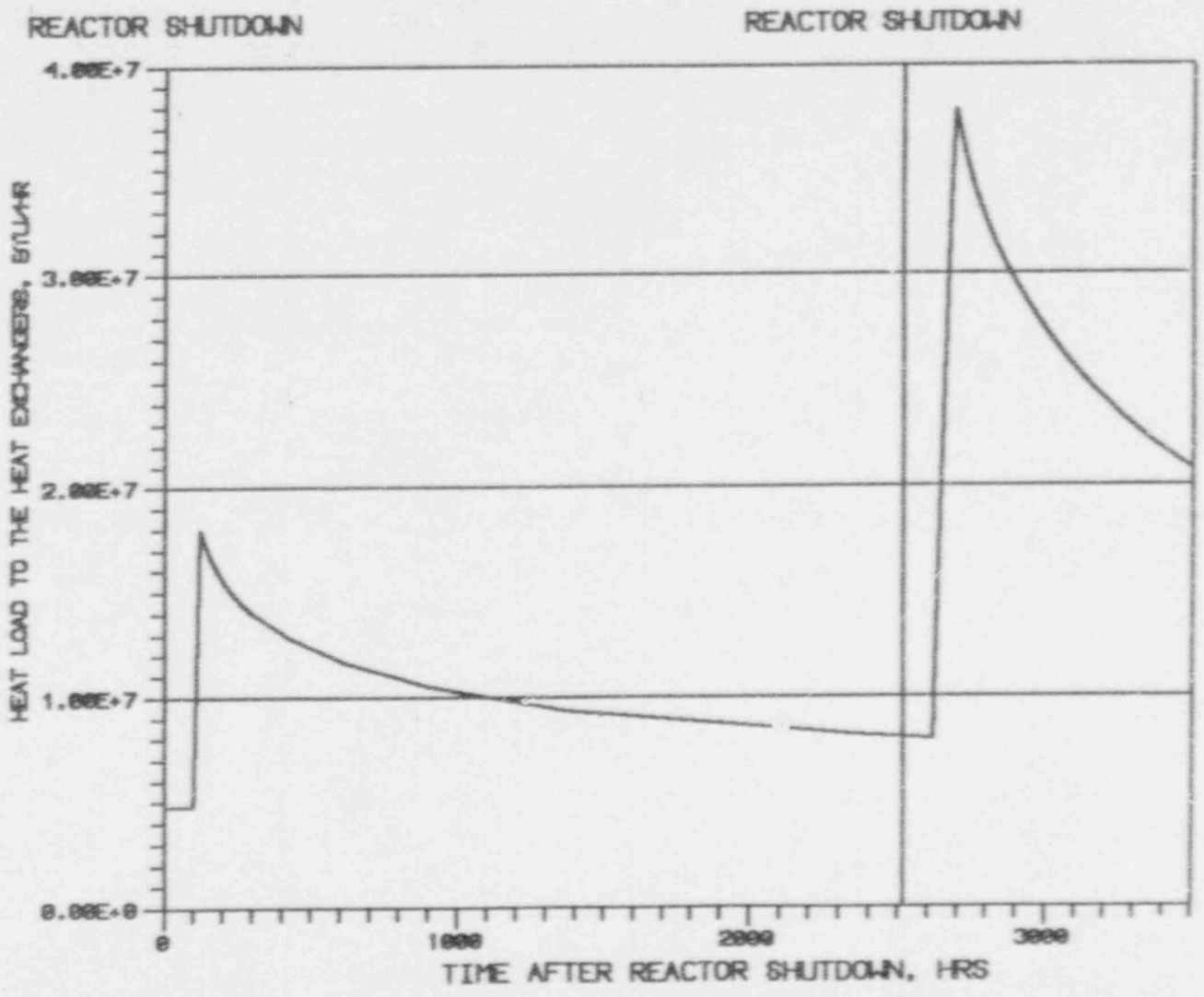
HOLTEC INTERNATIONAL
LaSalle UNIT 1 - CASE II
REACTOR SHUTDOWN
REACTOR SHUTDOWN
4.00E+7
3.00E+7
2.00E+7
1.00E+7
0.00E+0
HEAT LOAD TO THE HEAT EXCHANGERS, BTU/HR
0
1000
2000
3000
TIME AFTER REACTOR SHUTDOWN, HRS

FIGURE 5.8.4

6.0 STRUCTURAL/SEISMIC CONSIDERATIONS

6.1 Introduction

This section contains analyses to demonstrate structural adequacy of the high density spent fuel rack design under seismic loadings postulated for the plant spent fuel pool. Analyses and subsequent evaluations are in compliance with the requirements of the OT Position Paper, Section IV [6.1.1], and follow the USNRC Standard Review Plan (SRP) [6.1.2]. The dynamic analyses employ a time-history simulation code used in previous licensing efforts listed in Table 6.1.1. This section provides details of the method of analysis, modeling assumptions, numerical convergence studies and parametric evaluations performed to establish the required margins of safety.

Results reported herein show that the high density spent fuel racks are structurally and kinematically adequate to meet requirements defined in references [6.1.1], [6.1.2], and [6.1.3] with large margins of safety.

6.2 Analysis Outline

A spent fuel rack is a seismic category I structure [6.2.1]. Furthermore, it is a free-standing structure consisting of discrete storage cells which are loaded with free-standing fuel assemblies. As a result, the response of a rack module to seismic inputs is highly nonlinear involving a complex combination of motions (sliding, rocking, twisting, and turning), resulting in impacts and friction effects. Linear methods such as modal analysis and response spectrum techniques cannot accurately simulate the structural response of such a highly nonlinear structure to seismic excitation. A correct simulation is obtained only by direct integration of the nonlinear equations of motion using actual pool slab acceleration time-histories to provide the loading. Therefore, the initial step in spent fuel rack

qualification is to develop synthetic time-histories for three orthogonal directions which comply with the guidelines of USNRC SRP [6.1.2]. In particular, the synthetic time-histories must meet the criteria of statistical independence and enveloping of the design response spectra.

As stated above, a free-standing spent fuel rack, subject to a seismic loading, executes non-linear motions - even when isolated. The motion of an array of closely spaced racks in the spent fuel pool involves additional interactions due to fluid coupling between adjacent racks and between racks and adjacent walls. Further mechanical interactions between racks occur if rack-to-rack impacts take place during the event. To demonstrate structural qualification, it is required to show that stresses are within allowable limits and that displacements remain within the constraints of the contemplated design layout for the pool.

This implies that impacts between rack modules, if they occur, must be confined to locations engineered for this purpose, such as the baseplate edge and the top perimeter of the rack, above the active fuel region. Similarly, rack-to-pool wall impacts, if engineered into the rack design, (not contemplated for these racks) must be within stipulated limits. Accurate and reliable assessment of the stress field and kinematic behavior of the rack modules calls for a comprehensive and conservative dynamic model which incorporates all key attributes of the actual structure. This means that the model must feature the ability to execute concurrent sliding, rocking, bending, twisting and other motion forms available to the rack modules. Furthermore, the model must possess the capability to effect the momentum transfers which occur due to rattling of the fuel assemblies inside the storage cells and impacts of support pedestals on the bearing pads. Finally, the contribution of the water mass in the interstitial spaces around the rack modules and within storage cells must be modeled in an accurate manner because erring in the quantification

of fluid coupling on either side of the actual value is no guarantee of conservatism. The Coulomb friction coefficient at the pedestal-to-pool liner (or bearing pad) interface may lie within a rather wide range and a conservative value of friction cannot be prescribed a' priori. In fact, a perusal of results of rack dynamic analyses in numerous dockets (Table 6.1.1) indicate that an upper bound value of the coefficient of friction, μ, often maximizes the computed rack displacements as well as the equivalent elastostatic stresses. Further, the analysis must consider that a rack module may be fully or partially loaded with fuel assemblies or entirely empty. The pattern of loading in a partially loaded rack may also have innumerable combinations. In short, there are a large number of parameters with potential influence on the rack motion. A comprehensive structural evaluation should deal with all of these without sacrificing conservatism.

The 3-D single rack dynamic model introduced by Holtec International in the Enrico Fermi Unit Two rack project (ca. 1980) and used in some twenty rerack projects since that time (Table 6.1.1) tackles the above mentioned array of parameters in a most appropriate manner. The details of this classical methodology are published in the permanent literature [6.2.2] and have been widely replicated by other industry groups in recent years. Briefly speaking, the single rack 3-D model handles the array of variables as follows:

Interface Coefficient of Friction

Parametric runs are made with upper bound and lower bound values of the coefficient of friction. The limiting values are based on experimental data.

Impact Phenomena

Compression-only gap elements are used to provide for opening and closing of interfaces such as the pedestal-to-bearing pad interface.

Fuel Loading Scenarios

The fuel assemblies are conservatively assumed to rattle in unison which obviously exaggerates the contribution of impact against the cell wall. The different patterns of possible fuel assembly loadings in the rack are simulated by orienting the center of gravity column of the assemblage of fuel assemblies with respect of the module geometric centerline in an appropriate manner.

Fluid Coupling

The contribution of fluid coupling forces is ascertained by prescribing the motion of the racks (adjacent to the one being analyzed). The most commonly used assumption is that the adjacent racks vibrate out-of-phase with respect to the rack being analyzed.

Despite the above simplifying assumptions, targeted for accuracy and conservatism, a large menu of cases is run to foster confidence in the calculated safety margins. Most of the safety analyses reported in the previous dockets (Table 6.1.1) over the past decade have relied on a single rack 3-D model. From a conceptual standpoint, all aspects of the 3-D single rack model are satisfactory except for the fluid coupling effect. One intuitively expects the relative motion of the free-standing racks in the pool to be poorly correlated, given the random harmonics in the impressed slab motion. Single rack analyses cannot model this interactive behavior between racks. However, as described later, analytical and experimental research in this field has permitted rack analyses to be extended to all racks in the pool simultaneously. Holtec International had successfully extended Fritz's classical two body fluid coupling model to multiple bodies and utilized it to perform the first two dimensional multi-rack analysis (Diablo Canyon, ca. 1987). Subsequently, laboratory experiments were conducted to validate the multi-rack fluid coupling theory. This technology was incorporated in the computer code DYNARACK which now can treat simultaneous simulation of all racks in the pool. This development marked a pivotal expansion in the rack structural modeling capability and was first utilized in Chin Shan, Oyster Creek and Shearon Harris plants [6.2.3]. The Whole Pool Multi-Rack (WPMR) 3-D analyses have corroborated the uncanny accuracy of the single rack 3-D solutions in predicting the maximum structural stresses. The multi-rack analyses also serve to improve predictions of rack kinematics.

In order to ensure utmost confidence in the results of structural safety analyses, we present results for both single rack 3-D and Whole Pool Multi-Rack (WPMR) 3-D analyses. The intent of this parallel approach is to foster added confidence and to uncover any peculiarities in the dynamic response which are germane to the structural safety of the storage system.

In the following, we summarize the sequence of model development and analysis steps that are undertaken. Subsequent subsections provide model detail, limiting criteria for stress and displacement, and results of the analyses.

a. Prepare three-dimensional dynamic models of individual fuel racks which embody all elastostatic characteristics and structural nonlinearities of the plant specific free-standing rack modules.

b. Perform 3-D dynamic analyses on limiting module geometry types (from all those present in the spent fuel pool) and include various physical conditions (such as coefficient of friction, extent of cells containing fuel assemblies, and proximity of other racks).

c. Perform detailed stress analysis for the limiting case of all the dynamic analysis runs made in the foregoing steps. Demonstrate compliance with ASME Code Section III, subsection NF [6.1.3] limits on stress and displacement.

d. Calculate hydrodynamic mass contributions based on a model of the whole pool which incorporates all of the rack-to-rack and rack-to-wall spaces. This fluid model satisfies all required classical fluid mechanics principles.

e. Prepare a whole pool multi-rack dynamic model which includes all rack modules in the pool, and includes all fluid coupling interactions among them, as well as fluid coupling interactions between racks and pool walls. This 3-D simulation is referred to as a Whole Pool Multi-Rack (WPMR) model.

f. Perform 3-D Whole Pool Multi-Rack (WPMR) analyses to demonstrate that all kinematic criteria for the spent fuel rack modules are satisfied, and that resultant structure loads confirm the validity of the structural qualification. The principal kinematic criteria are (i) no rack-to-pool wall impact, and (ii) no rack-to-rack impact in the cellular region of the racks.

6.3 Artificial Time-Histories

6.3.1 Time-History Generation

Section 3.7.1 of the SRP [6.1.2] provides guidelines for establishing seismic time-histories. Subsection 3.7.1.II.1.b gives applicable criteria for generation of time-histories from design response spectra.

A generated artificial time-history is acceptable if the response spectrum in the free field at the specified level of the site, obtained from the generated time-history, envelops the design response spectrum at the same location for all damping values used in the analysis.

The acceptance criterion for spectrum enveloping is that no more than five points of the spectrum obtained from the time-history fall below, and no more than 10% below, the design response spectrum. The SRP states that an acceptable method of comparison is to choose a set of frequencies such that each frequency is within 10% of the previous one. The nature of the spent fuel rack structure is such that primary response is to excitations above 5-8 HZ. Within the 5-33HZ range, discrete check points are established from the above 10% criterion.

Generated artificial time-histories must also be statistically independent. Any two time-histories are considered to be statistically independent if their normalized correlation coefficient is less than 0.15.

Figures 6.3.1 - 6.3.6 show the three statistically independent synthetic time-histories generated at the pool slab level for two conditions, denoted for the La Salle plant as Levels B and C seismic conditions. 2% damping is associated with the Level B (UCBV) event and 4% damping is used for the Level C (FCBV) event [6.3.1]. The notations UCBV and FCBV are those used by

Commonwealth Edison in their Specification. The service Levels B and C dynamic input motion to the pool and the racks have been obtained by combining various SRV and LOCA spectra with the seismic OBE and SSE in-structure spectra. Note that the Level B designation used at this plant corresponds to Level B of [6.1.3] and that the Level C CECo designation corresponds to Level D of [6.1.3]. GENEQ [6.3.2] is used to generate three synthetic, statistically independent time-histories for two horizontal and the vertical directions, respectively, from the given design response spectra. The comparisons of the original response spectra and response spectra regenerated using the synthetic time-histories are shown in Figures 6.3.7-6.3.9 for the Level B event, and in Figures 6.3.10-6.3.12 for the Level C event. It is noted that the time-histories satisfy all USNRC bounding requirements and are therefore inherently conservative.

The normalized correlation coefficients p_{ij} between time-histories i and j are provided in Tables 6.3.1 and 6.3.2 and demonstrate compliance with the statistical independence requirement for both the CECo designated Level B (UCBV) and the CECo designated Level C (FCBV) event.

The enveloping requirement on the derived spectra and statistical noncoherence of artificial motions are satisfied.

6.3.2 Soil Structure Interaction

In addition to the conservatism built in the synthetic time-histories described in the foregoing, the mother spectra themselves have a large element of conservatism.

Seismic soil structure interaction (SSI) has been an evolving state-of-the-art during the last twenty years. The SSI analysis method used for La Salle plant is consistent with the present methodology, except that the control motion (seismic input motion in the free field) was

assumed at the foundation level. The assumption was according to the criteria given in the then available edition of SRP 3.7.2.

It is currently recognized that the above definition of control motion is a conservative criteria. During the NRC sponsored Workshop on SSI at Bethesda in 1986 [6.3.3], the experts and the panelists unanimously emphasized that the control motion should be defined at the ground surface. This criteria was endorsed in the ASCE Standard ASCE 4-86 [6.3.4] and also in the EPRI/NRC/TPC Workshop on Seismic Soil-Structure-Interation Analysis Techniques using data from Lotung, Taiwan, held at Palo Alto, California in December 1987. Subsequently, SRP 3.7.1 and SRP 3.7.2, 1989, adopted the control motion definition at the ground surface.

The La Salle soil site is such that if a surface definition of the control motion is used in the SSI analysis, the foundation level spectrum at the building's major contributing frequencies will be lower than the foundation level design basis input spectrum. It is conservatively estimated that this will result in about 25% reduction in the building response, i.e., the design basis in-structure response spectra are about 25% conservative.

The above estimate is based on the results of a study documented in Figures Q 130.23-2 of Amendment 49, May 1980 of La Salle FSAR. In response to NRC request, SSI analysis was also performed using Compliance Function approach, in addition to design basis Finite Element approach. By the time this study was done, it was recognized that the control motion should be defined at the ground surface, instead of the foundation level. Hence, in the Compliance Function approach, the control motion was defined at the ground surface (Plant grade level). Soil properties variation was also considered in this study. The above referred figures show that the design basis spectral amplitudes at the building foundation, for the predominant building frequencies, are about 30% to 50% higher than the results obtained from Compliance Function

approach. From this comparison, it is conservatively estimated that the design basis in-structure response spectra have 25% conservatism built into them.

6.4 Rack Modeling for Dynamic Simulations

6.4.1 General Remarks

Spent fuel storage racks are Seismic Class I equipment. They are required to remain functional during and after a CECo designated Level C (FCBV) event. The racks are free-standing; they are neither anchored to the pool floor nor attached to the sidewalls. Individual rack modules are not interconnected. Figure 6.4.1 shows a pictorial view of a typical module. The baseplate extends beyond the cellular region envelope ensuring that inter-rack impacts, if any occur at the baseplate level, occur in an area that is structurally qualifiable to withstand any large in-plane impact loads. Not shown in Figure 6.4.1 is an additional impact protection structure around the rack top (above the active fuel region) that is added to provide additional structure to where rack-to-rack impacts occur.

A rack may be completely loaded with fuel assemblies (which corresponds to greatest total mass), or it may be completely empty. The coefficient of friction, μ, between pedestal supports and pool floor is indeterminate. According to Rabinowicz [6.4.1], results of 199 tests performed on austenitic stainless steel plates submerged in water show a mean value of μ to be 0.503 with standard deviation of 0.125. Upper and lower bounds (based on twice standard deviation) are 0.753 and 0.253, respectively. Analyses are therefore performed for coefficient of friction values of 0.2 (lower limit) and for 0.8 (upper limit), and for random friction values clustered about a mean of 0.5. The bounding values of μ = 0.2 and 0.8 have been found to bracket the upper limit of module response in previous rerack projects.

Since free-standing racks are not anchored to the pool slab, not attached .to the pool walls, and not interconnected, they can execute a wide variety of motions. Racks may slide on the pool floor, one or more rack support pedestals may momentarily tip and lose contact with the floor slab liner, or racks may exhibit a combination of sliding and tipping. The structural models developed permit simulation of these kinematic events with inherent built-in conservatisms. The rack models also include components for simulation of potential inter-rack and rack-to-wall impact phenomena. Lift-off of support pedestals and subsequent liner impacts are modeled using impact (gap) elements, and Coulomb friction between rack and pool liner is simulated by piecewise linear (friction) elements. Rack elasticity, relative to the rack base, is included in the model with linear springs representing a beam like action. These special attributes of rack dynamics require strong emphasis on modeling of linear and nonlinear springs, dampers, and compression only gap elements. The term "nonlinear spring" is a generic term to denote the mathematical element representing the case where restoring force is not linearly proportional to displacem nt. In the fuel rack simulations, the Coulomb friction interface between rack support pedestal and liner is typical of a nonlinear spring. The mathematical development for these nonlinear springs is described in Ref. [6.4.2].

3-D dynamic analyses of single rack modules require a key modeling assumption. This relates to location and relative motion of neighboring racks. The gap between a peripheral rack and adjacent pool wall is known, with motion of the wall prescribed. However, another rack, adjacent to the rack being analyzed, is also free-standing and subject to motion during a seismic event. To conduct the seismic analysis of a given rack, its physical interface with neighboring modules must be specified. The standard procedure in analysis of a single rack module is that neighboring racks move 180° out-of-phase in relation to the subject rack. Thus, the

available gap before inter-rack impact occurs is 50% of the physical gap. This "opposed phase motion" assumption increases likelihood of intra-rack impacts and is thus conservative. However, it also increases the relative contribution of fluid coupling, which depends on fluid gaps and relative movements of bodies, making overall conservatism a less certain assertion. 3-D Whole Pool Multi-Rack analyses carried ou for Taiwan Power Company's Chin Shan Station, and for GPU Nuclear's Oyster Creek Nuclear Station demonstrate that single rack simulations predict smaller rack displacement during seismic responses. Nevertheless, 3-D analyses of single rack modules permit detailed evaluation of stress fields, and serve as a benchmark check for the much more involved, WPMR analysis.

Particulars of modeling details and assumptions for 3-D Single Rack analysis and for Whole Pool Multi-Rack analysis are given in the following subsections.

6.4.2 The 3-D 22 DOF Model for Single Rack Module

6.4.2.1 Assumptions

a. The fuel rack structure is very rigid; motion is captured by modeling the rack as a twelve degree-of-freedom structure. Movement of the rack cross-section at any height is described by six degrees-of-freedom of the rack base and six degrees-of-freedom at the rack top. Rattling fuel assemblies within the rack are modeled by five lumped masses located at H, .75H, .5H, .25H, and at the rack base (H is the rack height measured above the baseplate). Each lumped fuel mass has two horizontal displacement degrees-of-freedom. Vertical motion of the fuel assembly mass is assumed equal to rack vertical motion at the baseplate level. The centroid of each fuel assembly mass can be located off center, relative to the rack structure centroid at that level, to simulate a partially loaded rack.

b. Seismic motion of a fuel rack is characterized by random rattling of fuel assemblies in their individual storage locations. All fuel assemblies are assumed to move in-phase within a rack. This exaggerates computed dynamic loading on the rack structure and therefore yields conservative results.

c. Fluid coupling between rack and fuel assemblies, and between rack and wall, is simulated by appropriate inertial coupling in the system kinetic energy. Inclusion of these effects uses the methods of [6.4.3] and [6.4.4] for rack/assembly coupling and for rack-to-rack coupling, respectively. Fluid coupling terms for rack-to-rack coupling are based on opposed phase motion of adjacent modules.

d. In the dynamic analysis of the spent fuel racks, the damping due to fluid interaction is conservatively neglected. That is, in the damping matrix $(C + C_h)$, where C is the structural damping associated with the rack and C_h is the effective damping due to velocity drag effects of water, C_h is assumed to be zero.

The above assumption is reasonable for large gaps between the racks. However, for very small gaps in the case of reracking this assumption is overly conservative. Both analytical and experimental results show that for small gaps the damping is not small. The damping is estimated to be more than 5%, for the gap dimensions of La Salle reracking. Hence, additional conservatism has been introduced in the rack dynamic analysis by neglecting this damping effect. Because the hydrodynamic masses are very large, the conservatism introduced by neglecting the damping due to fluid interaction is expected to be substantial.

e. Sloshing is negligible at the top of the rack and is neglected in the analysis of the rack.

f. Potential impacts between rack and fuel assemblies are accounted for by appropriate "compression only" gap elements between masses involved. The possible incidence of rack-to-wall or rack-to-rack impact is simulated by gap elements at top and bottom of the rack in two horizontal directions. Bottom elements are located at the baseplate elevation.

g. Pedestals are modeled by gap elements in the vertical direction and as "rigid links" for transferring horizontal stress. Each pedestal support is linked to the pool liner by two friction springs. Local pedestal spring stiffness accounts for floor elasticity and for local rack elasticity just above the pedestal.

h. Rattling of fuel assemblies inside the storage locations causes the gap between fuel assemblies and cell wall to change from a maximum of twice the nominal gap to a theoretical zero gap. Fluid coupling coefficients are based on the nominal gap, which too is known to produce conservative results [6.4.3].

6.4.2.2 Model Details

Figure 6.4.2 shows a schematic of the model. S_i ($i = 1,\ldots,4$) represent support locations, p_i represent absolute degrees-of-freedom, and q_i represent degrees-of-freedom relative to the slab. H is the height of the rack above the baseplate. Not shown in Fig. 6.4.2 are gap elements used to model pedestal/liner impact locations and impact locations with adjacent racks.

Table 6.4.1 lists the degrees-of-freedom for the single rack model. Translational and rotational degrees-of-freedom 1-6 and 17-22 describe the rack motion; rattling fuel masses (nodes 1^*, 2^*, 3^*, 4^*, 5^* in Fig. 6.4.2) are described by translational degrees-of-freedom 7-16. $U_i(t)$ represents pool floor slab displacement seismic time-history.

Figures 6.4.3 and 6.4.4, respectively, show inter-rack impact springs (to track potential for impact between racks or between rack and wall), and fuel assembly/storage cell impact springs at one location of rattling fuel assembly mass.

Figures 6.4.5, 6.4.6, and 6.4.7 show the degrees-of-freedom and the modeling technique associated with rack elasticity. In each bending plane a shear and bending spring simulate elastic effects [6.4.2]. Linear elastic springs coupling rack vertical and torsional degrees-

of-freedom are also included in the model. Additional details concerning fluid coupling and determination of stiffness elements are provided below.

6.4.2.3 Fluid Coupling Details

The "fluid coupling effect" [6.4.3],[6.4.4] is described as follows: If one body (mass m_1) vibrates adjacent to a second body (mass m_2), and both bodies are submerged in frictionless fluid, then Newton's equations of motion for the two bodies are:

$$(m_1 + M_{11})\ddot{X}_1 + M_{12}\ddot{X}_2 = \text{applied forces on mass } m_1 + O(\dot{X}_1^2)$$

$$M_{21}\ddot{X}_1 + (m_2 + M_{22})\ddot{X}_2 = \text{applied forces on mass } m_2 + O(\dot{X}_2^2)$$

$\ddot{X}_1$, $\ddot{X}_2$ denote absolute accelerations of masses m_1 and m_2, respectively, and the notation $O(\dot{X}^2)$ denotes nonlinear terms.

M_{11}, M_{12}, M_{21}, and M_{22} are fluid coupling coefficients which depend on body shape, relative disposition, etc. Fritz [6.4.4] gives data for M_{ij} for various body shapes and arrangements. The fluid adds mass to the body (M_{11} to mass m_1), and an external force proportional to acceleration of the adjacent body (mass m_2). Thus, acceleration of one body affects the force field on another. This force field is a function of interbody gap, reaching large values for small gaps. Lateral motion of a fuel assembly inside a storage location encounters this effect. For example, fluid coupling is between nodes 2 and 2* in Figure 6.4.2. The rack analysis also contains inertial fluid coupling terms which model the effect of fluid in the gaps between adjacent racks. Terms modeling effects of fluid flowing between adjacent racks are computed assuming that all racks adjacent to the rack being analyzed are vibrating 180^0 out of phase from the rack being analyzed. Thus, the modeled rack is enclosed by a hydrodynamic mass computed as if there were a plane of symmetry located in the

middle of the gap region. Rack-to-rack gap elements (Figure 6.4.3) have initial gaps set to 50% of the physical gap to reflect this symmetry.

6.4.2.4 Stiffness Element Details

The cartesian coordinate system associated with the rack has the following nomenclature:

x = Horizontal coordinate along the short direction of rack rectangular planform

y = Horizontal coordinate along the long direction of the rack rectangular planform

z = Vertical coordinate upward from the rack base

Table 6.4.2 lists all spring elements used in the 3-D 22 DOF single rack model.

If the simulation model is restricted to two dimensions (one horizontal motion plus vertical motion, for example), for the purposes of model clarification only, then a descriptive model of the simulated structure which includes gap and friction elements is shown in Figure 6.4.8. This simpler model is used to elaborate on the various stiffness modeling elements.

Gap elements modeling impacts between fuel assemblies and rack have local stiffness K_I in Figure 6.4.8. In Table 6.4.2, for example, gap elements 5 through 8 act on the rattling fuel mass at the rack top. Support pedestal spring rates K_S are modeled by elements 1 through 4 in Table 6.4.2. Local compliance of the concrete floor is included in K_S. Friction elements 2 plus 8 and 4 plus 6 in Table 6.4.2 are shown in Figure 6.4.8. Friction at support/liner interface is modeled by the piecewise linear friction springs with suitably large stiffness K_f up to the limiting lateral load, μN, where N is the current compression load at the interface between support and liner. At every time step

during transient analysis, the current value of N (either zero if the pedestal has lifted-off the liner, or a compressive finite value) is computed. Finally, support rotational friction springs K_R may be included to reflect any rotational restraint that may be offered by the foundation. The rotational friction spring rate is calculated using a modified Bousinesq equation [6.4.2] and is included to simulate resistive moment by the slab to counteract rotation of the rack pedestal in a vertical plane. The nonlinearity of these springs (friction elements 9, 11, 13, and 15 in Table 6.4.2) reflects the edging limitation imposed on the base of the rack support pedestals and the shift in location of slab resistive load as the rack pedestal rotates.

The gap element K_S, modeling the effective compression stiffness of the structure in the vicinity of the support, includes stiffness of the pedestal, local stiffness of the underlying pool slab, and local stiffness of the rack cellular structure above the pedestal.

The previous discussion is limited to a 2-D model solely for simplicity. Actual analyses incorporate 3-D motions and include all stiffness elements listed in Table 6.4.2.

6.4.3 Whole Pool Multi-Rack (WPMR) Model

6.4.3.1 General Remarks

The single rack 3-D (22 DOF) model outlined in the preceding subsection is used to evaluate structural integrity, physical stability, and to initially assess kinematic compliance (no rack-to-rack impact in the cellular region) of the rack modules. Prescribing the motion of the racks adjacent to the module being analyzed is an assumption in the single rack simulations. For closely spaced racks, demonstration of kinematic compliance is further confirmed by modeling all modules in one comprehensive simulation using a Whole Pool Multi-Rack (WPMR) model. In WPMR

analysis, all racks are modeled, and their correct fluid interaction is included in the model.

6.4.3.2 Whole Pool Fluid Coupling

The presence of fluid moving in the narrow gaps between racks and between racks and pool walls causes both near and far field fluid coupling effects. A single rack simulation can effectively include only hydrodynamic effects due to contiguous racks when a certain set of assumptions is used for the motion of contiguous racks. In a Whole Pool Multi-Rack analysis, far field fluid coupling effects of all racks are accounted for using the correct model of pool fluid mechanics. The external hydrodynamic mass due to the presence of walls or adjacent racks is computed in a manner consistent with fundamental fluid mechanics principles [6.4.5] using conservative nominal fluid gaps in the pool at the beginning of the seismic event. Verification of the computed hydrodynamic effect by comparison with experiments is also provided in [6.4.5]. This formulation has been reviewed and approved by the Nuclear Regulatory Commission during post-licensing multi-rack analyses for the Diablo Canyon Unit I and II reracking project. The fluid flow model used to obtain the whole pool hydrodynamic effect reflects actual gaps and rack locations.

6.4.3.3 Coefficients of Friction

To eliminate the last significant element of uncertainty in rack dynamic analyses, the friction coefficient is ascribed to the support pedestal/pool bearing pad interface consistent with Rabinowicz's data [6.4.1]. Friction coefficients, developed by a random number generator with Gaussian normal distribution characteristics, are imposed on each pedestal of each rack in the pool. The assigned values are then held constant during the

entire simulation in order to obtain reproducible results.* Thus, the WPMR analysis can simulate the effect of different coefficients of friction at adjacent rack pedestals.

6.4.3.4 Modeling Details

Figure 6.4.9 shows a planform view of the spent fuel pool which includes rack and pedestal numbering scheme and the global coordinate system used for the WPMR analysis. Tables 2.1.2 and 2.1.3 give details on number of cells per rack, and on rack weights. In Whole Pool Multi-Rack analysis, each rack structure, together with contained fuel, is modeled as an eight degree-of-freedom system. Six degrees-of-freedom model the rack behavior and two degrees-of-freedom model the behavior of the rattling fuel. The portion of fuel assumed to rattle is chosen so as to match displacement maximum values predicted from a 22 DOF single rack analysis of the same configuration.

The Whole Pool Multi-Rack model includes gap elements representing compression only pedestals, representing impact potential at fuel assembly-fuel rack interfaces, and at rack-to-rack or rack-to-wall locations at top and bottom corners of each rack module. Each pedestal has two friction elements associated with force in the vertical compression element. Values used for spring constants for the various stiffness elements reflect values used in the single rack analyses. For any given fuel pool loading

---

* Note that DYNARACK has the capability to change the coefficient of friction at any pedestal at each instant of contact based on a random reading of the PC-clock cycle. However, exercising this option would yield results that could not be reproduced. Therefore, the random choice of coefficients is made only once per run.

configuration, a WPMR analysis yields time-histories of the motion of each rack, time-histories of the loads transmitted to the spent fuel pool slab, and time-histories of the hydrodynamic pressures applied to the walls.

6.5 Acceptance Criteria, Stress Limits, and Material Properties

6.5.1 Acceptance Criteria

There are two sets of criteria to be satisfied by the rack modules:

a. Kinematic Criteria

The rack must be a physically stable structure and it must be demonstrated that there are no inter-rack impacts in the active fuel region of the cellular structure. The criteria for physical stability is that an isolated rack in water exhibit no overturning tendency when a seismic event of magnitude 1.1 x Faulted condition event is applied [6.1.2].

b. Stress Limit Criteria

Stress limits must not be exceeded under certain load combinations. The following loading combinations are applicable [6.1.3] for La Salle Unit 1.

Loading Combination	Service Level
$D + L$ $D + L + T_o$ $D + L + T_o + E$	Level A
$D + L + T_a + E$ $D + L + T_o + P_f$	Level B
$D + L + T_a + E'$ $D + L + F_d$	Faulted condition (maintain functional capability)

Abbreviations are those used in Section 3.8.4 of the Standard Review Plan and the "Review and Acceptance of Spent Fuel Storage and Handling Applications" section:

D = Dead weight-induced internal moments (including fuel assembly weight)

L = Live Load (not applicable for the fuel rack, since there are no moving objects in the rack load path).

F_d = Force caused by the accidental drop of the heaviest load from the maximum possible height (see Chapter 7 of this report).

P_f = Upward force on the racks caused by postulated stuck fuel assembly (see Chapter 7).

E = CECo designated UCBV Event

E' = CECo designated FCBV Event

T_o = Differential temperature induced loads (normal operating or shutdown condition based on the most critical transient or steady state condition).

T_a = Differential temperature induced loads (the highest temperature associated with the postulated abnormal design conditions).

T_a and T_o cause local thermal stresses to be produced. For fuel rack analysis, only one scenario need be examined. The worst situation is obtained when an isolated storage location has a fuel assembly generating heat at maximum postulated rate and surrounding storage locations contain no fuel. Heated water makes unobstructed contact with the inside of the storage walls, thereby producing maximum possible temperature difference between adjacent cells. Secondary stresses produced are limited to the body of the rack; that is, support pedestals do not experience secondary (thermal) stresses. For rack qualification, T_o, T_a are the same.

6.5.2 Stress Limits for Various Conditions

Stress limits are derived from the ASME Code, Section III, Subsection NF [6.1.3]. Parameters and terminology are in accordance with the ASME Code.

6.5.2.1 Normal and Upset Conditions (Level A or Level B)

a. Allowable stress in tension on a net section is:

$F_t = 0.6\ S_y$ (S_y = yield stress at temperature)

(F_t is equivalent to primary membrane stress)

b. Allowable stress in shear on a net section is:

$F_v = .4\ S_y$

c. Allowable stress in compression on a net section

$$F_a = \frac{\left[1 - \frac{(kl)^2}{r^2} / 2C_c^2\right] S_y}{\left\{\left(\frac{5}{3}\right) + \left[3\left(\frac{kl}{r}\right)/8C_c\right] - \left[\left(\frac{kl}{r}\right)^3 / 8C_c^3\right]\right\}}$$

where:

$$C_c = \left[\frac{(2\pi^2 E)}{S_y}\right]^{1/2}$$

l = unsupported length of component

k = length coefficient which gives influence of boundary conditions; e.g.
k = 1 (simple support both ends)
= 2 (cantilever beam)
= 1/2 (clamped at both ends)

E = Young's Modulus

r = radius of gyration of component

kl/r for the main rack body is based on the full height and cross section of the honeycomb region.

d. Maximum allowable bending stress at the outermost fiber of a net section, due to flexure about one plane of symmetry is:

$F_b = 0.60\ S_y$
(equivalent to primary bending)

e. Combined flexure and compression on a net section satisfies:

$$\frac{f_a}{F_a} + \frac{C_{mx}\, f_{bx}}{D_x F_{bx}} + \frac{C_{my} f_{by}}{D_y F_{by}} \leq 1$$

where:

f_a = Direct compressive stress in the section

f_{bx} = Maximum flexural stress along x-axis

f_{by} = Maximum flexural stress along y-axis

$C_{mx} = C_{my} = 0.85$

$$D_x = 1 - \frac{f_a}{F'_{ex}}$$

$$D_y = 1 - \frac{f_a}{F'_{ey}}$$

$$F'_{ex,ey} = \frac{12\ \pi^2\ E}{23 \left(\frac{kl}{r} \right)^2_{x,y}}$$

and subscripts x,y reflect the particular bending plane.

f. Combined flexure and compression (or tension) on a net section:

$$\frac{f_a}{0.6S_y} + \frac{f_{bx}}{F_{bx}} + \frac{f_{by}}{F_{by}} \leq 1$$

The above requirements are to be met for both direct tension or compression.

6.5.2.2 Faulted Condition Service Limits

Section F-1370 (ASME Section III, Appendix F), states that limits for the Faulted condition are the minimum of 1.2 (S_y/F_t) or ($0.7S_u/F_t$) times the corresponding limits for the Level A condition. S_u is ultimate tensile stress at the specified rack design temperature. For example, if the material is such that $1.2S_y$ is less than $0.7S_u$, then the multiplier on the Level A limits, to obtain Faulted limits, is 2.0.

6.5.2.3 Dimensionless Stress Factors

Stress results are presented in dimensionless form. Dimensionless stress factors are defined as the ratio of the actual developed stress to the specified limiting value. Stress factors are only developed for the single rack analyses. The limiting value of each stress factor is 1.0 for the UCBV event and 2.0 (or less) for the Level FCBV (Faulted condition) event. Stress factors reported are:

R_1 = Ratio of direct tensile or compressive stress on a net section to its allowable value (note pedestals only resist compression.

R_2 = Ratio of gross shear on a net section in the x-direction to its allowable value.

R_3 = Ratio of maximum bending stress due to bending about the x-axis to its allowable value for the section.

R_4 = Ratio of maximum bending stress due to bending about the y-axis to its allowable value for the section.

R_5 = Combined flexure and compressive factor (as defined in 6.5.2.1e above)

R_6 = Combined flexure and tension (or compression) factor (as defined in 6.5.2.1f)

R_7 = Ratio of gross shear on a net section in the y-direction to its allowable value.

6.5.3 Material Properties

Physical properties of the rack and support materials, obtained from the ASME Boiler & Pressure Vessel Code, Section III, appendices, are listed in Table 6.5.1. Maximum pool bulk temperature is less than 200°F; this is used as the reference design temperature for evaluation of material properties. Stress limits for Levels A and Faulted, corresponding to conditions in Section 6.5.2 above, are evaluated using given yield strength data.

6.6 Governing Equations of Motion

Using the structural model for either a 22 DOF single rack analysis, or for the entire set of fuel racks that comprise a Whole Pool Multi-Rack model, equations of motion corresponding to each degree of freedom are obtained using Lagrange's Formulation [6.6.1]. The system kinetic energy includes contributions from solid structures and from trapped and surrounding fluid. The final system of equations obtained have the matrix form:

$$[M] \{q''\} = \{Q\} + \{G\}$$

where:

- $[M]$ - total mass matrix (including structural and fluid mass contributions);
- $\{q\}$ - the nodal displacement vector relative to the pool slab displacement; (double prime stands for second derivatives with respect to time);
- $\{G\}$ - a vector dependent on the given ground acceleration;
- $\{Q\}$ - a vector dependent on the spring forces (linear and nonlinear) and the coupling between degrees-of-freedom

The equations can be rewritten as:

$$\{q''\} = [M]^{-1} \{Q\} + [M]^{-1} \{G\}$$

This equation set is mass uncoupled, displacement coupled at each instant in time; numerical solution uses a central difference scheme built into the proprietary, computer program "DYNARACK" [6.6.2 - 6.6.5]. As indicated earlier, this program has been used in the licensing effort for a considerable number of reracking projects.

DYNARACK has been validated against exact solutions, experimental data, and solutions obtained using alternate numerical schemes [6.6.5]. These solutions are chosen to exercise all features of DYNARACK. It is demonstrated there that well known classical nonlinear phenomena (subharmonic resonance, bifurcation, stick-slip) can be reproduced using DYNARACK.

The application of DYNARACK to the spent fuel rack analysis requires the establishment of a time step to ensure convergence and stability of the results. DYNARACK utilizes the classical central difference algorithm [6.4.2]. Stability of the results is assured as long as the time step is significantly below the smallest period of the equivalent linear problem. Convergence is obtained by performing a series of rack analyses with different time steps to ascertain the upper limit on time step that will provide converged results. This is done by taking a typical rack module and subjecting it to the given time-histories using different integration time steps. Once an appropriate time step is determined, it is used in subsequent simulations.

Results of the dynamic simulations are time-history response of all degrees-of-freedom of the particular model, and of all forces and moments at important sections of the structure. From these results, maximum movements and stresses can be ascertained for the event, and appropriate structural qualifications can be carried out. Where required, DYNARACK automatically tracks maximum values of dimensionless factors R_1 to R_7 defined above in Section 6.5, and reports results for the entire rack cross section just above

the baseplate and for each pedestal cross section just below the baseplate. These are the critical sections which historically develop the highest stresses due to the geometry of a fuel rack structure. From the archived results, time-histories of all rack-to-rack fluid gaps, all rack-to-wall fluid gaps, and motion of any point on any rack can be generated. Sections 6.7 and 6.8 presents results obtained from single and multi-rack analyses, respectively. The results demonstrate satisfaction of all requirements on structure and kinematic integrity.

6.7 Results of 3-D Nonlinear Analyses of Single Racks

This section focuses on results from all 3-D single rack analyses. In the following section, we will present results from the whole pool multi-rack analysis and discuss the similarities and differences between single and multi-rack analysis.

A summary of results of all analyses performed for racks in the pool, using a single rack model, is presented in summary Tables 6.7.1 - 6.7.38. Table 6.7.1 lists all runs carried out. Table 6.7.2 presents the bounding results from all runs, and Tables 6.7.3 - 6.7.38 give details for each run. Analyses are carried out for different coefficients of friction, rack geometries, and fuel loading patterns. Analyses are also performed assuming channelled or unchannelled fuel. The assumption of channelled fuel increases the effective fuel weight, decreases the nominal cell wall-to-fuel assembly spacing, and adds additional elastic spring elements to model the bending stiffness of the channel. The choice of single rack simulations encompasses the heaviest rack, the rack with maximum moment of inertia differences in the two horizontal directions, and racks with larger than nominal surrounding water gaps. The tabular results for each run give maximax (maximum in time and in space) values of stress factors at important locations in the rack. Results are given for maximum rack displacements (see Section 6.4.2.2 for x,y orientation), maximum impact forces

at pedestal-liner interface, and rack cell-to-fuel, rack-to-rack, and rack-to-wall impact forces. It is shown that no rack-to-rack or rack-to-wall impacts occur in the active fuel region of the cellular structure. In the single rack analysis, kinematic criteria are checked by confirming that no inter-rack gap elements at the top of the rack close (see Figure 6.4.3). By virtue of the symmetry assumption discussed in subsection 6.4.2.4, impact is likely to occur if the local horizontal displacement exceeds 50% of the actual rack-to-rack gap.

Structural integrity at various rack sections is considered by computing the appropriate stress factors R_i. Results corresponding to the FCBV event yield the highest stress factors. Limiting stress factors for pedestals are at the upper section of the support and are to be compared with the bounding value of 1.0 (UCBV) or 2.0 (FCBV). Stress factors for the lower portion of the support are not limiting and are not reported. From Table 6.7.2, all stress factors are below the allowable limits. Note that only Faulted condition (FCBV) analyses are reported since the resulting stress factors also meet the Level B (UCBV) requirements.

Overturning has also been considered. A multiplier of 1.5 on FCBV horizontal earthquakes (more conservative than required by the USNRC Standard Review Plan) is applied to an isolated rack and the predicted displacements examined. Horizontal displacements do not grow to such an extent as to imply any possibility for overturning.

Additional investigation of important structural items is carried out and results are summarized in Table 6.7.39. A discussion of these items follows:

6.7.1.1 Impact Analyses

a. Impact Loading Between Fuel Assembly and Cell Wall

Local cell wall integrity is conservatively estimated from peak impact loads. Plastic analysis is used to obtain the limiting impact load. Table 6.7.39 gives the limiting impact load and compares the limit with the highest value obtained from any of the single rack analyses. The limiting load is much greater than the load obtained from any of the simulations reported in Tables 6.7.1 - 6.7.38. This limiting load is based on the cell wall. The actual impact loads, when considered as loads applied to the fuel assembly structure, are much lower than the load limits imposed by the fuel manufacturer.

b. Impacts Between Adjacent Racks

No non-zero impact loads are found for the rack-to-wall elements; it is concluded that no impacts between racks and walls are likely to occur during a seismic event. This is confirmed by the Whole Pool Multi-Rack analysis results in Section 6.8. Because of the closely spaced racks, impact protection is provided at the top corner of racks at potential impact sites. While the nominal rack-to-rack gap is used for calculation of hydrodynamic effects, the gap elements at the corners of the rack reflect the actual smaller gaps that are present at the top corners and at the baseplate level. These impact protection hard points ensure that impacts, if they occur, will be above or below the active fuel region. The results of the single rack analyses, using the opposed phase motion of adjacent racks, indicates that some rack-to-rack impacts are to be expected. The whole pool analysis confirms this. The design of these impact protection sites is based on the highest anticipated impact force from present and future fuel loading scenarios and limits the local stress in the cell wall near the impact protection site to prevent buckling.

6.7.1.2 Weld Stresses

Weld locations subjected to significant seismic loading are at the bottom of the rack at the baseplate-to-cell connection, at the top of the pedestal support at the baseplate connection, and at cell-to-cell connections. Results from dynamic analyses of single racks are surveyed and maximum loading used to qualify the welds.

a. Baseplate-to-Rack Cell Welds and Baseplate-to-Pedestal Welds

Reference [6.1.3] (ASME Code Section III, Subsection NF) permits, for the CECo Faulted condition (FCBV) event, an allowable weld stress $\tau = .42\ S_u$. A comparison of this allowable value with the highest weld stress predicted is given in Table 6.7.39. The highest predicted weld stress is less than the allowable weld stress value.

The weld between baseplate and support pedestal is checked using limit analysis techniques [6.7.1]. The structural weld at that location is considered safe if the interaction curve between net force and moment is such that:

$$G = \text{Function}(F/F_y, M/M_y) < 1.0$$

F_y, M_y are the limit load and moment under direct load only and direct moment only. These values depend on the configuration and on material yield strengths. F, M are absolute values of actual force and moments applied to the weld section. The calculated value of G for the pedestal/baseplate weld is presented in Table 6.7.39 and is less than the limit value of 1.0. This calculated value is conservatively based on instantaneous peak loading, and reflects results obtained from both single and multi-rack analyses.

b. Cell-to-Cell Welds

Cell-to-cell connections are made by fillet welds along the cell height. A total of 33" of lineal 1/16" fillet weld in a maximum of seven connecting bars connect each cell with its adjacent cell. Stresses in storage cell to storage cell welds develop along the length due to fuel assembly impact with the cell wall. This occurs if fuel assemblies in adjacent cells are moving out of phase with one another so that impact loads in two adjacent

cells are in opposite directions; this tends to separate the two cells from each other at the weld. Table 6.7.39 gives results for the maximum allowable load that can be transferred by these welds based on the available weld area. An upper bound on the load required to be transferred is also given in Table 6.7.39 and is less than the allowable load. This upper bound value is obtained by using the highest rack-to-fuel impact load from Table 6.7.2 (for any simulation), and multiplying the result by 2 (assuming that two impact locations are supported by every weld connection). Table 6.7.39 also reports the stress in the lowest connecting bar which develops due to the baseplate gross shear force.

6.8 Results from Whole Pool Multi-Rack Analyses

Tables 6.8.1 - 6.8.2 show maximum corner absolute displacements at both the top and bottom of each rack in global x and y directions (refer to Fig. 6.4.9) from two multi-rack runs. A random set of friction coefficients in the range of 0.2 - 0.8 with mean value of 0.5 are used. The input loadings are the governing earthquake time-histories for Level C (UCBV), and for Level B (FCBV), respectively. The maximum absolute displacement values are higher than those obtained from single rack analysis. Thus, it appears essential to perform Whole Pool Multi-Rack analyses to verify that racks do not impact or hit the wall.

Figures 6.8.1 - 6.8.5 show the time-histories of rack-to-rack and rack-to-wall gaps at typical locations (see Figure 6.4.9 for locations). A survey of all rack-to-wall impact elements confirms that there are no rack-to-wall impacts. Figures 6.8.3 - 6.8.5 show typical gap time-histories around the wall. Figures 6.8.1 and 6.8.2 show typical rack-to-rack gap time-histories. The presence of negative gaps is an indication of inter-rack impact at the top corners. The maximum impact force values predicted by these impact springs serves to size the impact protection plate. No real physical meaning, other than showing that the impact has occurred, should be ascribed to the actual value of the negative displacement.

Tables 6.8.4 - 6.8.5 present peak pedestal compressive loads for all pedestals in the pool for each of the two WPMR analyses (see Figure 6.4.9 for pedestal locations). In addition to a report of maximum pedestal loads, the time-history of each pedestal load vector for each rack is archived for future use, if necessary. Note that the maximum pedestal vertical load is 217500 lb. for Rack 19. This is higher than the maximum load predicted from the single rack analyses. However, the conclusions concerning rack structural integrity remain unchanged.

The Whole Pool Multi-Rack analyses confirms that no new concerns are identified; overall structural integrity is evaluated using the limiting loadings from either whole pool or from single rack analyses.

In view of the large margin of safety both in respect of stresses and displacements in the LSCS Unit 1 racks, CECo has determined that it is feasible to mount a work table on top of a fuel rack module to provide a working surface for underwater operation, such as LPRM cutting and for storage of miscellaneous items. Preliminary estimates show that such a table, qualified to a maximum gross load of 4 tons, can be designed for installation on certain rack modules. In the event that CECo decides to implement such a modification the appropriate safety evaluation in accordance with the provisions of 10CFR50:59, will be made with special emphasis on structural compliance.

6.9 Bearing Pad Analysis

To protect the slab from high localized dynamic loadings, 15"x15" (minimum) bearing pads are placed between the pedestal base and the slab. Fuel rack pedestals impact on these bearing pads during a seismic event and pedestal loading is transferred to the liner. Bearing pad dimensions are set to ensure that the average pressure on the slab surface due to a static load plus a dynamic impact

load does not exceed the American Concrete Institute [6.9.1] limit on bearing pressures. Pedestal locations are set to avoid overloading of leak chase regions under the slab. Time-history 22results from dynamic simulations for each pedestal are used to generate appropriate static and dynamic pedestal loads which are then used to develop the bearing pad size.

Section 10 of [6.9.1] gives the design bearing strength as:

$$f_b = \phi\ (.85\ f_c')\ \epsilon$$

where $\phi = .7$ and f_c' is the specified concrete strength for the spent fuel pool. $\epsilon = 1$ except when the supporting surface is wider on all sides than the loaded area. In that case, $\epsilon = (A_2/A_1)^{.5}$, but not more than 2. A_1 is the actual loaded area, and A_2 is an area greater than A_1 and is defined in [6.9.1]. Using a value of $\epsilon > 1$ includes credit for the confining effect of the surrounding concrete.

Bearing pads are sized so as to provide sufficient margin on average bearing pressure. Table 6.9.1 summarizes the limiting result. Rack pedestal placement is such that no bearing pads encroach on an existing leak chase. The result presented in Table 6.8.1 conservatively reflects the instantaneous peak pedestal load. In reality, the ACI Code limits should be applied using some lower "effective static load defined by a time-averaging of the dynamic load. Thus, our result has additional conservatism.

6.10 References for Section 6

[6.1.1] "OT Position for Review and Acceptance of Spent Fuel Storage and Handling Applications", dated April 14, 1978, and January 18, 1979 amendment thereto.

[6.1.2] USNRC Standard Review Plan, NUREG-0800 (1981).

[6.1.3] ASME Boiler & Pressure Vessel Code, Section III, Subsection NF, appendices (1989).

[6.2.1] USNRC Regulatory Guide 1.29, "Seismic Design Classification," Rev. 3, 1978.

[6.2.2] Soler, A.I. and Singh, K.P., "Seismic Responses of Free Standing Fuel Rack Constructions to 3-D Motions", Nuclear Engineering and Design, Vol. 80, pp. 315-329 (1984).

[6.2.3] Singh, K.P. and Soler, A.I., "Seismic Qualification of Free Standing Nuclear Fuel Storage Racks - the Chin Shan Experience, Nuclear Engineering International, UK (March 1991).

[6.3.1] Specification for Spent Fuel and Special Storage Racks, La Salle County Station Unit 1, Commonwealth Edison Company.

[6.3.2] Holtec Proprietary Report - Verification and User's Manual for Computer Code GENEQ, Report HI-89364, January, 1990.

[6.3.3] "Proceedings of the Workshop on Soil-Structure Interaction, Bethesda, Maryland, June 16-18, 1986", NUREG/CP-0054, BNL-NUREG-52011.

[6.3.4] ASCE Standard, "Seismic Analysis of Safety Related Nuclear Structures and Commentary on Standard for Seismic Analysis of Safety Related Nuclear Structures", ASCE 4-86, September 1986.

[6.4.1] Rabinowicz, E., "Friction Coefficients of Water Lubricated Stainless Steels for a Spent Fuel Rack Facility," MIT, a report for Boston Edison Company, 1976.

[6.4.2] Levy, S. and Wilkinson, J.P.D., "The Component Element Method in Dynamics with Application to Earthquake and Vehicle Engineering," McGraw Hill, 1976.

[6.4.3] Singh, K.P. and Soler, A.I., "Dynamic Coupling in a Closely Spaced Two-Body System Vibrating in Liquid Medium: The Case of Fuel Racks," 3rd International Conference on Nuclear Power Safety, Keswick, England, May 1982.

[6.4.4] Fritz, R.J., "The Effects of Liquids on the Dynamic Motions of Immersed Solids," Journal of Engineering for Industry, Trans. of the ASME, February 1972, pp 167-172.

[6.4.5] Paul, B., "Fluid Coupling in Fuel Racks: Correlation of Theory and Experiment , Holtec Proprietary Report HI-88243.

[6.6.1] "Dynamics of Structures," R.W. Clough and J. Penzien, McGraw Hill (1975).

[6.6.2] Soler, A.I., "User Guide for PREDYNA1 and DYNAMO", Holtec Proprietary Report HI-89343, Rev. 2, March, 1990.

[6.6.3] Soler, A.I., "Theoretical Background for Single and Multiple Rack Analysis", Holtec Proprietary Report HI-90439, Rev. 0, February, 1990.

[6.6.4] Soler, A.I., "DYNARACK Theoretical Manual", Holtec Proprietary Report HI-87162, Rev. 1, January, 1988.

[6.6.5] Soler, A.I., "DYNARACK Validation Manual, Holtec Proprietary Report HI-91760, Rev. 0, October, 1991.

[6.7.1] Singh, K.P., Soler, A.I., and Bhattacharya, S., "Design Strength of Primary Structural Welds in Free Standing Structures", ASME, Journ. of Pressure Vessel Technology, August, 1991.

[6.9.1] ACI 349-85, Code Requirements for Nuclear Safety Related Concrete Structures, American Concrete Institute, Detroit, Michigan, 1985.

Table 6.1.1

LISTING OF PLANTS WHERE DYNARACK WAS APPLIED

PLANT		DOCKET NO.
Enrico Fermi Unit 2	USNRC	50-341
Quad Cities 1 and 2	USNRC	50-254, 50-265
Rancho Seco	USNRC	50-312
Grand Gulf Unit 1	USNRC	50-416
Oyster Creek	USNRC	50-219
Pilgrim Unit I	USNRC	50-293
V.C. Summer	USNRC	50-395
Diablo Canyon Units 1 and 2	USNRC	50-275, 50-323
Byron Units 1 & 2	USNRC	50-454, 50-455
Braidwood Units 1 & 2	USNRC	50-456, 50-457
Vogtle Unit 2	USNRC	50-425
St. Lucie Unit 1	USNRC	50-335
Millstone Point Unit 1	USNRC	50-245
D.C. Cook Units 1 & 2	USNRC	50-315, 50-316
Indian Point Unit 2	USNRC	50-247
Three Mile Island Unit 1	USNRC	50-289
J.A. FitzPatrick	USNRC	50-333
Shearon Harris Unit 2	USNRC	50-401
Kuosheng Units 1 & 2	Taiwan Power Company	
Chin Shan Units 1 & 2	Taiwan Power Company	
Ulchin Unit 2	Korea Electric Power	
Laguna Verde Units 1 & 2	Comision Federal de Electricidad	
Zion Station Units 1 & 2	USNRC	50-295, 50-304

Table 6.3.1

CROSS-CORRELATION COEFFICIENTS OF THE SYNTHETIC
LEVEL B ACCELERATION TIME-HISTORIES FOR
LA SALLE UNIT 1 SPENT FUEL POOL SLAB

RESULTS OF COEFFICIENT OF CORRELATION

DATA1 TO DATA2 = -2.839259E-02
DATA1 TO DATA3 = -2.139747E-02
DATA2 TO DATA3 = -3.526679E-02

NOTE: DATA1: LEVEL B SEISMIC ACCELERATION TIME-HISTORY IN N-S DIRECTION

DATA2: LEVEL B SEISMIC ACCELERATION TIME-HISTORY IN E-W DIRECTION

DATA3: LEVEL B SEISMIC ACCELERATION TIME-HISTORY IN VERTICAL DIRECTION

Table 6.3.2

CROSS-CORRELATION COEFFICIENTS OF THE SYNTHETIC
LEVEL C ACCELERATION TIME-HISTORIES FOR
LA SALLE UNIT 1 SPENT FUEL POOL SLAB

RESULTS OF COEFFICIENT OF CORRELATION

DATA1 TO DATA2 = -4.453371E-02
DATA1 TO DATA3 = -1.967042E-02
DATA2 TO DATA3 = -4.879382E-03

NOTE: DATA1: LEVEL C SEISMIC ACCELERATION TIME-HISTORY IN N-S DIRECTION

DATA2: LEVEL C SEISMIC ACCELERATION TIME-HISTORY IN E-W DIRECTION

DATA3: LEVEL C SEISMIC ACCELERATION TIME-HISTORY IN VERTICAL DIRECTION

Table 6.4.1

DEGREES-OF-FREEDOM

Location (Node)	Displacement			Rotation		
	U_x	U_y	U_z	θ_x	θ_y	θ_z
1	P1	P2	P3	q4	q5	q6
2	P17	P18	P19	q20	q21	q22
Point 2 is assumed attached to rigid rack at the top most point.						
2*	P7	P8				
3*	P9	P10				
4*	P11	P12				
5*	P13	P14				
1*	P15	P16				

where:

$P_i = q_i(t) + U_1(t)$ $\quad i = 1,7,9,11,13,15,17$

$= q_i(t) + U_2(t)$ $\quad i = 2,8,10,12,14,16,18$

$= q_i(t) + U_3(t)$ $\quad i = 3,19$

$U_i(t)$ are the 3 known earthquake displacements.

Table 6.4.2
NUMBERING SYSTEM FOR GAP ELEMENTS AND FRICTION ELEMENTS

I. Nonlinear Springs (Gap Elements) (64 Total)

Number	Node Location	Description
1	Support S1	Z compression only element
2	Support S2	Z compression only element
3	Support S3	Z compression only element
4	Support S4	Z compression only element
5	2,2*	X rack/fuel assembly impact element
6	2,2*	X rack/fuel assembly impact element
7	2,2*	Y rack/fuel assembly impact element
8	2,2*	Y rack/fuel assembly impact element
9-24	Other rattling masses for nodes 1*, 3*, 4* and 5*	
25	Bottom cross-section of rack (around edge)	Inter-rack impact elements
.		Inter-rack impact elements
.		Inter-rack impact elements
.		Inter-rack impact elements
.		Inter-rack impact elements
.		Inter-rack impact elements
44		Inter-rack impact elements
45	Top cross-section of rack (around edge)	Inter-rack impact elements
.		Inter-rack impact elements
.		Inter-rack impact elements
.		Inter-rack impact elements
.		Inter-rack impact elements
.		Inter-rack impact elements
.		Inter-rack impact elements
64		Inter-rack impact elements

Table 6.4.2 (continued)

NUMBERING SYSTEM FOR GAP ELEMENTS AND FRICTION ELEMENTS

II. Friction Elements (16 total)

Number	Node Location	Description
1	Support S1	X direction friction
2	Support S1	Y direction friction
3	Support S2	X direction friction
4	Support S2	Y direction friction
5	Support S3	X direction friction
6	Support S3	Y direction friction
7	Support S4	X direction friction
8	Support S4	Y direction friction
9	S1	X Slab moment
10	S1	Y Slab moment
11	S2	X Slab moment
12	S2	Y Slab moment
13	S3	X Slab moment
14	S3	Y Slab moment
15	S4	X Slab moment
16	S4	Y Slab moment

Table 6.5.1

Material	Young's Modulus E (psi)	Yield Strength S_y (psi)	Ultimate Strength S_u (psi)
304 S.S.	27.9×10^6	25,000	71,000
Section III Reference	Table I-6.0	Table I-2.2	Table I-3.2

SUPPORT MATERIAL DATA (200°F)

	Material	Young's Modulus E (psi)	Yield Strength S_y (psi)	Ultimate Strength S_u (psi)
1	SA-240, Type 304 (upper part of support feet)	27.9×10^6	25,000	71,000
2	SA-564-630 (lower part of support feet; age hardened at 1100°F)	27.9×10^6	106,300	140,000

Table 6.7.1

RESULTS OF SINGLE RACK ANALYSES

List of All Runs

Holtec Run I.D.	Rack I.D.	Fuel I.D.	Fuel Loading Condition	Seismic Loading	Coefficient of Friction	Motion Mode
dc15x17a.rf8	A	GE 8x8-C chan'led	Fully Loaded 255 cells	Level C	0.8	opposed phase
dc15x17a.rf5	A	GE 8x8-C chan'led	Fully loaded 255 cells	Level C	0.5	opposed phase
dc15x17a.rf2	A	GE 8x8-C chan'led	Fully loaded 255 cells	Level C	0.2	opposed phase
dc15x17a.rh8	A	GE 8x8-C chan'led	Half loaded 127 cells	Level C	0.8	opposed phase
dc15x17a.rh5	A	GE 8x8-C chan'led	Half loaded 127 cells	Level C	0.5	opposed phase
dc15x17a.rh2	A	GE 8x8-C chan'led	Half loaded 127 cells	Level C	0.2	opposed phase
dc15x17a.re8	A	GE 8x8-C chan'led	" Empty " 15 cells	Level C	0.8	opposed phase
dc15x17a.re5	A	GE 8x8-C chan'led	" Empty " 15 cells	Level C	0.5	opposed phase
dc15x17a.re2	A	GE 8x8-C chan'led	" Empty " 15 cells	Level C	0.2	opposed phase
dc15x17a.uf8	A	GE 8x8-C uncha'ed	Fully Loaded 255 cells	Level C	0.8	opposed phase
dc15x17a.uf5	A	GE 8x8-C uncha'ed	Fully loaded 255 cells	Level C	0.5	opposed phase
dc15x17a.uf2	A	GE 8x8-C uncha'ed	Fully loaded 255 cells	Level C	0.2	opposed
dc15x17a.uh8	A	GE 8x8-C uncha'ed	Half loaded 127 cells	Level C	0.8	opposed
dc15x17a.uh5	A	GE 8x8-C uncha'ed	Half loaded 127 cells	Level C	0.5	opposed

(to be continued)

Table 6.7.1 (continued)

dc15x17a.uh2	A	GE 8x8-C uncha'ed	Half loaded 127 cells	Level C	0.2	opposed
dc15x17a.ue8	A	GE 8x8-C uncha'ed	" Empty " 15 cells	Level C	0.8	opposed phase
dc15x17a.ue5	A	GE 8x8-C uncha'ed	" Empty " 15 cells	Level C	0.5	opposed
dc15x17a.ue2	A	GE 8x8-C uncha'ed	" Empty " 15 cells	Level C	0.2	opposed
dc15x18f.rf8	F	GE 8x8-C chan'led	Fully Loaded 270 cells	Level C	0.8	opposed phase
dc15x18f.rf5	F	GE 8x8-C chan'led	Fully loaded 270 cells	Level C	0.5	opposed phase
dc15x18f.rf2	F	GE 8x8-C chan'led	Fully loaded 270 cells	Level C	0.2	opposed phase
dc15x18f.rh8	F	GE 8x8-C chan'led	Half loaded 135 cells	Level C	0.8	opposed phase
dc15x18f.rh5	F	GE 8x8-C chan'led	Half loaded 135 cells	Level C	0.5	opposed phase
dc15x18f.rh2	F	GE 8x8-C chan'led	Half loaded 135 cells	Level C	0.2	opposed phase
dc15x18f.re8	F	GE 8x8-C chan'led	" Empty " 15 cells	Level C	0.8	opposed phase
dc15x18f.re5	F	GE 8x8-C chan'led	" Empty " 15 cells	Level C	0.5	opposed phase
dc15x18f.re2	F	GE 8x8-C chan'led	" Empty " 15 cells	Level C	0.2	opposed phase
dc9x18k.rf8	K	GE 8x8-C chan'led	Fully Loaded 162 cells	Level C	0.8	opposed phase
dc9x18k.rf5	K	GE 8x8-C chan'led	Fully Loaded 162 cells	Level C	0.5	opposed phase
dc9x18k.rf2	K	GE 8x8-C chan'led	Fully Loaded 162 cells	Level C	0.2	opposed phase

(to be continued)

Table 6.7.1 (continued)

dc9x18k.rh8	K	GE 8x8-C chan'led	Half Loaded 81 cells	Level C	0.8	opposed phase
dc9x18k.rh5	K	GE 8x8-C chan'led	Half Loaded 81 cells	Level C	0.5	opposed phase
dc9x18k.rh2	K	GE 8x8-C chan'led	Half Loaded 81 cells	Level C	0.2	opposed phase
dc9x18k.re8	K	GE 8x8-C chan'led	" Empty " 9 cells	Level C	0.8	opposed phase
dc9x18k.re5	K	GE 8x8-C chan'led	" Empty " 9 cells	Level C	0.5	opposed phase
dc9x18k.re2	K	GE 8x8-C chan'led	" Empty " 9 cells	Level C	0.2	opposed phase

Table 6.7.2

SUMMARY OF WORST RESULTS
FROM 36 RUNS OF SINGLE RACK ANALYSIS

(LOADED WITH REGULAR FUEL ASSEMBLIES)

Item	Value		Run I.D.
1. Maximum total vertical pedestal load:	427,140	lbs.	dc15x17a.rf2
2. Maximum vertical load in any single pedestal:	152,117	lbs.	dc15x17a.rf5
3. Maximum shear load in any single pedestal:	90,010	lbs.	dc8x18k.rf8
4. Maximum fuel assembly-to-cell wall impact load at one local position:	970	lbs.	dc15x17a.ue2
5. Maximum rack-to-wall impact load at baseplat level:	0	lbs.	
6. Maximum rack-to-wall impact load at the top of rack:	0	lbs.	
7. Maximum rack-to-rack impact load at baseplat level:	0	lbs.	dc9x18k.rf2
8. Maximum rack-to-rack impact load at the top of rack:	172	lbs.	dc15x17a.uh8
9. Maximum corner displacements			
Top corner in x direction:	0.1556	in.	dc9x18k.uf8
in y direction:	0.2248	in.	dc15x17a.rf8
Baseplate corner in x direction:	0.0604	in.	dc15x17a.uh2
in y direction:	0.1981	in.	dc15x17a.uh2
10. Maximum stress factors			
Above baseplate:	0.249 (R6)		dc15x17a.rf8
Support pedestals:	0.740 (R6)		dc15x17a.rf8

Table 6.7.3

SUMMARY RESULTS OF 3-D SINGLE RACK ANALYSIS FOR RACK MODULE: A15x17

Holtec Run I.D.: dc15x17a.rf8 Seismic Loading: Level-C

Fuel Assembly I.D. and Weight: GE 8x8-C ; 680.0 (lbs.)

Fuel Loading: 255 cells loaded; Fuel centroid X,Y: .0, .0 (in.)

Coefficient of friction at the bottom of support pedestal: 0.8

$Revision: 3.46 $
$Logfile: C:/racks/dynam0/dynam0.fov $
$Revision: 2.5 $
$Logfile: C:/racks/dynam0/dynas1.fov $
$Revision: 3.36 $
$Logfile: C:/racks/dynam0/dynas2.fov $

DYNAMIC IMPACT LOADS (lbs.)

(1) Maximum total vertical pedestal load:	422535.0
(2) Maximum vertical load in any single pedestal:	147815.2
(3) Maximum shear load in any single pedestal:	73787.4
(4) Maximum fuel-cell impact at one local position:	870.7
(5) Maximum rack-to-wall impact at baseplate:	.0
(6) Maximum rack-to-wall impact at rack top:	.0
(7) Maximum rack-to-rack impact at baseplate:	.0
(8) Maximum rack-to-rack impact at rack top:	.0

MAXIMUM CORNER DISPLACEMENTS (in.)

Location:	X-direction	Y-direction
Top corner:	.1465	.1214
Baseplate corner:	.0048	.0050

MAXIMUM STRESS FACTORS *

Stress factor:	R1	R2	R3	R4	R5	R6	R7
Above baseplate:	.056	.032	.135	.107	.218	.249	.040
Support pedestal:	.312	.167	.367	.281	.666	.740	.218

* See Section 6.5.2.3 of the Licensing Report for definitions.

Table 6.7.4

SUMMARY RESULTS OF 3-D SINGLE RACK ANALYSIS FOR RACK MODULE: A15x17

Holtec Run I.D.: dc15x17a.rf5 Seismic Loading: Level-C

Fuel Assembly I.D. and Weight: GE 8x8-C ; 680.0 (lbs.)

Fuel Loading: 255 cells loaded; Fuel centroid X,Y: .0, .0 (in.)

Coefficient of friction at the bottom of support pedestal: 0.5

$Revision: 3.46 $
$Logfile: C:/racks/dynam0/dynam0.fov $
$Revision: 2.5 $
$Logfile: C:/racks/dynam0/dynas1.fov $
$Revision: 3.36 $
$Logfile: C:/racks/dynam0/dynas2.fov $

DYNAMIC IMPACT LOADS (lbs.)

(1) Maximum total vertical pedestal load:	419264.0
(2) Maximum vertical load in any single pedestal:	152117.5
(3) Maximum shear load in any single pedestal:	52304.3
(4) Maximum fuel-cell impact at one local position:	825.2
(5) Maximum rack-to-wall impact at baseplate:	.0
(6) Maximum rack-to-wall impact at rack top:	.0
(7) Maximum rack-to-rack impact at baseplate:	.0
(8) Maximum rack-to-rack impact at rack top:	.0

MAXIMUM CORNER DISPLACEMENTS (in.)

Location:	X-direction	Y-direction
Top corner:	.1452	.1188
Baseplate corner:	.0052	.0073

MAXIMUM STRESS FACTORS *

Stress factor:	R1	R2	R3	R4	R5	R6	R7
Above baseplate:	.055	.031	.133	.105	.210	.238	.045
Support pedestal:	.321	.128	.270	.216	.541	.588	.160

* See Section 6.5.2.3 of the Licensing Report for definitions.

Table 6.7.5

SUMMARY RESULTS OF 3-D SINGLE RACK ANALYSIS FOR RACK MODULE: A15x17

Holtec Run I.D.: dc15x17a.rf2 Seismic Loading: Level-C

Fuel Assembly I.D. and Weight: GE 8x8-C ; 680.0 (lbs.)

Fuel Loading: 255 cells loaded; Fuel centroid X,Y: .0, .0 (in.)

Coefficient of friction at the bottom of support pedestal: 0.2

$Revision: 3.46 $
$Logfile: C:/racks/dynam0/dynam0.fov $
$Revision: 2.5 $
$Logfile: C:/racks/dynam0/dynas1.fov $
$Revision: 3.36 $
$Logfile: C:/racks/dynam0/dynas2.fov $

DYNAMIC IMPACT LOADS (lbs.)

(1) Maximum total vertical pedestal load:	427140.7
(2) Maximum vertical load in any single pedestal:	132255.4
(3) Maximum shear load in any single pedestal:	26415.6
(4) Maximum fuel-cell impact at one local position:	754.1
(5) Maximum rack-to-wall impact at baseplate:	.0
(6) Maximum rack-to-wall impact at rack top:	.0
(7) Maximum rack-to-rack impact at baseplate:	.0
(8) Maximum rack-to-rack impact at rack top:	.0

MAXIMUM CORNER DISPLACEMENTS (in.)

Location:	X-direction	Y-direction
Top corner:	.1113	.2248
Baseplate corner:	.0463	.1462

MAXIMUM STRESS FACTORS *

Stress factor:	R1	R2	R3	R4	R5	R6	R7
Above baseplate:	.055	.021	.125	.107	.205	.234	.028
Support pedestal:	.279	.076	.141	.128	.427	.455	.084

* See Section 6.5.2.3 of the Licensing Report for definitions.

Table 6.7.6

SUMMARY RESULTS OF 3-D SINGLE RACK ANALYSIS FOR RACK MODULE: A15x17

Holtec Run I.D.: dc15x17a.rh8 Seismic Loading: Level-C

Fuel Assembly I.D. and Weight: GE 8x8-C ; 680.0 (lbs.)

Fuel Loading: 127 cells loaded; Fuel centroid X,Y: 1.4,-26.7 (in.)

Coefficient of friction at the bottom of support pedestal: 0.8

$Revision: 3.46 $
$Logfile: C:/racks/dynam0/dynam0.fov $
$Revision: 2.5 $
$Logfile: C:/racks/dynam0/dynas1.fov $
$Revision: 3.36 $
$Logfile: C:/racks/dynam0/dynas2.fov $

DYNAMIC IMPACT LOADS (lbs.)

(1) Maximum total vertical pedestal load:	248294.1
(2) Maximum vertical load in any single pedestal:	104926.1
(3) Maximum shear load in any single pedestal:	40094.7
(4) Maximum fuel-cell impact at one local position:	863.5
(5) Maximum rack-to-wall impact at baseplate:	.0
(6) Maximum rack-to-wall impact at rack top:	.0
(7) Maximum rack-to-rack impact at baseplate:	.0
(8) Maximum rack-to-rack impact at rack top:	.0

MAXIMUM CORNER DISPLACEMENTS (in.)

Location:	X-direction	Y-direction
Top corner:	.1071	.1235
Baseplate corner:	.0044	.0043

MAXIMUM STRESS FACTORS *

Stress factor:	R1	R2	R3	R4	R5	R6	R7
Above baseplate:	.037	.017	.092	.078	.133	.154	.017
Support pedestal:	.221	.091	.166	.154	.470	.515	.099

* See Section 6.5.2.3 of the Licensing Report for definitions.

Table 6.7.7

SUMMARY RESULTS OF 3-D SINGLE RACK ANALYSIS FOR RACK MODULE: A15x17

Holtec Run I.D.: dc15x17a.rh5 Seismic Loading: Level-C

Fuel Assembly I.D. and Weight: GE 8x8-C ; 680.0 (lbs.)

Fuel Loading: 127 cells loaded; Fuel centroid X,Y: 1.4,-26.7 (in.)

Coefficient of friction at the bottom of support pedestal: 0.5

$Revision: 3.46 $
$Logfile: C:/racks/dynam0/dynam0.fov $
$Revision: 2.5 $
$Logfile: C:/racks/dynam0/dynas1.fov $
$Revision: 3.36 $
$Logfile: C:/racks/dynam0/dynas2.fov $

DYNAMIC IMPACT LOADS (lbs.)

(1) Maximum total vertical pedestal load:	248356.8
(2) Maximum vertical load in any single pedestal:	108286.5
(3) Maximum shear load in any single pedestal:	41030.4
(4) Maximum fuel-cell impact at one local position:	840.6
(5) Maximum rack-to-wall impact at baseplate:	.0
(6) Maximum rack-to-wall impact at rack top:	.0
(7) Maximum rack-to-rack impact at baseplate:	.0
(8) Maximum rack-to-rack impact at rack top:	15.2

MAXIMUM CORNER DISPLACEMENTS (in.)

Location:	X-direction	Y-direction
Top corner:	.1030	.1266
Baseplate corner:	.0091	.0091

MAXIMUM STRESS FACTORS *

Stress factor:	R1	R2	R3	R4	R5	R6	R7
Above baseplate:	.037	.020	.091	.084	.132	.152	.020
Support pedestal:	.222	.121	.209	.204	.424	.467	.124

* See Section 6.5.2.3 of the Licensing Report for definitions.

Table 6.7.8

SUMMARY RESULTS OF 3-D SINGLE RACK ANALYSIS FOR RACK MODULE: A15x17

Holtec Run I.D.: dc15x17a.rh2 Seismic Loading: Level-C

Fuel Assembly I.D. and Weight: GE 8x8-C ; 680.0 (lbs.)

Fuel Loading: 127 cells loaded; Fuel centroid X,Y: 1.4,-26.7 (in.)

Coefficient of friction at the bottom of support pedestal: 0.2

$Revision: 3.46 $
$Logfile: C:/racks/dynam0/dynam0.fov $
$Revision: 2.5 $
$Logfile: C:/racks/dynam0/dynas1.fov $
$Revision: 3.36 $
$Logfile: C:/racks/dynam0/dynas2.fov $

DYNAMIC IMPACT LOADS (lbs.)

(1) Maximum total vertical pedestal load:	243972.2
(2) Maximum vertical load in any single pedestal:	103189.2
(3) Maximum shear load in any single pedestal:	18945.1
(4) Maximum fuel-cell impact at one local position:	892.0
(5) Maximum rack-to-wall impact at baseplate:	.0
(6) Maximum rack-to-wall impact at rack top:	.0
(7) Maximum rack-to-rack impact at baseplate:	.0
(8) Maximum rack-to-rack impact at rack top:	.0

MAXIMUM CORNER DISPLACEMENTS (in.)

Location:	X-direction	Y-direction
Top corner:	.0930	.1923
Baseplate corner:	.0468	.1781

MAXIMUM STRESS FACTORS *

Stress factor:	R1	R2	R3	R4	R5	R6	R7
Above baseplate:	.036	.012	.081	.053	.121	.136	.014
Support pedestal:	.218	.049	.101	.082	.324	.342	.060

* See Section 6.5.2.3 of the Licensing Report for definitions.

Table 6.7.9

SUMMARY RESULTS OF 3-D SINGLE RACK ANALYSIS FOR RACK MODULE: A15x17

Holtec Run I.D.: dc15x17a.re8 Seismic Loading: Level-C

Fuel Assembly I.D. and Weight: GE 8x8-C ; 680.0 (lbs.)

Fuel Loading: 15 cells loaded; Fuel centroid X,Y: .0,-50.2 (in.)

Coefficient of friction at the bottom of support pedestal: 0.8

$Revision: 3.46 $
$Logfile: C:/racks/dynam0/dynam0.fov $
$Revision: 2.5 $
$Logfile: C:/racks/dynam0/dynas1.fov $
$Revision: 3.36 $
$Logfile: C:/racks/dynam0/dynas2.fov $

DYNAMIC IMPACT LOADS (lbs.)

(1) Maximum total vertical pedestal load:	61823.1
(2) Maximum vertical load in any single pedestal:	43045.3
(3) Maximum shear load in any single pedestal:	14798.3
(4) Maximum fuel-cell impact at one local position:	914.3
(5) Maximum rack-to-wall impact at baseplate:	.0
(6) Maximum rack-to-wall impact at rack top:	.0
(7) Maximum rack-to-rack impact at baseplate:	.0
(8) Maximum rack-to-rack impact at rack top:	.0

MAXIMUM CORNER DISPLACEMENTS (in.)

Location	X-direction	Y-direction
Top corner:	.0664	.0694
Baseplate corner:	.0036	.0043

MAXIMUM STRESS FACTORS *

Stress factor:	R1	R2	R3	R4	R5	R6	R7
Above baseplate:	.010	.006	.034	.028	.049	.056	.008
Support pedestal:	.087	.042	.073	.071	.170	.185	.043

* See Section 6.5.2.3 of the Licensing Report for definitions.

Table 6.7.10

SUMMARY RESULTS OF 3-D SINGLE RACK ANALYSIS FOR RACK MODULE: A15x17

Holtec Run I.D.: dc15x17a.re5 Seismic Loading: Level-C

Fuel Assembly I.D. and Weight: GE 8x8-C ; 680.0 (lbs.)

Fuel Loading: 15 cells loaded; Fuel centroid X,Y: .0,-50.2 (in.)

Coefficient of friction at the bottom of support pedestal: 0.5

$Revision: 3.46 $
$Logfile: C:/racks/dynam0/dynam0.fov $
$Revision: 2.5 $
$Logfile: C:/racks/dynam0/dynas1.fov $
$Revision: 3.36 $
$Logfile: C:/racks/dynam0/dynas2.fov $

DYNAMIC IMPACT LOADS (lbs.)

(1) Maximum total vertical pedestal load:	59282.7
(2) Maximum vertical load in any single pedestal:	44541.7
(3) Maximum shear load in any single pedestal:	16830.3
(4) Maximum fuel-cell impact at one local position:	914.2
(5) Maximum rack-to-wall impact at baseplate:	.0
(6) Maximum rack-to-wall impact at rack top:	.0
(7) Maximum rack-to-rack impact at baseplate:	.0
(8) Maximum rack-to-rack impact at rack top:	.0

MAXIMUM CORNER DISPLACEMENTS (in.)

Location:	X-direction	Y-direction
Top corner:	.0719	.0669
Baseplate corner:	.0154	.0264

MAXIMUM STRESS FACTORS *

Stress factor:	R1	R2	R3	R4	R5	R6	R7
Above baseplate:	.010	.007	.03[illegible]	.028	.050	.057	.006
Support pedestal:	.090	.041	.080	.070	.185	.204	.036

* See Section 6.5.2.3 of the Licensing Report for definitions.

Table 6.7.11

SUMMARY RESULTS OF 3-D SINGLE RACK ANALYSIS FOR RACK MODULE: A15x17

Holtec Run I.D.: dc15x17a.re2 Seismic Loading: Level-C

Fuel Assembly I.D. and Weight: GE 8x.-C ; 680.0 (lbs.)

Fuel Loading: 15 cells loaded; Fuel centroid X,Y: .0,-50.2 (in.)

Coefficient of friction at the bottom of support pedestal: 0.2

$Revision: 3.46 $
$Logfile: C:/racks/dynam0/dynam0.fov $
$Revision: 2.5 $
$Logfile: C:/racks/dynam0/dynas1.fov $
$Revision: 3.36 $
$Logfile: C:/racks/dynam0/dynas2.fov $

DYNAMIC IMPACT LOADS (lbs.)

(1) Maximum total vertical pedestal load:	52062.3
(2) Maximum vertical load in any single pedestal:	25200.9
(3) Maximum shear load in any single pedestal:	5013.5
(4) Maximum fuel-cell impact at one local position:	912.3
(5) Maximum rack-to-wall impact at baseplate:	.0
(6) Maximum rack-to-wall impact at rack top:	.0
(7) Maximum rack-to-rack impact at baseplate:	.0
(8) Maximum rack-to-rack impact at rack top:	.0

MAXIMUM CORNER DISPLACEMENTS (in.)

Location:	X-direction	Y-direction
Top corner:	.0344	.0580
Baseplate corner:	.0179	.0463

MAXIMUM STRESS FACTORS *

Stress factor:	R1	R2	R3	R4	R5	R6	R7
Above baseplate:	.009	.003	.021	.018	.037	.042	.003
Support pedestal:	.053	.014	.026	.024	.080	.084	.016

* See Section 6.5.2.3 of the Licensing Report for definitions.

Table 6.7.12

SUMMARY RESULTS OF 3-D SINGLE RACK ANALYSIS FOR RACK MODULE: A15x17

Holtec Run I.D.: dc15x17a.uf8 Seismic Loading: Level-C

Fuel Assembly I.D. and Weight: GE 8x8-C ; 600.0 (lbs.)

Fuel Loading: 255 cells loaded; Fuel centroid X,Y: .0, .0 (in.)

Coefficient of friction at the bottom of support pedestal: 0.8

$Revision: 3.46 $
$Logfile: C:/racks/dynam0/dynam0.fov $
$Revision: 2.5 $
$Logfile: C:/racks/dynam0/dynas1.fov $
$Revision: 3.36 $
$Logfile: C:/racks/dynam0/dynas2.fov $

DYNAMIC IMPACT LOADS (lbs.)

(1) Maximum total vertical pedestal load:	376328.0
(2) Maximum vertical load in any single pedestal:	127294.1
(3) Maximum shear load in any single pedestal:	70796.3
(4) Maximum fuel-cell impact at one local position:	954.6
(5) Maximum rack-to-wall impact at baseplate:	.0
(6) Maximum rack-to-wall impact at rack top:	.0
(7) Maximum rack-to-rack impact at baseplate:	.0
(8) Maximum rack-to-rack impact at rack top:	.0

MAXIMUM CORNER DISPLACEMENTS (in.)

Location:	X-direction	Y-direction
Top corner:	.1556	.1169
Baseplate corner:	.0065	.0041

MAXIMUM STRESS FACTORS *

Stress factor:	R1	R2	R3	R4	R5	R6	R7
Above baseplate:	.051	.042	.120	.107	.190	.216	.044
Support pedestal:	.264	.149	.377	.252	.535	.589	.224

* See Section 6.5.2.3 of the Licensing Report for definitions.

Table 6.7.13

SUMMARY RESULTS OF 3-D SINGLE RACK ANALYSIS FOR RACK MODULE: A15x17

Holtec Run I.D.: dc15x17a.uf5 Seismic Loading: Level-C

Fuel Assembly I.D. and Weight: GE 8x8-C ; 600.0 (lbs.)

Fuel Loading: 255 cells loaded; Fuel centroid X,Y: .0, .0 (in.)

Coefficient of friction at the bottom of support pedestal: 0.5

$Revision: 3.46 $
$Logfile: C:/racks/dynam0/dynam0.fov $
$Revision: 2.5 $
$Logfile: C:/racks/dynam0/dynas1.fov $
$Revision: 3.36 $
$Logfile: C:/racks/dynam0/dynas2.fov $

DYNAMIC IMPACT LOADS (lbs.)

(1) Maximum total vertical pedestal load:	377324.7
(2) Maximum vertical load in any single pedestal:	131552.2
(3) Maximum shear load in any single pedestal:	55182.7
(4) Maximum fuel-cell impact at one local position:	953.9
(5) Maximum rack-to-wall impact at baseplate:	.0
(6) Maximum rack-to-wall impact at rack top:	.0
(7) Maximum rack-to-rack impact at baseplate:	.0
(8) Maximum rack-to-rack impact at rack top:	.0

MAXIMUM CORNER DISPLACEMENTS (in.)

Location:	X-direction	Y-direction
Top corner:	.1538	.1133
Baseplate corner:	.0068	.0071

MAXIMUM STRESS FACTORS *

Stress factor:	R1	R2	R3	R4	R5	R6	R7
Above baseplate:	.051	.042	.124	.107	.202	.231	.052
Support pedestal:	.278	.131	.295	.221	.535	.584	.175

* See Section 6.5.2.3 of the Licensing Report for definitions.

Table 6.7.14

SUMMARY RESULTS OF 3-D SINGLE RACK ANALYSIS FOR RACK MODULE: A15x17

Holtec Run I.D.: dc15x17a.uf2 Seismic Loading: Level-C

Fuel Assembly I.D. and Weight: GE 8x8-C ; 600.0 (lbs.)

Fuel Loading: 255 cells loaded; Fuel centroid X,Y: .0, .0 (in.)

Coefficient of friction at the bottom of support pedestal: 0.2

$Revision: 3.46 $
$Logfile: C:/racks/dynam0/dynam0.fov $
$Revision: 2.5 $
$Logfile: C:/racks/dynam0/dynas1.fov $
$Revision: 3.36 $
$Logfile: C:/racks/dynam0/dynas2.fov $

DYNAMIC IMPACT LOADS (lbs.)

(1) Maximum total vertical pedestal load:	383149.6
(2) Maximum vertical load in any single pedestal:	1208
(3) Maximum shear load in any single pedestal:	23792.7
(4) Maximum fuel-cell impact at one local position:	952.0
(5) Maximum rack-to-wall impact at baseplate:	.0
(6) Maximum rack-to-wall impact at rack top:	.0
(7) Maximum rack-to-rack impact at baseplate:	.0
(8) Maximum rack-to-rack impact at rack top:	.0

MAXIMUM CORNER DISPLACEMENTS (in.)

Location:	X-direction	Y-direction
Top corner:	.1056	.1922
Baseplate corner:	.0583	.1226

MAXIMUM STRESS FACTORS *

Stress factor:	R1	R2	R3	R4	R5	R6	R7
Above baseplate:	.052	.021	.114	.101	.186	.212	.024
Support pedestal:	.251	.067	.127	.114	.397	.424	.075

* See Section 6.5.2.3 of the Licensing Report for definitions.

Table 6.7.15

'SUMMARY RESULTS OF 3-D SINGLE RACK ANALYSIS FOR RACK MODULE: A15x17

Holtec Run I.D.: dc15x17a.uh8 Seismic Loading: Level-C

Fuel Assembly I.D. and Weight: GE 8x8-C ; [illegible] (lbs.)

Fuel Loading: 127 cells loaded; Fuel centroid X,Y: [illegible] -26.7 (in.)

Coefficient of friction at the bottom of support pedestal: 0.8

$Revision: 3.46 $
$Logfile: C:/racks/dynam0/dynam0.fov $
$Revision: 2.5 $
$Logfile: C:/racks/dynam0/dynas1.fov $
$Revision: 3.36 $
$Logfile: C:/racks/dynam0/dynas2.fov $

DYNAMIC IMPACT LOADS (lbs.)

(1) Maximum total vertical pedestal load:	207950.7
(2) Maximum vertical load in any single pedestal:	106936.1
(3) Maximum shear load in any single pedestal:	61892.6
(4) Maximum fuel cell impact at one local position:	952.9
(5) Maximum rack-to-wall impact at baseplate:	.0
(6) Maximum rack-to-wall impact at rack top:	.0
(7) Maximum rack-to-rack impact at baseplate:	.0
(8) Maximum rack-to-rack impact at rack top:	171.6

MAXIMUM CORNER DISPLACEMENTS (in.)

Location:	X-direction	Y-direction
Top corner:	.1373	.1440
Baseplate corner:	.0098	.0099

MAXIMUM STRESS FACTORS *

Stress factor:	R1	R2	R3	R4	R5	R6	R7
Above baseplate:	.029	.038	.086	.079	.119	.138	.020
Support pedestal:	.222	.149	.256	.252	.559	.629	.152

* See Section 6.5.2.3 of the Licensing Report for definitions.

Table 6.7.16

SUMMARY RESULTS OF 3-D SINGLE RACK ANALYSIS FOR RACK MODULE: A15x17

Holtec Run I.D.: dc15x17a.uh5 Seismic Loading: Level-C

Fuel Assembly I.D. and Weight: GE 8x8-C ; 600.0 (lbs.)

Fuel Loading: 127 cells loaded; Fuel centroid X,Y: 1.4,-26.7 (in.)

Coefficient of friction at the bottom of support pedestal: 0.5

$Revision: 3.46 $
$Logfile: C:/racks/dynam0/dynam0.fov $
$Revision: 2.5 $
$Logfile: C:/racks/dynam0/dynas1.fov $
$Revision: 3.36 $
$Logfile: C:/racks/dynam0/dynas2.fov $

DYNAMIC IMPACT LOADS (lbs.)

(1) Maximum total vertical pedestal load:	217531.7
(2) Maximum vertical load in any single pedestal:	104898.5
(3) Maximum shear load in any single pedestal:	38398.1
(4) Maximum fuel-cell impact at one local position:	952.3
(5) Maximum rack-to-wall impact at baseplate:	.0
(6) Maximum rack-to-wall impact at rack top:	.0
(7) Maximum rack-to-rack impact at baseplate:	.0
(8) Maximum rack-to-rack impact at rack top:	153.3

MAXIMUM CORNER DISPLACEMENTS (in.)

Location:	X-direction	Y-direction
Top corner:	.1292	.1420
Baseplate corner:	.0170	.0145

MAXIMUM STRESS FACTORS *

Stress factor:	R1	R2	R3	R4	R5	R6	R7
Above baseplate:	.031	.026	.084	.071	.123	.142	.020
Support pedestal:	.218	.110	.188	.186	.403	.445	.112

* See Section 6.5.2.3 of the Licensing Report for definitions.

Table 6.7.17

SUMMARY RESULTS OF 3-D SINGLE RACK ANALYSIS FOR RACK MODULE: A15x17

Holtec Run I.D.: dc15x17a.uh2 Seismic Loading: Level-C

Fuel Assembly I.D. and Weight: GE 8x8-C ; 600.0 (lbs.)

Fuel Loading: 127 cells loaded; Fuel centroid X,Y: 1.4,-26.7 (in.)

Coefficient of friction at the bottom of support pedestal: 0.2

$Revision: 3.46 $
$Logfile: C:/racks/dynam0/dynam0.fov $
$Revision: 2.5 $
$Logfile: C:/racks/dynam0/dynas1.fov $
$Revision: 3.36 $
$Logfile: C:/racks/dynam0/dynas2.fov $

DYNAMIC IMPACT LOADS (lbs.)

(1) Maximum total vertical pedestal load:	214142.4
(2) Maximum vertical load in any single pedestal:	94827..
(3) Maximum shear load in any single pedestal:	17356.9
(4) Maximum fuel-cell impact at one local position:	952.2
(5) Maximum rack-to-wall impact at baseplate:	.0
(6) Maximum rack-to-wall impact at rack top:	.0
(7) Maximum rack-to-rack impact at baseplate:	.0
(8) Maximum rack-to-rack impact at rack top:	.0

MAXIMUM CORNER DISPLACEMENTS (in.)

Location:	X-direction	Y-direction
Top corner:	.1141	.2031
Baseplate corner:	.0604	.1981

MAXIMUM STRESS FACTORS *

Stress factor:	R1	R2	R3	R4	R5	R6	R7
Above baseplate:	.032	.010	.076	.064	.111	.125	.013
Support pedestal:	.200	.045	.091	.076	.296	.313	.054

* See Section 6.5.2.3 of the Licensing Report for definitions.

Table 6.7.18

SUMMARY RESULTS OF 3-D SINGLE RACK ANALYSIS FOR RACK MODULE: A15x17

Holtec Run I.D.: dc15x17a.ue8 Seismic Loading: Level-C

Fuel Assembly I.D. and Weight: GE 8x8-C ; 600.0 (lbs.)

Fuel Loading: 15 cells loaded; Fuel centroid X,Y: .0,-50.2 (in.)

Coefficient of friction at the bottom of support pedestal: 0.8

$Revision: 3.46 $
$Logfile: C:/racks/dynam0/dynam0.fov $
$Revision: 2.[illegible] $
$Logfile: C:/racks/dynam0/dynas1.fov $
$Revision: 3.36 $
$Logfile: C:/racks/dynam0/dynas2.fov $

DYNAMIC IMPACT LOADS (lbs.)

(1) Maximum total vertical pedestal load:	53667.5
(2) Maximum vertical load in any single pedestal:	38707.7
(3) Maximum shear load in any single pedestal:	23053.1
(4) Maximum fuel-cell impact at one local position:	967.8
(5) Maximum rack-to-wall impact at baseplate:	.0
(6) Maximum rack-to-wall impact at rack top:	.0
(7) Maximum rack-to-rack impact at baseplate:	.0
(8) Maximum rack-to-rack impact at rack top:	.0

MAXIMUM CORNER DISPLACEMENTS (in.)

Location:	X-direction	Y-direction
Top corner:	.0685	.0801
Baseplate corner:	.0057	.0046

MAXIMUM STRESS FACTORS *

Stress factor:	R1	R2	R3	R4	R5	R6	R7
Above baseplate:	.009	.008	.034	.028	.053	.061	.010
Support pedestal:	.082	.057	.089	.096	.228	.254	.053

* See Section 6.5.2.3 of the Licensing Report for definitions.

Table 6.7.19

SUMMARY RESULTS OF 3-D SINGLE RACK ANALYSIS FOR RACK MODULE: A15x17

Holtec Run I.D.: dc15x17a.ue5 Seismic Loading: Level-C

Fuel Assembly I.D. and Weight: GE 8x8-C ; 600.0 (lbs.)

Fuel Loading: 15 cells loaded; Fuel centroid X,Y: .0,-50.2 (in.)

Coefficient of friction at the bottom of support pedestal: 0.5

$Revision: 3.46 $
$Logfile: C:/racks/dynam0/dynam0.fov $
$Revision: 2.5 $
$Logfile: C:/racks/dynam0/dynas1.fov $
$Revision: 3.36 $
$Logfile: C:/racks/dynam0/dynas2.fov $

DYNAMIC IMPACT LOADS (lbs.)

(1) Maximum total vertical pedestal load:	57119.1
(2) Maximum vertical load in any single pedestal:	38493.3
(3) Maximum shear load in any single pedestal:	18456.7
(4) Maximum fuel-cell impact at one local position:	968.9
(5) Maximum rack-to-wall impact at baseplate:	.0
(6) Maximum rack-to-wall impact at rack top:	.0
(7) Maximum rack-to-rack impact at baseplate:	.0
(8) Maximum rack-to-rack impact at rack top:	.0

MAXIMUM CORNER DISPLACEMENTS (in.)

Location:	X-direction	Y-direction
Top corner:	.0687	.0781
Baseplate corner:	.0118	.0175

MAXIMUM STRESS FACTORS *

Stress factor:	R1	R2	R3	R4	R5	R6	R7
Above baseplate:	.010	.006	.034	.028	.051	.058	.006
Support pedestal:	.079	.040	.074	.068	.196	.217	.044

* See Section 6.5.2.3 of the Licensing Report for definitions.

Table 6.7.20

SUMMARY RESULTS OF 3-D SINGLE RACK ANALYSIS FOR RACK MODULE: A15x17

Holtec Run I.D.: dc15x17a.ue2 Seismic Loading: Level-C

Fuel Assembly I.D. and Weight: GE 8x8-C ; 600.0 (lbs.)

Fuel Loading: 15 cells loaded; Fuel centroid X,Y: .0,-50.2 (in.)

Coefficient of friction at the bottom of support pedestal: 0.2

$Revision: 3.46 $
$Logfile: C:/racks/dynam0/dynam0.fov $
$Revision: 2.5 $
$Logfile: C:/racks/dynam0/dynas1.fov $
$Revision: 3.36 $
$Logfile: C:/racks/dynam0/dynas2.fov $

DYNAMIC IMPACT LOADS (lbs.)

(1) Maximum total vertical pedestal load:	49945.7
(2) Maximum vertical load in any single pedestal:	24058.3
(3) Maximum shear load in any single pedestal:	4793.1
(4) Maximum fuel-cell impact at one local position:	969.9
(5) Maximum rack-to-wall impact at baseplate:	.0
(6) Maximum rack-to-wall impact at rack top:	.0
(7) Maximum rack-to-rack impact at baseplate:	.0
(8) Maximum rack-to-rack impact at rack top:	.0

MAXIMUM CORNER DISPLACEMENTS (in.)

Location:	X-direction	Y-direction
Top corner:	.0380	.0495
Baseplate corner:	.0219	.0479

MAXIMUM STRESS FACTORS *

Stress factor:	R1	R2	R3	R4	R5	R6	R7
Above baseplate:	.009	.003	.021	.018	.037	.041	.003
Support pedestal:	.051	.012	.025	.021	.077	.082	.015

* See Section 6.5.2.3 of the Licensing Report for definitions.

Table 6.7.21

SUMMARY RESULTS OF 3-D SINGLE RACK ANALYSIS FOR RACK MODULE: K9x18

Holtec Run I.D.: dc9x18k.rf8 Seismic Loading: Level-C

Fuel Assembly I.D. and Weight: GE 8x8-C ; 680.0 (lbs.)

Fuel Loading: 162 cells loaded; Fuel centroid X,Y: .0, .0 (in.)

Coefficient of friction at the bottom of support pedestal: 0.8

$Revision: 3.46 $
$Logfile: C:/racks/dynam0/dynam0.fov $
$Revision: 2.5 $
$Logfile: C:/racks/dynam0/dynas1.fov $
$Revision: 3.36 $
$Logfile: C:/racks/dynam0/dynas2.fov $

DYNAMIC IMPACT LOADS (lbs.)

(1) Maximum total vertical pedestal load:	252590.0
(2) Maximum vertical load in any single pedestal:	113789.2
(3) Maximum shear load in any single pedestal:	90010.1
(4) Maximum fuel-cell impact at one local position:	802.4
(5) Maximum rack-to-wall impact at baseplate:	.0
(6) Maximum rack-to-wall impact at rack top:	.0
(7) Maximum rack-to-rack impact at baseplate:	.0
(8) Maximum rack-to-rack impact at rack top:	.0

MAXIMUM CORNER DISPLACEMENTS (in.)

Location:	X-direction	Y-direction
Top corner:	.1259	.1064
Baseplate corner:	.0054	.0039

MAXIMUM STRESS FACTORS *

Stress factor:	R1	R2	R3	R4	R5	R6	R7
Above baseplate:	.052	.040	.191	.083	.212	.242	.034
Support pedestal:	.238	.137	.480	.231	.673	.750	.285

* See Section 6.5.2.3 of the Licensing Report for definitions.

Table 6.7.22

SUMMARY RESULTS OF 3-D SINGLE RACK ANALYSIS FOR RACK MODULE: K9x18

Holtec Run I.D.: dc9x18k.rf5 Seismic Loading: Level-C

Fuel Assembly I.D. and Weight: GE 8x8-C ; 680.0 (lbs.)

Fuel Loading: 162 cells loaded; Fuel centroid X,Y: .0, .0 (in.)

Coefficient of friction at the bottom of support pedestal: 0.5

$Revision: 3.46 $
$Logfile: C:/racks/dynam0/dynam0.fov $
$Revision: 2.5 $
$Logfile: C:/racks/dynam0/dynas1.fov $
$Revision: 3.36 $
$Logfile: C:/racks/dynam0/dynas2.fov $

DYNAMIC IMPACT LOADS (lbs.)

(1) Maximum total vertical pedestal load:	246963.0
(2) Maximum vertical load in any single pedestal:	112069.4
(3) Maximum shear load in any single pedestal:	54704.1
(4) Maximum fuel-cell impact at one local position:	802.4
(5) Maximum rack-to-wall impact at baseplate:	.0
(6) Maximum rack-to-wall impact at rack top:	.0
(7) Maximum rack-to-rack impact at baseplate:	.0
(8) Maximum rack-to-rack impact at rack top:	.0

MAXIMUM CORNER DISPLACEMENTS (in.)

Location:	X-direction	Y-direction
Top corner:	.1238	.1006
Baseplate corner:	.0061	.0053

MAXIMUM STRESS FACTORS *

Stress factor:	R1	R2	R3	R4	R5	R6	R7
Above baseplate:	.050	.033	.197	.079	.207	.238	.037
Support pedestal:	.231	.088	.292	.149	.495	.543	.173

* See Section 6.5.2.3 of the Licensing Report for definitions.

Table 6.7.23

SUMMARY RESULTS OF 3-D SINGLE RACK ANALYSIS FOR RACK MODULE: K9x18

Holtec Run I.D.: dc9x18k.rf2 Seismic Loading: Level-C

Fuel Assembly I.D. and Weight: GE 8x8-C ; 680.0 (lbs.)

Fuel Loading: 162 cells loaded; Fuel centroid X,Y: .0, .0 (in.)

Coefficient of friction at the bottom of support pedestal: 0.2

$Revision: 3.46 $
$Logfile: C:/racks/dynam0/dynam0.fov $
$Revision: 2.5 $
$Logfile: C:/racks/dynam0/dynas1.fov $
$Revision: 3.36 $
$Logfile: C:/racks/dynam0/dynas2.fov $

DYNAMIC IMPACT LOADS (lbs.)

(1) Maximum total vertical pedestal load:	244480.7
(2) Maximum vertical load in any single pedestal:	100113.8
(3) Maximum shear load in any single pedestal:	19968.3
(4) Maximum fuel-cell impact at one local position:	871.2
(5) Maximum rack-to-wall impact at baseplate:	.0
(6) Maximum rack-to-wall impact at rack top:	.0
(7) Maximum rack-to-rack impact at baseplate:	.0
(8) Maximum rack-to-rack impact at rack top:	.0

MAXIMUM CORNER DISPLACEMENTS (in.)

Location:	X-direction	Y-direction
Top corner:	.1130	.1094
Baseplate corner:	.0134	.0709

MAXIMUM STRESS FACTORS *

Stress factor:	R1	R2	R3	R4	R5	R6	R7
Above baseplate:	.048	.020	.154	.080	.172	.196	.023
Support pedestal:	.211	.050	.104	.084	.319	.338	.062

* See Section 6.5.2.3 of the Licensing Report for definitions.

Table 6.7.24

SUMMARY RESULTS OF 3-D SINGLE RACK ANALYSIS FOR RACK MODULE: K9x18

Holtec Run I.D.: dc9x18k.rh8 Seismic Loading: Level-C

Fuel Assembly I.D. and Weight: GE 8x8-C ; 680.0 (lbs.)

Fuel Loading: 81 cells loaded; Fuel centroid X,Y: .0, 28.3 (in.)

Coefficient of friction at the bottom of support pedestal: 0.8

$Revision: 3.46 $
$Logfile: C:/racks/dynam0/dynam0.fov $
$Revision: 2.5 $
$Logfile: C:/racks/dynam0/dynas1.fov $
$Revision: 3.36 $
$Logfile: C:/racks/dynam0/dynas2.fov $

DYNAMIC IMPACT LOADS (lbs.)

(1) Maximum total vertical pedestal load:	134093.9
(2) Maximum vertical load in any single pedestal:	59940.5
(3) Maximum shear load in any single pedestal:	33427.6
(4) Maximum fuel-cell impact at one local position:	765.2
(5) Maximum rack-to-wall impact at baseplate:	.0
(6) Maximum rack-to-wall impact at rack top:	.0
(7) Maximum rack-to-rack impact at baseplate:	.0
(8) Maximum rack-to-rack impact at rack top:	.0

MAXIMUM CORNER DISPLACEMENTS (in.)

Location:	X-direction	Y-direction
Top corner:	.1440	.0836
Baseplate corner:	.0028	.0024

MAXIMUM STRESS FACTORS *

Stress factor:	R1	R2	R3	R4	R5	R6	R7
Above baseplate:	.027	.020	.095	.056	.104	.120	.020
Support pedestal:	.127	.064	.173	.109	.292	.325	.102

* See Section 6.5.2.3 of the Licensing Report for definitions.

Table 6.7.25

SUMMARY RESULTS OF 3-D SINGLE RACK ANALYSIS FOR RACK MODULE: K9x18

Holtec Run I.D.: dc9x18k.rh5 Seismic Loading: Level-C

Fuel Assembly I.D. and Weight: GE 8x8-C ; 680.0 (lbs.)

Fuel Loading: 81 cells loaded; Fuel centroid X,Y: .0, 28.3 (in.)

Coefficient of friction at the bottom of support pedestal: 0.5

$Revision: 3.46 $
$Logfile: C:/racks/dynam0/dynam0.fov $
$Revision: 2.5 $
$Logfile: C:/racks/dynam0/dynas1.fov $
$Revision: 3.36 $
$Logfile: C:/racks/dynam0/dynas2.fov $

DYNAMIC IMPACT LOADS (lbs.)

(1) Maximum total vertical pedestal load:	137211.9
(2) Maximum vertical load in any single pedestal:	60458.1
(3) Maximum shear load in any single pedestal:	24744.3
(4) Maximum fuel-cell impact at one local position:	875.6
(5) Maximum rack-to-wall impact at baseplate:	.0
(6) Maximum rack-to-wall impact at rack top:	.0
(7) Maximum rack-to-rack impact at baseplate:	.0
(8) Maximum rack-to-rack impact at rack top:	.0

MAXIMUM CORNER DISPLACEMENTS (in.)

Location:	X-direction	Y-direction
Top corner:	.1434	.0847
Baseplate corner:	.0032	.0026

MAXIMUM STRESS FACTORS *

Stress factor:	R1	R2	R3	R4	R5	R6	R7
Above baseplate:	.029	.015	.099	.043	.106	.121	.019
Support pedestal:	.127	.044	.131	.074	.244	.267	.078

* See Section 6.5.2.3 of the Licensing Report for definitions.

Table 6.7.26

SUMMARY RESULTS OF 3-D SINGLE RACK ANALYSIS FOR RACK MODULE: K9x18

Holtec Run I.D.: dc9x18k.rh2 Seismic Loading: Level-C

Fuel Assembly I.D. and Weight: GE 8x8-C ; 680.0 (lbs.)

Fuel Loading: 81 cells loaded; Fuel centroid X,Y: .0, 28.3 (in.)

Coefficient of friction at the bottom of support pedestal: 0.2

$Revision: 3.46 $
$Logfile: C:/racks/dynam0/dynam0.fov $
$Revision: 2.5 $
$Logfile: C:/racks/dynam0/dynas1.fov $
$Revision: 3.36 $
$Logfile: C:/racks/dynam0/dynas2.fov $

DYNAMIC IMPACT LOADS (lbs.)

(1) Maximum total vertical pedestal load:	118068.6
(2) Maximum vertical load in any single pedestal:	58743.2
(3) Maximum shear load in any single pedestal:	11725.7
(4) Maximum fuel-cell impact at one local position:	826.5
(5) Maximum rack-to-wall impact at baseplate:	.0
(6) Maximum rack-to-wall impact at rack top:	.0
(7) Maximum rack-to-rack impact at baseplate:	.0
(8) Maximum rack-to-rack impact at rack top:	.0

MAXIMUM CORNER DISPLACEMENTS (in.)

Location:	X-direction	Y-direction
Top corner:	.0963	.0902
Baseplate corner:	.0244	.0794

MAXIMUM STRESS FACTORS *

Stress factor:	R1	R2	R3	R4	R5	R6	R7
Above baseplate:	.023	.010	.084	.057	.104	.119	.012
Support pedestal:	.124	.028	.057	.048	.199	.212	.034

* See Section 6.5.2.3 of the Licensing Report for definitions.

Table 6.7.27

SUMMARY RESULTS OF 3-D SINGLE RACK ANALYSIS FOR RACK MODULE: K9x18

Holtec Run I.D.: dc9x18k.re8 Seismic Loading: Level-C

Fuel Assembly I.D. and Weight: GE 8x8-C ; 680.0 (lbs.)

Fuel Loading: 9 cells loaded; Fuel centroid X,Y: .0, 53.4 (in.)

Coefficient of friction at the bottom of support pedestal: 0.8

$Revision: 3.46 $
$Logfile: C:/racks/dynam0/dynam0.fov $
$Revision: 2.5 $
$Logfile: C:/racks/dynam0/dynas1.fov $
$Revision: 3.36 $
$Logfile: C:/racks/dynam0/dynas2.fov $

DYNAMIC IMPACT LOADS (lbs.)

(1) Maximum total vertical pedestal load:	32627.4
(2) Maximum vertical load in any single pedestal:	16441.7
(3) Maximum shear load in any single pedestal:	11710.2
(4) Maximum fuel-cell impact at one local position:	902.8
(5) Maximum rack-to-wall impact at baseplate:	.0
(6) Maximum rack-to-wall impact at rack top:	.0
(7) Maximum rack-to-rack impact at baseplate:	.0
(8) Maximum rack-to-rack impact at rack top:	.0

MAXIMUM CORNER DISPLACEMENTS (in.)

Location:	X-direction	Y-direction
Top corner:	.0674	.0403
Baseplate corner:	.0011	.0011

MAXIMUM STRESS FACTORS *

Stress factor:	R1	R2	R3	R4	R5	R6	R7
Above baseplate:	.009	.004	.036	.016	.040	.046	.006
Support pedestal:	.035	.022	.063	.037	.100	.112	.037

* See Section 6.5.2.3 of the Licensing Report for definitions.

Table 6.7.28

SUMMARY RESULTS OF 3-D SINGLE RACK ANALYSIS FOR RACK MODULE: K9x18

Holtec Run I.D.: dc9x18k.re5 Seismic Loading: Level-C

Fuel Assembly I.D. and Weight: GE 8x8-C ; 680.0 (lbs.)

Fuel Loading: 9 cells loaded; Fuel centroid X,Y: .0, 53.4 (in.)

Coefficient of friction at the bottom of suppor pedestal: 0.5

$Revision: 3.46 $
$Logfile: C:/racks/dynam0/dynam0.fov $
$Revision: 2.5 $
$Logfile: C:/racks/dynam0/dynas1.fov $
$Revision: 3.36 $
$Logfile: C:/racks/dynam0/dynas2.fov $

DYNAMIC IMPACT LOADS (lbs.)

(1) Maximum total vertical pedestal load:	32057.4
(2) Maximum vertical load in any single pedestal:	17202.2
(3) Maximum shear load in any single pedestal:	7388.6
(4) Maximum fuel-cell impact at one local position:	927.9
(5) Maximum rack-to-wall impact at baseplate:	.0
(6) Maximum rack-to-wall impact at rack top:	.0
(7) Maximum rack-to-rack impact at baseplate:	.0
(8) Maximum rack-to-rack impact at rack top:	.0

MAXIMUM CORNER DISPLACEMENTS (in.)

Location:	X-direction	Y-direction
Top corner:	.0622	.0384
Baseplate corner:	.0022	.0016

MAXIMUM STRESS FACTORS *

Stress factor:	R1	R2	R3	R4	R5	R6	R7
Above baseplate:	.009	.006	.036	.014	.039	.044	.004
Support pedestal:	.036	.014	.039	.024	.071	.077	.023

* See Section 6.5.2.3 of the Licensing Report for definitions.

Table 6.7.29

SUMMARY RESULTS OF 3-D SINGLE RACK ANALYSIS FOR RACK MODULE: K9x18

Holtec Run I.D.: dc9x18k.re2 Seismic Loading: Level-C

Fuel Assembly I.D. and Weight: GE 8x8-C ; 680.0 (lbs.)

Fuel Loading: 9 cells loaded; Fuel centroid X,Y: .0, 53.4 (in.)

Coefficient of friction at the bottom of support pedestal: 0.2

$Revision: 3.46 $
$Logfile: C:/racks/dynam0/dynam0.fov $
$Revision: 2.5 $
$Logfile: C:/racks/dynam0/dynas1.fov $
$Revision: 3.36 $
$Logfile: C:/racks/dynam0/dynas2.fov $

DYNAMIC IMPACT LOADS (lbs.)

(1) Maximum total vertical pedestal load:	33808.9
(2) Maximum vertical load in any single pedestal:	17750.0
(3) Maximum shear load in any single pedestal:	3549.8
(4) Maximum fuel-cell impact at one local position:	825.8
(5) Maximum rack-to-wall impact at baseplate:	.0
(6) Maximum rack-to-wall impact at rack top:	.0
(7) Maximum rack-to-rack impact at baseplate:	.0
(8) Maximum rack-to-rack impact at rack top:	.0

MAXIMUM CORNER DISPLACEMENTS (in.)

Location:	X-direction	Y-direction
Top corner:	.0573	.0464
Baseplate corner:	.0269	.0347

MAXIMUM STRESS FACTORS *

Stress factor:	R1	R2	R3	R4	R5	R6	R7
Above baseplate:	.009	.003	.028	.008	.033	.037	.004
Support pedestal:	.037	.007	.019	.011	.054	.057	.011

* See Section 6.5.2.3 of the Licensing Report for definitions.

Table 6.7.30

SUMMARY RESULTS OF 3-D SINGLE RACK ANALYSIS FOR RACK MODULE: R-P198

Holtec Run I.D.: dc198p.rf8 Seismic Loading: Level-C

Fuel Assembly I.D. and Weight: GE 8x8-C ; 680.0 (lbs.)

Fuel Loading: 198 cells loaded; Fuel centroid X,Y: .0, .0 (in.)

Coefficient of friction at the bottom of support pedestal: 0.8

$Revision: 3.46 $
$Logfile: C:/racks/dynam0/dynam0.fov $
$Revision: 2.5 $
$Logfile: C:/racks/dynam0/dynas1.fov $
$Revision: 3.36 $
$Logfile: C:/racks/dynam0/dynas2.fov $

DYNAMIC IMPACT LOADS (lbs.)

(1) Maximum total vertical pedestal load:	297291.2
(2) Maximum vertical load in any single pedestal:	112242.7
(3) Maximum shear load in any single pedestal:	43223.2
(4) Maximum fuel-cell impact at one local position:	829.7
(5) Maximum rack-to-wall impact at baseplate:	.0
(6) Maximum rack-to-wall impact at rack top:	.0
(7) Maximum rack-to-rack impact at baseplate:	.0
(8) Maximum rack-to-rack impact at rack top:	.0

MAXIMUM CORNER DISPLACEMENTS (in.)

Location:	X-direction	Y-direction
Top corner:	.1137	.1233
Baseplate corner:	.0039	.0046

MAXIMUM STRESS FACTORS *

Stress factor:	R1	R2	R3	R4	R5	R6	R7
Above baseplate:	.041	.029	.102	.117	.179	.204	.032
Support pedestal:	.235	.130	.221	.220	.444	.483	.131

* See Section 6.5.2.3 of the Licensing Report for definitions.

Table 6.7.31

SUMMARY RESULTS OF 3-D SINGLE RACK ANALYSIS FOR RACK MODULE: R-P198

Holtec Run I.D.: dc198p.rf5 Seismic Loading: Level-C

Fuel Assembly I.D. and Weight: GE 8x8-C ; 680.0 (lbs.)

Fuel Loading: 198 cells loaded; Fuel centroid X,Y: .0, .0 (in.)

Coefficient of friction at the bottom of support pedestal: 0.5

$Revision: 3.46 $
$Logfile: C:/racks/dynam0/dynam0.fov $
$Revision: 2.5 $
$Logfile: C:/racks/dynam0/dynas1.fov $
$Revision: 3.36 $
$Logfile: C:/racks/dynam0/dynas2.fov $

DYNAMIC IMPACT LOADS (lbs.)

(1) Maximum total vertical pedestal load:	312497.0
(2) Maximum vertical load in any single pedestal:	109492.6
(3) Maximum shear load in any single pedestal:	42211.1
(4) Maximum fuel-cell impact at one local position:	785.7
(5) Maximum rack-to-wall impact at baseplate:	.0
(6) Maximum rack-to-wall impact at rack top:	.0
(7) Maximum rack-to-rack impact at baseplate:	.0
(8) Maximum rack-to-rack impact at rack top:	.0

MAXIMUM CORNER DISPLACEMENTS (in.)

Location:	X-direction	Y-direction
Top corner:	.1122	.1112
Baseplate corner:	.0043	.0037

MAXIMUM STRESS FACTORS *

Stress factor:	R1	R2	R3	R4	R5	R6	R7
Above baseplate:	.046	.026	.094	.105	.172	.196	.034
Support pedestal:	.230	.131	.161	.220	.435	.473	.096

* See Section 6.5.2.3 of the Licensing Report for definitions.

Table 6.7.32

SUMMARY RESULTS OF 3-D SINGLE RACK ANALYSIS FOR RACK MODULE: R-P198

Holtec Run I.D.: dc198p.rf2 Seismic Loading: Level-C

Fuel Assembly I.D. and Weight: GE 8x8-C ; 680.0 (lbs.)

Fuel Loading: 198 cells loaded; Fuel centroid X,Y: .0, .0 (in.)

Coefficient of friction at the bottom of support pedestal: 0.2

$Revision: 3.46 $
$Logfile: C:/racks/dynam0/dynam0.fov $
$Revision: 2.5 $
$Logfile: C:/racks/dynam0/dynas1.fov $
$Revision: 3.36 $
$Logfile: C:/racks/dynam0/dynas2.fov $

DYNAMIC IMPACT LOADS (lbs.)

(1) Maximum total vertical pedestal load:	308847.9
(2) Maximum vertical load in any single pedestal:	105309.2
(3) Maximum shear load in any single pedestal:	20886.4
(4) Maximum fuel-cell impact at one local position:	884.7
(5) Maximum rack-to-wall impact at baseplate:	.0
(6) Maximum rack-to-wall impact at rack top:	.0
(7) Maximum rack-to-rack impact at baseplate:	.0
(8) Maximum rack-to-rack impact at rack top:	.0

MAXIMUM CORNER DISPLACEMENTS (in.)

Location:	X-direction	Y-direction
Top corner:	.1015	.1172
Baseplate corner:	.0203	.0292

MAXIMUM STRESS FACTORS *

Stress factor:	R1	R2	R3	R4	R5	R6	R7
Above baseplate:	.045	.020	.097	.106	.164	.187	.018
Support pedestal:	.221	.066	.108	.111	.353	.376	.064

* See Section 6.5.2.3 of the Licensing Report for definitions.

Table 6.7.33

SUMMARY RESULTS OF 3-D SINGLE RACK ANALYSIS FOR RACK MODULE: R-P198

Holtec Run I.D.: dc198p.rh8 Seismic Loading: Level-C

Fuel Assembly I.D. and Weight: GE 8x8-C ; 680.0 (lbs.)

Fuel Loading: 97 cells loaded; Fuel centroid X,Y: .0, 22.0 (in.)

Coefficient of friction at the bottom of support pedestal: 0.8

$Revision: 3.46 $
$Logfile: C:/racks/dynam0/dynam0.fov $
$Revision: 2.5 $
$Logfile: C:/racks/dynam0/dynas1.fov $
$Revision: 3.36 $
$Logfile: C:/racks/dynam0/dynas2.fov $

DYNAMIC IMPACT LOADS (lbs.)

(1) Maximum total vertical pedestal load:	157210.6
(2) Maximum vertical load in any single pedestal:	74952.8
(3) Maximum shear load in any single pedestal:	40519.8
(4) Maximum fuel-cell impact at one local position:	857.9
(5) Maximum rack-to-wall impact at baseplate:	.0
(6) Maximum rack-to-wall impact at rack top:	.0
(7) Maximum rack-to-rack impact at baseplate:	.0
(8) Maximum rack-to-rack impact at rack top:	.0

MAXIMUM CORNER DISPLACEMENTS (in.)

Location:	X-direction	Y-direction
Top corner:	.0972	.1577
Baseplate corner:	.0048	.0053

MAXIMUM STRESS FACTORS *

Stress factor:	R1	R2	R3	R4	R5	R6	R7
Above baseplate:	.024	.017	.066	.065	.093	.107	.018
Support pedestal:	.158	.087	.203	.146	.349	.392	.120

* See Section 6.5.2.3 of the Licensing Report for definitions.

Table 6.7.34

SUMMARY RESULTS OF 3-D SINGLE RACK ANALYSIS FOR RACK MODULE: R-P198

Holtec Run I.D.: dc198p.rh5 Seismic Loading: Level-C

Fuel Assembly I.D. and Weight: GE 8x8-C ; 680.0 (lbs.)

Fuel Loading: 97 cells loaded; Fuel centroid X,Y: .0, 22.0 (in.)

Coefficient of friction at the bottom of support pedestal: 0.5

$Revision: 3.46 $
$Logfile: C:/racks/dynam0/dynam0.fov $
$Revision: 2.5 $
$Logfile: C:/racks/dynam0/dynas1.fov $
$Revision: 3.36 $
$Logfile: C:/racks/dynam0/dynas2.fov $

DYNAMIC IMPACT LOADS (lbs.)

(1) Maximum total vertical pedestal load:	167954.4
(2) Maximum vertical load in any single pedestal:	77911.0
(3) Maximum shear load in any single pedestal:	28694.6
(4) Maximum fuel-cell impact at one local position:	823.3
(5) Maximum rack-to-wall impact at baseplate:	.0
(6) Maximum rack-to-wall impact at rack top:	.0
(7) Maximum rack-to-rack impact at baseplate:	.0
(8) Maximum rack-to-rack impact at rack top:	.0

MAXIMUM CORNER DISPLACEMENTS (in.)

Location:	X-direction	Y-direction
Top corner:	.0998	.1376
Baseplate corner:	.0133	.0171

MAXIMUM STRESS FACTORS *

Stress factor:	R1	R2	R3	R4	R5	R6	R7
Above baseplate:	.026	.016	.071	.064	.099	.115	.017
Support pedestal:	.164	.075	.151	.127	.300	.329	.090

* See Section 6.5.2.3 of the Licensing Report for definitions.

Table 6.7.35

SUMMARY RESULTS OF 3-D SINGLE RACK ANALYSIS FOR RACK MODULE: R-P198

Holtec Run I.D.: dc198p.rh2 Seismic Loading: Level-C

Fuel Assembly I.D. and Weight: [illegible] ; 680.0 (lbs.)

Fuel Loading: 97 cells loaded; Fuel centroid X,Y: .0, 22.0 (in.)

Coefficient of friction at the bottom of support pedestal: 0.2

$Revision: 3.46 $
$Logfile: C:/racks/dynam0/dynam0.fov $
$Revision: 2.5 $
$Logfile: C:/racks/dynam0/dynas1.fov $
$Revision: 3.36 $
$Logfile: C:/racks/dynam0/dynas2.fov $

DYNAMIC IMPACT LOADS (lbs.)

(1) Maximum total vertical pedestal load:	153457.5
(2) Maximum vertical load in any single pedestal:	71809.2
(3) Maximum shear load in any single pedestal:	13508.1
(4) Maximum fuel-cell impact at one local position:	793.3
(5) Maximum rack-to-wall impact at baseplate:	.0
(6) Maximum rack-to-wall impact at rack top:	.0
(7) Maximum rack-to-rack impact at baseplate:	.0
(8) Maximum rack-to-rack impact at rack top:	.0

MAXIMUM CORNER DISPLACEMENTS (in.)

Location:	X-direction	Y-direction
Top corner:	.0837	.1061
Baseplate corner:	.0235	.0605

MAXIMUM STRESS FACTORS *

Stress factor:	R1	R2	R3	R4	R5	R6	R7
Above baseplate:	.023	.010	[illegible]	.064	.095	.110	.009
Support pedestal:	.149	.042	[illegible]	.070	.218	.232	.042

* See Section 6.5.2.3 of the Licensing Report for definitions.

Table 6.7.36

SUMMARY RESULTS OF 3-D SINGLE RACK ANALYSIS FOR RACK MODULE: R-P198

Holtec Run I.D.: dc198p.re8 Seismic Loading: Level-C

Fuel Assembly I.D. and Weight: GE 8x8-C ; 680.0 (lbs.)

Fuel Loading: 14 cells loaded; Fuel centroid X,Y: .0, 40.8 (in.)

Coefficient of friction at the bottom of support pedestal: 0.8

$Revision: 3.46 $
$Logfile: C:/racks/dynam0/dynam0.fov $
$Revision: 2.5 $
$Logfile: C:/racks/dynam0/dynas1.fov $
$Revision: 3.36 $
$Logfile: C:/racks/dynam0/dynas2.fov $

DYNAMIC IMPACT LOADS (lbs.)

(1) Maximum total vertical pedestal load:	46546.5
(2) Maximum vertical load in any single pedestal:	30305.7
(3) Maximum shear load in any single pedestal:	13697.3
(4) Maximum fuel-cell impact at one local position:	854.9
(5) Maximum rack-to-wall impact at baseplate:	.0
(6) Maximum rack-to-wall impact at rack top:	.0
(7) Maximum rack-to-rack impact at baseplate:	.0
(8) Maximum rack-to-rack impact at rack top:	.0

MAXIMUM CORNER DISPLACEMENTS (in.)

Location:	X-direction	Y-direction
Top corner:	.0675	.0823
Baseplate corner:	.0051	.0051

MAXIMUM STRESS FACTORS *

Stress factor:	R1	R2	R3	R4	R5	R6	R7
Above baseplate:	.009	.005	.025	.030	.044	.050	.006
Support pedestal:	.064	.036	.066	.060	.126	.141	.039

* See Section 6.5.2.3 of the Licensing Report for definitions.

Table 6.7.37

SUMMARY RESULTS OF 3-D SINGLE RACK ANALYSIS FOR RACK MODULE: R-P198

Holtec Run I.D.: dc198p.re5 Seismic Loading: Level-C

Fuel Assembly I.D. and Weight: GE 8x8-C ; 680.0 (lbs.)

Fuel Loading: 14 cells loaded; Fuel centroid X,Y: .0, 40.8 (in.)

Coefficient of friction at the bottom of support pedestal: 0.5

$Revision: 3.46 $
$Logfile: C:/racks/dynam0/dynam0.fov $
$Revision: 2.5 $
$Logfile: C:/racks/dynam0/dynas1.fov $
$Revision: 3.36 $
$Logfile: C:/racks/dynam0/dynas2.fov $

DYNAMIC IMPACT LOADS (lbs.)

(1) Maximum total vertical pedestal load:	46544.4
(2) Maximum vertical load in any single pedestal:	29501.6
(3) Maximum shear load in any single pedestal:	10973.7
(4) Maximum fuel-cell impact at one local position:	808.0
(5) Maximum rack-to-wall impact at baseplate:	.0
(6) Maximum rack-to-wall impact at rack top:	.0
(7) Maximum rack-to-rack impact at baseplate:	.0
(8) Maximum rack-to-rack impact at rack top:	.0

MAXIMUM CORNER DISPLACEMENTS (in.)

Location:	X-direction	Y-direction
Top corner:	.0849	.0743
Baseplate corner:	.0110	.0183

MAXIMUM STRESS FACTORS *

Stress factor:	R1	R2	R3	R4	R5	R6	R7
Above baseplate:	.009	.006	.024	.028	.039	.044	.006
Support pedestal:	.062	.031	.054	.053	.116	.128	.032

* See Section 6.5.2.3 of the Licensing Report for definitions.

Table 6.7.38

SUMMARY RESULTS OF 3-D SINGLE RACK ANALYSIS FOR RACK MODULE: R-P198

Holtec Run I.D.: dc198p.re2 Seismic Loading: Level-C

Fuel Assembly I.D. and Weight: GE 8x8-C ; 680.0 (lbs.)

Fuel Loading: 14 cells loaded; Fuel centroid X,Y: .0, 40.8 (in.)

Coefficient of friction at the bottom of support pedestal: 0.2

$Revision: 3.46 $
$Logfile: C:/racks/dynam0/dynam0.fov $
$Revision: 2.5 $
$Logfile: C:/racks/dynam0/dynas1.fov $
$Revision: 3.36 $
$Logfile: C:/racks/dynam0/dynas2.fov $

DYNAMIC IMPACT LOADS (lbs.)

(1) Maximum total vertical pedestal load:	45888.1
(2) Maximum vertical load in any single pedestal:	26887.3
(3) Maximum shear load in any single pedestal:	5377.2
(4) Maximum fuel-cell impact at one local position:	865.2
(5) Maximum rack-to-wall impact at baseplate:	.0
(6) Maximum rack-to-wall impact at rack top:	.0
(7) Maximum rack-to-rack impact at baseplate:	.0
(8) Maximum rack-to-rack impact at rack top:	.0

MAXIMUM CORNER DISPLACEMENTS (in.)

Location:	X-direction	Y-direction
Top corner:	.0507	.0539
Baseplate corner:	.0243	.0392

MAXIMUM STRESS FACTORS *

Stress factor:	R1	R2	R3	R4	R5	R6	R7
Above baseplate:	.009	.003	.021	.019	.039	.045	.00
Support pedestal:	.057	.014	.028	.023	.090	.096	.01

* See Section 6.5.2.3 of the Licensing Report for definitions.

Table 6.7.39

COMPARISON OF CALCULATED AND ALLOWABLE LOADS/STRESSES AT IMPACT LOCATIONS AND AT WELDS

Item/Location	Value	
	Calculated	Allowable
Fuel assembly/ cell wall impact, lbs.	970.	3528.
Rack/Baseplate weld psi	9204	29820
Pedestal/Baseplate weld (dimensionless limit load ratio)	.845*	1.0
Cell/Cell welds	1940 lb. along height for impacts 2577 lb. for base shear	6588 lbs.

* Reflects limiting case of either single or multi-rack analysis. Also, the result conservatively neglects effect of pedestal gussets.

Table 6.8.1

MAXIMUM ABSOLUTE DISPLACEMENTS OF RACK CORNERS
AT BOTH THE TOP AND BOTTOM OF EACH RACK
FROM WHOLE POOL MULTI RACK ANALYSIS
(20 racks in the pool; cof.=random with mean=0.5;
Fully loaded with reg.fuel; Level-C seismic.)

rack	uxt	uyt	uxb	uyb
1	.5879E+00	.5602E+00	.2656E+00	.2993E+00
2	.4331E+00	.4335E+00	.1921E+00	.1645E+00
3	.4195E+00	.4719E+00	.2267E+00	.3792E+00
4	.4037E+00	.3067E+00	.2637E+00	.2059E+00
5	.6641E+00	.4404E+00	.5063E+00	.4389E+00
6	.4858E+00	.3352E+00	.1764E+00	.2568E+00
7	.5589E+00	.6253E+00	.4927E+00	.5220E+00
8	.5286E+00	.2956E+00	.3991E+00	.1874E+00
9	.1196E+01	.5968E+00	.1202E+01	.6141E+00
10	.9648E+00	.4538E+00	.8878E+00	.3998E+00
11	.7592E+00	.4347E+00	.7238E+00	.4347E+00
12	.7187E+00	.4705E+00	.6508E+00	.4343E+00
13	.7315E+00	.8103E+00	.4021E+00	.7119E+00
14	.8767E+00	.4927E+00	.5160E+00	.3756E+00
15	.6008E+00	.3769E+00	.3907E+00	.3201E+00
16	.5597E+00	.5122E+00	.4994E+00	.4628E+00
17	.7324E+00	.8415E+00	.4514E+00	.7339E+00
18	.6161E+00	.3370E+00	.5087E+00	.2601E+00
19	.7499E+00	.7927E+00	.6522E+00	.6502E+00
20	.6989E+00	.7682E+00	.4525E+00	.5690E+00

$Revision: 1.8 $
$Logfile: C:/racks/multirac/maxdisp.fov $

Table 6.8.2

MAXIMUM ABSOLUTE DISPLACEMENTS OF RACK CORNERS
AT BOTH THE TOP AND BOTTOM OF EACH RACK
FROM WHOLE POOL MULTI RACK ANALYSIS
(20 racks in the pool; cof.=random with mean=0.5;
Fully loaded with reg.fuel; Level-B seismic.)

rack	uxt	uyt	uxb	uyb
1	.3655E+00	.2095E+00	.2795E+00	.1993E+00
2	.2605E+00	.2051E+00	.2641E+00	.1771E+00
3	.1491E+00	.1788E+00	.1230E+00	.1580E+00
4	.1957E+00	.1378E+00	.1903E+00	.9076E-01
5	.3085E+00	.1643E+00	.2215E+00	.1587E+00
6	.2682E+00	.1723E+00	.2854E+00	.1450E+00
7	.2439E+00	.1970E+00	.2062E+00	.1374E+00
8	.1448E+00	.1951E+00	.1180E+00	.1722E+00
9	.3596E+00	.1987E+00	.3081E+00	.1818E+00
10	.2520E+00	.1419E+00	.2482E+00	.1404E+00
11	.3586E+00	.2097E+00	.3662E+00	.2157E+00
12	.3838E+00	.1492E+00	.4045E+00	.1437E+00
13	.2375E+00	.2311E+00	.2293E+00	.2256E+00
14	.3528E+00	.2465E+00	.3680E+00	.2386E+00
15	.2368E+00	.1267E+00	.1580E+00	.9439E-01
16	.1616E+00	.1214E+00	.1591E+00	.9232E-01
17	.1448E+00	.2161E+00	.1178E+00	.1711E+00
18	.2340E+00	.1244E+00	.2253E+00	.9398E-01
19	.2917E+00	.2448E+00	.2181E+00	.2230E+00
20	.2434E+00	.1908E+00	.2154E+00	.1941E+00

$Revision: 1.8 $
$Logfile: C:/racks/multirac/maxdisp.fov $

Table 6.8.3

MAXIMUM PEDESTAL VERTICAL LOADS
FROM WHLE POOL MULTI-RACK ANALYSIS
(Fully loaded with regular fuel;
Seismic: level-c; cof.=random.)

RACK AND PEDESTAL NO.	MAX.FORCE lbs.	TIME
RACK-1:		
1	1.482D+05	3.447D+00
2	1.525D+05	1.178D+01
3	1.444D+05	1.193D+01
4	1.337D+05	7.899D+00
5	1.534D+05	8.034D+00
RACK-2:		
1	1.315D+05	1.235D+01
2	1.625D+05	1.193D+01
3	1.040D+05	3.541D+00
4	1.285D+05	1.223D+01
RACK-3:		
1	1.201D+05	1.567D+01
2	1.515D+05	1.192D+01
3	1.272D+05	1.062D+01
4	1.356D+05	1.223D+01
RACK-4:		
1	8.807D+04	1.227D+01
2	9.473D+04	1.193D+01
3	1.377D+05	1.059D+01
4	1.184D+05	1.602D+01
5	1.010D+05	1.177D+01
RACK-5:		
1	1.327D+05	1.587D+01
2	1.303D+05	1.193D+01
3	1.219D+05	8.032D+00
4	1.743D+05	1.108D+01
RACK-6:		
1	1.428D+05	8.438D+00
2	1.049D+05	1.162D+01
3	1.054D+05	5.320D+00
4	1.517D+05	1.108D+01
RACK-7:		
1	1.186D+05	8.435D+00
2	1.119D+05	1.389D+01
3	1.292D+05	5.314D+00
4	1.317D+05	1.108D+01

Table 6.8.3 (continued)

RACK-8:		
1	9.657D+04	8.554D+00
2	1.002D+05	1.612D+01
3	1.024D+05	5.314D+00
4	9.205D+04	1.587D+01
RACK-9:		
1	1.377D+05	1.567D+01
2	1.322D+05	1.186D+01
3	2.058D+05	1.122D+01
4	1.487D+05	1.108D+01
5	9.460D+04	1.108D+01
RACK-10:		
1	1.473D+05	1.088D+01
2	1.709D+05	6.118D+00
3	1.416D+05	1.122D+01
4	1.517D+05	1.107D+01
RACK-11:		
1	1.416D+05	9.323D+00
2	1.470D+05	1.184D+01
3	1.732D+05	1.058D+01
4	1.747D+05	9.865D+00
RACK-12:		
1	1.111D+05	1.203D+01
2	1.218D+05	1.192D+01
3	1.149D+05	5.311D+00
4	1.120D+05	8.029D+00
RACK-13:		
1	1.680D+05	8.364D+00
2	1.931D+05	1.194D+01
3	1.373D+05	8.675D+00
4	1.755D+05	8.245D+00
RACK-14:		
1	1.348D+05	1.587D+01
2	1.863D+05	1.195D+01
3	1.047D+05	1.121D+01
4	1.071D+05	1.112D+01
RACK-15:		
1	1.021D+05	9.309D+00
2	1.565D+05	1.193D+01
3	1.112D+05	8.557D+00
4	1.616D+05	1.229D+01

Table 6.8.3 (continued)

RACK-16:		
1	1.063D+05	1.568D+01
2	1.276D+05	1.193D+01
3	7.910D+04	1.058D+01
4	1.254D+05	1.229D+01
RACK-17:		
1	1.582D+05	1.587D+01
2	1.805D+05	1.194D+01
3	1.196D+05	1.059D+01
4	1.623D+05	1.236D+01
5	1.054D+05	8.032D+00
RACK-18:		
1	1.403D+05	1.037D+01
2	1.586D+05	1.194D+01
3	1.315D+05	1.063D+01
4	1.641D+05	1.109D+01
RACK-19:		
1	1.380D+05	9.319D+00
2	1.[illegible]D+05	1.194D+01
3	1.480D+05	1.064D+01
4	2.175D+05	1.108D+01
RACK-20:		
1	1.201D+05	1.236D+01
2	1.750D+05	1.195D+01
3	1.105D+05	1.058D+01
4	1.524D+05	1.122D+01
5	1.179D+05	8.360D+00

Table 6.8.4

MAXIMUM PEDESTAL VERTICAL LOADS
FROM WHLE POOL MULTI-RACK ANALYSIS
(Fully loaded with regular fuel;
Seismic: Level-B; cof.=random.)

RACK AND PEDESTAL NO.	MAX. FORCE lbs.	TIME
RACK-1:		
1	9.686D+04	1.361D+01
2	1.045D+05	1.353D+01
3	6.598D+04	1.374D+01
4	9.513D+04	7.520D+00
5	7.327D+04	1.373D+01
RACK-2:		
1	9.074D+04	1.367D+01
2	9.027D+04	1.367D+01
3	6.196D+04	7.523D+00
4	8.161D+04	7.519D+00
RACK-3:		
1	7.284D+04	7.433D+00
2	7.350D+04	1.528D+01
3	8.828D+04	1.527D+01
4	1.004D+05	7.515D+00
RACK-4:		
1	6.565D+04	7.362D+00
2	7.058D+04	6.712D+00
3	6.768D+04	6.[illegible]0D+00
4	7.809D+04	7.[illegible]8D+00
5	6.381D+04	1.340D+01
RACK-5:		
1	8.547D+04	1.366D+01
2	8.342D+04	1.375D+01
3	6.844D+04	1.537D+01
4	6.821D+04	7.518D+00
RACK-6:		
1	7.319D+04	1.096D+01
2	9.705D+04	1.374D+01
3	5.901D+04	8.560D+00
4	6.715D+04	7.632D+00
RACK-7:		
1	7.273D+04	1.366D+01
2	7.139D+04	1.373D+01
3	7.469D+04	1.535D+01
4	8.307D+04	7.520D+00

Table 6.8.4

RACK-8:		
1	6.951D+04	1.366D+01
2	7.621D+04	1.352D+01
3	5.936D+04	6.759D+00
4	5.352D+04	1.545D+01
RACK-9:		
1	1.039D+05	1.361D+01
2	1.072D+05	1.352D+01
3	9.073D+04	8.082D+00
4	6.868D+04	7.432D+00
5	6.570D+04	7.432D+00
RACK-10:		
1	1.163D+05	1.367D+01
2	1.093D+05	1.353D+01
3	7.961D+04	1.006D+01
4	8.397D+04	1.414D+01
RACK-11:		
1	1.102D+05	1.361D+01
2	7.821D+04	1.354D+01
3	9.440D+04	1.394D+01
4	9.227D+04	7.520D+00
RACK-12:		
1	7.606D+04	1.367D+01
2	8.254D+04	1.373D+01
3	6.154D+04	1.535D+01
4	5.875D+04	7.354D+00
RACK-13:		
1	1.080D+05	1.367D+01
2	8.591D+04	1.367D+01
3	7.138D+04	1.382D+01
4	7.941D+04	7.430D+00
RACK-14:		
1	6.804D+04	1.360D+01
2	9.156D+04	1.367D+01
3	6.145D+04	1.538D+01
4	5.908D+04	1.420D+01
RACK-15:		
1	7.549D+04	1.367D+01
2	7.654D+04	1.367D+01
3	6.452D+04	8.762D+00
4	7.864D+04	7.520D+00

Table 6.8.4

RACK-16:		
1	6.144D+04	1.096D+01
2	5.877D+04	6.761D+00
3	4.523D+04	1.529D+01
4	5.671D+04	7.451D+00
RACK-17:		
1	1.076D+05	1.367D+01
2	8.289D+04	5.079D+00
3	6.726D+04	8.556D+00
4	6.543D+04	4.937D+00
5	6.416D+04	1.420D+01
RACK-18:		
1	9.900D+04	1.367D+01
2	8.248D+04	8.186D+00
3	6.051D+04	1.389D+01
4	7.107D+04	1.432D+01
RACK-19:		
1	8.362D+04	1.366D+01
2	7.858D+04	1.354D+01
3	8.376D+04	1.407D+01
4	8.476D+04	1.407D+01
RACK-20:		
1	6.237D+04	1.546D+01
2	6.787D+04	1.224D+01
3	6.438D+04	7.630D+00
4	8.854D+04	1.592D+01
5	8.220D+04	1.366D+01

Table 6.9.1

AVERAGE BEARING PAD PRESSURE
COMPARISON OF CALCULATED AND ALLOWABLE STRESSES

Pad Size	Max. Load (lb.)	STRESS (psi) Calculated	Allowable
15.0 x 15.0 (no leak chase)	217500	967	2380*

(based on concrete strength f_c' = 2000 psi)

* factor ϵ = 2

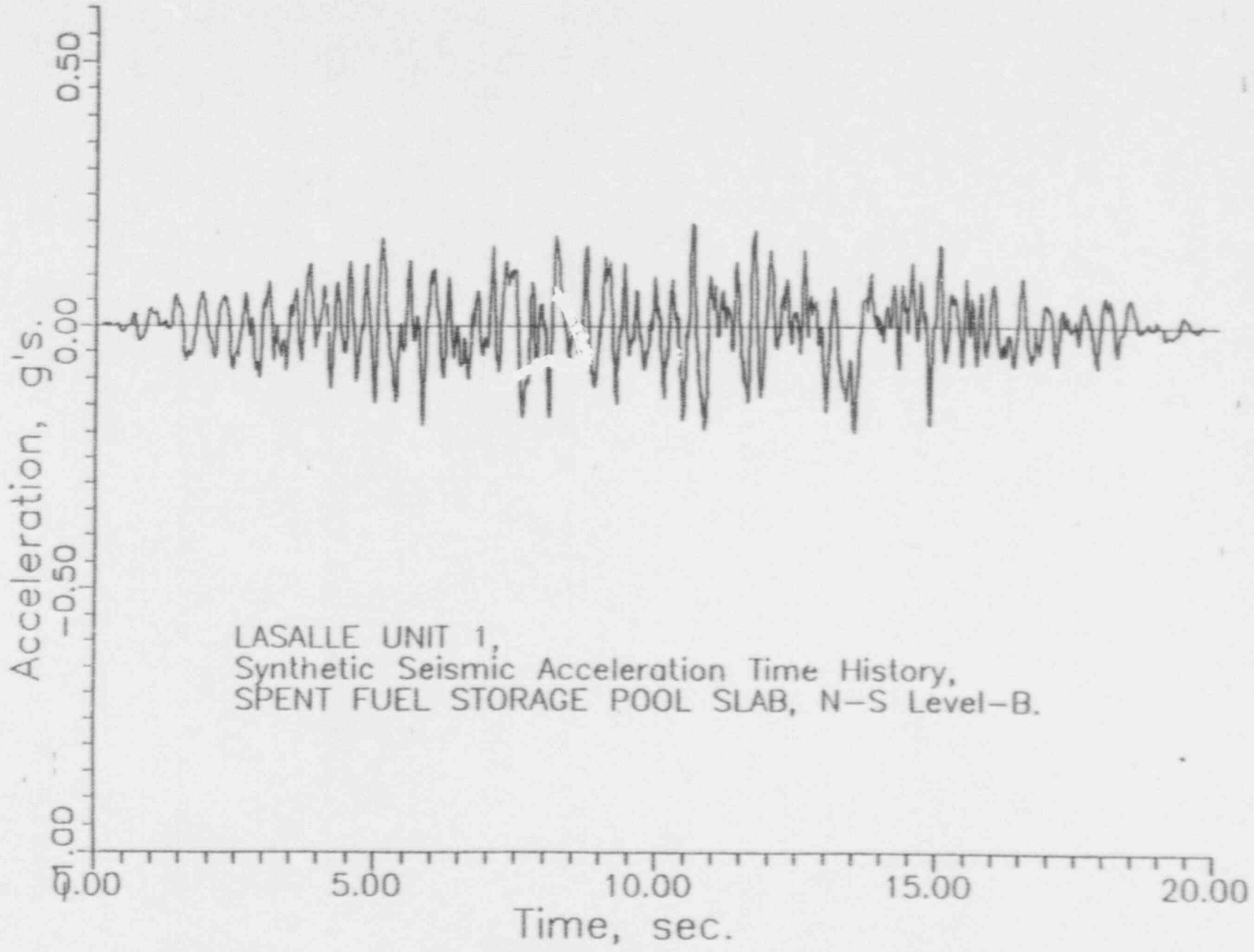
0.50
0.00
-0.50
-1.00
Acceleration, g's.
0.00
5.00
10.00
15.00
20.00
Time, sec.
LASALLE UNIT 1,
Synthetic Seismic Acceleration Time History,
SPENT FUEL STORAGE POOL SLAB, N-S Level-B.

FIGURE 6.3.1

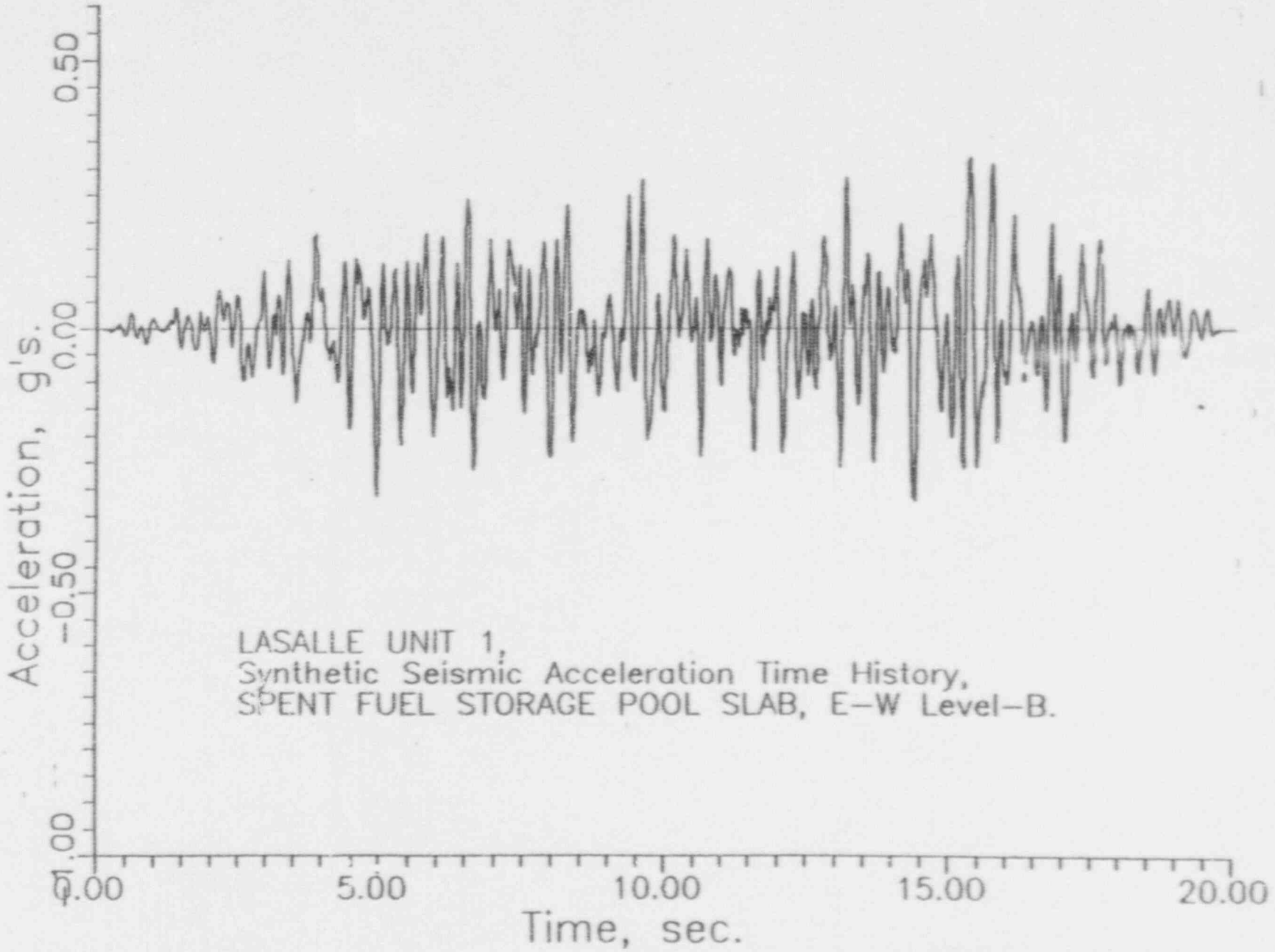
0.50
0.00
-0.50
-1.00
Acceleration, g's.
0.00
5.00
10.00
15.00
20.00
Time, sec.
LASALLE UNIT 1,
Synthetic Seismic Acceleration Time History,
SPENT FUEL STORAGE POOL SLAB, E-W Level-B.

FIGURE 6.3.2

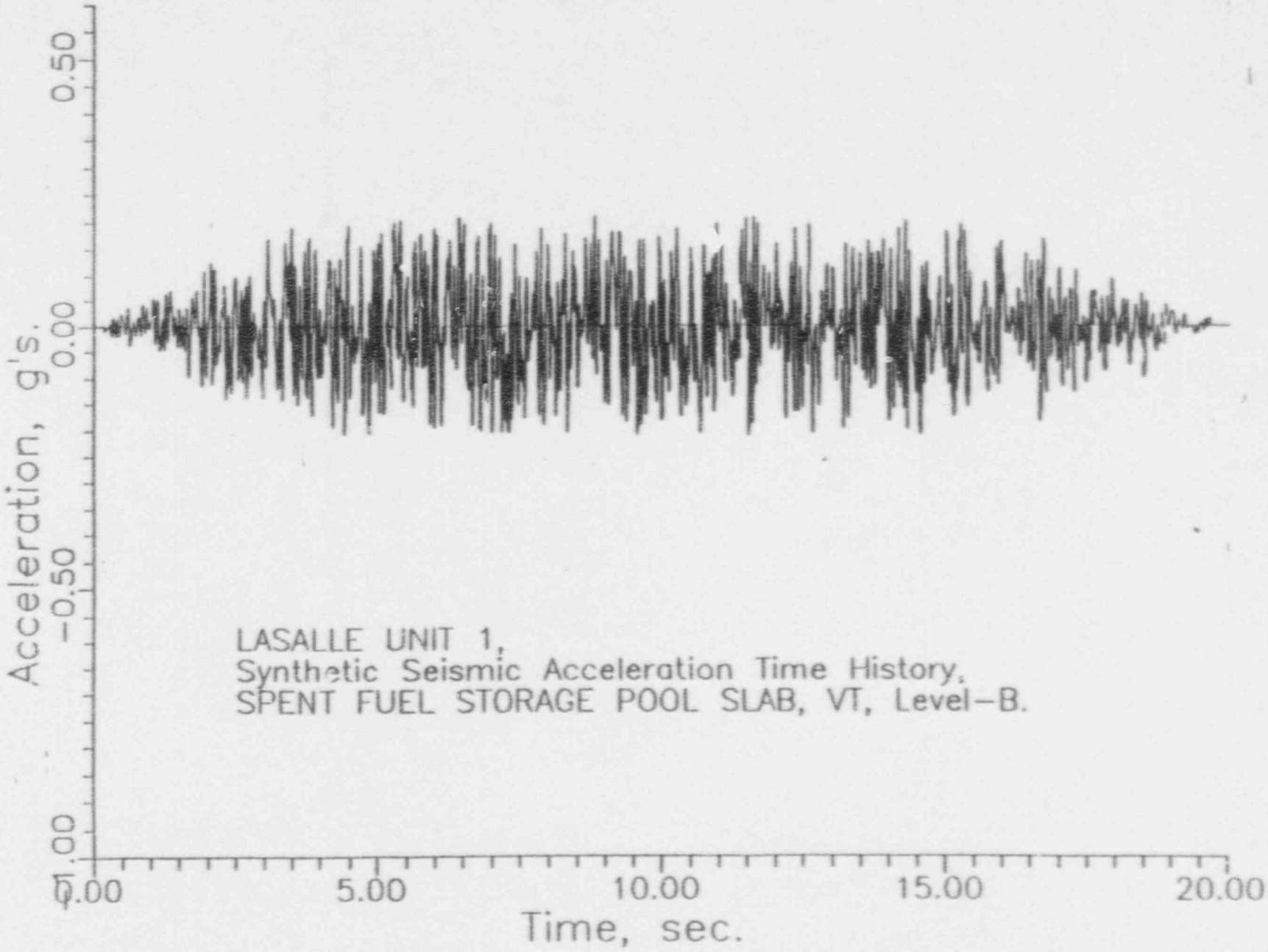
0.50
0.00
-0.50
-1.00
Acceleration, g's.
0.00
5.00
10.00
15.00
20.00
Time, sec.
LASALLE UNIT 1,
Synthetic Seismic Acceleration Time History,
SPENT FUEL STORAGE POOL SLAB, VT, Level-B.

FIGURE 6.3.3

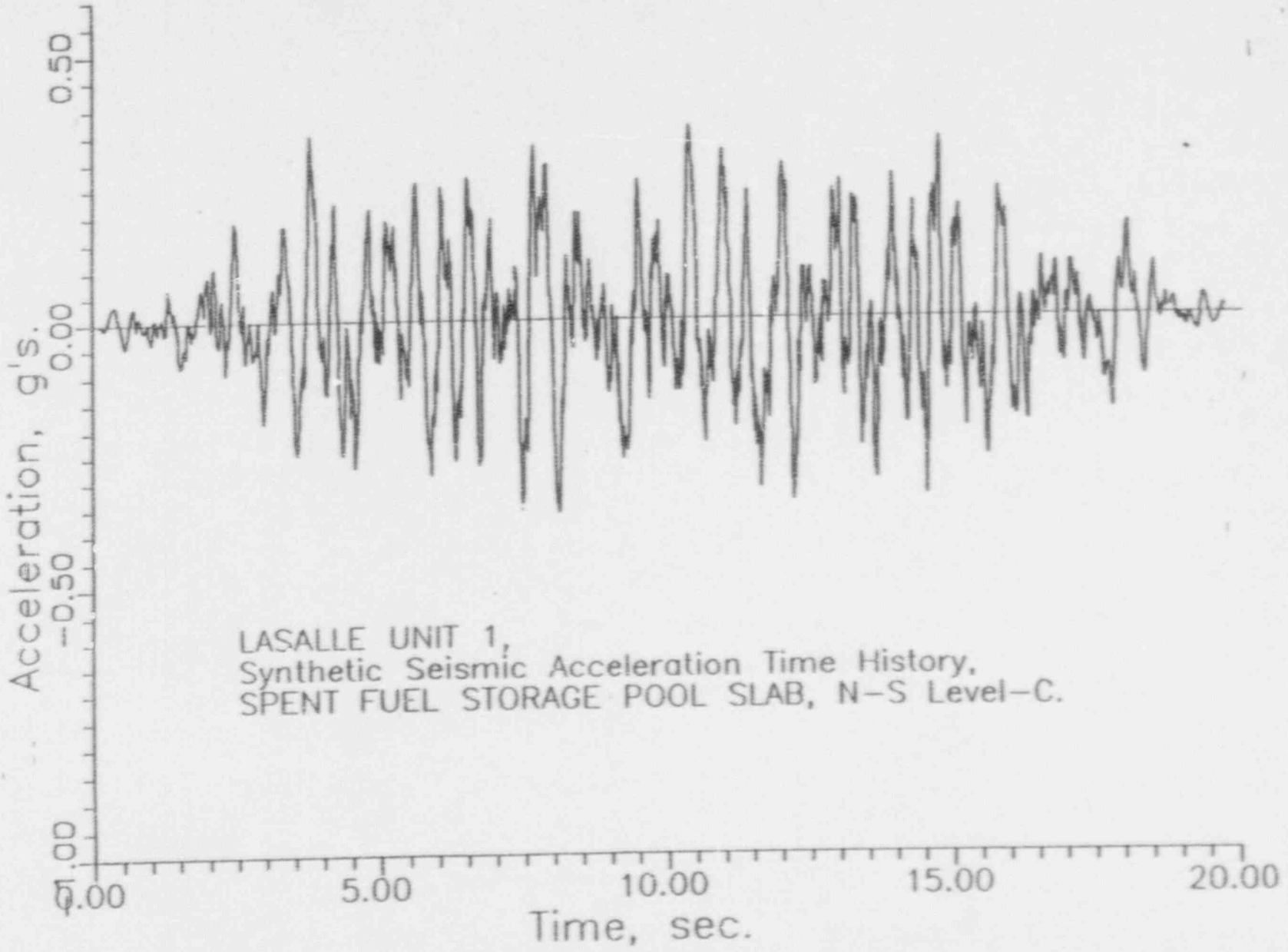

96-9

FIGURE 6.3.4

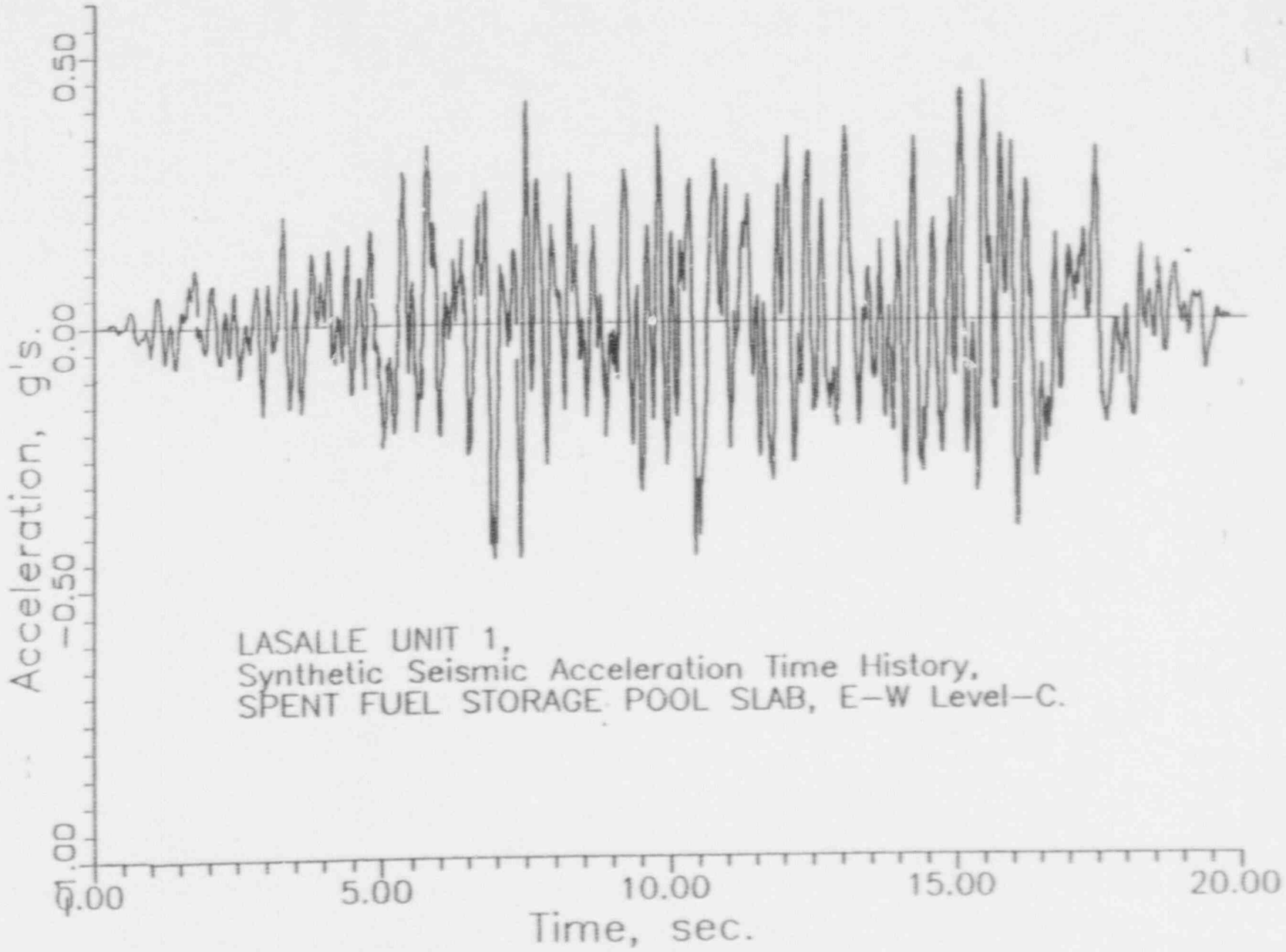

96-9

FIGURE 6.3.5

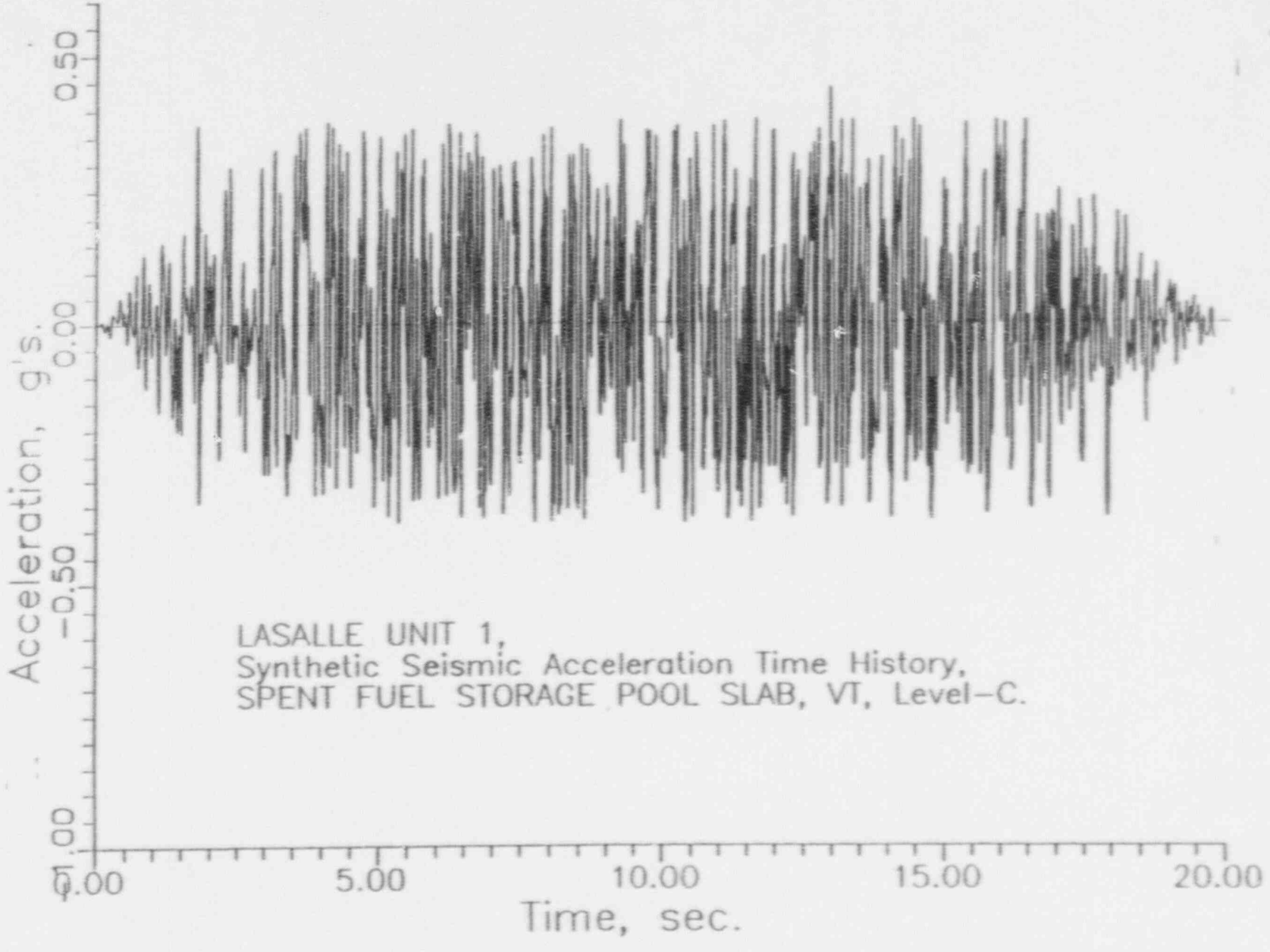
Acceleration, g's.
0.50
0.00
-0.50
-1.00
0.00
5.00
10.00
15.00
20.00
Time, sec.
LASALLE UNIT 1,
Synthetic Seismic Acceleration Time History,
SPENT FUEL STORAGE POOL SLAB, VT, Level-C.

FIGURE 6.3.6

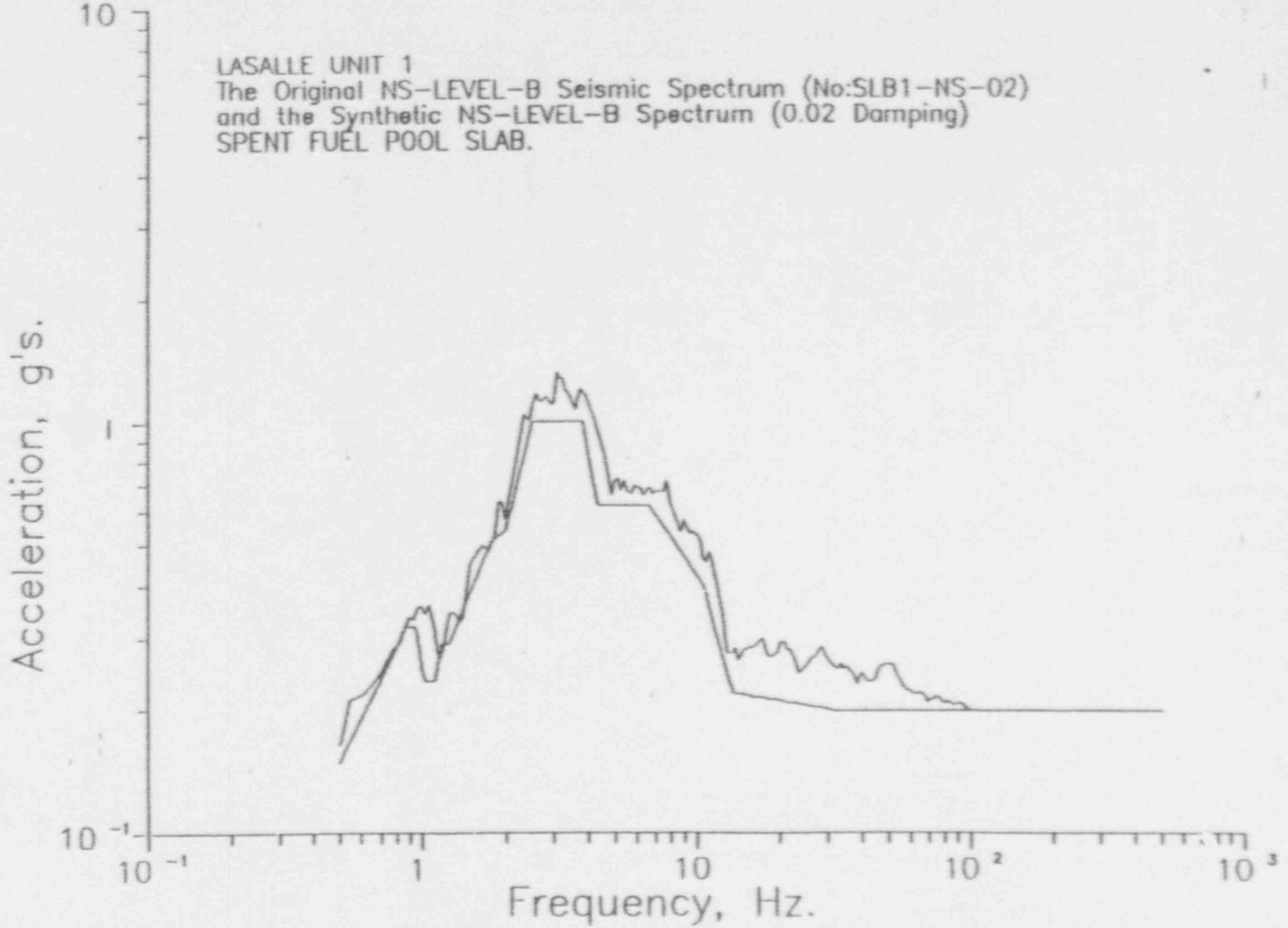

86-9

FIGURE 6.3.7

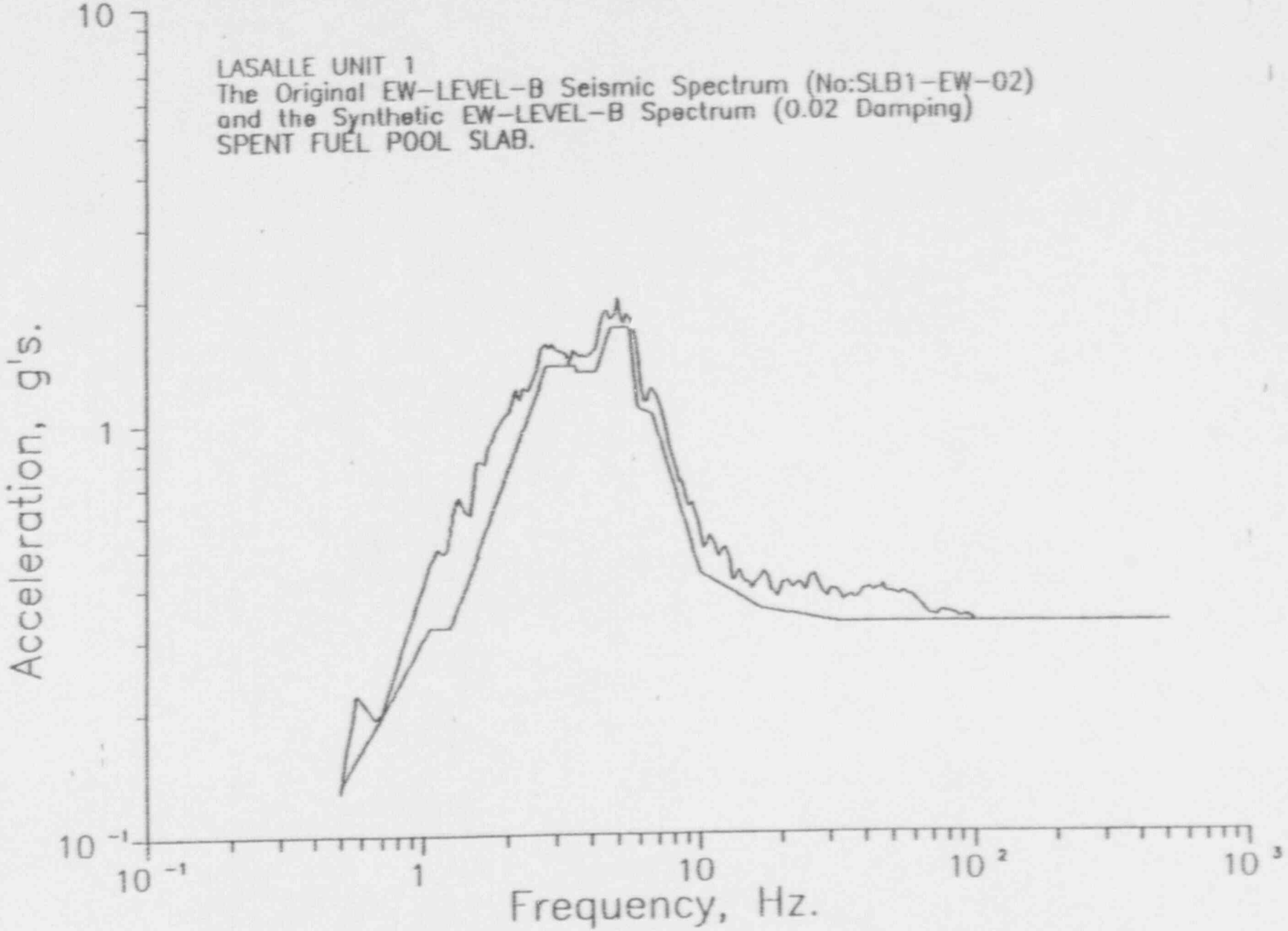
LASALLE UNIT 1
The Original EW-LEVEL-B Seismic Spectrum (No:SLB1-EW-02)
and the Synthetic EW-LEVEL-B Spectrum (0.02 Damping)
SPENT FUEL POOL SLAB.
Acceleration, g's.
10
1
10 -1
10 -1
1
10
10 2
10 3
Frequency, Hz.

FIGURE 6.3.8

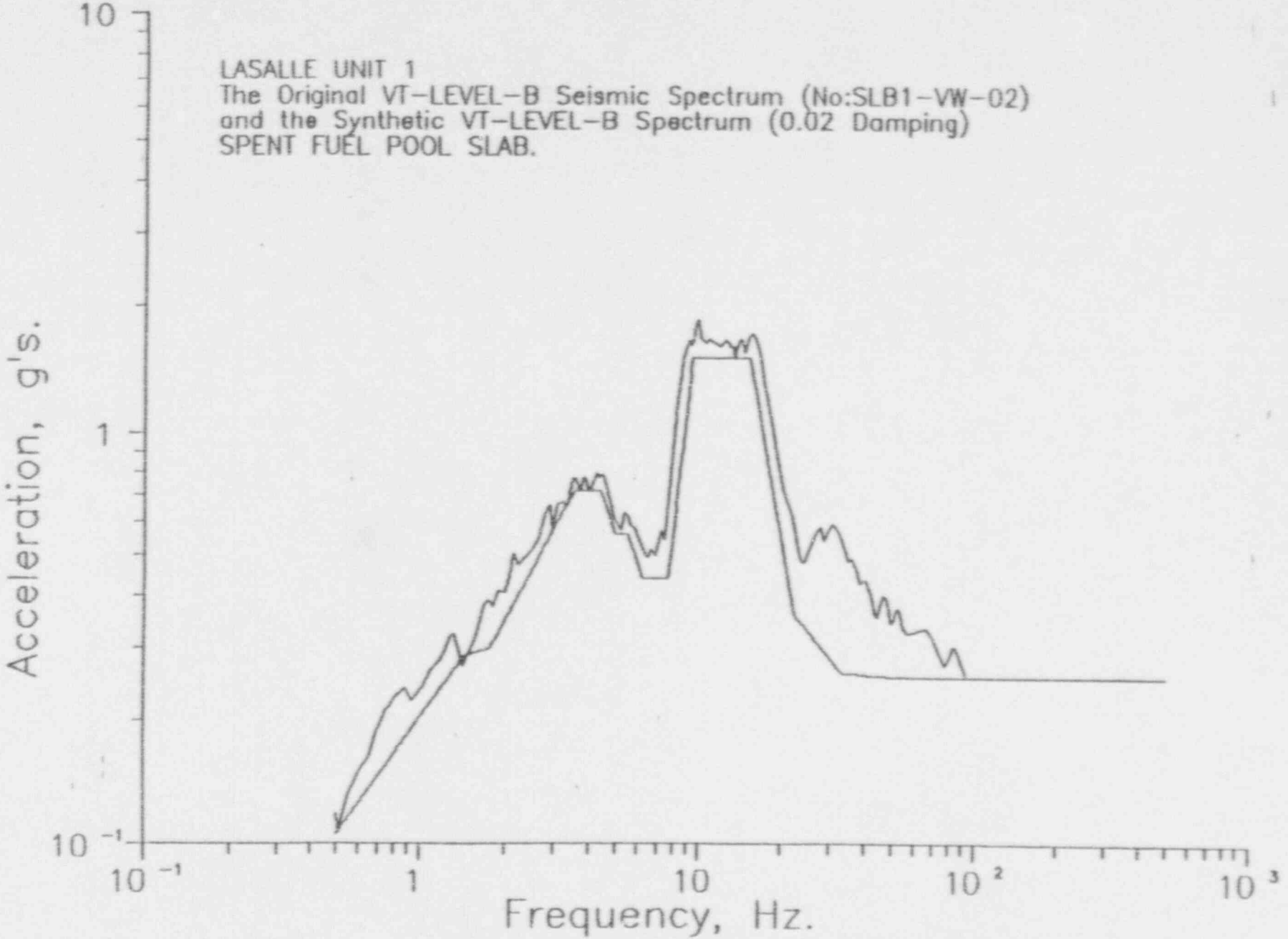

001-9

FIGURE 6.3.9

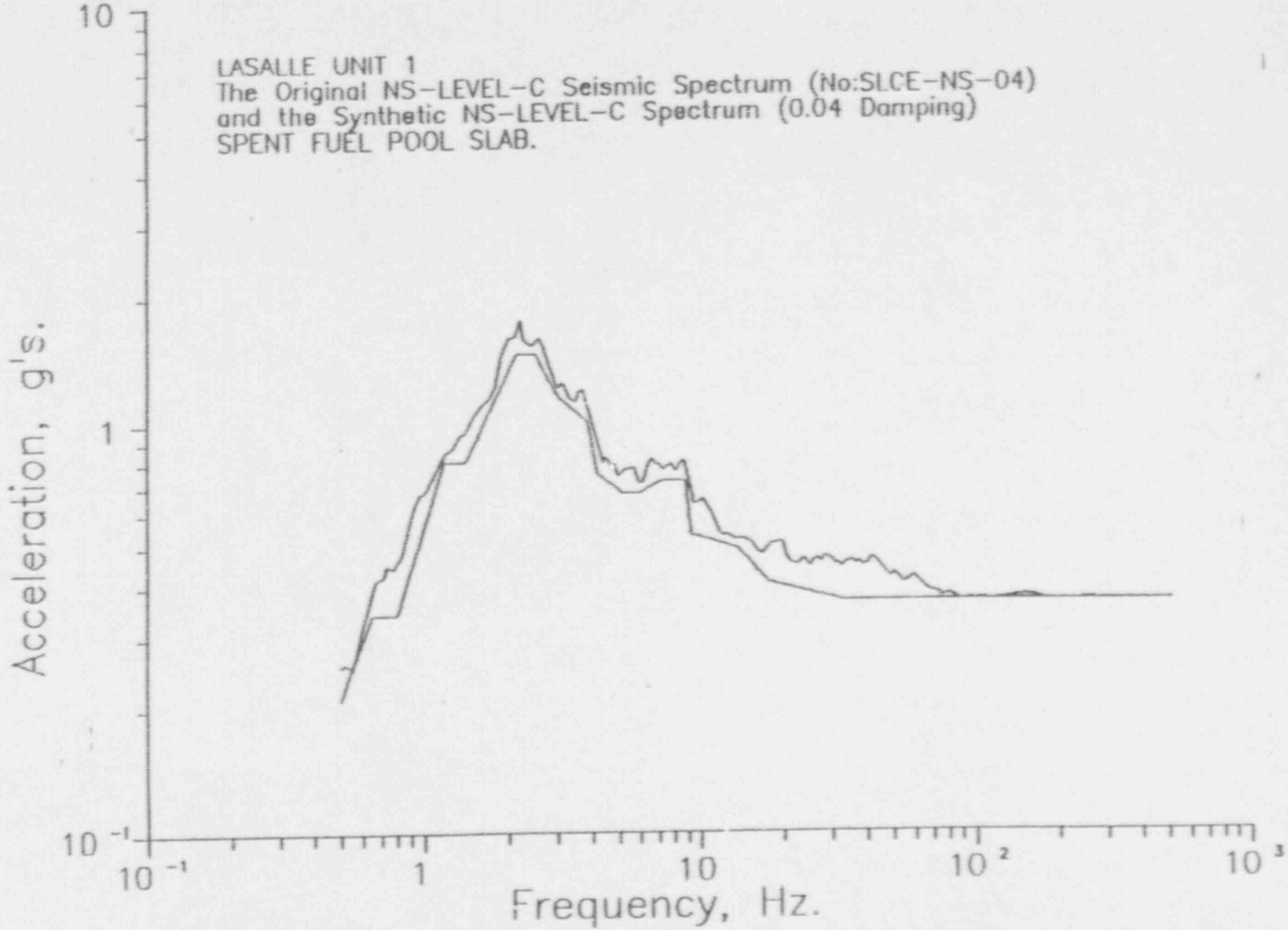
LASALLE UNIT 1
The Original NS-LEVEL-C Seismic Spectrum (No:SLCE-NS-04)
and the Synthetic NS-LEVEL-C Spectrum (0.04 Damping)
SPENT FUEL POOL SLAB.
Acceleration, g's.
10
1
10 -1
10 -1
1
10
10 2
10 3
Frequency, Hz.

FIGURE 6.3.10

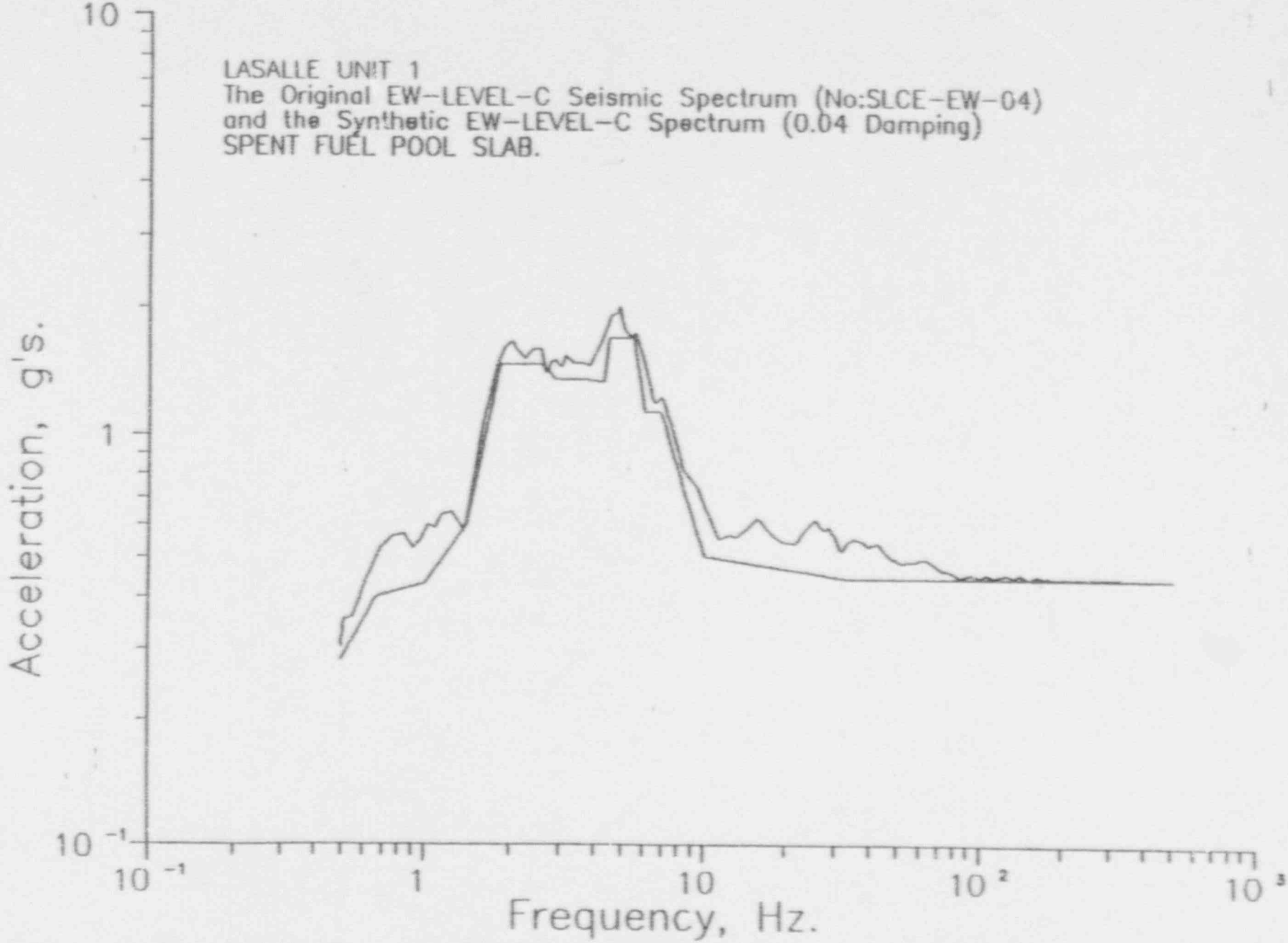
LASALLE UNIT 1
The Original EW-LEVEL-C Seismic Spectrum (No:SLCE-EW-04)
and the Synthetic EW-LEVEL-C Spectrum (0.04 Damping)
SPENT FUEL POOL SLAB.
Acceleration, g's.
Frequency, Hz.
10
1
10 -1
10 -1
1
10
10 2
10 3

FIGURE 6.3.11

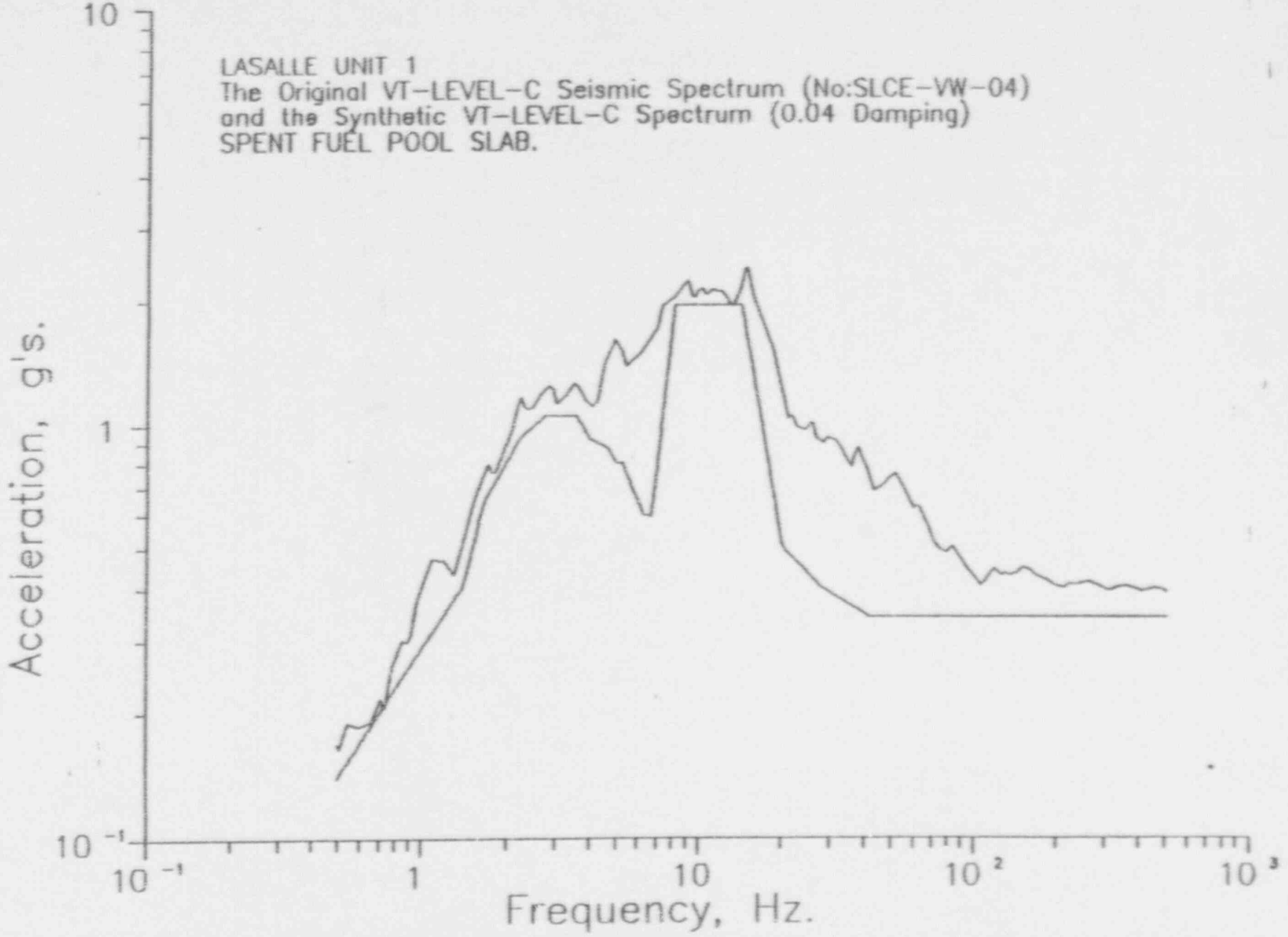
LASALLE UNIT 1
The Original VT-LEVEL-C Seismic Spectrum (No:SLCE-VW-04)
and the Synthetic VT-LEVEL-C Spectrum (0.04 Damping)
SPENT FUEL POOL SLAB.
Acceleration, g's.
10
1
10 -1
10 -1
1
10
10 2
10 3
Frequency, Hz.

FIGURE 6.3.12

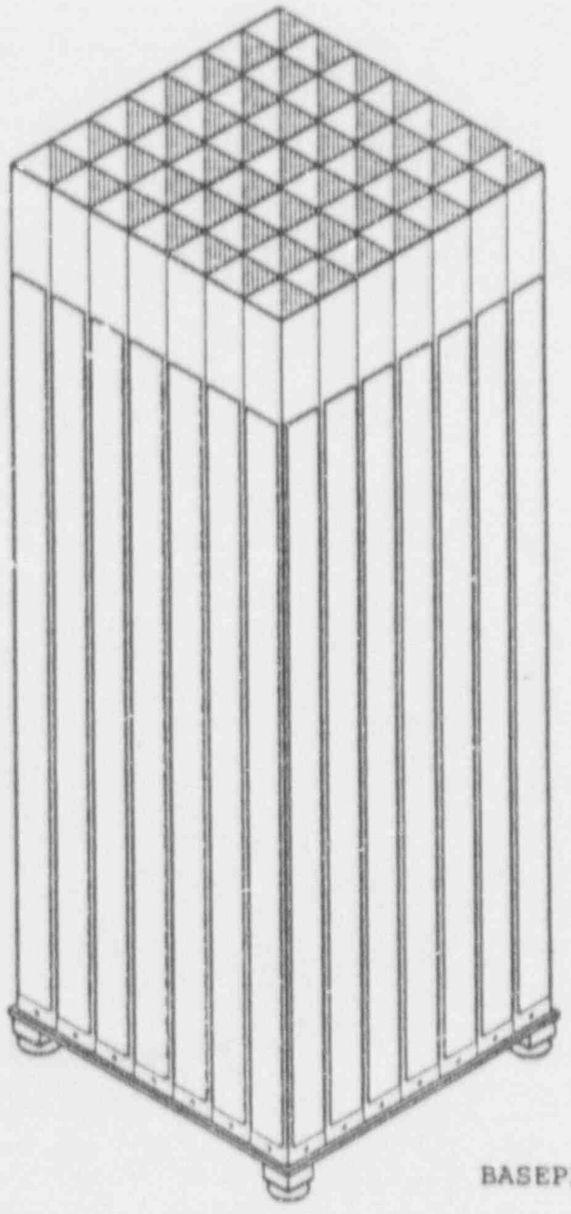

FIGURE 6.4.1 PICTORIAL VIEW OF RACK STRUCTURE

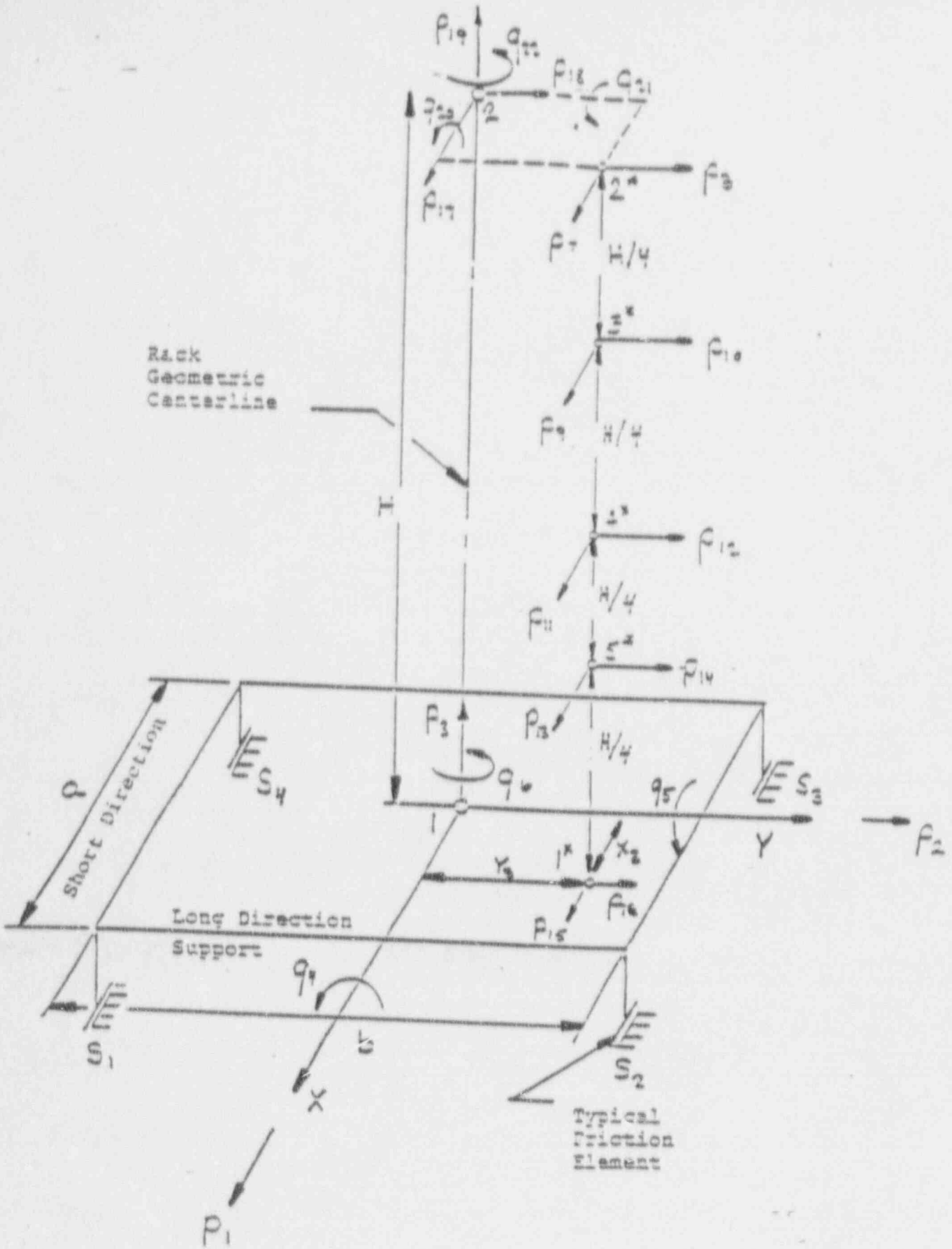

FIGURE 6.4.2 SCHEMATIC MODEL FOR DYNARACK

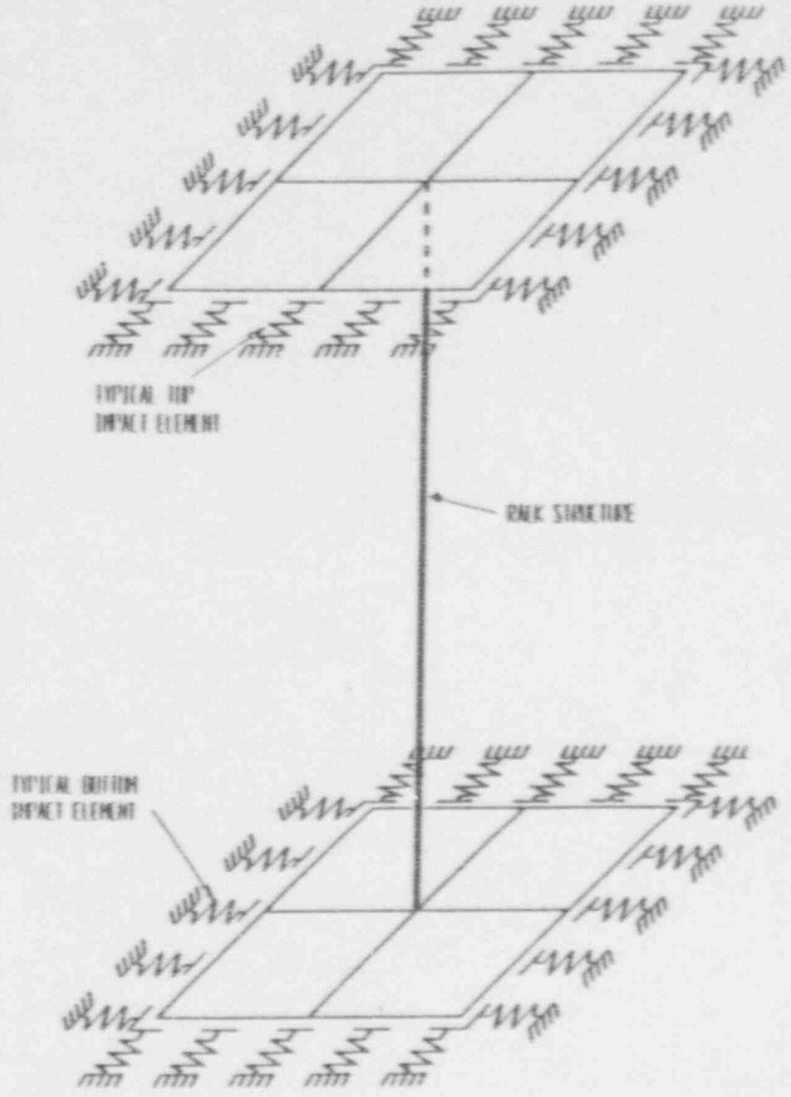

FIGURE 6.4.3 RACK-TO-RACK IMPACT SPRINGS

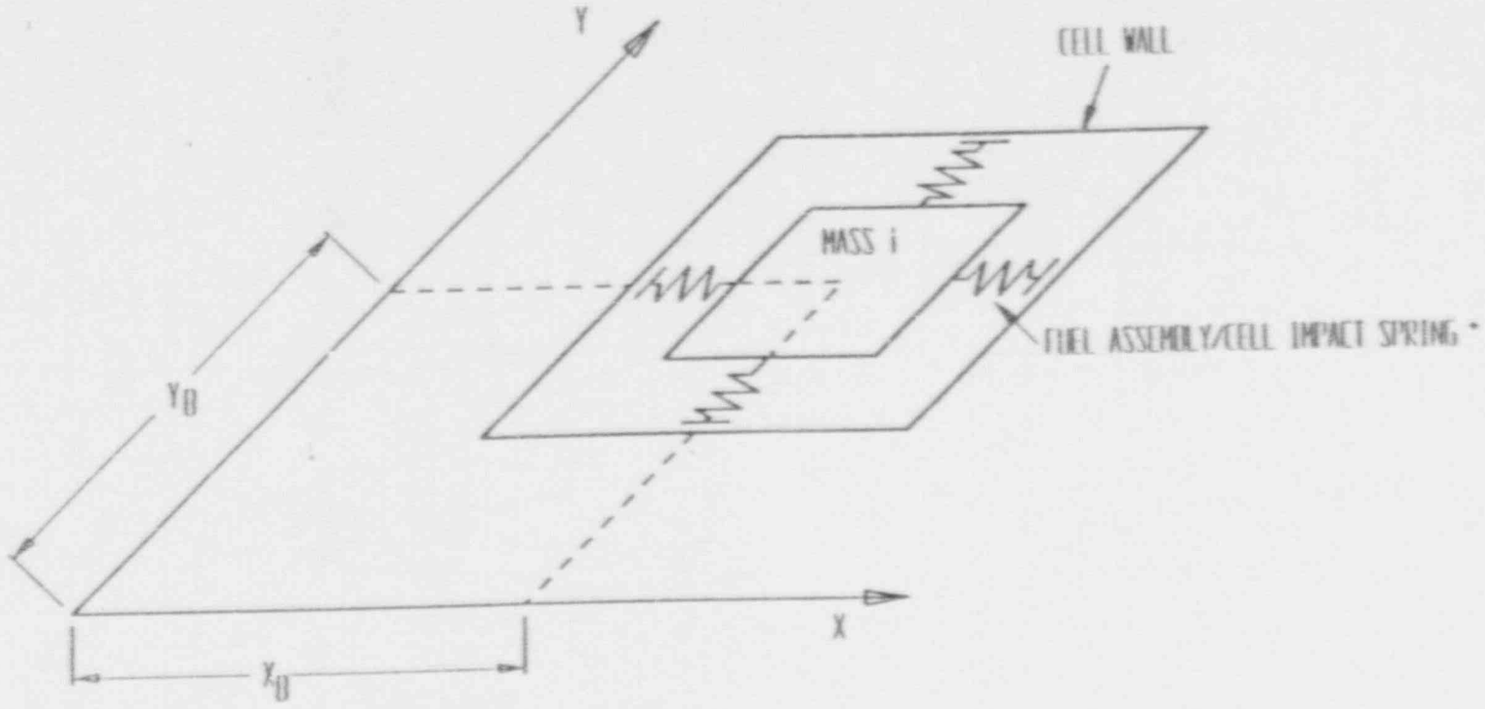

FIGURE 6.4.4 FUEL-TO-RACK IMPACT SPRINGS

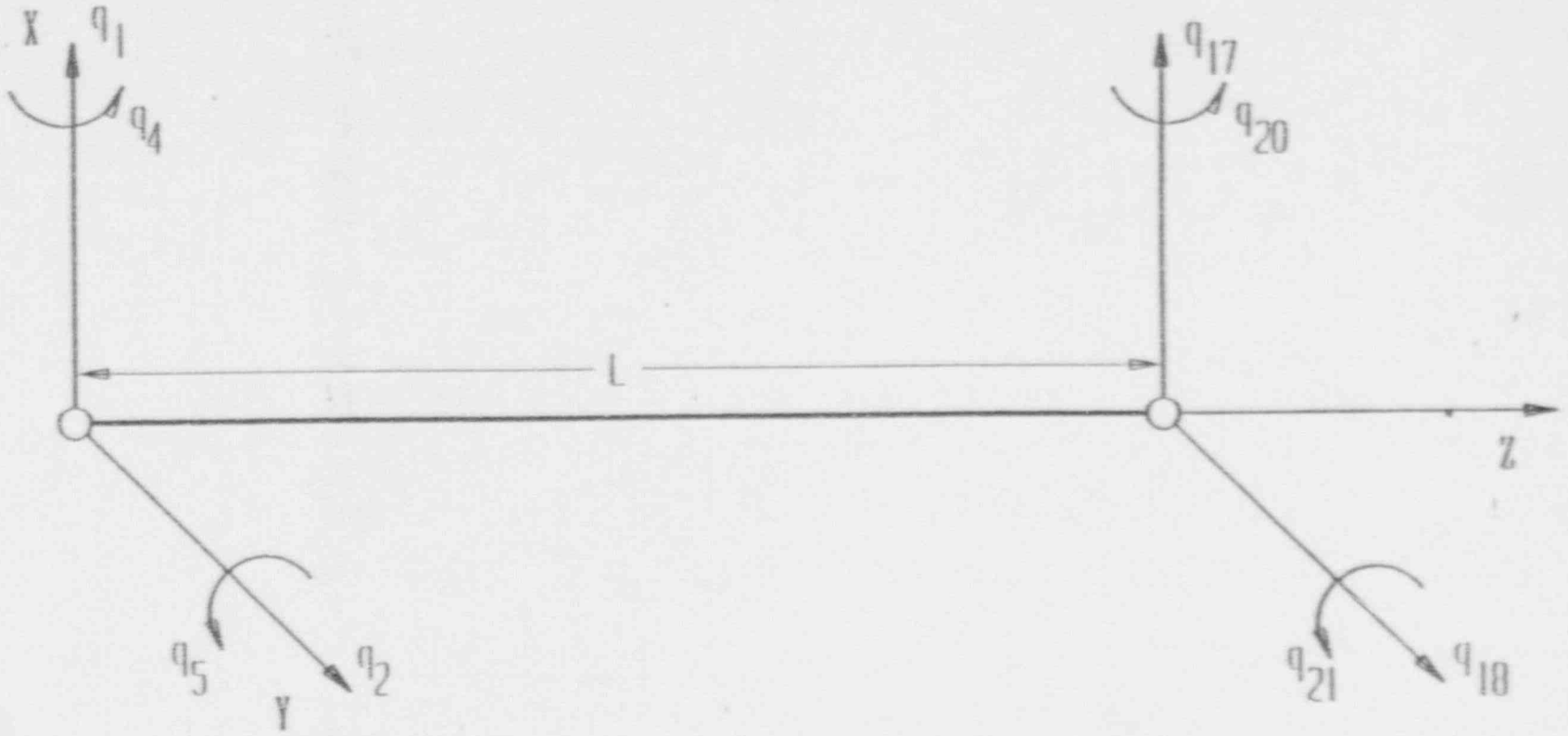

FIGURE 6.4.5 DEGREES-OF-FREEDOM
MODELING RACK MOTION

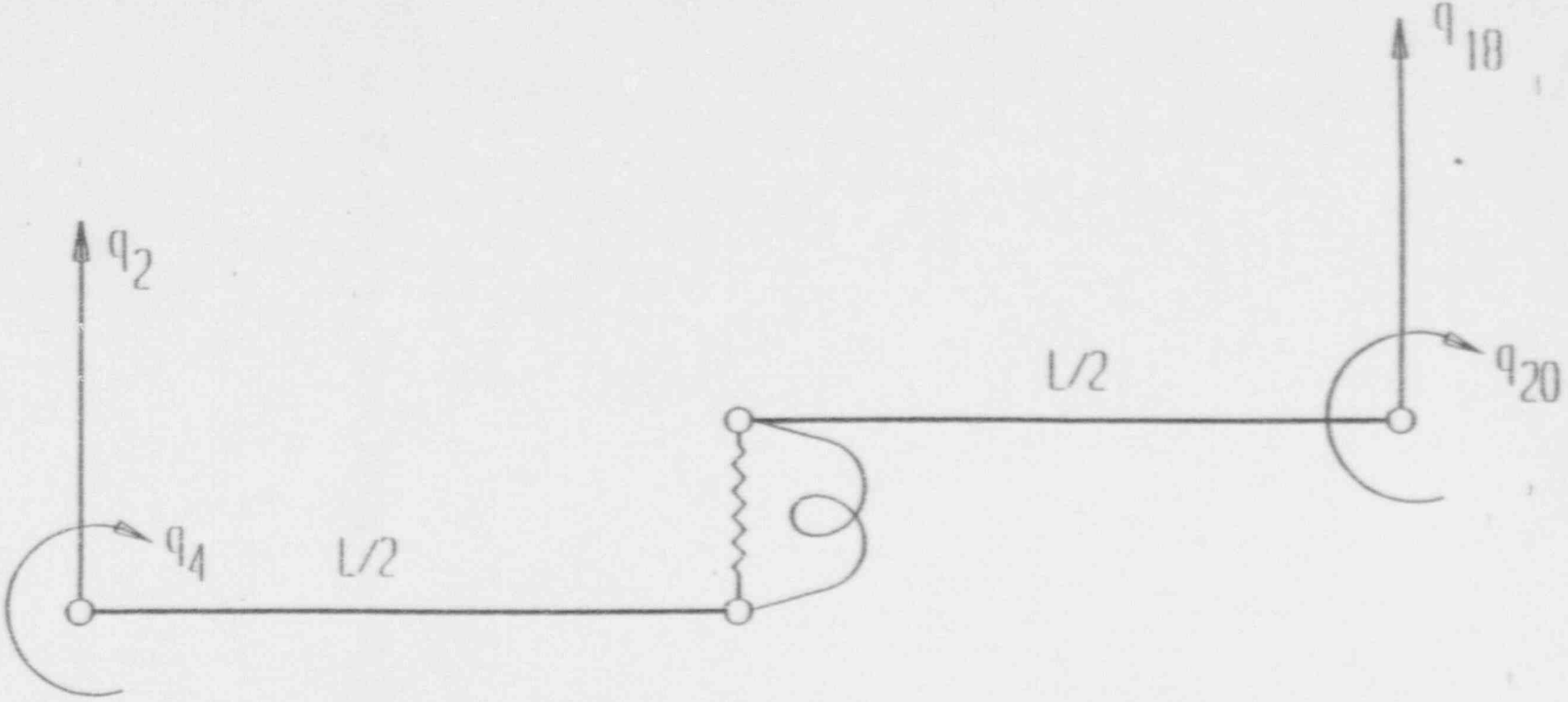

FIGURE 6.4.6 RACK DEGREE-OF-FREEDOM
FOR Y-Z PLANE BENDING

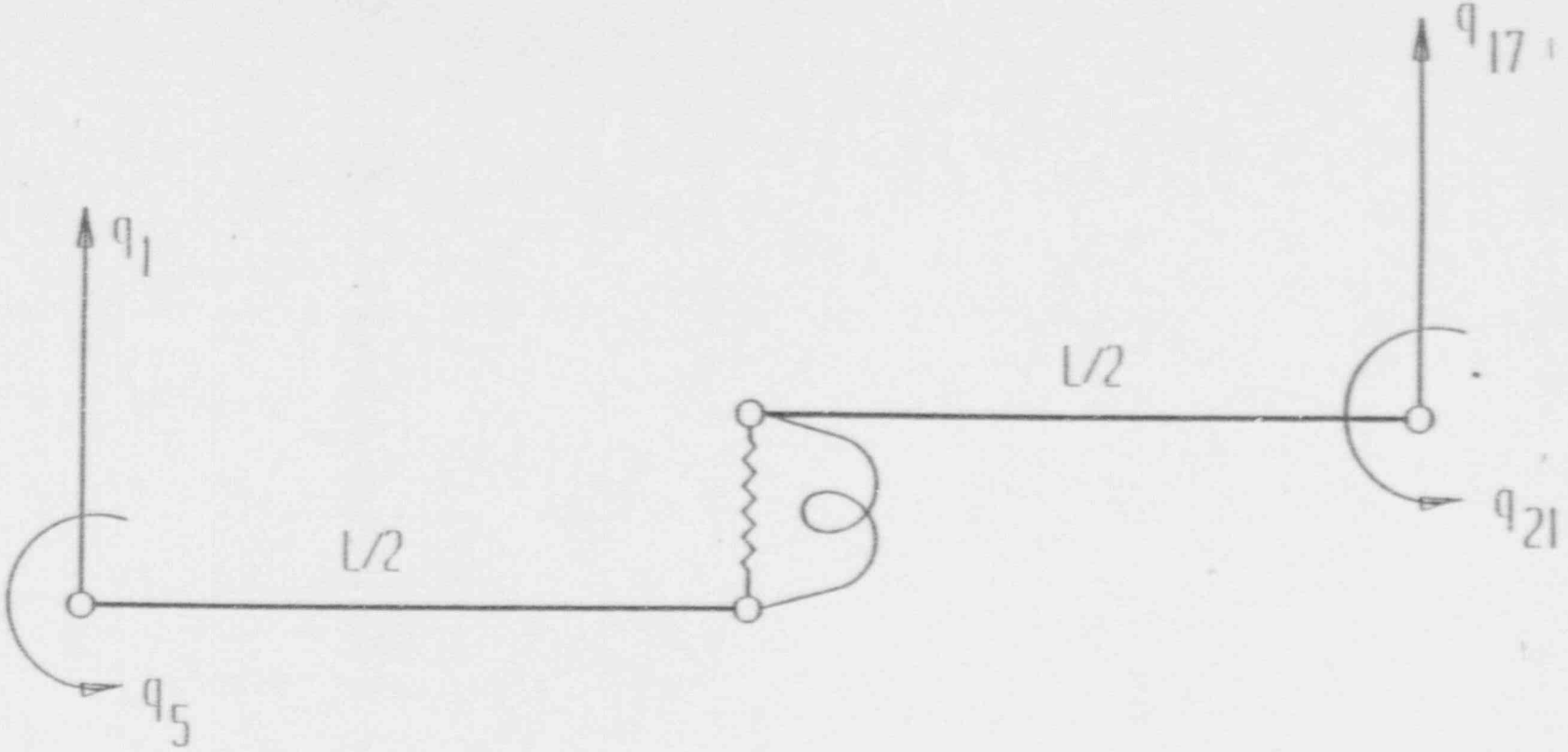

FIGURE 6.4.7 RACK DEGREE-OF-FREEDOM
FOR X-Z PLANE BENDING

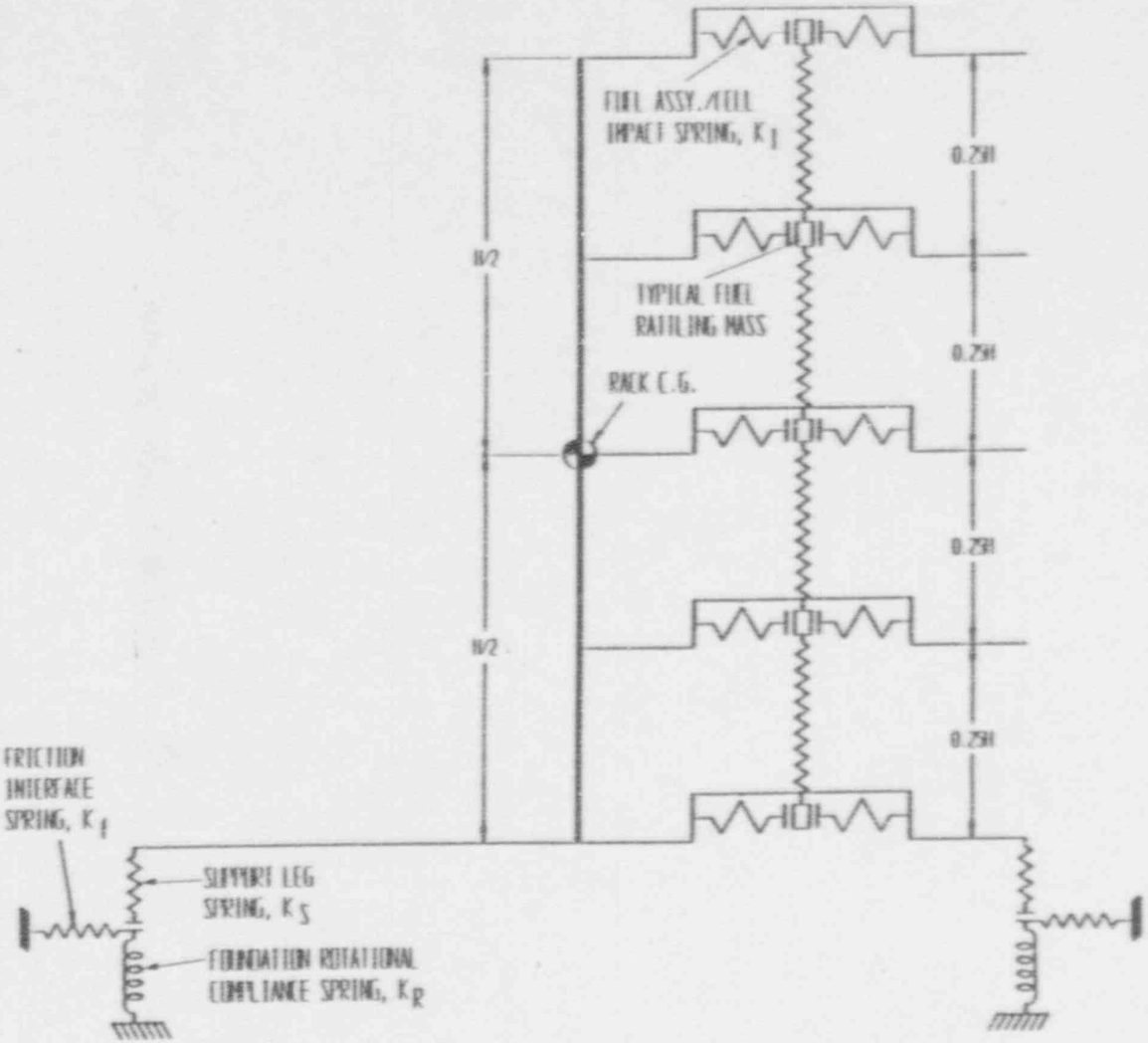

FIGURE 6.4.8 2-D VIEW OF RACK MODULE

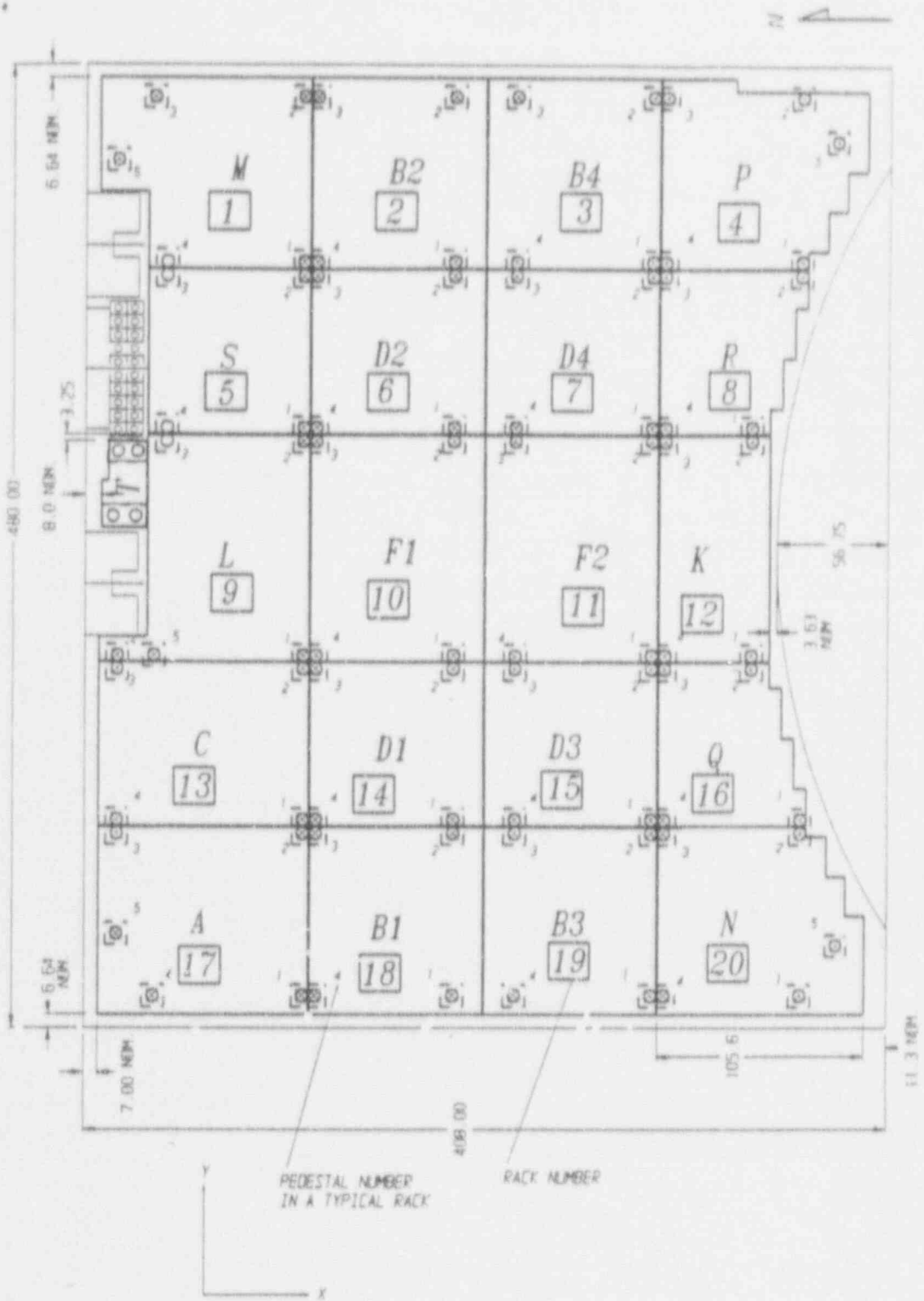

LAYOUT FOR LA SALLE UNIT 1 FUEL POOL

FIG 6.4.9

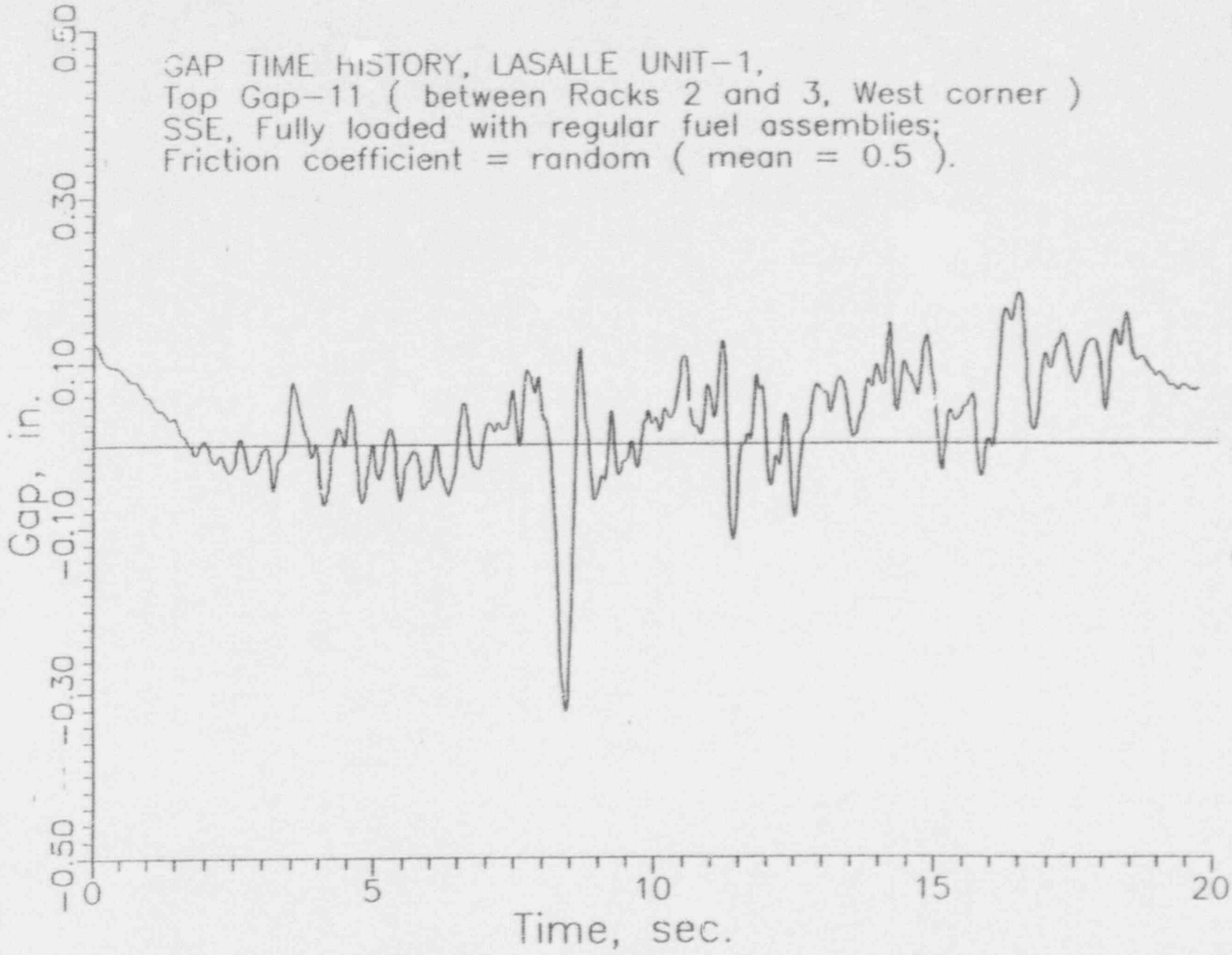
GAP TIME HISTORY, LASALLE UNIT-1,
Top Gap-11 (between Racks 2 and 3, West corner)
SSE, Fully loaded with regular fuel assemblies;
Friction coefficient = random (mean = 0.5).
Gap, in.
0.50
0.30
0.10
-0.10
-0.30
-0.50
0
5
10
15
20
Time, sec.

FIGURE 6.8.1

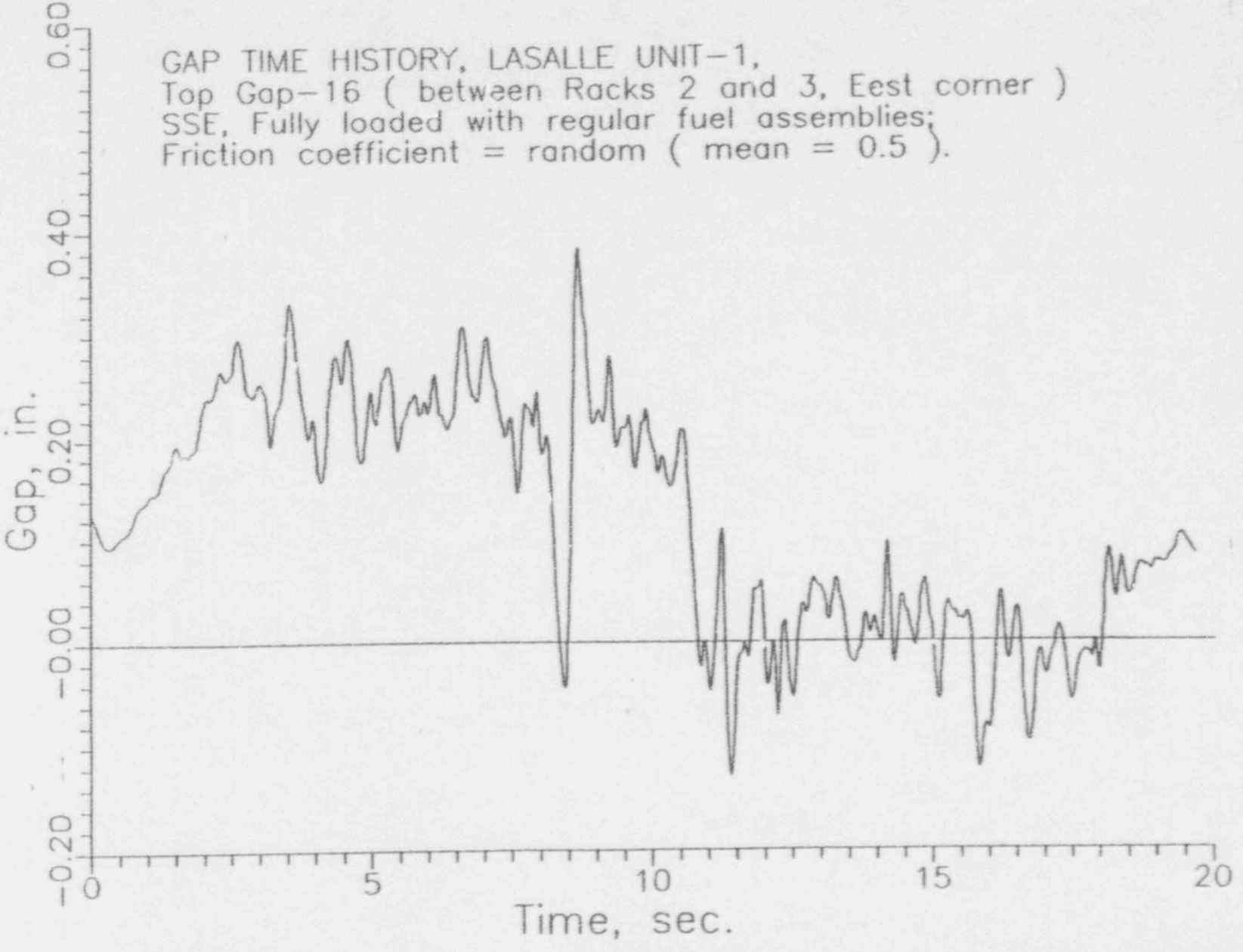
GAP TIME HISTORY, LASALLE UNIT-1,
Top Gap-16 (between Racks 2 and 3, East corner)
SSE, Fully loaded with regular fuel assemblies;
Friction coefficient = random (mean = 0.5).
Gap, in.
0.60
0.40
0.20
-0.00
-0.20
0
5
10
15
20
Time, sec.

FIGURE 6.8.2

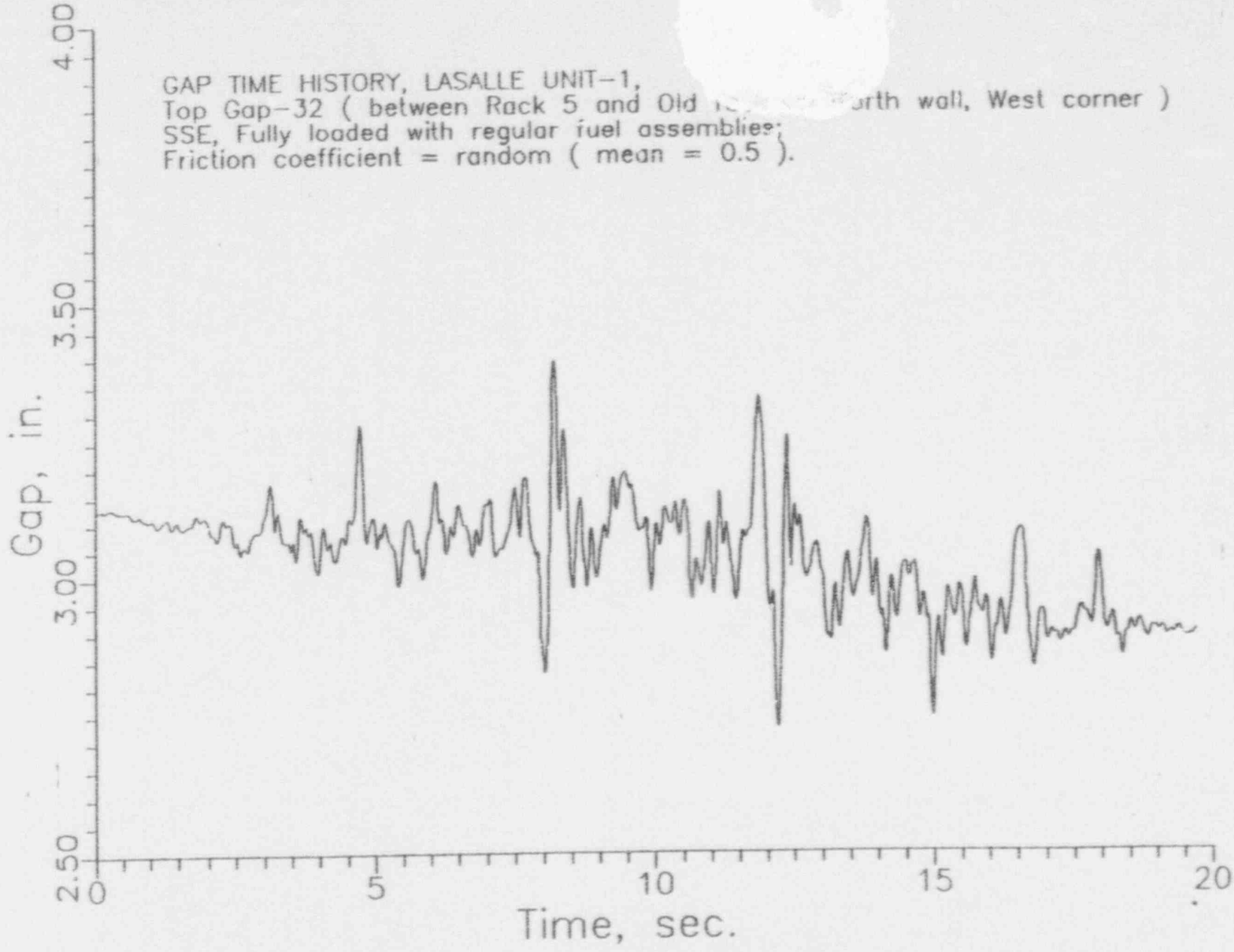
GAP TIME HISTORY, LASALLE UNIT-1,
Top Gap-32 (between Rack 5 and Old
orth wall, West corner)
SSE, Fully loaded with regular fuel assemblies;
Friction coefficient = random (mean = 0.5).
Gap, in.
4.00
3.50
3.00
2.50
0
5
10
15
20
Time, sec.

FIGURE 6.8.3

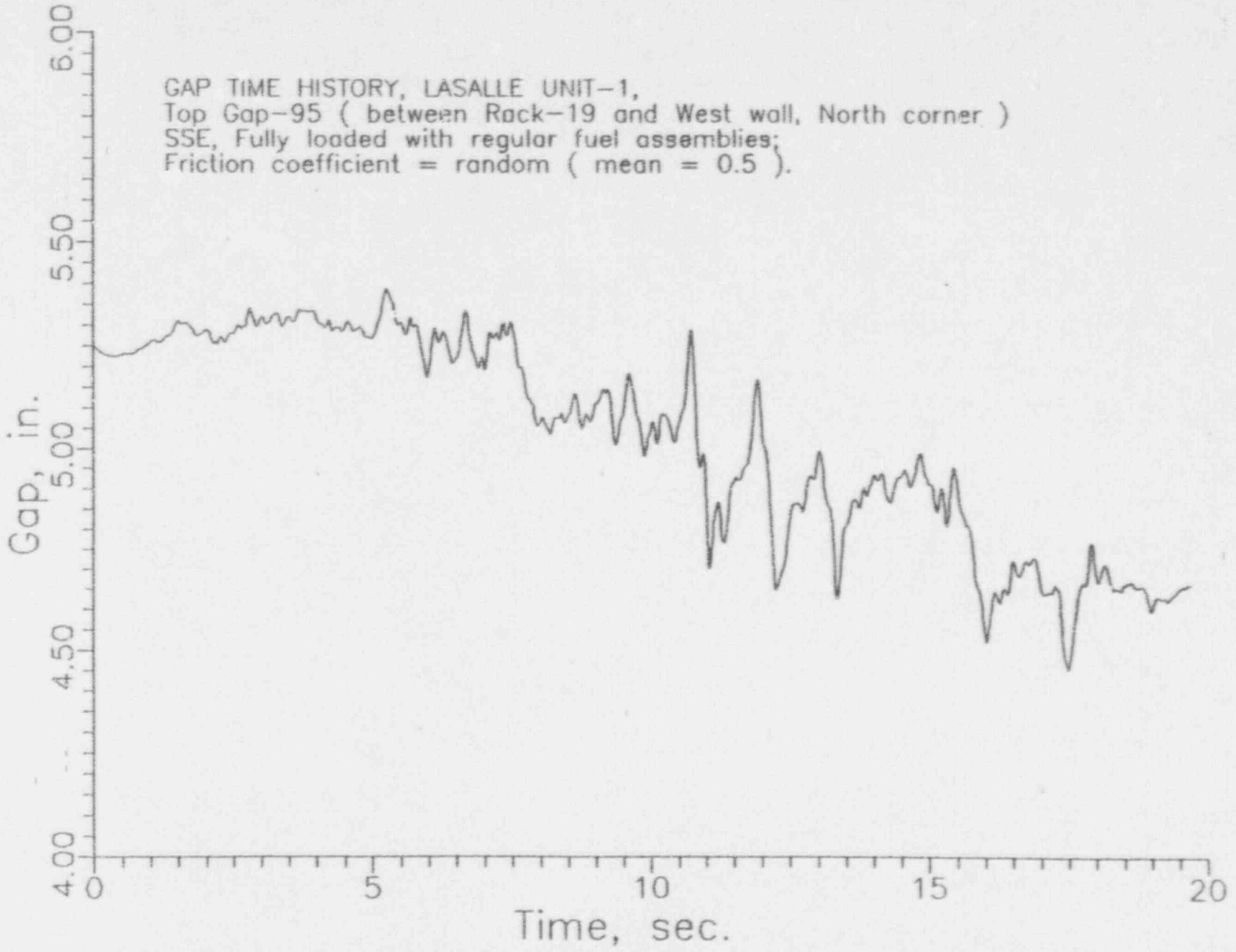
GAP TIME HISTORY, LASALLE UNIT-1,
Top Gap-95 (between Rack-19 and West wall, North corner)
SSE, Fully loaded with regular fuel assemblies;
Friction coefficient = random (mean = 0.5).
Gap, in.
6.00
5.50
5.00
4.50
4.00
0
5
10
15
20
Time, sec.

FIGURE 6.8.4

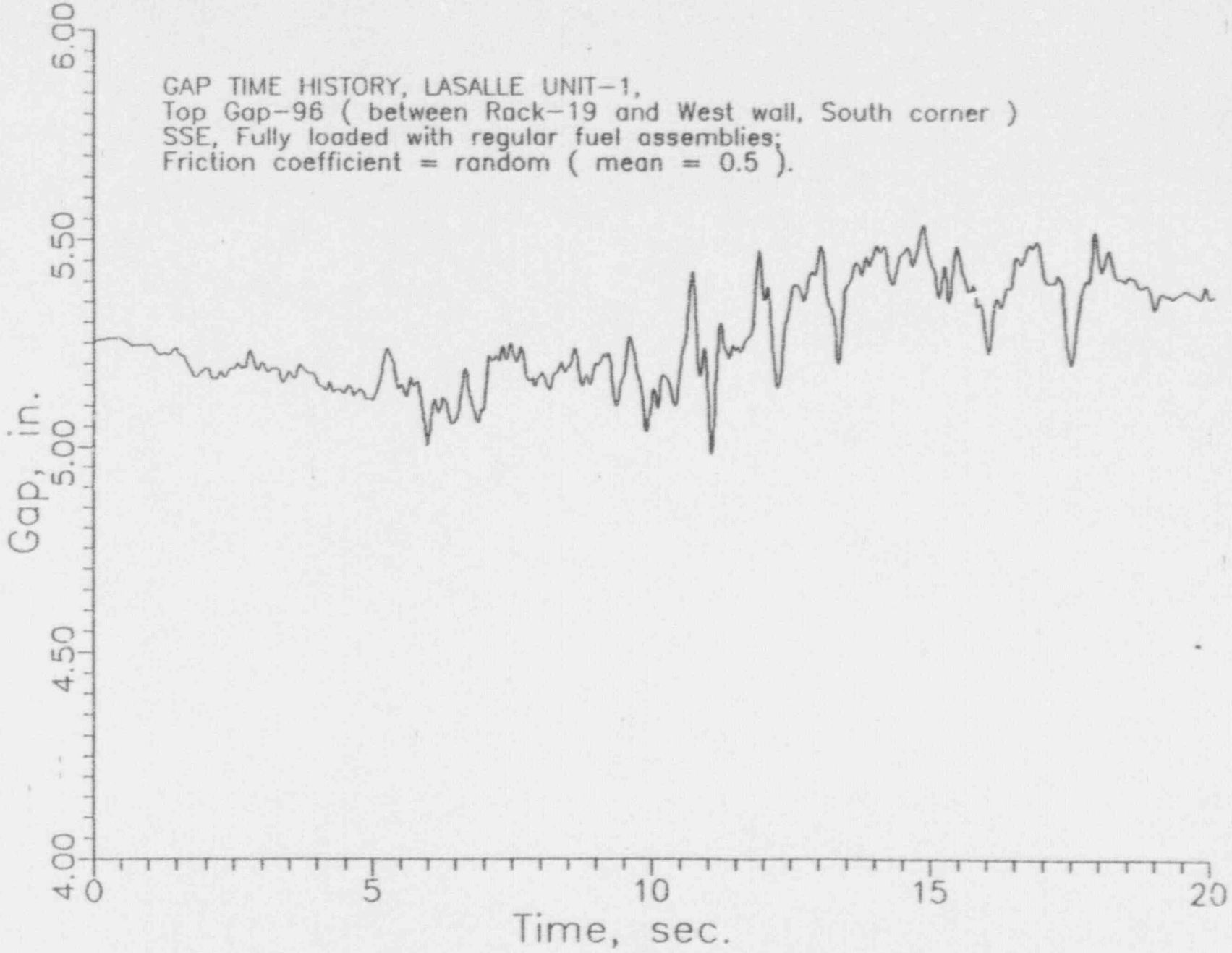
GAP TIME HISTORY, LASALLE UNIT-1,
Top Gap-96 (between Rack-19 and West wall, South corner)
SSE, Fully loaded with regular fuel assemblies;
Friction coefficient = random (mean = 0.5).
Gap, in.
6.00
5.50
5.00
4.50
4.00
0
5
10
15
20
Time, sec.

FIGURE 6.8.5

7.0 ACCIDENT ANALYSIS AND MISCELLANEOUS STRUCTURAL EVALUATIONS

7.1 Introduction

This section provides results of accident analyses and miscellaneous evaluations performed to demonstrate regulatory compliance of the new fuel racks.

The following limiting accident and miscellaneous structural evaluations are considered:

- Refueling accidents - drop of fuel assembly from 30" above the rack to top of rack or through a cell to the baseplate
- Analyses of tool drops from the elevated worktable
- Uplift load of 1200 lb. (UFSAR condition)
- Local cell wall buckling
- Analysis of welded joints due to isolated hot cell

7.2 Refueling Accidents

7.2.1 Dropped Fuel Assembly

The consequences of dropping a fuel assembly as it is being moved over stored fuel is discussed below. Based on the highest lift of a fuel assembly, the maximum distance from the bottom of a fuel assembly, travelling over fuel racks, to the top of the rack is 30".

a. Dropped Fuel Assembly Accident (Deep Drop Scenario)

A bounding 680 lb. fuel assembly plus channel is assumed to be dropped from 30" above the top of a storage location and impacts the base of the module. Local failure of the baseplate is acceptable; however, the rack design should ensure that gross structural failure does not occur and the subcriticality of the adjacent fuel assemblies is not violated. Calculated results show that there will be no change in the spacing between cells. Local deformation of the baseplate in the neighborhood of the impact will occur, but the dropped assembly will

be contained and not impact the liner. We show that the maximum movement of the baseplate toward the liner after the impact is less than 1.25". Any load transmitted to the liner through the support by such an accident is well below the loads caused by seismic events (given in Section 6).

b. Dropped Fuel Assembly Accident (Shallow Drop Scenario)

One fuel assembly plus the channel is assumed to be dropped from 30" above the top of the rack and impacts the top of the rack. Permanent deformation of the rack is acceptable, but is required to be limited to the top region such that the rack cross-sectional geometry at the level of the top of the active fuel (and below) is not altered. It is shown that damage, if it occurs, will be restricted to a depth of 3.2" below the top of the rack. This is above the active fuel region.

c. Dropped Fuel Assembly Accident (Inclined Drop)

One fuel assembly is assumed to be dropped from 30" above the top of the rack and hits the rack so as to impose both horizontal and vertical impulsive force. We show that damage to the fuel rack is also confined to regions above the active fuel.

d. Analysis of Tool Drops

Commonwealth Edison intends to retain the hinged worktable over the spent fuel pool, and therefore, an evaluation of the effects of dropped tools and equipment is required. It is shown that damage is again confined to a region of the cell above the active fuel if we consider a bounding scenario of tool weight and drop height.

e. Uplift Loads

An uplift load of 1200 lb. may be imposed on one cell. The stresses in the rack imposed by this load are bounded by the stresses induced from other accident conditions described in this section.

7.3 Local Buckling of Fuel Cell Walls

This subsection and the next one presents details on the secondary stresses produced by buckling and by temperature effects.

The allowable local buckling stresses in the fuel cell walls are obtained by using classical plate buckling analysis. The following formula for the critical stress has been used based on a width of cell "b" [7.3.1]:

$$\sigma_{cr} = \frac{\beta \pi^2 E t^2}{12 b^2 (1 - \mu^2)} \times \frac{2}{3}$$

The factor 2/3 is applied to ensure an appropriate safety margin.

σ_{cr} is the limiting vertical compressive stress in the tube, E = 27.9×10^6 psi, μ = 0.3, (Poison's ratio), t = .09", b = 6.05". The factor β is suggested in (Ref. 7.3.1) to be 4.0 for a long panel.

For the given data,

$$\sigma_{cr} = 14881 \text{ psi}$$

It should be noted that this stability calculation is based on the applied stress being uniform along the entire length of the cell wall. In the actual fuel rack, the compressive stress comes from consideration of overall bending of the rack structures during a seismic event and as such is negligible at the rack top and maximum at the rack bottom. It is conservative to apply the above equation to the rack cell wall if we compare σ_{cr} with the maximum compressive stress anywhere in the cell wall. As shown in Section 6, the local buckling stress limit is not violated anywhere in the body of the rack modules. The maximum compressive stress in the outermost cell is obtained by multiplying the limiting value of the stress factor R_6 (for the cell cross-section just above the baseplate) by the allowable stress. Thus, from Table 6.7.2, $\sigma = R_6 \times$ allowable stress = .249 x 25000 = 6225 psi under faulted conditions.

7.4 Analysis of Welded Joints in Rack due to Isolated Hot Cell

In this subsection, in-rack welded joints are examined under the loading conditions arising from thermal effects due to an isolated hot cell.

A maximum thermal gradient between cells will develop when an isolated storage location contains a fuel assembly emitting maximum postulated heat, while the surrounding locations are empty. We can obtain a conservative estimate of weld stresses along the length of an isolated hot cell by considering a beam strip (a cell wall) uniformly heated and restrained from growth along one long edge. The strip is subject to a uniform temperature rise $\Delta T = 41.8°F$. The temperature rise has been calculated from the difference of the maximum local water temperature and bulk water temperature in the spent fuel pool. (see Tables 5.8.2 and 5.8.4). Then, using a shear beam theory, we can calculate an estimate of the maximum value of the average shear stress in the strip (see Figure 7.4.1).

The final result for wall maximum shear stress, under conservative restraint assumptions is given as [7.5.1]:

$$\tau_{max} = \frac{E \alpha \Delta T}{.931}$$

where $\alpha = 9.5 \times 10^{-6}$ in/in °F and $E = 27.9 \times 10^{6}$ psi.

Therefore, we obtain an estimate of maximum weld shear stress in an isolated hot cell as

$$\tau_{max} = 11900 \text{ psi}$$

since this is a secondary thermal stress, it is appropriate to compare this to the allowable weld shear stress for a faulted event $\tau < .42S_u = 29820$ psi. In the fuel rack, this maximum stress occurs near the top of the rack and does not interact with any other critical stress.

7.5 References for Section 7

[7.3.1] "Strength of Materials", S.P. Timoshenko, 3rd Edition, Part II, pp 194-197 (1956).

[7.5.1] "Seismic Analysis of High Density Fuel Racks, Part III -Structural Design Calculations - Theory", HI-89330, Revision 1, 1989.

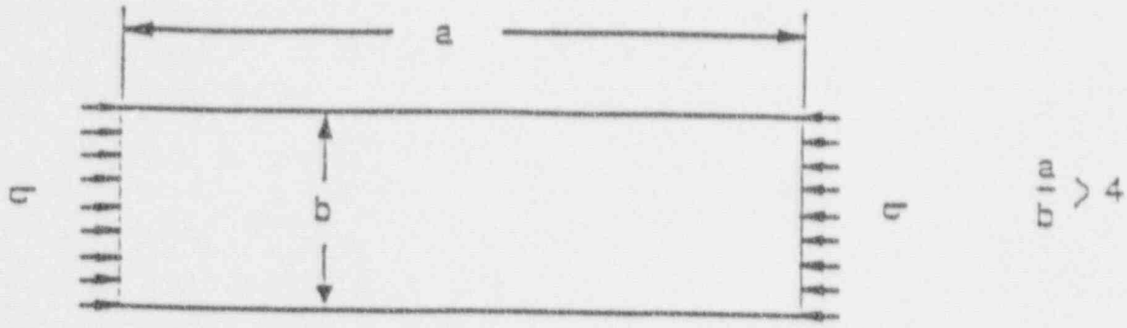

FIGURE 7.3.1 LOADING ON RACK WALL

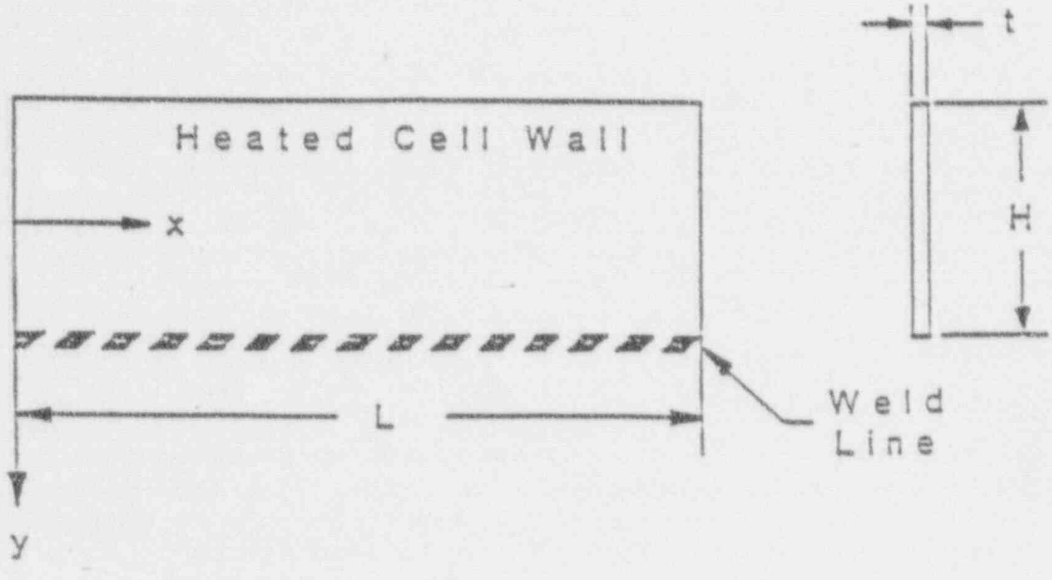

FIGURE 7.4.1 WELDED JOINT IN RACK

8.0 ANALYSIS OF SPENT FUEL POOL STRUCTURE

8.1 Description of Spent Fuel Pool

The La Salle spent fuel pool (SFP) is a stainless steel lined reinforced concrete structure in the La Salle Reactor Building. Sketches of the pool structure are provided in Figures 8.1 through 8.4. The pool is 38 feet deep, 40 feet long and 34 feet wide with walls that are a minimum of 6 feet thick. The pool floor and walls are lined with a 1/4 inch continuously welded stainless steel liner anchored to steel embedments. The pool structure consisting of the cask storage area, spent fuel pool, and new fuel storage area is supported by the containment and Reactor Building walls which extend down to the Reactor Building mat foundation. The SFP north-south walls span between the Unit 1 and Unit 2 containment structures with intermediate support provided at the center of their spans by the east-west wall along column line 15, which separates the two units. The pool slab varies in thickness from 6'-0" in the SFP to 4'-10" in the cask storage area and 1'-6" in the new fuel storage area.

The SFP slab is reinforced with #11 bars at 6" typical in each direction and in both faces. An additional layer of #11 bars at 12" in each direction in the top face is provided in the corners of the SFP slab. The cask shipping slab is reinforced with #11 bars at 6" in each direction and in both faces. The new fuel storage area slab is reinforced with #10 bars at 6" in each direction and in both faces. The pool structure walls are reinforced with #11 bars at 6" vertically and horizontally in both faces.

8.2 Codes, Standards and Specifications

The La Salle design basis codes were utilized in the analysis. Consistent with the UFSAR [8.1], the concrete SFP structure was evaluated using ACI 318-71 [8.2]. ACI 349-85 [8.3] guidelines were utilized for treatment of thermal effects.

The loads and load combinations used to evaluate the SFP and supporting elements are consistent with the La Salle Design Assessment Report [8.4] load combinations. In addition, the load combinations meet or exceed the load combinations specified in the La Salle UFSAR. Loads and load combinations are presented in Section 8.5, and the resulting design margins are discussed in Section 8.6.

8.3 Seismic, Impact and Thermal Loads

Interaction between the high density fuel racks (HDFRs) and the SFP is considered in the structural evaluation of the slab and walls. The HDFRs may be completely or partially filled with spent fuel assemblies to achieve the critical loading conditions. The loads from the high density spent fuel racks based on dynamic time history analyses, and the associated hydrodynamic loads, are used to obtain pressure loads for the SFP static finite element analyses.

The overall vertical and horizontal seismic and SRV loads on the slab consider the effects of all pool contents including fuel assemblies, racks and water. The seismic and SRV loads from the water were determined by taking the water mass times the appropriate vertical accelerations. The Level B and Level C vertical response spectra are shown in Figures 6.3.9 and 6.3.12, respectively. The vertical and horizontal forces acting on the slab from the HDFRs were determined by taking the maximum value of the sum of all pedestal forces at each time step in the pedestal

force time histories obtained from the whole pool dynamic time history analysis of the high density fuel racks.

The critical loading on the slab is produced when all fuel racks are fully loaded. The DYNARACK analysis method produces a time history of all support pedestal/pool slab loadings including the condition of pedestal lift-off. These pedestal loads include the contribution of rack-to-bearing pad impact and therefore, there is no need to apply empirical impact factors. Other analyses involving partially loaded and empty racks are addressed in Section 6.

Hydrodynamic effects on the pool walls from the bulk pool water and the effects of the racks as they approach the wall during a postulated dynamic event are considered in the analysis of the spent fuel pool. Fluid coupling pressures on the walls are given in Table 8.1. The effects of sloshing of the pool water during a seismic event have been applied as pressure loads on the wall in accordance with the procedure described in Reference [8.5]. The Level B and Level C horizontal dynamic response spectra are shown in Figures 6.3.7, 6.3.8, 6.3.10 and 6.3.11.

The maximum rack loads determined from dynamic rack analyses and used in the SFP evaluation are tabulated in Table 8.1. Table 8.2 gives the bounding temperatures for the La Salle SFP as 128°F for the normal condition and 212°F for the abnormal condition.

8.4 Liner Leak Tightness

To provide for the leak tightness of the liner, the rack layout has been established to ensure that none of the rack pedestal feet or bearing plates rest on the liner leak chase system. The rack layout drawings clearly show the relationship between the rack feet

and the leak chase system. The liner, liner welds, and anchorages have been assessed for the effects of horizontal forces from the rack pedestals and have been found to be acceptable.

8.5 Loads and Load Combinations

Loads and load combinations for evaluation of the SFP are listed in Table 8.3. These loads and load combinations envelop the criteria as delineated in the La Salle UFSAR [8.1] and the La Salle Design Assessment Report [8.4]. Governing loads and load combinations were determined to calculate the controlling stresses. Thermal effects are considered in accordance with ACI 349-85, Appendix A [8.3].

Original design basis loads such as dead load, hydrostatic load, and earthquake loads resulting from the overall seismic analysis of the Reactor Building were considered in the SFP evaluation. As discussed in Section 8.3, hydrodynamic loads on the spent fuel pool have been determined based on the La Salle design basis response spectra. The dynamic loads were conservatively assumed to act in phase when determining the maximum stresses in the pool. For example, the peak rack seismic, pool water seismic and slab inertia effects were all assumed to act downward on the pool slab at the same time.

8.6 Analysis Procedure

A Finite Element Method (FEM) analysis was utilized to investigate the structural behavior of the entire pool. A plot of the FEM model is presented in Figure 8.5. The FEM analysis results were used in concrete section analyses to determine reinforcing and concrete stresses. These stresses were used to establish the design margin in the pool and its ability to safely support the loads associated with the new high density fuel racks.

When excited by the various postulated dynamic events, the racks are capable of producing vertical loads, horizontal friction loads on the floor and horizontal fluid coupling forces on the walls. The rack loads in the analysis were treated as overall uniformly distributed loads.

The local effect of the concentrated loads at the rack feet has been determined to be within the allowable stresses for the concrete fill slab.

The pool temperatures of 128°F and 212°F were considered as uniform temperatures in the FEM analysis. Based on the guidelines of ACI 349-85, the cracked section properties of the SFP walls were used in the analyses. The effect of the thermal gradient through the walls was then considered in the concrete section analyses.

Seismic shear forces in the pool walls were calculated in the original La Salle design basis seismic analysis of the Reactor Building. These shear forces have been included in the evaluation of the SFP walls. Seismic input for the analysis of the Reactor Building was based on the La Salle SSE ground motion acceleration of 0.20g and OBE ground motion acceleration of 0.10g as specified in the La Salle Updated Final Safety Analysis Report [8.1].

The FEM personal computer (PC) program, SAP90 [8.6], was used for the analysis of the SFP. SAP90 has been validated in accordance with the appropriate quality assurance requirements. Validation of the program has shown that results produced by the program are comparable to results from other FEM programs used to perform safety-related finite element analysis of spent fuel pools. The concrete SFP structure is modeled utilizing quadrilateral shell elements.

The results of the FEM structural analysis were used as input to the TEMCO computer program [8.7] which calculates reinforcing steel and concrete stresses. TEMCO, which has been validated in accordance with the appropriate quality assurance requirements, calculates reinforcing and concrete stresses based on cracked section properties of a plate section subjected to in-plane axial and shear loads, bending and torsional moments, and thermal gradient load. Calculated stresses are compared with allowables to verify that tension in reinforcing steel does not exceed 0.9 Fy and compression stress in concrete does not exceed 0.85 f'c. Temperature gradient effects are accounted for in the program by calculating the stresses in the reinforcing due to the thermal gradient and the applied section loads. Section geometry and reinforcing are shown in Figures 8.1 through 8.4. Five locations for TEMCO analysis were chosen, based on the results of the finite element analysis of the pool structure, to determine the maximum stress conditions. Figures 8.1 and 8.2 identify these locations. The FEM analysis results for the remaining pool elements confirmed selection of the controlling sections.

The resulting reinforcing steel stresses from TEMCO are presented in Table 8.4 and show a minimum reinforcing tensile stress design margin of 1.7. The maximum compressive stress in the concrete occurred in Section 5 under load case 7. The ratio of the allowable stress over the actual stress was 1.6. Design margins have been calculated based on an allowable concrete compressive stress of 0.85 f'c and an allowable tensile stress of 0.90 Fy. The critical element for shear stress is Section 2. The ratio of the allowable shear stress over the actual shear stress was 1.7 for this element for critical load case 7.

8.7 Conclusion

A finite element analysis has been performed to provide a structural assessment to demonstrate that the spent fuel pool for La Salle Station, Unit 1 can support new loads associated with the installation of HDFRs. The stresses in the pool have been shown to be well within the La Salle UFSAR allowables and the ACI 318-71 allowables demonstrating that the La Salle spent fuel pool is capable of supporting the new rack and fuel loads.

8.8 References for Section 8

[8.1] La Salle Station Updated Final Safety Analysis Report.

[8.2] ACI 318-71, "Building Code Requirements for Reinforced Concrete," American Concrete Institute.

[8.3] ACI 349-85, "Requirements for Nuclear Safety-Related Structures," American Concrete Institute.

[8.4] La Salle Station Design Assessment Report, Revision 9, June 1981.

[8.5] "Dynamic Pressure on Fluid Containers", Nuclear Reactors and Earthquakes, TID-7024, U.S. Atomic Energy Commission, August 1963.

[8.6] E. L. Wilson and A. Habibullah, "SAP90, A Series of Computer Programs for the Static and Dynamic Finite Element Analysis of Structures", Computers and Structures, Inc. Berkeley, California, July 1989.

[8.7] TEMCO/PC, Peinforced Concrete Sections Under Eccentric Loads and Thermal Gradients, S&L Program No. 03.7.255-1.0, dated June 1991.

TABLE 8.1
SUMMARY OF MAXIMUM RACK LOADS ON SFP

DEAD LOAD	
Submerged Rack and Fuel Assembly	2.29 ksf
VERTICAL LOAD ON SLAB	
Level B Spectrum	0.697 KSF
Level C Spectrum	1.464 ksf
FRICTION ON SLAB	
Level B Spectrum	0.74 ksf (N-S); 1.12 ksf (E-W)
Level C Spectrum	1.19 ksf (N-S); 1.55 ksf (E-W)
FLUID COUPLING PRESSURE ON WALLS (MAXIMUM)	
Level B Spectrum	0.43 ksf
Level C Spectrum	0.60 ksf

TABLE 8.2
TEMPERATURE CONDITIONS

Normal Operating Temperature	128°F
Accident Temperature	212°F

TABLE 8.3
CRITICAL LOAD COMBINATIONS

Description	No.	D	L	L_h	T_o	E	T_a	E_s	SRV
Normal	1	1.4	1.7	1.4	1.3	-	-	-	-
Normal + SRV (without To)	2	1.4	1.7	1.4	-	-	-	-	1.5 (1)
Normal with SRV + To	3	1.0	1.3	1.0	1.0	-	-	-	1.3 (1)
Severe Environmental	4	1.05	1.3	1.05	1.05	1.4	-	-	-
Severe Environmental + SRV	5	1.0	1.0	1.0	1.0	1.25	-	-	1.25 (1)
Abnormal with SRV	6	1.0	1.0	1.0	-	-	1.0	-	1.25 (2)
Abnormal Extreme Environmental with SRV	7	1.0	1.0	1.0	-	-	1.0	1.0	1.0 (2)

where:

D = Dead loads and vertical water pressure

L = Live loads

L_h = Lateral hydrostatic water pressure

T_o = Normal operating temperature

E = Operating basis earthquake

T_a = Accident Temperature

E_s = Safe shutdown earthquake

SRV = Safety/Relief Valve Loads

Notes:

1) Use level B SRV
2) Use level C SRV

TABLE 8.4
SPENT FUEL POOL STRUCTURE
REINFORCEMENT TENSILE STRESS SUMMARY
FOR DESIGN BASIS LOAD COMBINATIONS

Section (Note 1)	Max Tensil Stress (ksi)		Design Margin (Note 4)	Critical Load Case (Note 6)
	Horizontal East-West (Note 2)	Vertical North-South (Note 3)		
1	14.9	15.7	3.4	7
2	7.5	7.4	7.2	7
3	25.8	32.7	1.7	2
4	20.0	26.2	2.1	2
5	7.4	13.4	4.0	7

---

1. See Figures 8.1 and 8.2 for section locations.

2. Tensile stress in horizontal steel for walls or in East-West direction for steel in the SFP slab.

3. Tensile stress in vertical steel for walls or in North-South direction for steel in the SFP slab.

4. Design Margin = Allowable Stress/Actual Stress

5. Allowable stress in reinforcement = 0.90 Fy = 54 ksi

6. Sections 1 and 2 were controlled by load combination 7 without thermal

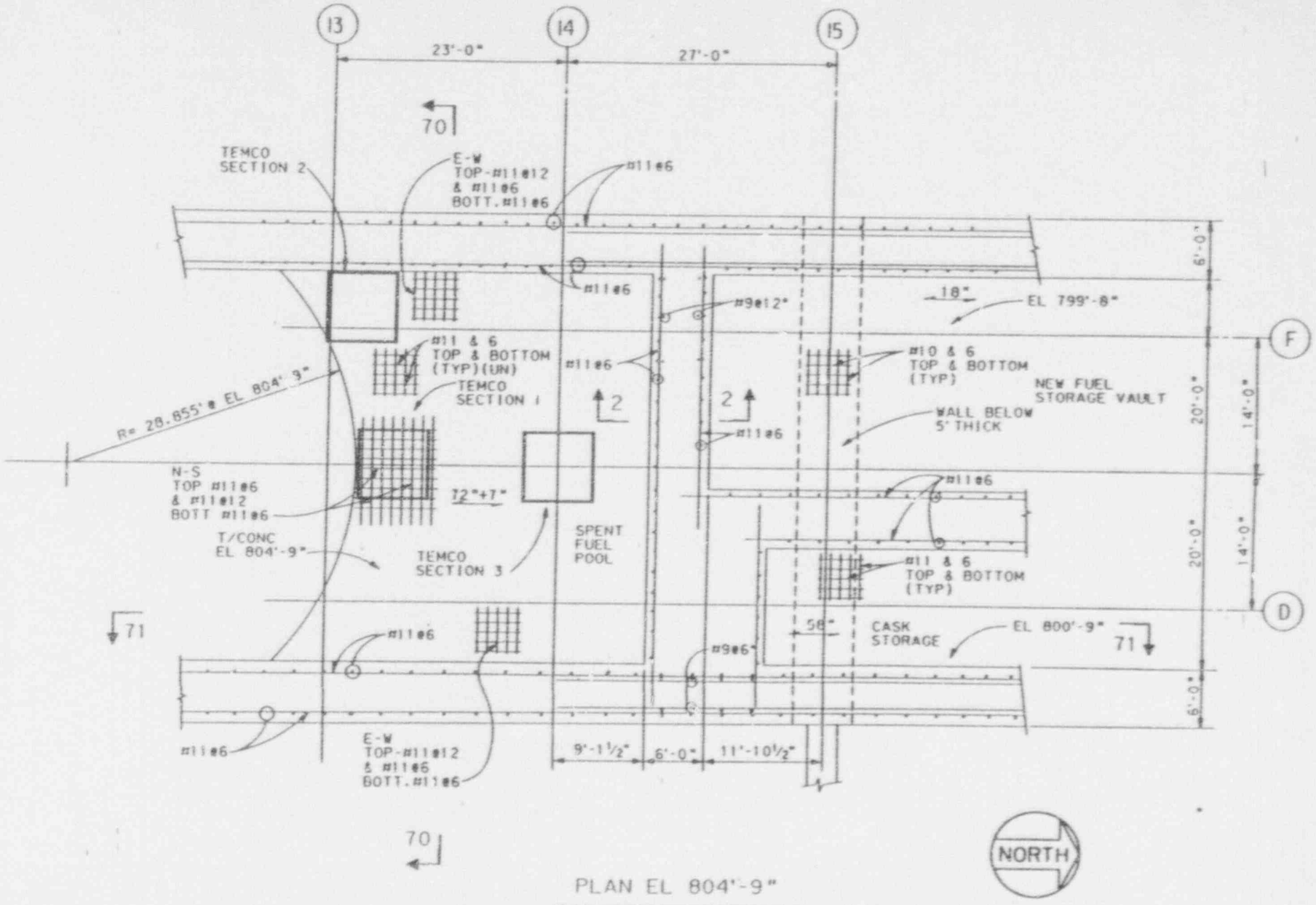

PLAN EL 804'-9"

FIGURE 8.1 LASALLE SPENT FUEL POOL FLOOR PLAN

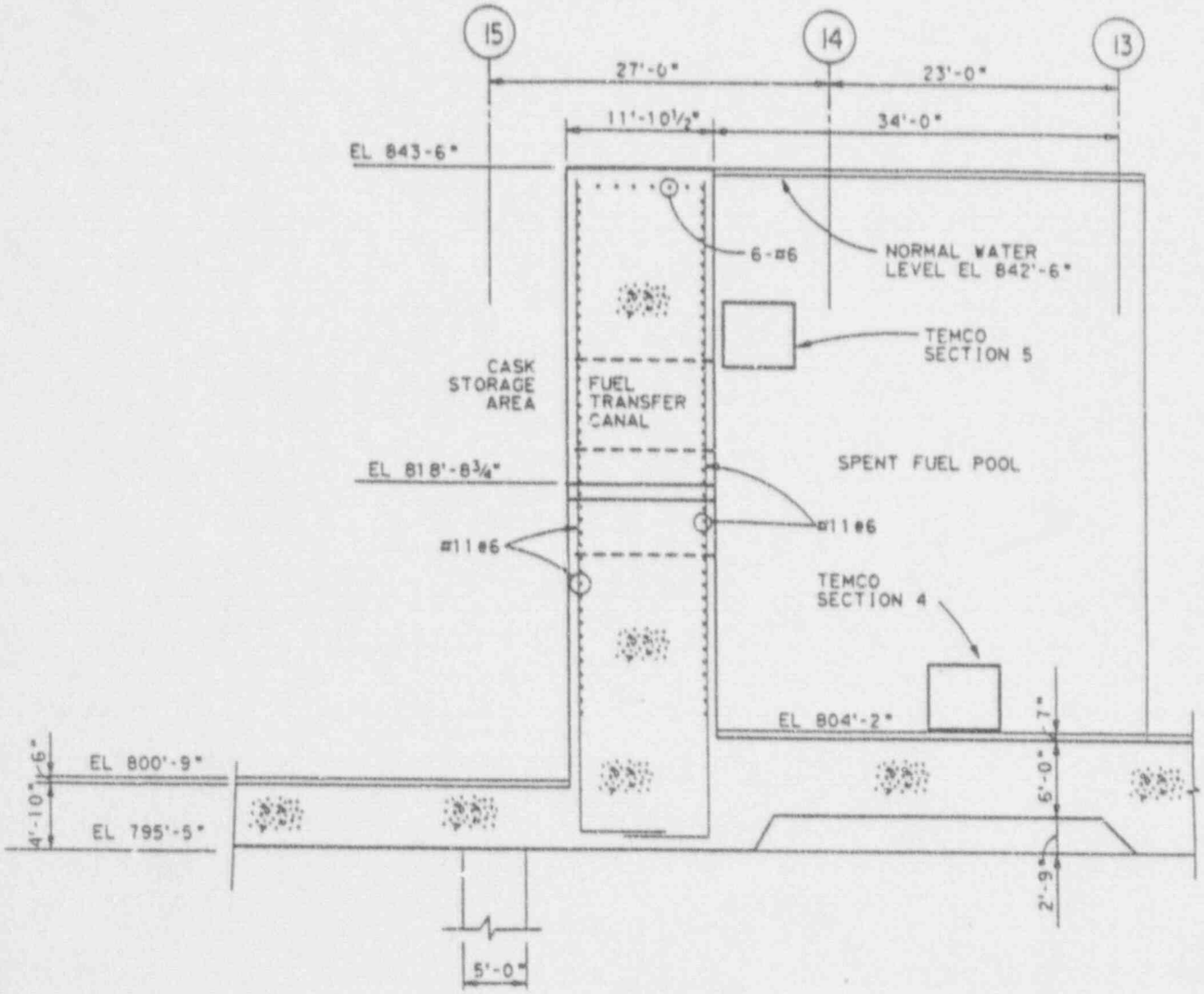

SECTION 71

FIGURE 8.2 SECTION THROUGH CASK STORAGE AREA LOOKING AT EAST WALL

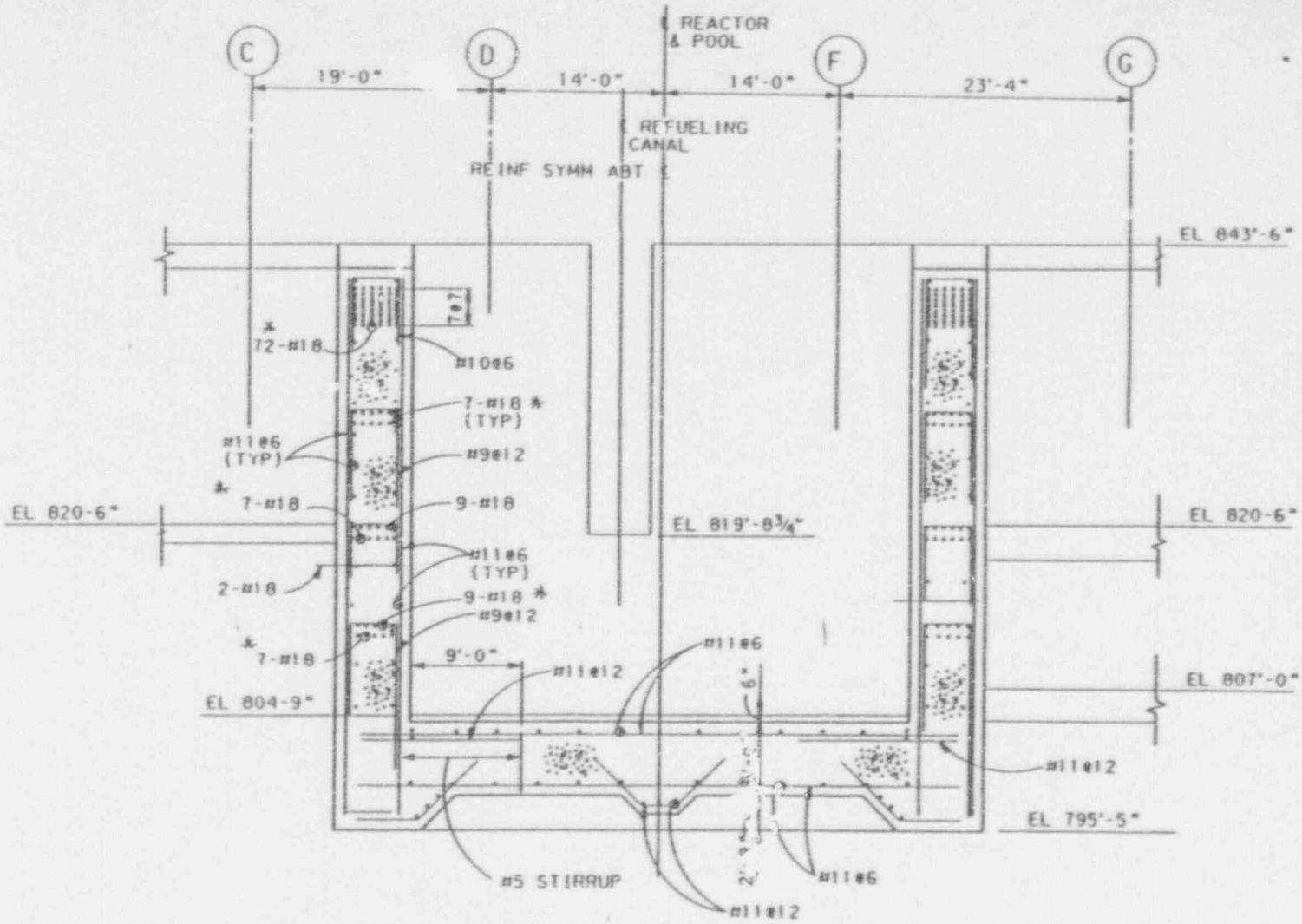

* BARS ARE TERMINATED. SEE DWG S-228. SECT 3

SECTION 70

FIGURE 8.3 SECTION THROUGH EAST AND WEST POOL WALLS LOOKING SOUTH

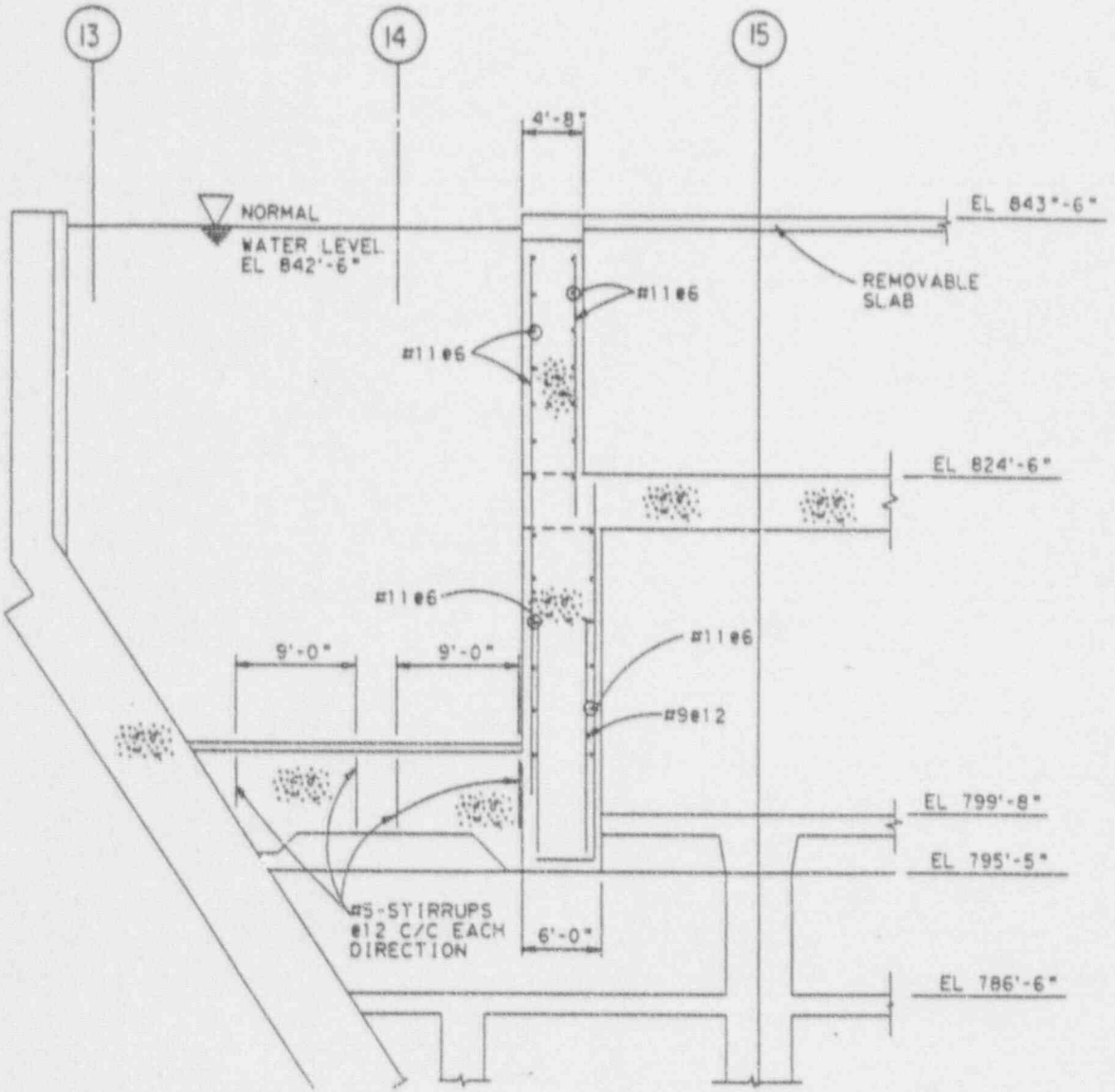

SECTION 2

FIGURE 8.4 SECTION THROUGH NORTH POOL WALL
LOOKING AT WEST WALL

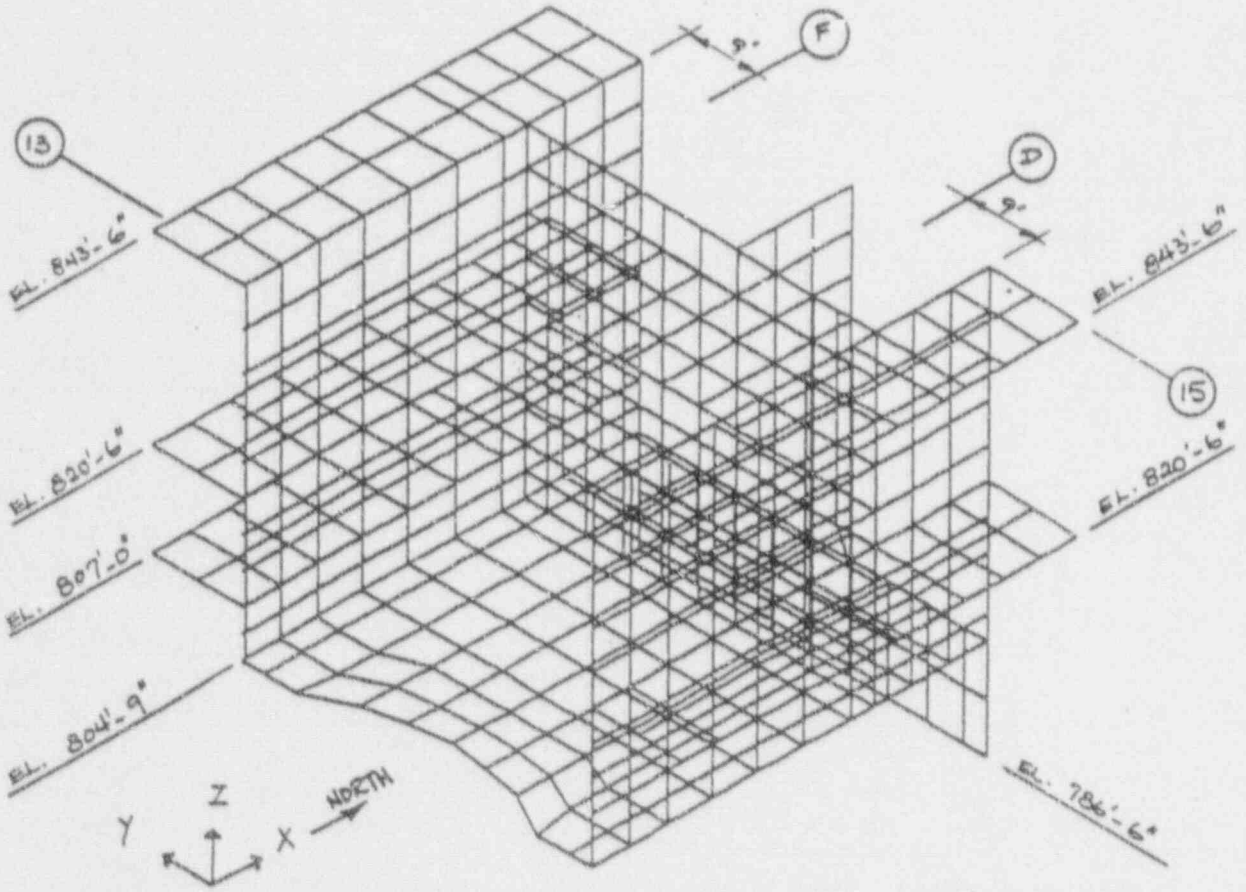

FIGURE 8.5 LaSALLE SPENT FUEL POOL ANALYTICAL MODEL

9.0 RADIOLOGICAL EVALUATION

9.1 Fuel Handling Accident

The design basis fuel handling accident (dropped assembly) is described in Section 15.7.4 of the LSCS UFSAR. The accident involves a drop of a spent fuel assembly onto the reactor core when the reactor vessel head is removed. Analysis of the design basis fuel handling accident is based on the methodology given in Regulatory Guide 1.25 and NRC Standard Review Plan (SRP) 15.7.4.

In accordance with Regulatory Guide 1.25: a peaking factor of 1.5 was applied to the radionuclidic inventory of each damaged fuel rod; 10% of the radioactive iodine and 10% of the noble gasses (30% for Kr-85) are assumed to be released from the damaged fuel rods into the pool water; 100% of the released noble gasses and 1% of the released radioactive iodines are assumed to exit the water and become airborne in the secondary containment; airborne activity within the secondary containment is released to the atmosphere over a 2-hour period through the SGTS; SGTS exhaust filter removes 90% of the iodines. The number of fuel rods damaged by the dropped assembly was calculated based on the kinetic energy of the falling fuel assembly, on the number of fuel assemblies impacted, and the minimum impact energy required to result in cladding failure. Radiological consequences of the accident were determined to be well within 10CFR100 limits.

The severity (i.e., radiological consequences) of a fuel handling accident in the spent fuel storage pool, incorporating a high density storage configuration, would not exceed that due to the design basis analysis addressed in Section 15.7.4 of the LSCS UFSAR. As such, the fuel handling accident analysis presented in the LSCS UFSAR remains valid.

9.2 Gaseous Releases

The LSCS - 1 spent fuel racks are currently authorized to store approximately one-and-a-half full cores. The proposed expanded capacity racks can accommodate more than five full core loads. To evaluate the radiological impact of the existing pool arrangement, it is assumed to contain one full core of newly removed spent fuel assemblies with the remaining storage spots (316) occupied by fuel which has been stored for one year or more. The proposed new storage arrangement will permit the storage of fuel assemblies as above, plus more fuel assemblies that are much older. Table 9-1 illustrates the age of the fuel assemblies that can be stored in the current pool vs. the new proposed pool arrangement with a refueling discharge of 256 fuel assemblies per refueling.

It is important to note that the difference between the radiological impact for the currently authorized storage pool capacity and the expanded storage pool capacity is attributable to the presence of the additional aged spent fuel in the expanded capacity racks.

The aged spent fuel in the expanded capacity racks will not contain significant amounts of radioactive iodine or short-lived gaseous fission products, since these would have decayed during the storage period. Based on the information in Reference 1, Krypton-85 that might escape from defective fuel assemblies has been shown to do so quickly (i.e., within a short time after discharge from the core). Further, the residual Krypton-85 will be contained within the fuel pellet matrix and hence, any leakage would occur at very low rates.

Based on this information, the only significant gaseous radionuclide remaining in the old spent fuel is Kr-85. The release rate of this nuclide from old spent fuel is negligible. Therefore,

the addition of two or more year old spent fuel to the pool is not expected to have any significant impact on airborne releases from the station.

9.3 Solid Radwaste

In a survey (Reference 2) of spent fuel storage pool experience, Johnson, at Battelle Pacific Northwest Laboratories, has shown that typical concentrations of radionuclides in spent fuel pool water range from 10^{-4} μCi/ml, or less, to 10^{-2} μCi/ml with the higher value associated with refueling operation. Isotopic measurements of the nuclides confirm that a major fraction of the radionuclide activity in the spent fuel pool water results from activated corrosion products dislodged from fuel element surfaces during refueling operations or carried into the spent fuel pool water (with some fission-product radionuclides) by mixing the pool water with primary system water during refueling. These sources of storage pool radionuclides depend upon the frequency of refueling operations and are basically independent of the total number of spent fuel assemblies in storage.

Once fuel-handling operations are completed, the mixing of pool water with primary system water ceases and these sources of radionuclides decrease significantly; only dissolution of fission-products absorbed on the surface of fuel assemblies and low erosion levels of corrosion product (crud) depositions remain. These, however, are removed through the operation of the fuel pool cooling and cleanup system. With aged fuel (5 or more years of storage), neither of these latter sources would be expected to contribute significantly to the concentrations of radionuclides in the storage pool.

This is further supported by measurements of the principal radionuclide concentrations made in both Quad Cities (QC) spent fuel storage pools during reactor operation (Reference 3). As shown in Table 9-2, the pool water radionuclide concentrations are not significantly affected by the number of spent fuel assemblies stored in the pool; over three (3) times as many spent fuel assemblies are stored in the QC Unit 1 pool as in the QC Unit 2 pool, but both pools have essentially the same Cs-134, Cs-137 and Co-60 radionuclide concentrations. This observation lends credibility to the expected low contribution from aged spent fuel in storage.

Similar measurements made at the Dresden Unit 2 pool (which is similar to the Quad Cities pool) indicated that the contribution, if any, from aged spent fuel will be very small or negligible in comparison to the higher activity levels (especially during refueling) of freshly discharged spent fuel assemblies. The Dresden measurements also show that the higher radionuclide concentrations that are measured during refueling operations dropped rapidly (within 2 months) to near the pre-fueling levels even though the pool contained the freshly discharged spent fuel removed from the reactor.

In view of the above, it is concluded that the additional storage capacity of the expanded spent fuel pool will not measurably alter the currently approved radiological impact or impose any significant additional burden on the cleanup system as a result of corrosion-product radionuclides or fission-product carry-over from the primary system during refueling operations.

Operation of the cleanup demineralizer system and frequency of resin replacement is determined primarily by requirements for water clarity rather than the loading of fission product radionuclides.

The amount of suspended particulate material that must be removed to maintain the desired water clarity is determined by the frequency of refueling operations and should be independent of the number of spent fuel assemblies stored. Thus, the expanded capacity of the storage pool is not expected to significantly alter the frequency of resin or filter media replacement above what is currently experienced, or the personnel radiation exposures during maintenance operations.

9.4 Personnel Exposure

The spent fuel pool at LaSalle County Station - Unit 1 is provided with
6-foot thick concrete shielding on the sides and bottom. A minimum of 23 feet of water will be maintained above the top of the active fuel in the stored assemblies (Reference 4). Area radiation levels that would be caused by stored spent fuel assemblies in the existing racks are presented in the LSCS UFSAR (Reference 5). The shielding effectiveness and the projected area radiation levels have been recalculated based on the proposed new racks.

For the new calculations (Reference 6), the fuel was assumed to be in the core for three years while the reactor was operating continuously at a power level of 3323 MWt. For conservatism, the full core of 764 fuel assemblies was assumed to have been removed from the reactor and stored in a 28 x 28 storage matrix next to the pool walls. The calculated dose rates at the side and bottom of the pool are plotted in Figure 9-1, as a function of time after shutdown. As can be seen from Figure 9-1, the dose rates below the pool remain well under 1 mrem/hr and those outside the pool walls are 2.5 mrem/hr with 5-day old discharged fuel and 1 mrem/hr with approximately 22 day old discharged fuel. In other words, by the time a normal refueling outage is over, the dose rates all around

the pool would be less than 1 mrem/hr. For up to two weeks following discharge, the dose rates in a few areas around the pool may be in the range of 1 to 2.5 mrem/hr. Based on these conservative calculations, the areas affected are: the storage area north of the pool, access corridors west of the pool at elevation 807 feet 0 inches and 820 feet 6 inches, and the equipment removal areas east of the pool at elevation 807 feet 0 inches and 820 feet 6 inches. The effect on personnel exposure is expected to be negligible.

The dose rates above the pool due to direct radiation shine from the stored spent fuel were calculated to be less than 1×10^{-5} mrem/hr.

Based on industry experience (Reference 2), LSCS-1 pool water is expected to have a radionuclide concentration of approximately 10^{-4} μCi/cc. The addition of two or more year old aged spent fuel should have no significant impact on the radionuclide concentration in the water. Therefore, the activity in the fuel pool water due to spent fuel storage within the expanded storage capacity will not impact the dose rates in the vicinity of the fuel pool.

It can also be concluded from the trend seen in Figure 9-1 that the presence of additional spent fuel, which would be at least one-year old, will have no significant impact on the dose rates to areas surrounding the pool. Therefore, it is concluded that the increased spent fuel storage capacity and new rack arrangements do not have any adverse effects on the in-plant radiation levels.

9.5 Anticipated Exposures During Reracking

Prior to the installation of the new racks, the spent fuel assemblies stored in the Unit 1 spent fuel pool will be transferred underwater through the spent fuel transfer canals and spent fuel cask pit to the Unit 2 spent fuel storage pool.

After underwater transfer of all the spent fuel elements and stored radioactive items to the Unit 2 pool, the Unit 1 pool and racks will be monitored and decontaminated as required. The racks will be disassembled into their components using divers. The components will be cut to convenient lengths before or after being lifted out of the pool by the reactor building crane. The rack components/pieces will be monitored and decontaminated as required. The pieces will then be prepared for offsite shipment in accordance with NRC requirements and CECo procedures. The rack pieces will be moved to the Unit 1 refueling floor equipment hatch and lowered down to the ground floor by the reactor building crane.

The high-density spent fuel storage rack modules will arrive onsite on the carrier's trucks. Any necessary pre-installation examination by station personnel will be made before the rack modules are moved up the Unit 1 equipment hatch area of the reactor building. The requirements for reactor building secondary containment will be maintained as the racks enter the reactor building.

The reactor building crane will raise the new storage rack modules to the refueling floor for interim storage, preferably along the east wall. The reactor building crane will move the new storage rack modules at an approximate height of two feet above the floor, except for obstacles where a height of approximately 6 feet above the floor is permitted. The crane will transport the new storage

racks to the Unit 1 spent fuel storage pool and lower them into the pool. When the storage racks are positioned and leveled in the pool, the final check and tests, if any, will be completed. The Unit 1 spent fuel elements temporarily stored in the Unit 2 pool will then be transferred underwater through the spent fuel cask storage pit and transfer canals to the Unit 1 pool, as desired.

For the purposes of estimating exposure, the reracking operation is broken into three tasks. The first is the underwater decontamination and disassembly of the existing racks. The second task is the packaging and preparation for shipment of the racks removed from the pool. The last task is the installation of the new racks. The dose received by workers transferring the spent fuel assemblies to the Unit 2 spent fuel pool and back into the Unit 1 pool is expected to be small because this operation will be similar to a normal refueling operation.

The estimated exposure associated with the Unit 1 reracking for high density storage is less than 10 men-rem. This estimate is based on the Unit 2 reracking, which resulted in a total exposure of 11.1 man-rem (6.5 man-rem for underwater operations, 3.7 man-rem for packaging and 0.9 man-rem for installation). The exposure during Unit 1 reracking is expected to be less than that acquired during Unit 2 reracking, because experience gained from the Unit 2 reracking job will be incorporated into job planning for Unit 1 reracking. Additional measures are being taken to minimize the dose which will result from Unit 1 reracking (e.g., the Unit 1 spent fuel storage pool was vacuumed in February 1992, in order to reduce radioactive crud deposits).

9.6 References for Section 9

1. NUREG-0575, Vol. 1, "Final Generic Environmental Impact Statement on Handling and Storage of Spent Light Water Power Reactor Fuel," USNRC, August 1979.

2. A. B. Johnson, Jr., "Behavior of Spent Nuclear Fuel in Water Pool Storage," BNWL-2256, September 1977.

3. "Spent Fuel Pool Modification for Increased Storage Capacity," Quad Cities Nuclear Units 1 & 2, Docket Nos. 50-254 & 50-265, March 1981 (with addendum).

4. LaSalle County Station - Unit 2 Technical Specification, Section 3.9.9.

5. LaSalle County Station Updated Final Safety Analysis Report.

6. Sargent & Lundy Shielding Calculation No. 3-SF-2, Rev. 1, for LSCS-2, October 20, 1986.

7. Sargent & Lundy Shielding Calculation No. 2-FH-2, Rev. 1, for LSCS-2, May 26, 1987.

TABLE 9-1

EXISTING VERSUS PROPOSED SPENT FUEL STORAGE POOL CAPACITY

Age of Fuel (Years)	Existing Racks	New Proposed Racks
0	764	764
1	256	256
2	60	256
3	-	256
4	-	256
5	-	256
6	-	256
7	-	256
8	-	256
9	-	256
10	-	256
11	-	256
12	-	256
13	-	150
Total	1080	3986

TABLE 9-2

OBSERVED RADIONUCLIDE CONCENTRATIONS IN QUAD CITIES SPENT FUEL STORAGE POOL WATER
(Both Units Operating)

Date	Spent Fuel Assemblies in Pool	µCi/cc Cs-134	Cs-137	Co-60
QC Unit 1				
4/27/81	1139	2.6×10^{-4}	7.9×10^{-4}	7.1×10^{-5}
5/18/81	1139	5.5×10^{-5}	1.8×10^{-4}	1.8×10^{-4}
5/24/81	1139	4.5×10^{-5}	1.7×10^{-4}	1.9×10^{-5}
6/1/81	1139	9.2×10^{-5}	3.0×10^{-4}	3.9×10^{-4}
QC Unit 2				
4/27/81	353	2.4×10^{-4}	7.8×10^{-4}	2.7×10^{-4}
5/18/81	353	7.1×10^{-5}	2.2×10^{-4}	9.5×10^{-4}
5/24/81	353	6.5×10^{-5}	2.6×10^{-4}	6.1×10^{-5}
6/1/81	353	8.5×10^{-5}	2.8×10^{-4}	2.1×10^{-4}

* Reference 3

Figure 9-1. Calculated Dose Rate Near the Spent Fuel Storage Pool With High Density Storage Racks

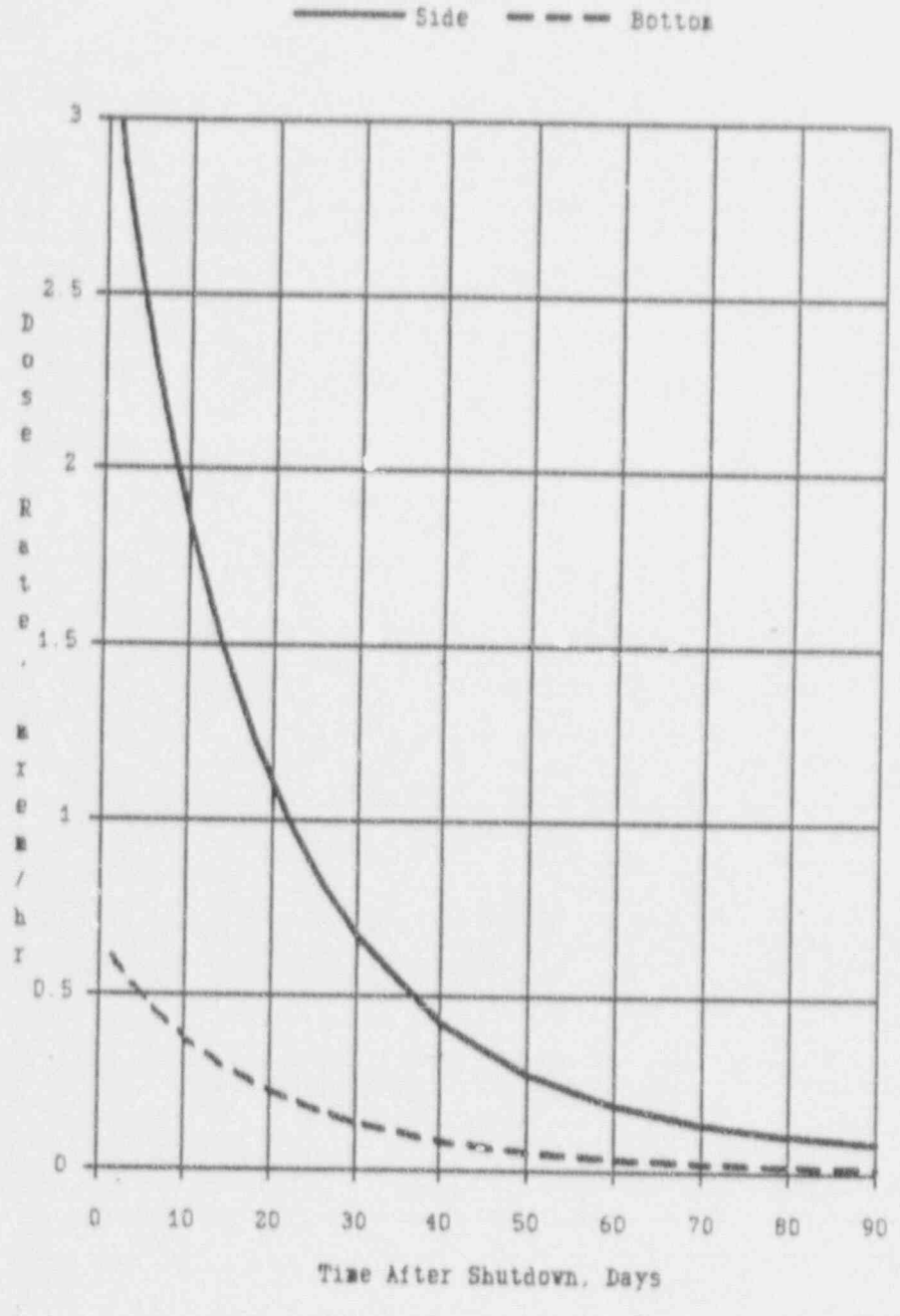

10.0 BORAL SURVEILLANCE PROGRAM

10.1 Purpose

Boral™, the neutron absorbing material incorporated in the spent fuel storage rack design to assist in controlling system reactivity, consists of finely divided particles of boron carbide (B_4C) uniformly distributed in type 1100 aluminum powder, clad in type 1100 aluminum and pressed and sintered in a hot-rolling process. Tests simulating the radiation, thermal and chemical environment of the spent fuel pool have demonstrated the stability and chemical inertness of Boral (References 1 - 3). The accumulated dose to the Boral over the expected rack lifetime is estimated to be about 3×10^{10} to 3×10^{11} rads depending upon how the racks are used and the number of full-core off-loads they may experience. Based upon the available information, Boral is considered a satisfactory material for reactivity control in spent fuel storage racks and is fully expected to fulfill its design function over the lifetime of the racks. Nevertheless, it is prudent to establish a surveillance program to monitor the integrity and performance of Boral on a continuing basis and to assure that slow, long-term synergistic effects, if any, do not become significant. Furthermore, the April 14, 1978 USNRC letter to all power reactor licensees (Reference 4), specifies that

> "Methods for verification of long-term material stability and mechanical integrity of special poison materials utilized for neutron absorption should include actual tests."

The purpose of the surveillance program, is to characterize certain properties of the Boral with the objective of providing data necessary to assess the capability of the Boral panels in the racks to continue to perform their intended function.

The surveillance program should also be capable of detecting the onset of any significant degradation with ample time to take such corrective action as may be necessary.

The Boral surveillance program depends primarily on representative coupon samples to monitor performance of the absorber material. The principal parameters to be measured are the neutron attenuation (to monitor for the continued presence of boron) and the Boral thickness (to monitor for possible swelling).

While degradation is not expected, should the measured parameters suggest possible degradation of the Boral, additional coupons may then be tested. Should these additional tests confirm degradation, an engineering evaluation will be undertaken to define the magnitude of the problem, if any, and prudent corrective action taken. Provision is also included to augment the coupon measurement program by in-situ testing (Blackness Tests) as required in the event significant degradation may be indicated by the coupon measurements.

10.2 COUPON SURVEILLANCE PROGRAM

The coupon measurement program includes coupons suspended in a high radiation area of the storage pool. Coupons will be removed for testing on a predetermined schedule and certain physical and chemical properties measured from which the stability and integrity of the Boral in the storage cells may be inferred. Each surveillance coupon (12 in number) will be mounted in stainless steel jackets, simulating as nearly as possible the in-service geometry, physical mounting, and materials representative of the environment of the Boral in the storage racks. The coupons will be positioned axially within the central 8 feet of the fuel zone where the gamma flux is expected to be reasonably uniform.

The coupon measurement program is intended to monitor changes in physical properties of the Boral absorber material by performing the following measurements on the pre-planned schedule:

- o Visual Observation and Photography,
- o Neutron Attenuation,
- o Dimensional Measurements (length, width and thickness),
- o Weight and Specific Gravity (including the volume by immersion).

The most significant measurements are neutron attenuation* (to confirm the concentration of Boron-10 in the absorber material) and thickness (to monitor for swelling). In the event loss of boron is observed or suspected, the data may be augmented by wet-chemical analysis (a destructive gravimetric technique for total boron).

Each coupon will be carefully pre-characterized prior to insertion in the pool to provide reference initial values for comparison with measurements made after irradiation. As a minimum, the surveillance coupons will be pre-characterized for weight, dimensions (especially thickness) and neutron attenuation. Two additional coupons will be preserved as archive samples for comparison with subsequent test coupon measurements.

---

* Neutron attenuation measurements are a precise instrumental method of chemical analysis for Boron-10 content using a non-destructive technique in which the percentage of thermal neutrons transmitted through the panel is measured and compared with pre-determined calibration data. Boron-10 is the nuclide of principal interest since it is the isotope responsible for neutron absorption in the Boral panel.

By locating the coupons in an area of higher gamma flux, the coupons will be exposed to a higher radiation dose than the Boral in the racks. Evaluation of the coupons removed will provide information of the effects of the radiation, thermal and chemical environment of the pool and by inference, comparable information on the Boral panels in the racks. Over the duration of the coupon testing program, the coupons will have accumulated more radiation dose than the expected lifetime dose for normal storage cells.

Some coupons may optionally be returned to the storage pool. They will then be available for subsequent investigation of defects, should any be found.

10.3 Surveillance Coupon Acceptance Criteria

Of the measurements to be performed on the Boral surveillance coupons, the most important are (1) the neutron attenuation measurements (to verify the continued presence of the boron) and (2) the thickness measurement (as a monitor of potential swelling). Acceptance criteria for these measurements are as follows:

- The Boron-10 content, as determined by neutron attenuation, shall not be more than 5% below the design basis B-10 loading, including analytical uncertainties. (The design basis tolerance in the criticality analysis is ± 8%).

- An increase in thickness at any point shall not exceed 10% of the initial thickness at that point (ie, approximately twice the tolerance in thickness).

Changes in excess of either of these two criteria requires investigation and engineering evaluation which may include early retrieval and measurement of one or more of the remaining coupons

to provide corroborative evidence that the indicated change(s) is real. If the deviation is determined to be real, an engineering evaluation shall be performed to identify further testing or any corrective action that may be necessary.

The remaining measurement parameters serve a supporting role and should be examined for early indications of the potential onset of Boral degradation that would suggest a need for further attention and possibly a change in measurement schedule. These include (1) visual or photographic evidence of unusual surface or edge deterioration, (2) unaccountable weight loss in excess of the measurement accuracy, or (3) significant change in the observed specific gravity.

10.4 In-Service Inspection (Blackness Tests)

In-service inspection involves directly testing the Boral panels in the storage racks by neutron logging* (sometimes called "Blackness Testing"). This technique is able to detect areas of significant boron loss or the existence of gaps in the Boral, but cannot determine other physical properties such as those measured in the coupon program.

Normally, Blackness testing should not be needed. However, in the event that the surveillance coupon program shows a confirmed indication of degradation, blackness testing may be one of the techniques employed to investigate the extent of degradation, if any, in the racks.

---

* Neutron logging, is a derivative of well-logging methods successfully used in the petroleum industry for many years.

10.5 References

(1) "Spent Fuel Storage Module Corrosion Report", Brooks & Perkins Report 554, June 1, 1977

(2) "Suitability of Brooks & Perkins Spent Fuel Storage Module for Use in PWR Storage Pools", Brooks & Perkins Report 578, July 7, 1978

(3) "Boral Neutron Absorbing/Shielding Material - Product Performance Report", Brooks & Perkins Report 624, July 20, 1982

(4) USNRC Letter to All Power Reactor Licensees, transmitting the "OT Position for Review and Acceptance of Spent Fuel Storage and Handling Applications", April 14, 1978

11.0 ENVIRONMENTAL COST/BENEFIT EVALUATION

11.1 Introduction

This section addresses the NRC informational needs for an environmental cost/benefit assessment, as is expressed within Section V of the USNRC OT Position paper entitled "Review and Acceptance of Spent Fuel Storage and Handling Applications", transmitted via Generic letter dated April 14, 1978.

In addition, this section summarizes the evaluations and analyses which were performed by Commonwealth Edison prior to the selection of reracking as the preferred option for expansion of the La Salle Unit 1 spent fuel storage capacity. A discussion of the relative merits associated with each category of technically viable spent fuel storage alternatives is also presented below.

11.2 Need for Increased Storage Capacity

11.2.1 Historical Perspective

All domestic nuclear plants were originally designed and constructed under the assumption that fuel reprocessing would become available for commercially-generated spent nuclear fuel. As a result, the spent fuel pools were designed to accommodate a very limited inventory.

However, fuel reprocessing services did not become generally available to the industry. As a result, the need to expand wet pool storage capacity arose, since it has only been in recent years that the new dry storage technologies have emerged. Therefore, many plants backfitted their spent fuel storage pools with stainless steel racks containing no neutron absorbing materials, but possessing a closer interspacing between individual spent fuel storage cells.

As the need arose for yet more spent fuel storage capacity, since no reprocessing or other alternatives had become available, new technical innovations were developed during the latter 1970s for alternative spent fuel storage rack designs. These new designs reflected the incorporation of neutron absorbing materials. The integral use of the fixed neutron poison material within this new generation of rack designs permitted a highest density fuel storage array, reflecting a closest possible approach (or "pitch") between adjacently stored spent fuel assemblies.

In light of both a) the site spent fuel inventories which continued to grow as well as b) the lack of alternative storage or reprocessing under federal programs, the industry was presented with a strong incentive to develop other methods; new technologies to accommodate these ever-growing spent fuel inventories. Therefore, under cooperative programs, new technologies were developed and demonstrated to expand wet pool capacity via rod consolidation and to provide storage outside of the wet pools via dry casks.

11.2.2 Status of the DOE OCRWM Program

As a result of the Nuclear Waste Policy Act of 1982, the Department of Energy was congressionally-mandated to develop a permanent geologic repository to accept shipments of commercially-generated spent nuclear fuel with operations commencing in the year 1998. Subsequent to the passage of the NWPA, all commercial utilities which own nuclear reactors entered into a mandatory contractual agreement with the DOE. Per the provisions of the generic DOE contract, all utilities must make payments corresponding to one-mil-per-kilowatt-hour of their net nuclear electrical generation into the Nuclear Waste Fund.

The DOE Office of Civilian Radioactive Waste Management has responsibility for the development of the repository. Funding for this program is being provided via the Nuclear Waste Fund, in order to develop the permanent geologic repository, as well as the proposed Monitored Retrievable Storage Facility as was authorized by Congress in the years following the passage of the 1982 Act.

Since the time that the Department of Energy was first charged by Congress with the task of repository development, there have been a total of three announcements of delay in the schedule for repository readiness. Whereas the generic DOE contract still reflects a 1998 fuel "pickup" date, the most recent DOE announcement was that the repository will be ready no sooner than the year 2010.

While the MRS concept continues to be studied at this time, it is unlikely that such a facility will be operational by the year 1998. In addition, the DOE fuel acceptance schedules reflecting their "oldest fuel first" policy, offer very little relief to the utilities during the early years of DOE facility operation. It is not until approximately the fifteenth year of the DOE's facility operation that the DOE spent fuel acceptance rate is projected to match the utility generation rate.

11.2.3 Summary of CECo Evaluations

In light of the unavailability of federal facilities to accommodate the growing inventory of spent nuclear fuel, both currently and apparently well into the future, Commonwealth Edison continues to evaluate all technically viable options to expand at-reactor interim spent fuel storage capacity for all CECo plants, including La Salle Station. Such options include new wet pool construction, rod consolidation within the existing spent fuel pools, and dry storage within modular vaults, concrete silos, or casks.

La Salle Station evaluations have indicated that on both a programmatic as well as economic basis, the installation of high density spent fuel storage racks within the La Salle Unit 1 pool is by far the preferred option. Expansion of wet pool storage capacity via high density rack installation has for all practical purposes become the industry convention. Wet storage of spent fuel assemblies is certainly the most common method utilized by the nuclear industry, and many years of operating experience have demonstrated that wet storage provides excellent performance in terms of long term fuel integrity. In addition, wet storage of spent fuel reflects the least extent of fuel handling operations.

Furthermore, evaluations for La Salle Station have indicated that the addition of high density spent fuel storage racks offers the most favorable economic profile. The rerack of the La Salle Unit 1 spent fuel pool will provide 2,949 more storage cells beyond the current capacity of 1,080 spaces. In terms of the equivalent dry storage capacity, this incremental increase of 2,949 storage spaces corresponds to approximately a) 54 vertical concrete silos or b) 56 extra large metal casks or NUHOMS horizontal concrete silo modules. Overall the La Salle Unit 1 spent fuel pool rerack option is less than one-third the cost of the most economical dry storage option.

In addition, we note that while an industry demonstration of BWR fuel rod consolidation has not yet been completed, CECo economic evaluations have projected these costs (the present value of revenue requirements) are very nearly equivalent to the cost of the most economical dry storage option.

For La Salle Unit 1, the installation of free-standing high density spent fuel storage racks with neutron absorbing materials is clearly more economical than any other available option, given the absence of both federal storage and commercial fuel reprocessing. It is clearly the most prudent direction to take in order to expand the at-reactor storage capability for La Salle Station. Storage

provisions must be provided in order to avert unit shutdown, at a cost of over $1 Million per day, as well as to retain eligibility for the Federal Interim Storage Program under NRC guidelines.

11.2.4 La Salle-Specific Needs

La Salle Station was originally constructed with a combined spent fuel storage capacity of 2,160 assemblies to serve both La Salle Units 1 and 2. In 1987, the La Salle Unit 2 spent fuel pool was modified to feature high density racks with a storage capacity of 4,073 spaces. However, 63 cells near the periphery of the La Salle Unit 2 pool are inaccessible due to physical interferences located above them. Therefore, La Salle Unit 2 has a current usable capacity of 4,010 available cells, and combined, the two La Salle units currently have a total of 5,090 accessible spent fuel storage cells.

Based upon the 192 average number of assemblies in reload for each reactor core with an 18-month operating cycle basis, it is projected, given the current usable storage capacity of 5,090 cells for the interconnected pools, that La Salle Station will lose full core offload capability in the year 2002.

However, given that the La Salle Unit 1 fuel pool was originally fitted with only 1,080 storage spaces, which was sufficient for the first 7 1/2 years of operation, La Salle has been forced to store Unit 1 spent fuel within the Unit 2 storage pool. The very limited storage capacity in the Unit 1 spent fuel pool has led to additional fuel handling operations to accommodate the storage of the Unit 1 fuel.

The La Salle Unit 1 rerack will provide a total of 8,059 spent fuel storage spaces among the two La Salle spent fuel storage pools. After the La Salle Unit 1 is fitted with the high density spent fuel storage racks, it is projected that a loss of full core

offload capability will not occur at La Salle Station until the year 2013, and a loss of reload discharge capability will not be encountered until the year 2016. Once the full complement of high density racks has been installed at La Salle, there will be sufficient spent fuel storage capacity to maintain full core reserve well into the future, for 30 years of La Salle Station operation.

11.3 Environmental Considerations

It is Commonwealth Edison's position that an environmental impact statement is not warranted, as there will be no environmental impact beyond that which has been predicted and described in the NRC's Final Environmental Statement related to the operation of La Salle Station. The results of the thermal/hydraulic analysis associated with the La Salle Unit 1 rerack are described in detail within Section 5.0 of this report.

Under the worst case analyzed, the total heat load is less than 38 million BTU per hour. Evaporative heat losses comprise approximately 0.4% of this total heat load to the environs. In addition, the 38 million BTU/hr is less than 0.05% of the total plant heat loss to the environment. Note that this additional heat load is well within the capability of the plant cooling system.

11.4 Natural Resource Commitment

The Boral racks for La Salle Unit 1 will require the use of a limited amount of the earth's natural resources, for metal and boron. Both the stainless steel rack structural material and the aluminum contained within the Boral product comprise well under .001% of the total world output. The world's production of boron carbide powder (contained within the Boral neutron absorbing material) is highly variable, is based upon demand, and can easily be expanded at any time to accommodate worldwide needs.